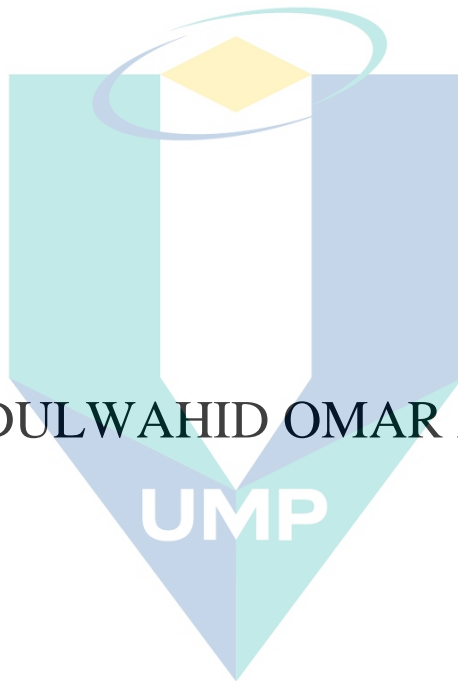


NUMERICAL INVESTIGATION OF EXHAUST  
GAS REFORMING OF NATURAL GAS FOR  
ON-BOARD HYDROGEN-RICH SYNGAS  
PRODUCTION IN SPARK IGNITION ENGINE



ABDULWAHID OMAR ARMAN

UMP

اونیورسیتی ملیسیا قہق  
MASTER OF SCIENCE

UNIVERSITI MALAYSIA PAHANG  
UNIVERSITI MALAYSIA PAHANG

## UNIVERSITI MALAYSIA PAHANG

### DECLARATION OF THESIS AND COPYRIGHT

Author's Full Name : ABDULWAHID OMAR ARMAN  
Date of Birth : 01/01/1994  
Title : NUMERICAL INVESTIGATION OF EXHAUST GAS  
REFORMING OF NATURAL GAS FOR ON-BOARD  
HYDROGEN-RICH SYNGAS PRODUCTION IN SPARK  
IGNITION ENGINE  
Academic Session : SEMESTER 1 2020-2021

I declare that this thesis is classified as:

- CONFIDENTIAL (Contains confidential information under the Official Secret Act 1997)\*
- RESTRICTED (Contains restricted information as specified by the organization where research was done)\*
- OPEN ACCESS I agree that my thesis to be published as online open access (Full Text)

I acknowledge that Universiti Malaysia Pahang reserves the following rights:

1. The Thesis is the Property of Universiti Malaysia Pahang
2. The Library of Universiti Malaysia Pahang has the right to make copies of the thesis for the purpose of research only.
3. The Library has the right to make copies of the thesis for academic exchange.

Certified by:



(Student's Signature)

08405677

New IC/Passport Number  
Date: 1/2/2021



(Supervisor's Signature)

Ftwi Yohaness Hagos

Name of Supervisor  
Date: 1/2/2021

NOTE : \* If the thesis is CONFIDENTIAL or RESTRICTED, please attach a thesis declaration letter.

## SUPERVISOR'S DECLARATION

We hereby declare that We have checked this thesis and in our opinion, this thesis is adequate in terms of scope and quality for the award of the degree of Master of Science.



DR. FTWI YOHANESS HAGOS (CEng , MIMechE)  
SENIOR LECTURER  
DEPARTMENT OF MECHANICAL ENGINEERING  
COLLEGE OF ENGINEERING  
UNIVERSITI MALAYSIA PAHANG  
LEBUHRAYA TUN RAZAK  
26300 GAMBANG, KUANTAN  
TEL : +609-424 6367 FAX : +609-549 2589

(Supervisor's Signature)

Full Name : Dr Ftwi Yohaness Hagos  
Position : Senior Lecturer  
Date : 3 February 2021



(Co-supervisor's Signature)

Full Name : Professor Madya Dr. Abdul Adam Bin Abdullah  
Position :  
Date :

PROF. MADYA DR. ABDUL ADAM BIN ABDULLAH  
Datan Inovasi Industri  
Jabatan Penyelidikan dan Inovasi  
Universiti Malaysia Pahang

## STUDENT'S DECLARATION

I hereby declare that the work in this thesis is based on my original work except for quotations and citations which have been duly acknowledged. I also declare that it has not been previously or concurrently submitted for any other degree at Universiti Malaysia Pahang or any other institutions.



(Student's Signature)

Full Name : ABDULWAHID OMAR ARMAN

ID Number : MML18004

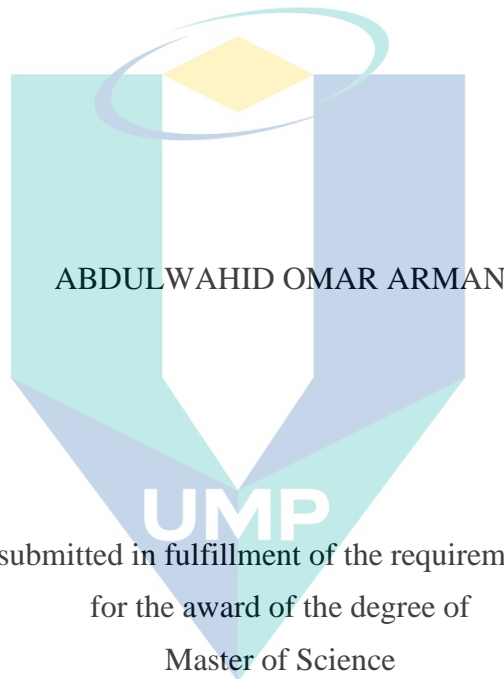
Date : 3 February 2021

UMP

اونيورسيتي ملايسيا قهغ

UNIVERSITI MALAYSIA PAHANG

NUMERICAL INVESTIGATION OF EXHAUST GAS REFORMING OF  
NATURAL GAS FOR ON-BOARD HYDROGEN-RICH SYNGAS PRODUCTION  
IN SPARK IGNITION ENGINE



اونيورسيتي ملايسيا قهغ

UNIVERSITI MALAYSIA PAHANG

College of Engineering

UNIVERSITI MALAYSIA PAHANG

FEBRUARY 2021

## ACKNOWLEDGEMENTS

In the name of Allah, the most Beneficent, the most Merciful.

Firstly, all praises to Allah, Almighty, on whom we ultimately depend for sustenance, guidance and for having everything possible by giving me the strength and courage to do this work.

Secondly, I would like to express my sincere gratitude to my supervisor Dr. Ftwi Yohannes Hagos for the continuous support during my master research. I would like to thank him for his, patience, motivation, valuable advices and immense knowledge; and without his extensive support and assistance, this thesis would not have been possible.

Next, I would like to express my deepest and warmest thanks to my family members, my father, mother, sister brothers and my wife. I am so grateful for their emotional and financial support.

My sincere and special thanks also go to the people who stand by my side at the critical moments that I passed during my research. I would like to thank E Abdullah who is considered as my psychological consultant and his words were as a light in the middle of the darkness. I still remember and I will never forget his words that made me a better person and be myself. I wish him all success and happiness in his life.

I would also like to send my sincere gratitude and thanks M Abdulmajed who stands with me in the most critical moments. His words and advices helped me a lot to overcome the worst situation I faced in my life. His words were like snow and rain that come down from the sky to water and restoes my soul and without her words I would not be able to finish this work.

My sincere thanks also go to my friends who always share me the bad and good moments, Saif, Salman, Feda'a, Azzat, Mohammed Hammod, Amri, Mukhtar, Abdullah and other friends for their assistance and moral support throughout this project. I also deeply appreciate Professor Dr. Abdul Adam. Cheng, Dr Azri, Dr Mass, Dr Ahmed Nurye and Dr Fadthlur for their helpfulness and willingness in providing a useful and valuable information, suggestions, and research materials.

Last but not lease, I would like to thank everyone supported me spiritually throughout writing this thesis and my life in general.

## ABSTRAK

Pembaharuan gas ekzos adalah kaedah yang menarik bagi meningkatkan prestasi enjin pembakaran dalaman yang menggunakan gas asli kerana gas sintesis dapat dihasilkan sejajar dengan proses pembaharuan. Tujuan kajian ini adalah untuk memodelkan dan mensimulasikan pembaharuan gas ekzos bagi pengeluaran gas sintesis yang kaya dengan hidrogen dan mengkaji kesan pembaharu pada ciri pembakaran dalam enjin. Kajian ini dijalankan dengan beban enjin 100% dan kecepatan enjin bervariasi dari 1200 hingga 3000 rpm dengan selang 300 rpm. Yang pertama sekali, pemodelan 1D digunakan bagi memerhatikan ciri-ciri pembaharuan untuk menentukan jumlah laju aliran pemangkin dan gas asli ( $\text{CH}_4$ ) yang diperlukan untuk mencapai tahap prestasi pembaharuan setinggi yang mungkin. Kajian mendapati bahawa ketika kecepatan enjin meningkat, kadar pemangkin lebih sedikit diperlukan, dan kadar gas asli yang lebih tinggi diperlukan. Yang kedua, pengoptimuman CCD (*central composite design*) RSM (*response surface method*) telah digunakan bagi mendapatkan penukaran metana secara maksimum dan pengeluaran gas sintesis pada satu kadar aliran metana minimum serta berat pemangkin pada semua tahap kelajuan enjin. Pengoptimuman CCD RSM menunjukkan bahawa kadar aliran gas asli dan berat pemangkin yang diperlukan masing-masing adalah 35 mol / jam dan 850 g. Yang ketiga, dimensi pembaharu telah dipilih dan simulasi CFD 2D telah dijalankan bagi menyiasat ciri-ciri pembaharuan saiz model pembaharu. Ciri-ciri pembaharuan telah dinilai dalam pelbagai keadaan. Kajian menunjukkan, penukaran metana yang maksimum dan pengeluaran gas sintesis diperoleh masing-masing pada 3000 rpm dan 2100 rpm. Peningkatan pecahan gas ekzos yang dikitar semula menghasilkan penggunaan metana yang lebih tinggi dan penjanaan  $\text{H}_2$  dan CO. Penambahan wap telah meningkatkan kadar penukaran metana. Namun begitu, apabila jumlah wap melebihi aras metana, hidrogen kurang dihasilkan. Kenaikan suhu dinding meningkatkan penukaran metana dan mengurangkan nisbah  $\text{H}_2$  / CO. Penambahan udara meningkatkan penukaran metana dan mengurangkan jumlah hidrogen yang dihasilkan dalam campuran gas sintesis. Akhir sekali, simulasi CFD 3D enjin telah dijalankan bagi mengkaji kesan gas yang diperbaharui pada ciri-ciri pembakaran berbanding dengan gas asli tulen menggunakan sistem bahan bakar berganda. Penambahan gas yang diperbaharui menyumbang kepada tekanan silinder dan kadar pembebasan haba yang lebih tinggi yang mana dianggap sebagai petanda kepada ciri pembakaran yang lebih baik berbanding gas asli tulen.

UNIVERSITI MALAYSIA PAHANG

## ABSTRACT

Exhaust gas reforming is an attractive method for performance enhancement of internal combustion engines fuelled by natural gas since syngas can be generated inline from the reforming process to overcome the hydrogen storage issue. The aim of this study was to model and simulate exhaust gas reformer for on-board hydrogen-rich syngas production and study the effect of the reformed gas on the combustion characteristics of the engine. The study was carried out at 100% engine load, and the engine speeds were varying from 1,200 to 3,000 rpm with an interval of 300 rpm. Firstly, 1D Modelling was used to observe the reforming characteristics to determine the amount of needed catalyst and natural gas ( $\text{CH}_4$ ) flow rate to achieve the highest possible reforming performance. Secondly, CCD (central composite design) RSM (response surface method) optimization was used to obtain the maximum methane conversion and syngas production at one minimum methane flow rate and catalyst weight at all the engine speeds. Thirdly, the reformer dimensions were selected, and 2D CFD simulation was conducted to investigate the reforming characteristics of the sized reformer model. Moreover, the reforming characteristics were evaluated at various conditions. Finally, 3D CFD simulation of the engine was conducted to study the effect of the reformed gas on the combustion characteristics and compared with purely natural gas using dual fuelling system. The 1D Modelling showed that as the engine speed increased, less amount of catalyst is needed, and a higher amount of natural gas is required. The demanded amount of catalyst mass and natural that determined by using RSM CCD was 850 g and 35 mol/hr, respectively. 2D CFD simulation found that the maximum methane conversion and syngas production were obtained at 3,000 rpm and 2,100 rpm, respectively. Increasing the rate of recirculated exhaust gas resulted in higher consumption of methane and the generation of  $\text{H}_2$  and CO. Steam addition enhanced methane conversion. However, when the amount of steam exceeded that of methane, less hydrogen was produced. At the same time, the rise of the wall temperature increased the methane conversion and reduced the  $\text{H}_2/\text{CO}$  ratio. The air addition increased methane conversion and reduced the amount of produced hydrogen in the syngas mixture. Lastly, 3D CFD simulation of the combustion characteristics showed that the addition of the reformed gas contributed to higher in-cylinder pressure and rate of heat release as well which is considered as a sign of better combustion characteristics than purely natural gas. Overall, the numerical investigation demonstrated that the amount of syngas generated through exhaust gas reforming process was sufficient to achieve a significant enhancement in the SI engine combustion fuelled by natural gas.

## TABLE OF CONTENT

**DECLARATION**

**TITLE PAGE**

**ACKNOWLEDGEMENTS** **ii**

**ABSTRAK** **iii**

**ABSTRACT** **iv**

**TABLE OF CONTENT** **v**

**LIST OF TABLES** **x**

**LIST OF FIGURES** **xii**

**LIST OF SYMBOLS** **xv**

**LIST OF ABBREVIATIONS** **xvii**

**LIST OF APPENDICES** **xviii**

**CHAPTER 1 INTRODUCTION** **1**

1.1 Research Background 1

1.2 Problem Statement 3

1.3 Research Questions 5

1.4 Research Objectives 5

1.5 Scope of the Research 6

1.6 Research Significance 7

1.7 Thesis Outline 7

**CHAPTER 2 LITERATURE REVIEW** **9**

2.1 Introduction 9

2.2 Syngas background 9

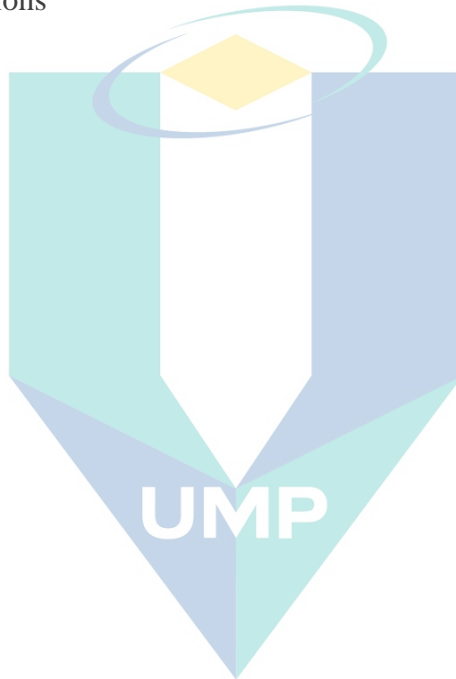
2.3 Applications of syngas 10

2.3.1	Fuel Processing for Fuel cells	11
2.3.2	Syngas in IC Engines	12
2.4	Syngas Production by Exhaust Gas Reforming of Natural Gas	15
2.4.1	Mechanism and Chemical reactions of the exhaust gas fuel reforming	15
2.5	Reaction Scheme and Kinetic of Exhaust Gas Reforming of Natural Gas	22
2.6	Catalyst	27
2.6.1	Catalyst Performance in Reforming Process	27
2.6.2	Catalyst in Exhaust Gas Reforming	30
2.7	Design of Exhaust Gas Fuel Reformer	31
2.8	Exhaust Gas Reforming F Natural Gas in an Internal Combustion Engine (Si Engine)	32
2.8.1	Overall Performance	32
2.8.2	Rate of exhaust gas recirculation	35
2.9	Effect of Hydrogen-Rich Syngas on Combustion Characteristics, Performance, and Emission of SI Engine Fuelled by Natural Gas	35
2.10	Summary	38
<b>CHAPTER 3 METHODOLOGY</b>		<b>40</b>
3.1	Overview	40
3.2	Thermodynamics Analysis	43
3.2.1	The Engine Specifications and Conditions	43
3.2.2	Injection Timing	44
3.2.3	Exhaust Gas Calculation	45
3.2.4	Natural Gas Flow Rate	47
3.2.5	Thermodynamic Properties for The Gas Mixtures	48
3.3	Catalyst Selection	50

3.4	Chemical Kinetic and Mathematical Modelling	51
3.4.1	Chemical kinetic	51
3.4.2	Mathematical Modelling	55
3.4.3	Boundary Conditions	56
3.4.4	Model of Validation	57
3.5	Optimization by Response Surface Method (RSM)	57
3.5.1	Independent Variables and Response Determination	60
3.5.2	Statistical Analysis	61
3.6	2D CFD Modeling of The Reforming Characteristics	62
3.6.1	Reactor Sizing	63
3.6.2	Boundary conditions	64
3.6.3	Governing Equations	67
3.6.4	Solution Procedure	73
3.6.5	Grid Independency Test	74
3.6.6	Model Validation	75
3.7	3D CFD Simulation of the Combustion Characteristics of The SI Engine Fuel by Natural Gas with the Addition of Reforming Products in Dual Fueling System	77
3.7.1	Model Design	78
3.7.2	Mesh Geometry	80
3.7.3	Cold Flow Simulation	81
3.7.4	Combustion Simulation	82
3.7.5	Mathematical Model and Numerical Solution	86
3.7.6	Flow Rates and Mole Fractions of The Fuels	88
3.7.7	Fuel Properties	90
3.7.8	Combustion Characteristics Calculation	93
3.8	Combustion validation	94

<b>CHAPTER 4 RESULTS AND DISCUSSION</b>	<b>96</b>
4.1 Introduction	96
4.2 The Demanded Amount of Catalyst Mass, Natural Gas Flow Rate and The Effect of Engine Speed on Reforming Characteristics	97
4.2.1 Variation of Natural Gas Flow and Catalyst Mass with the Engine speed	97
4.2.2 Effect of Engine Speeds on Reforming Characteristics	106
4.2.3 Optimization of The Amount of Demanded Natural Gas Flow Rate and Catalyst Mass	107
4.2.4 Statistical Analysis	108
4.2.5 Syngas Production	114
4.2.6 Methane Conversion	117
4.2.7 Selection of catalyst mass and natural gas (CH <sub>4</sub> ) flow rate	120
4.2.8 Syngas Production and Methane Conversion at The Selected Methane Flow Rate and Catalyst Mass	122
4.3 Reforming Characteristics of The Optimized Model (Sized Model) At Different Parameters	124
4.3.1 Effect of Engine Speed on Reforming Characteristics	124
4.3.2 Effect of EGR Rate on Reforming Characteristics	130
4.3.3 Effect of Steam Addition on Reforming Characteristics	131
4.3.4 Effect of Air Addition on Reforming Characteristics	132
4.3.5 Effect of Wall Temperature on Reforming Characteristics	132
4.4 Effect Of Reformmate Gas On The Combustion Characteristics	133
4.4.1 Cold Flow	134
4.4.2 Fuel Injection	135
4.4.3 Combustion Characteristics	137

<b>CHAPTER 5 CONCLUSION AND RECOMMENDATIONS</b>	<b>141</b>
5.1 Introduction	141
5.2 Conclusion Remarks	142
5.2.1 Objective 1	142
5.2.2 Objective 2	143
5.2.3 Objective 3	144
5.3 Recommendations	144
<b>REFERENCES</b>	<b>145</b>



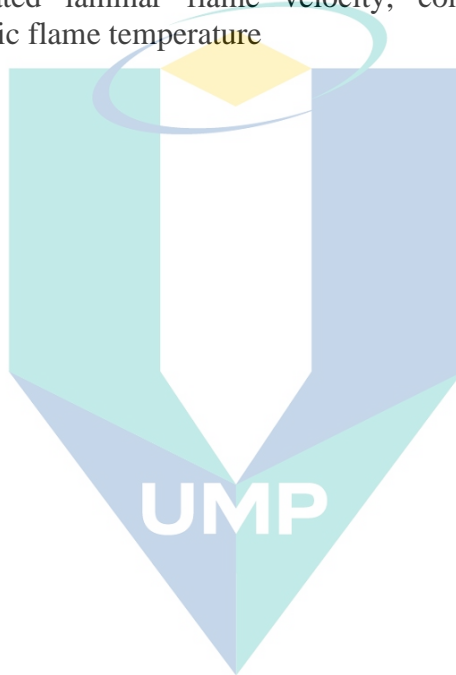
اونيورسيتي مليسيا قهغ

UNIVERSITI MALAYSIA PAHANG

## LIST OF TABLES

Table 2.1	Main reactions of the exhaust gas reforming reaction	16
Table 2.2	The kinetic rate equations based on the mentioned models for the tri-reforming process	25
Table 2.3	Properties of different catalyst at various temperature	29
Table 2.4	Main reaction in the reforming process of methane	33
Table 3.1	Engine specifications.	43
Table 3.2	Inlet fuel rate, air-fuel ratio and exhaust gas flow rate at each engine speed	46
Table 3.3	Exhaust gas volume fraction at 25% EGR	47
Table 3.4	Exhaust gas volume fraction at 1,800 rpm at various EGR rates	47
Table 3.5	Molar flow rate of natural gas at each engine speed based on the exhaust flow rate.	48
Table 3.6	Constants for polynomial in Equation 3.4	49
Table 3.7	Constants for calculation of $C_{p,i}$	50
Table 3.8	Catalyst properties	51
Table 3.9	Main reactions in the exhaust gas reforming process	52
Table 3.10	Equilibrium constant and Arrhenius kinetic coefficient	53
Table 3.11	Equilibrium constant and Arrhenius kinetic coefficient	53
Table 3.12	Heat transfer coefficient	54
Table 3.13	Independent variables and responses	60
Table 3.14	Design layout of the CCD model design for the process optimization and the corresponding responses	61
Table 3.15	The mixture volume fractions and flow region at engine speed	66
Table 3.16	Catalytic reaction scheme	72
Table 3.17	Meshing details	74
Table 3.18	Comparison between experimental, 1D and 2D modelling mole fractions values	76
Table 3.19	Comparison between experimental, 1D modelling and 2D simulation of Hydrogen and methane mole fraction	76
Table 3.20	Boundary condition for cold flow simulation	82
Table 3.21	Boundary condition for combustion simulation CNG fuel	83
Table 3.22	Mole fraction and flow rate of the reformat gas	89
Table 3.23	Mole and mass fractions and molar and mass flow rate of the reformat gas	89
Table 3.24	Properties of the pure gases	90

Table 3.25	Volume basis and mass basis LHV of the reformat gas	92
Table 4.1	Catalyst mass and methane flow rate at each engine speed.	106
Table 4.2	Analysis of variance (ANOVA) for syngas response	111
Table 4.3	Analysis of variance (ANOVA) for Methane conversion response	112
Table 4.4	Actual modeling and empirical regression model validation of Syngas	113
Table 4.5	Actual modelling and empirical regression model validation of Methane conversion	114
Table 4.6	Calculated laminar flame velocity, combustion duration and adiabatic flame temperature	140



اونيورسيتي ملايسيا قهغ

UNIVERSITI MALAYSIA PAHANG

## LIST OF FIGURES

Figure 2.1	Fuel processing of gaseous, liquid, and solid fuels for syngas and hydrogen production for different fuel cells	11
Figure 2.2	Exhaust gas reforming mechanism	16
Figure 2.3	Effect of reforming Pressure on the CH <sub>4</sub> & H <sub>2</sub> O Conversion and H <sub>2</sub> & CO yield	18
Figure 2.4	CH <sub>4</sub> /CO <sub>2</sub> ratio on conversion of CH <sub>4</sub> and CO <sub>2</sub> and yield of CO and H <sub>2</sub> at 850 °C and 1atm	20
Figure 2.5	Typical temperature profile of a CPO reactor with concentration profile les of fuel and O <sub>2</sub> along a COX catalyst bed	21
Figure 2.6	Different kinds of heat exchange reformers	32
Figure 2.7	Principle of the exhaust reforming process	33
Figure 3.1	Flow chart of the research	42
Figure 3.2	Schematics of exhaust gas reforming mechanism	44
Figure 3.3	Position of the crank angles at different injection timing	45
Figure 3.4	Catalytic fixed bed tube	57
Figure 3.5	CCD RSM optimization steps	59
Figure 3.6	Physical domain of fixed bed of exhaust gas reformer	63
Figure 3.7	Model of the single fixed bed reactor tube.	74
Figure 3.8	Variation of the molar fraction of methane with the size of the mesh	75
Figure 3.9	Schematic diagram of the single tube reforming test bench systemx	77
Figure 3.10	Engine simulation steps	78
Figure 3.11	Schematic diagram of direct-injection spark-ignition engine	79
Figure 3.12	Engine geometry (a) before decomposition (b) decmposed geometry	80
Figure 3.13	A generated mesh of the geometry	81
Figure 3.14	Variation Coordinates file of footprint CNG injection	84
Figure 3.15	Variation Labelled beam, spark, and footprint point	84
Figure 3.16	Decomposed geometry with spray cone	85
Figure 3.17	Coordinates file of footprint reformate injection	85
Figure 3.18	Labelled EGR beam point and footprint	86
Figure 3.19	Comparison between experimental data and CFD simulation	95
Figure 4.1	Methane conversion and syngas percentage at different ratio of methane flow rate to exhaust gas flow rate (a) reforming	

	characteristics at 1,200 rpm at 0.15 ratio of methane to exhaust (b).	98
Figure 4.2	Methane conversion and syngas percentage 1500 rpm at different ratio of methane flow rate to exhaust gas flow rate (a) reforming characteristics at 0.15 ratio of CH <sub>4</sub> to exhaust (b).	99
Figure 4.3	Reforming performance at different ratio of methane flow rate to exhaust gas flowrate (a) reforming characteristics at 1,800 rpm at 0.2 ratio of CH <sub>4</sub> to exhaust at 1,800 rpm (b).	100
Figure 4.4	Reforming performance at different ratio of methane flow rate to exhaust gas flow rate (a) reforming characteristics at 2,100 rpm at 0.2 ratio of CH <sub>4</sub> to exhaust (b).	102
Figure 4.5	Reforming performance at different ratio of methane flow rate to exhaust gas flow rate (a), reforming characteristics at 2,400 rpm at 0.2 ratio of CH <sub>4</sub> to exhaust (b).	103
Figure 4.6	Reforming performance at different ratio of methane flow rate to exhaust gas flow rate (a) reforming characteristics at 2,700 rpm at 0.2 ratios of CH <sub>4</sub> to exhaust (b). (Continoued)	104
Figure 4.7	Reforming performance at different ratio of methane flow rate to exhaust gas flow rate (a) reforming characteristics at 0.2 ratio of CH <sub>4</sub> to exhaust (b). at at 3,000 rpm	105
Figure 4.8	Effect of engine speed on methane conversion and syngas production	106
Figure 4.9	The predicted vs actual modeling using various transform models of syngas response, a) Non, b) square root, c) Natural log model, d) Inverse square root mode and e) Inverse model.	108
Figure 4.10	The predicted vs actual modelling using various transform models of methane conversion response, a) Non, b) square root, c) Natural log model, d) Inverse square root mode and e) Inverse model.	110
Figure 4.11	3D Surface of syngas production at each engine speed with the various catalyst mass and methane flow rate.	116
Figure 4.12	3D surface of variation of catalyst mass and flow rate and their effect on the methane conversion at each engine speed.	119
Figure 4.13	Optimal numerical solutions	121
Figure 4.14	Desirability of the numerical solutions with syngas production and methane conversion.	122
Figure 4.15	Syngas production in 3D surface (a) and 2D contour (b) at different engine speed and catalyst mass at 35 mol/hr	123
Figure 4.16	Effect of engine speed and catalyst mass on methane conversion at 35 mol/hr in 3D surface (a) and contour 2D (b)	124
Figure 4.17	Effect of engine speed on temperature profile along the reactor with EGR rate of 25%.	125
Figure 4.18	Mole fraction of natural gas and exhaust gas components disruption and temperature profile in the EGR reformer at 1800 rpm and EGR	

	rate of 25% of 1D and 2D modelling. (a) 1D modeling, (b) CH <sub>4</sub> contours, (c) H <sub>2</sub> O contours, (d) CO <sub>2</sub> contours and (e) CO contour (f) H <sub>2</sub> contour (g) temperature contour	127
Figure 4.19	Effect of engine speed on methane conversion (a) and syngas production (b)	129
Figure 4.20	Effect of EGR rate on methane, carbon dioxide conversion (a) and syngas production (b) in 1D and 2D at 1,800 rpm	130
Figure 4.21	Effect of steam addition on methane conversion and syngas production at 1800 rpm.	131
Figure 4.22	Effect of O <sub>2</sub> /C ratio in methane conversion (a), H <sub>2</sub> and CO fraction at the reformer outlet at 1,800 rpm	132
Figure 4.23	Effect of wall temperature on methane conversion (a) and H <sub>2</sub> /CO ratio (b)	133
Figure 4.24	The airflow velocity from the intake flow (a), compression stage (b) and the open of exhaust valve (c) (continued)	134
Figure 4.25	Natural gas injection to the combustion chamber (Countinoud)	136
Figure 4.26	EGR addition to air manifold to the combustion chamber	137
Figure 4.27	Variation of in-cylinder pressure with crank angle degree at 1800 RPM in pure natural gas and natural gas with the addition of the reformed gas (continued)	138
Figure 4.28	Effect of EGR addition on the heat release rate at 1,800 rpm	139
Figure 4.29	Effect of EGR addition on the mass burned fraction at 1,800 rpm	140

اونيورسيتي ملايسيا قهغ

UNIVERSITI MALAYSIA PAHANG

## LIST OF SYMBOLS

$\gamma$	Initial sticking coefficient
$\Gamma$	density of the catalyst active base
$\varepsilon$	Porosity of the fixed bed
$\theta$	Surface coverage
$\mu$	Dynamic viscosity (Pa s)
$\nu$	stoichiometric coefficient of the reactant species
$\xi_{i,n}$	exponent of surface coverage
$\rho$	Fluid density (kg/m <sup>3</sup> )
$\rho_{cat}$	Density of catalyst bed (kg/m <sup>3</sup> )
$\tau$	
$\varphi$	Exponent of surface coverage
$A$	Pre-exponential factor (s <sup>-1</sup> or m <sup>2</sup> /mol.s)
$A_a$	Cross-section area of the reformer, m <sup>2</sup>
$C_2$	Inertial loss factor (m <sup>-1</sup> )
$C_1, C_2$	Calibration constants
$C_{pj}$	Specific heat of component $j$ , (J/kg.K)
$E_j$	Activation energy (kJ/mol)
$F_j$	Molar flow rate of component $j$ , (mol/hr)
$J_{i,j}$	Diffusion flux of the species $i$ in $j$ direction (kg/s)
$k_1$	Reaction constant of the for the first-rate equation (mol.kg <sup>-1</sup> .s <sup>-1</sup> )
$k_2$	Reaction constant of the for the second rate equation (mol.kg <sup>-1</sup> .s <sup>-1</sup> )
$k_3$	Reaction constant of the for the third rate equation (mol.kg <sup>-1</sup> .s <sup>-1</sup> )
$k_{4a}$	Reaction constant of the for the fourth rate equation (mol.kg <sup>-1</sup> .s <sup>-1</sup> )
$k_{4b}$	Reaction constant of the for the fourth rate equation (mol.kg <sup>-1</sup> .s <sup>-1</sup> )
$k_{eff}$	Effective heat transfer coefficient
$k_{f,n}$	Dynamic constant of elementary reactions (s <sup>-1</sup> or m <sup>2</sup> /mol.s)

$M_i$	Molecular weight of the species (kg/mol)
$m$	Mass (kg)
$P_j$	Partial pressure of component $j$ in reaction side (bar)
$R$	Ideal gas constant (J/K.mol)
$R_1$	First-rate of reaction for steam reforming (mol.kg <sup>-1</sup> .s <sup>-1</sup> )
$R_2$	Second rate of reaction for steam reforming (mol.kg <sup>-1</sup> .s <sup>-1</sup> )
$R_3$	Third rate of reaction for water-gas shift reaction (mol.kg <sup>-1</sup> .s <sup>-1</sup> )
$R_4$	Fourth rate of reaction for total combustion of methane (mol.kg <sup>-1</sup> .s <sup>-1</sup> )
$Re$	Reynolds number
$r_j$	Reaction rate of component $j$ (mol.kg <sup>-1</sup> .s <sup>-1</sup> )
$S_i$	Molar net production rate (mol/m <sup>3</sup> .s)
$T$	Fluid temperature (K)
$T_w$	Wall temperature (K)
$\nu$	Stoichiometric coefficient
$w$	Characteristics charge velocity
$Y_i$	Mass fraction of component $i$

اونيورسيتي ملايسيا قهغ

UNIVERSITI MALAYSIA PAHANG

## LIST OF ABBREVIATIONS

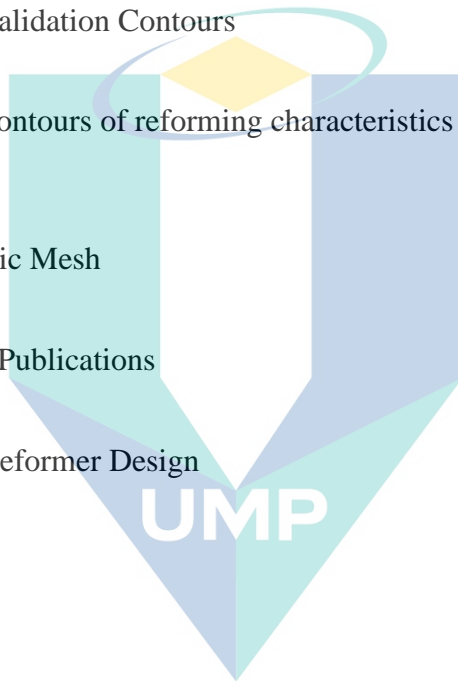
ICE	Internal Combustion Engine
SI	Spark Ignition Engine
PAFCs	Phosphoric Acid Fuel Cells
AFCs	Alkaline Fuel Cells
MCFCs	Molten Carbonate Fuel Cells
PEMFCs	Membrane Fuel Cell Exchange Protons
CNG	Compressed Natural Gas
DI	Direct Injection
MBT	Maximum Brake Torque
SR	Steam reforming
DRM	Dry reforming of methane
POX	Partial oxidation
COX	Complete Oxidation
TOX	Total oxidation
RSM	Response surface method
CCD	Central composite design
WGS	Water gas shift reaction
ATR	Autothermal reforming
LHHW	Langmuir-Hinshelwood-Hougen-Watson Reaction model
LNG	Liquid natural gas
EGR	Exhaust gas recirculation

اونیورسیتی ملیسیا قهق

UNIVERSITI MALAYSIA PAHANG

## LIST OF APPENDICES

Appendix A	Chemkin Code of Surface of Surface Mechanism Reaction of CH <sub>4</sub> Over Rhodium	154
Appendix B	Chemkin Code of H <sub>2</sub> /CO Combustion Mechanism	165
Appendix C	CFD scaled residual	170
Appendix D	CFD Validation Contours	171
Appendix E	CFD Contours of reforming characteristics of the optimized model	172
Appendix F	Dynamic Mesh	174
Appendix H	List of Publications	175
Appendix G	Final Reformer Design	176



اونيورسيتي ملايسيا قهغ

UNIVERSITI MALAYSIA PAHANG

# CHAPTER 1

## INTRODUCTION

### 1.1 Research Background

In the last two decades, transportation was considered the most blamed sector for the rise in fuel consumption globally. Transportation is responsible for over 23% of the global emission of CO<sub>2</sub> in 2018 (Chen et al. 2018). In China, this sector accounted for 348.19 million of coal equivalent, and the emission of the vehicles in 2018 was 45.71 tons (D. Chen, et al., 2018; Özener, et al., 2020). Today, the dependency on fossil fuel in road transportation is about 95%. However, to achieve a significant reduction in greenhouse gas emission, the dependence on crude oil must be reduced without any negative effects on the patterns of automobile populations (Tartakovsky, et al., 2018). As a result, the restriction on the harmful exhaust gas emissions from the internal combustion engines (ICEs) has increased in recent years. However, finding cleaner and more economical alternative sources of energy has become a crucial issue. Natural gas is one of the energy sources which is widely used in many applications such as electricity generation, for industrial heat supply and in transportation engines. In the transportation sector, it is considered as the most feasible fuel compared to conventional fuels such as gasoline and diesel (Altın, et al., 2017). Natural gas has advantages over the traditional fuels due to its lower cost, lower emissions and its abundant availability as alternative. Furthermore, its capability to be used in compression ignition (CI) and spark ignition (SI) engines with no or little modifications of the engine hardware put natural gas forefront as a fuel in an internal combustion engine. The amount of exhaust gas emissions from ICE powered with natural gas significantly reduces mainly the concentrations of polycyclic aromatic hydrocarbons (PAHs), SO<sub>2</sub>, CO and CO<sub>2</sub>. Besides, higher brake thermal efficiency (BTE) can be attained through the operation of the engine at a higher compression ratio. However, the use of natural gas faces various difficulties because its

combustion at lower engine speeds is less complete compared to gasoline which results in lower performance.

Hydrogen is an alternative fuel that can be utilized in ICE to substitute the gasoline and diesel in both the SI and CI engines. Hydrogen has superior combustion characteristics which can enhance the performance of the engine. However, the usage of hydrogen in ICE is hindered due to its high cost, difficulties of storage and its high combustion temperature. Therefore, hydrogen is being utilized in ICE as an additive, and it was found that a small amount of hydrogen can enhance the engine combustion and performance due its combustion characteristics (Liu, et al., 2018).

In recent years, the interest of syngas application in ICE has reemerged. Many experimental and numerical studies have shown that syngas addition contributes to the enhancement of natural gas engine performance and emission reduction. Utilization of syngas as an additive in the SI engine fueled by natural gas decreases the knock tendency and intensity of the engine. This is attributed to the rise of the energy density of the in-cylinder mixture and the flame speed promotion due to the higher flame propagation of hydrogen in the mix. It is also found that the addition of H<sub>2</sub>:CO extends the lean limit and stabilize the combustion (Liu, et al., 2018),(Changpeng Liu, et al., 2018).

Syngas is industrially produced through a reforming process of natural gas in the presence of a catalyst such as steam methane reforming, dry reforming and auto-thermal reforming. The reforming technology of natural gas and other hydrocarbon fuels was used in industry for the purpose of hydrogen and chemical production. Whereas in recent years, the technology of reforming has started to be used in the automotive sector by reforming the fuel with the use of the exhaust gas in the catalytic reactors (Baxter, et al., 2008a).

Exhaust gas reforming (EGR) is a technology of fuel conversion that offers a potential enhancement of the engine efficiency and emissions reduction in ICE. It is performed in a catalytic reactor which is integrated to exhaust gas recirculation loop and use the heat of the exhaust and the exhaust composition. The exhaust components: CO<sub>2</sub>, H<sub>2</sub>O (steam), O<sub>2</sub>, a small amount of CO and unburnt hydrocarbon are mixed with the primary fuel in the catalytic reactor to produce H<sub>2</sub>-rich reformat gas. Exhaust gas

reforming involves steam reforming, dry reforming and partial and complete oxidation of the fuel in the same catalytic reactor zone. This combination contributes to the reduction of the demanded external energy which contributes to the increase of hydrogen and monoxide production, primarily when the engine is powered by natural gas. Therefore, the application of this technology in the natural gas engine will be extremely beneficial because the syngas produced from the reforming process can enhance the performance of the engine due to the higher energy released from the hydrogen combustion (Tartakovsky, et al., 2018).

## 1.2 Problem Statement

Natural gas is considered one of the best options for fossil fuel replacement in transportation sector due to its worldwide availability, intrinsic clean-burning, cost-effective as fuel and flexibility to be used in gasoline and diesel engines. The burning of natural gas is cleaner than gasoline. This is mainly due to its mixture's thermodynamic properties, lowered peak cylinder temperatures that reduce engine heat losses and reduced pumping losses due to reduced throttling (Imran, et al., 2016).

Despite all the advantages of natural gas, it still has various difficulties to be used in SI and CI engines because its rare energy release from combustion is low compared to gasoline and diesel. Natural gas has low flame propagation speed which results in longer ignition delay compared to conventional fuels. The lower speed of propagation affects the engine performance and reduces the brake horsepower of the engine by 5-10% at the low speed and high load (A. H. Kakaee, et al., 2014)(A. Kakaee, et al., 2013). The lower performance of the natural gas in SI engines contributes to preventing the achievement of the idle conditions in natural gas vehicles. Idle condition is important for any vehicle to achieve more stability, fuel economy, exhaust emissions, comfortable and operational performance. They also influence the combustion stability during the motion, especially at higher loads (Ravindra, et al., 2006),(Fotache, et al., 1997).

Hydrogen has various combustion characteristics that can improve engine performance, such as the higher burning velocity and low ignition energy (Açikgöz, et al., 2015). Despite the prospect of hydrogen as a greener fuel in ICEs, the technical challenges on the production and storage are hindering its commercial viability. Besides

its role as a standalone fuel, hydrogen is being investigated as a prospective fuel additive in different power generation. It was experimentally proven that a tiny amount of hydrogen could improve performance and reduce exhaust gas emissions. Adding hydrogen to natural gas increases the cylinder pressure and temperature of natural gas engine as results of the improvement of heat release rate which contribute to shorten the combustion duration and achieve more engine stability (Kamil, et al., 2015; Raviteja, et al., 2015; Zhuoyao He , Zhan Gao , Lei Zhu , Shujing Li b, Ang Li , Wugao Zhang, 2016).

Despite all the advantages of hydrogen addition on the natural gas engine performance, it still has many challenges to be used in ICE. The issue of hydrogen storage can be avoided through the syngas production inline as hydrogen can be provided in the form of syngas mixture ( $H_2$ : CO) through the reforming reaction of the exhaust gas mixture and the primary engine fuel in the presence of a catalyst (Iulianelli, et al., 2014). Since syngas can enhance the combustion and performance of SI engine. This enhancement is due to the increasing of the energy density in-cylinder mixture and the promotion of the flame speed due to the higher propagation of hydrogen. It also found that the introducing of  $H_2$ /CO to the CNG-DISI extends the lean limit and stabilize the combustion (Changpeng Liu, et al., 2018; Hagos, et al., 2014a; Liu, et al., 2018).

Due to the difficulty of syngas storage and availability in petrol stations, exhaust gas reforming of natural gas can be used for on-board syngas production in SI engine. The technology of fuel and exhaust gas reforming is used in gasoline and diesel engines, and it shows a great improvement in the engine combustion, performance and emission characteristics. This technology has not been used yet in natural gas engines, despite the high performance of the reforming of natural gas in hydrogen-rich syngas production compared to other liquid fuels. No study to date has applied the reforming process of natural gas in ICE. In all the earlier studies, there is no linkage of the exhaust gas reforming modelling with the amount of exhaust gas recirculation and the engine operating condition. Therefore, the modelling and simulation of exhaust gas reforming of natural gas in SI engines at low engine speed and high load conditions needs to be investigated taking in consideration the effect of the reformed gas on the combustion characteristics of the engine.

The current studies are conducted by the simulation to test the availability of the reforming process of the recirculated exhaust. Thus, numerical simulation is preferred for various reasons, such as the cost-effective of the experiment setup. Besides, the reformer design can be enhanced and optimized through the simulation by calculating the amount of catalyst needs and natural gas flow rate demanded to achieve a satisfying reforming performance. Moreover, CFD simulation provides the availability to observe the conversion of exhaust components and formation of syngas ( $H_2+CO$ ) through contours which can indicate the chemical transport and thermal distribution along the reformer tube which is difficult to be obtained experimentally. Lastly, due to the complexity of the combustion experiments of dual fuelling system to investigate the effect of the reforming products (Syngas) on combustion characteristics, 3D CFD simulation is favoured to overcome the experiment challenges.

### 1.3 Research Questions

- i. How much natural gas and catalyst needed to achieve a satisfying reforming performance?
- ii. How much syngas can be produced from the exhaust gas reforming of natural gas at low speeds and high load?
- iii. How much methane conversion can be achieved in the reforming process?
- iv. Why the addition of reformed gas can effectively enhance the combustion characteristics?

### 1.4 Research Objectives

This study aims to investigate the availability of the on-board syngas production from the reforming process of the recirculated exhaust gas and the natural gas in the SI engine. Moreover, this study aims to evaluate the effect of reformed gas on combustion characteristics. The following specific objectives are to be achieved

- i. To analyze the minimum demanded amount of catalyst and natural gas flow rate to achieve the maximum reforming performance at all the engine speeds used in this study.

- ii. To investigate the reforming characteristics of the optimized model at different parameters using 2D CFD simulation and compare it with the 1D mathematical modelling.
- iii. To evaluate the effect of reformed gas addition on the combustion characteristics and compare it with the combustion characteristics of purely natural gas using CFD simulation.

### 1.5 Scope of the Research

- i. The composition of syngas considered in the current study is H<sub>2</sub> and CO.
- ii. In the current study, natural gas is represented by pure methane (CH<sub>4</sub>).
- iii. Reforming performance is evaluated by the amount of syngas production and methane conversion.
- iv. The exhaust gas emission composition includes CO<sub>2</sub>, H<sub>2</sub>O (steam), O<sub>2</sub> and N<sub>2</sub>. CO, NO<sub>x</sub>, and HC emissions are negligible in this study because they are less than 1%.
- v. This study is carried out at 100% engine load. The engine speed is varied from 1,200 to 3,000 rpm with an interval of 300 rpm.
- vi. The minimum and maximum EGR rate used in this study range from 5 to 25%.
- vii. The injection timing of the engine is considered at 180° BTDC which simulate the direct injection fuelling strategy.
- viii. The catalyst mass at each engine speeds is determined by using 1D mathematical modelling.
- ix. The mathematical model is developed based on the 1D packed-bed reactor design algorithms and heterogenous kinetic model of auto-thermal reforming.
- x. The porous medium model is used to describe the packed-bed reactor in 2D CFD Modelling.
- xi. Response surface method (RSM) and Central composite design (CCD) are used to optimize the reforming parameters.
- xii. 3D CFD model is used to study the effect of reformed gas on the combustion characteristics.
- xiii. The combustion characteristics considered are in-cylinder pressure, heat release, mass burned fraction.

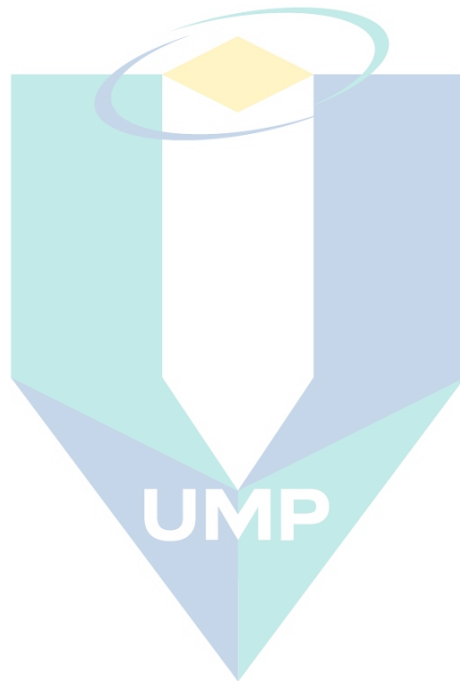
## 1.6 Research Significance

The technique of mixing syngas with natural gas in CNG-DISI engine acquires great attention due to its ability to enhance the engine combustion, performance and harmful emission reduction. Whereas, it still has a difficulty to be integrated into the natural gas vehicles due to the storage system of syngas complexity and the availability of syngas. Therefore, reforming can be used to produce a syngas mixture ( $H_2+CO$ ) in the inline system by using a catalytic reactor. The catalytic reactor provides an onboard hydrogen-rich syngas in a continuous supply which can solve the problem of syngas storage. In many previous studies, the investigations had been conducted to study the availability of the syngas production at various temperature ranges and another controlled parameter. Whereas in this study, the syngas production is investigated depending on the engine behaviour to provide a sufficient amount of syngas ( $H_2+CO$ ). However, the produced amount of syngas is able to make a significant enhancement on the engine combustion and performance and exhaust gas emission reduction. Most of the current studies still in the numerical modelling stage without linkage with the engine operating conditions. Whereas in this study, the engine conditions are taken in consideration, such as the low engine speed at maximum load and their effect on the reforming characteristics. Also, the reforming parameters that mainly affect the reforming characteristics such as the amount of syngas production and methane conversion are optimized. Moreover, the effect of the produced reformed gas on the combustion characteristics is also evaluated.

## 1.7 Thesis Outline

This thesis is arranged in five chapters. The first chapter provides an introduction that includes the research background, problem statement, research questions, objectives, scope, and research significance. Chapter 2 is mainly a review of the literature on the syngas applications, syngas production, syngas production in ICE and the effect of reformate-rich syngas addition on the combustion characteristics of SI engines. Chapter 3 shows the methods that were used to achieve the objectives of this study. It showed the description of the, 1D modelling, optimization, 2D modelling and 3D modelling in details. In chapter 4, the results obtained from the modelling and simulation are presented

and discussed. The reforming characteristics at each engine speed are discussed, and optimization of the amount of natural gas and catalyst mass is presented in graphs, 3D surfaces and contours. The 2D and 3D CFD modelling of the reforming and combustion characteristics are presented and discussed in detail. Finally, chapter 5 is the conclusion and recommendation of the overall study.



اونيورسيتي ملايسيا قهغ

UNIVERSITI MALAYSIA PAHANG

## CHAPTER 2

### LITERATURE REVIEW

#### 2.1 Introduction

This chapter discusses the principles of the reforming process and how it can be used in an internal combustion engine by reviewing the previous researches. Firstly, the syngas background is discussed to show its importance in industrial applications and its characteristics in energy generation. Secondly, since this study aims to explore the ability to produce hydrogen-rich syngas from natural gas combustion by reforming the exhaust gas with a percentage of natural gas, the production technologies are discussed in detail because the same technique is implemented in the current research. Therefore, the most reliable technologies of natural gas reforming are presented, including steam reforming, dry reforming and auto-thermal reforming. Thirdly, the effect of the addition of hydrogen-rich syngas on the combustion characteristics is discussed. Then, the fuel reforming in IC engines are reviewed to show the demands and characteristics of the reforming process. Finally, a discussion is presented on the exhaust gas reforming of natural for an onboard hydrogen-rich syngas production in SI engines powered by natural gas.

#### 2.2 Syngas background

The discovery by the Italian physicist Felice Fontana in 1780 of the fuel gas mixture consisting of hydrogen and carbon monoxide produced by the reaction of steam with hydrocarbons at a temperature of more than 500°C was the first step to know the syngas. This process has become the global standard in the generation of syngas. The synthesis of syngas fuels and chemicals started at the beginning of the 20<sup>th</sup> century. In 1902, the first synthesis of synthetic methane was performed by Sabatier and Sanderens, passing CO and H<sub>2</sub> on Ni, Fe and Co catalysts. (Baxter, et al., 2008a). At the same time, the first commercial hydrogen generated by steam reforming of methane was introduced

to the market. After this achievement, Haber, and Bosch invented ammonia synthesis from  $H_2$  and  $N_2$  in 1910, and the first industrial plants of ammonia synthesis was established in 1913. The methanol synthesis of  $H_2$  and CO catalyzed by ZnO were first reported in 1921. (Baxter, et al., 2008b).

Syngas processing and purification technology have been attracted significant by researchers and industry over the last few years, as its advancement is one of the main efforts to make the use of fossil hydrocarbon resources more efficient, safe and reduce the environmental threats. The reduction in the fossil fuel supply, petroleum, natural gas and coal globally, and the demand of renewable and green energy have become the key reasons for global research into sustainable energy growth. Today, the world's energy supply still relies heavily on fossil fuel combustion for stationary systems, domestic use, and automobiles. Alternative fuels are extremely demanded to fill the gap that will continue to expand. Today, humanity faces three major challenges related to fuel issues (Baxter, et al., 2008a):

- to supply the alternative fuels that can meet the rise of the demands of the fossil fuels,
- to improve energy efficiency using fuels and electricity generation, and
- to minimize the pollutants and manage the greenhouse gas emission by reducing the  $CO_2$ ,  $CH_4$  and  $NO_x$  in the industrial and energy generation sectors.

Emerging syngas processing technologies have opened up more substantial opportunities for syngas use and have enhanced its global economic. Several advanced technologies can be used for syngas generation, involving gasification and reforming. (Antonius Indarto, 2007).

### 2.3 Applications of syngas

In the industrial chemical plants, syngas is utilized as the primary feedstock for the synthesis of different chemical products, such as the methanol or ammonia. Besides, syngas is desired raw material for industrial synthesis, the rise of demand for the usage of renewable synthetic fuels is motivated by a high degree of interest in syngas research and production. Production of syngas is essential due to its momentum by the high need

of hydrogen generation. Syngas conversion to liquid fuels is valuable because syngas can be generated from any hydrocarbons, natural gas, coal, and petroleum resources .

### 2.3.1 Fuel Processing for Fuel cells

The principle of hydrogen and syngas production is used in fuel cell applications, as shown in Figure 2.1. All fuel cells normally work without combustion of fuel. Therefore it is desired for both an energy generation and environmental impacts. When converting fuel into electricity, a fuel cell has higher efficiency than an internal combustion engine (ICE) by tow up to three times. There are five types of fuel cells depend on the use of the electrolyte. They vary in electrolyte composition and operating temperature levels and are at various developmental stages. There are alkaline fuel cells (AFCs), phosphoric acid fuel cells (PAFCs), membrane fuel cell exchange protons (PEMFCs), molten carbonate fuel cells (MCFCs) and solid oxide fuel cells (SOFCs). In all forms, anode and cathode have different reactions, so ions with charge pass through the electrolyte when electrons travel through an external circuit. A more typical characteristic is that the electrodes should be porous, since the gasses must be in contact with the electrode and the electrolyte constantly (Baxter, et al., 2008a).

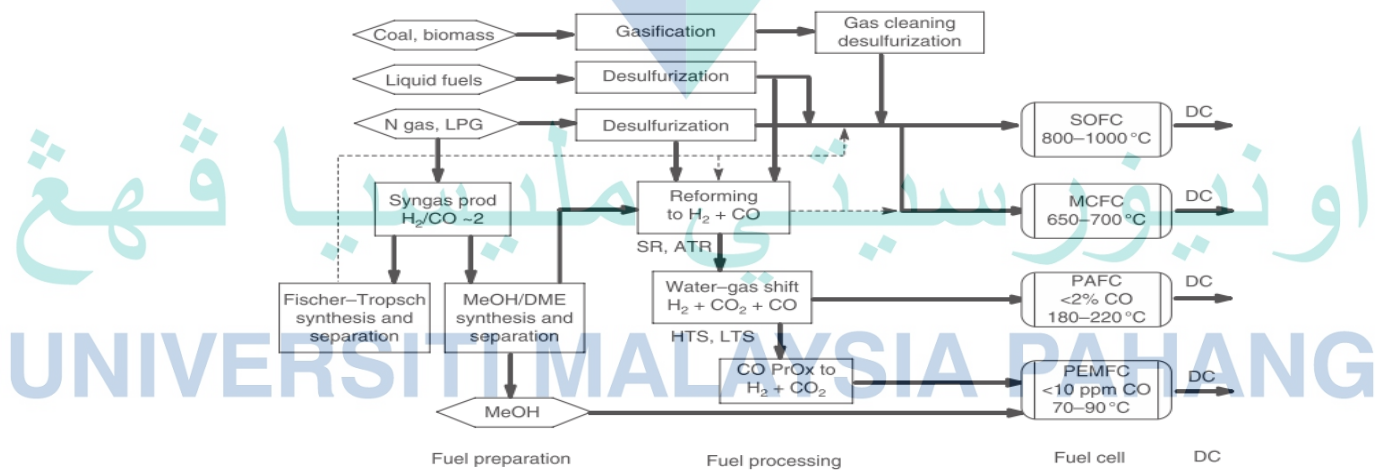


Figure 2.1 Fuel processing of gaseous, liquid, and solid fuels for syngas and hydrogen production for different fuel cells

Source: Baxter, et al., (2008a)

Hydrogen, syngas or reformat (carbon converted hydrogen-rich syngas), and alcohol (methanol or ethanol) are the primary fuels required for today fuel cells applications. Reformed gas can be utilized as a primary fuel for fuel cells at high temperature like SOFC and MCFC to for the fuel's conversion. Hydrogen normally is the main fuel for fuel cells at a low- temperature such as PEMFC and PAFC that can be produced on-site by fuel conversion for stationary applications or in the on-board application in vehicles. In the case of using natural gas or any hydrocarbon fuel in the system of PAFC, the reforming products should be processed by water - gas shift reaction. A PAFC can tolerate about 1% – 2% CO. (Baxter, et al., 2008a; Nathan, et al., 2012).

### **2.3.2 Syngas in IC Engines**

The future of hydrogen and syngas as ICE fuel is considered to be very promising and economical in cost. ICE is more contaminant-tolerant compared with gas turbines. While they are not substantial in number as they are in the IGCC region, ICE does have some research work on the usage of syngas. Most work can be classified into the application of spark-ignition (SI) explicitly in the naturally aspirated carburettor and port form of injection and dual fuel compression ignition (CI) engines. Carbureted and port injection engines mix the fuel and air before the combustion chamber, and the volumetric efficiency of the engine drops at the cost of the voluminous syngas displacing air. In addition, they have higher pumping and heat losses compared to SI direct injection (DI) engines, which results in high fuel consumption. Consequently, syngas-fueled carbureted and port-injection engines' estimated power output is smaller than gasoline and CNG engines. The gasoline in the combustion chamber is mixed with air for DI systems, so there is no limit to the air capacity in the chamber. A syngas-fueled engine with a DI system is predicted to have improved engine performance efficiency in addition to other engine operating parameters (Hagos, et al., 2014b).

#### **2.3.2.1 Syngas as Dual Fuel Injection on CI Engine**

Strict rules on diesel engine emissions restrict the development of the most efficient ICE. The use of syngas in diesel engines is considered a feasible solution for both the pollution and the energy crises. However, syngas has a high self-ignition

temperature (typically above 500°C), and as a result, it cannot be ignited by compression ignition in a diesel engine. One possible way to use syngas in the CI engine is through dual fueling, in which diesel is injected as a pilot fuel to start the ignition while syngas is injected into the induction system. The main motivation for the use of syngas and other gaseous fuels in a diesel engine is to replace diesel as it can reduce costs, minimize emissions (NO<sub>x</sub> and particulate matter), and increase engine performance. There are many kinds of research regarding syngas dual fueling in CI engine (Hagos, et al., 2014b).

Sahoo et al. conducted a study by the second law analysis for CI engine fueled by syngas in a dual fuel configuration, in which diesel was used as pilot fuel. The effect of the H<sub>2</sub>/CO ratio on the engine's dual-fuel efficiency and thermomechanical availability was explored. The synthetic syngas composed of H<sub>2</sub> and CO combined in a gas mixer and charged to the carburettor (Sahoo, et al., 2011). The experiments were performed with a 20 interval at various load levels ranging from 20% to 100%. They stated that the dual fuel syngas had a better quality of function at higher loads compared with diesel fuel. In fact, an improvement in the hydrogen content of syngas has increased the efficiency of dual fueling research. In another study the same researchers explored the effect of the H<sub>2</sub>/CO ratio on a dual-fuel engine output under the same testing conditions. Brake thermal efficiency (BTE), diesel substitution, pressure profile, maximum cylinder pressure, and exhaust gas temperature were the performance parameters examined in the study. Also, the resulting pollutants such as CO, NO<sub>x</sub>, and hydrocarbon (HC) were also investigated. The concentration of syngas H<sub>2</sub> and CO in the percentage range was 50: 50, 75: 25 and 100%. They found a significant increase in H<sub>2</sub> in the syngas contributing to an improvement in the thermal brake efficiency. The highest diesel replacement with syngas and maximum in-cylinder pressure was observed at 80% load with 100% H<sub>2</sub>. On emissions, NO<sub>x</sub> was observed to increase with H<sub>2</sub> content in syngas. As expected, the CO emission in syngas was directly related to the CO content. With 100% H<sub>2</sub> the HC emission was found to be minimum (Sahoo, et al., 2012).

### **2.3.2.2 Syngas in SI Engine Fuelled by Gasoline**

The application of syngas in SI engines was limited to carbureted, and port-injection engines and such fueling systems are now obsolete due to their poor

performance. Several studies indicated that the increase in the CO content advanced the ignition timing of the maximum brake torque (MBT). The overall conclusion of the study was that there is an increase in the combustion duration with an increase in the CO content

Xiaoxu Dai (Dai, et al., 2012) examined the impact of the introduction of syngas on a gasoline engine's combustion and emission efficiency under lean conditions. On-board fuel reformer was used to generate the syngas by recovering the exhaust heat from the engine. The engine was operated at a steady speed which is 1,800 rpm and a 61.5 kPa MAP with two fractions of the syngas volume intake of 0% and 2.5%. The test results demonstrate that the concentration of hydrogen in the syngas decreases as the excess air ratio increases due to the elevated exhaust gas temperature under lean conditions. Both the peak cylinder pressure and indicated thermal efficiency are enhanced with the increase of syngas addition. The indicated thermal efficiency of the engine is improved at an excess air ratio of 1.36 from 38.6 % to 40.0 % after syngas blending. Because hydrogen and carbon monoxide have slightly lower combustion energies and higher flammability than gasoline, both CA<sub>0-10</sub> and CA<sub>10-90</sub> are shortened with the introduction of syngas. Due to the shortened combustion period, the coefficient of variation of indicated mean effective pressure (COV<sub>imep</sub>) decreased after syngas addition. COV<sub>imep</sub> lowers after syngas enrichment from 3.1% to 1.6 % at an excess air ratio of 1.36. Upon the introduction of syngas CO and NO<sub>x</sub> emissions were significantly decreased. The introduction of syngas helps minimize HC emissions when the excess air ratio is less than 1.21. However, as the engine is leaned out further, the introduction of syngas continues to cause increased HC emissions. The impact of the application of syngas on a gasoline engine's combustion and emission efficiency at the lean condition. The engine was run at 1800 rpm constant speed, 61.5 kPa MAP and 1.20 global excess air ratio. The test results demonstrate that, due to the elevated exhaust temperature, the hydrogen content in the syngas decreases with the change of the fraction of the syngas amount. When the syngas volume fraction varies from 0% to 1.84%, indicated thermal efficiency is increased from 35.88% to 39.54%. CA<sub>0-10</sub> and CA<sub>10-90</sub> of a syngas-blended gasoline engine are shortened by about 8.4% and 6.8% compared with those of the original engine, respectively. Moreover, the total number per cubic centimeter sharply

decreased from  $8.77 \times 10^6$  to  $3.21 \times 10^5$  with the syngas addition. HC and NO<sub>x</sub> emissions are reduced after the syngas enrichment at the lean condition.

## **2.4 Syngas Production by Exhaust Gas Reforming of Natural Gas**

Exhaust gas fuel reforming is a catalytic conversion of the hydrocarbon fuels into the hydrogen-rich mixture. Conversion is conducted in a catalytic reactor through various mechanisms, and the well-known ones are, steam reforming, partial oxidation, dry reforming, and oxidative steam reforming. Each reaction is affected by different factors, such as heat, pressure, feed composition and primary fuels. Catalyst and reactor design are also important factors in the exhaust gas reforming performance, and they influence the reforming process. Thus, in this section, all the main factors that can affect the reforming process are considered.

### **2.4.1 Mechanism and Chemical reactions of the exhaust gas fuel reforming**

Exhaust gas reforming process includes steam reforming, dry reforming, and oxidation reactions, as shown in Table 2.1. These reactions are a combination of endothermic and exothermic reactions, and the oxidative reactions are highly endothermic reactions such as partial and complete oxidations. Whereas, steam reforming and dry reforming are highly exothermic reactions that require a high amount of heat to achieve the desired conversion of a hydrocarbon to produce the combustible gases (H<sub>2</sub>/CO). The mechanism principle of this process is dependent on the achievement of the energy recovery from the high heat of the exhaust by endothermic and exothermic catalytic reactions of the primary fuel and fraction of the engine exhaust. Then, the produced hydrogen-rich reformat mixture will be recirculated to the combustion chamber through the intake manifold as shown in Figure 2.2 (Daniel Fennell, et al., 2014; Zhang, Xie, et al., 2017). therefore, it is important to study the behaviour of each reaction in the process separately to understands its path in the exhaust gas reforming process.

Table 2.1 Main reactions of the exhaust gas reforming reaction

Reaction	General chemical formula	Enthalpy
Steam reforming	$C_xH_y + xH_2O \rightarrow xCO + \left(x + \frac{y}{2}\right) H_2$	$\Delta h_R = +1259$
Dry reforming	$C_xH_y + xCO_2 \rightarrow x2CO + \left(\frac{y}{2}\right) H_2$	$\Delta h_R = +1588$
Combustion	$C_xH_y + \left(x + \frac{y}{4}\right) O_2 \rightarrow x2CO_2 + \frac{y}{2} H_2O$	$\Delta h_R = -5116$
Partial oxidation	$C_xH_y + \frac{y}{2} O_2 \rightarrow x2CO_2 + \frac{y}{2} H_2O$	$\Delta h_R = -676$
Water gas shift	$CO + H_2O \leftrightarrow CO_2 + H_2$	$\Delta h_R = -283$

Source: (D. Fennell, et al., 2015)

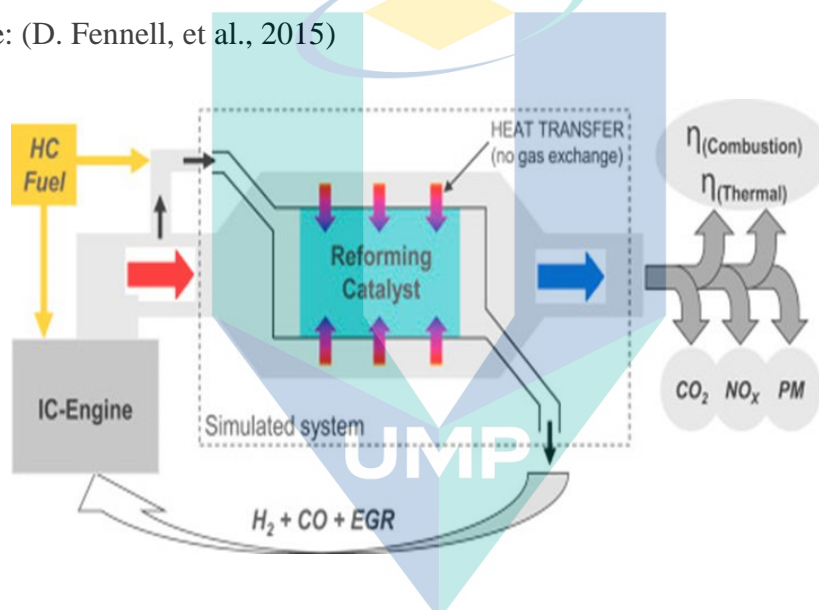
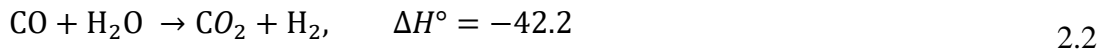
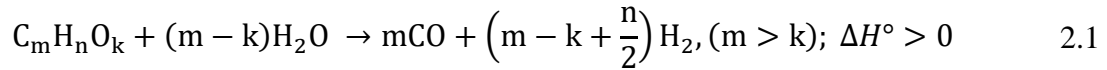


Figure 2.2 Exhaust gas reforming mechanism

Source: Daniel Fennell, et al., (2014)

### 2.4.1.1 Steam Reforming

Steam reforming is the reaction of hydrocarbons with steam, such as methane and steam reaction at elevated temperature to produce the syngas mixture of hydrogen and carbon monoxide, as shown in equation 2.1. Steam reforming reaction prefers water-gas shift reaction, as shown in equation 2.2 as an essential side reaction. WGS reaction rapidly occurs by consuming the fraction of the produced carbon dioxide with the amount of steam at the same time of the main steam reaction. Another reaction that can influence the hydrogen production through steam reforming is decomposition reaction due to the produced methane as shown in equation 2.3 (Baxter, et al., 2008a; Delgado, et al., 2015).



Steam reforming reaction is considered to be reversible in the case of natural gas (methane), but it is almost irreversible in the case of higher hydrocarbons, such as diesel and gasoline. Generally, steam reforming requires an elevated temperature, but in the case of the higher hydrocarbon, the temperature should be higher than the lower one, due to the pre reforming process which requires an additional heat with a range of temperature between 400-500°C, (Fauteux-Lefebvre, et al., 2010; Ilse Önsan, et al., 2011; Subramani, et al., 2009).

Steam reforming of natural gas (methane) is the most efficient way that can produce a high ratio of H<sub>2</sub>/CO, which is favoured in fuel reforming applications. Methane steam reforming is thermodynamically preferred at high elevated temperature, low pressure and high steam to methane ratio in the feed composition (Arman, et al., 2020; Ilse Önsan, et al., 2011). According to thermodynamic analysis, 90% of methane conversion can be achieved at a temperature above 600°C, 1 bar and 3 steam to methane ratio. The methane conversion and hydrogen production decrease with the rise of the reformer pressure, therefore the ambient conditions is the desired for reformer design to reduce the cost of the reformer design (Baxter, et al., 2008a; García, 2015). The catalyst is one of the factors that play an important role in the parameters of the reformer design. A non-noble catalyst like Ni-based is attractive due to the low cost and higher availability compared to the noble catalyst, such as Rh and Pd. Noble catalysts can give higher activity, but their low availability and high cost are the major drawbacks that reduce their utilization in the industrial applications of hydrogen/syngas production. In steam reforming of natural gas, carbon formation is a common issue that always occurs during steam reforming reaction as shown in equation 2.3. This issue mainly depends on the catalyst and the operating condition with S/C (steam to carbon ratio) in the feed stream. Therefore, the S/C ratio should be above the value of the stoichiometric and prefer to be

between 2.5-3 to minimize the coke formation and methane decomposition (Angeli, et al., 2014a; Arman, et al., 2020; Pashchenko, 2019).

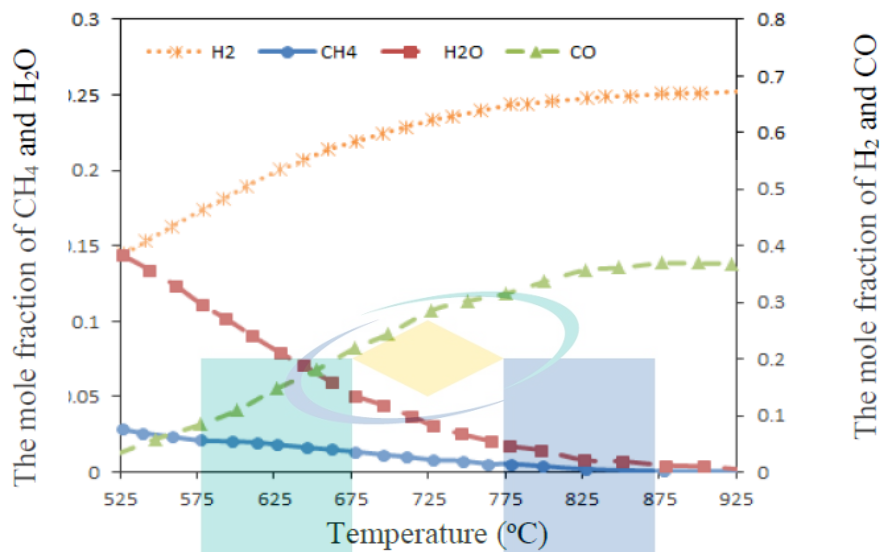
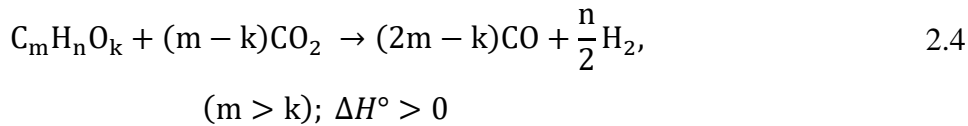


Figure 2.3 Effect of reforming Pressure on the CH<sub>4</sub> & H<sub>2</sub>O Conversion and H<sub>2</sub> & CO yield

Source: Angeli, et al., (2014)

#### 2.4.1.2 Dry Reforming

Dry reforming is a reforming reaction between hydrocarbons and carbon dioxide for hydrogen-rich syngas generation, as shown in equation 2.4. This method is attractive due to its advantage in the carbon dioxide conversion, which is considered as the most abundant factor in the greenhouse's gas emission. At the same time, CO<sub>2</sub> is one of the main exhaust gas composition of hydrocarbon combustion in ICE; therefore, it is important to study its characteristics for a high amount of carbon dioxide conversion into syngas. Dry reforming is an endothermic reaction that requires a high amount of energy for high hydrocarbon conversion, CO<sub>2</sub>, and higher syngas generation. The main disadvantage of this reaction is high carbon formation and deposition, which cause rapid catalyst deactivation. Most of the current catalysts cannot be operated for a long time, which make it difficult for commercialization in the industry (Abdullah, et al., 2017a; Aramouni, et al., 2018a; Usman, et al., 2015; Yabe, et al., 2017).



On the other hand, the equilibrium generation of syngas is influenced by the reverse water gas shift reaction, which occurs simultaneously with the main reaction, as shown in Equation 2.5 . This reaction causes a high conversion of carbon dioxide and some cases higher than the hydrocarbon conversion. This reaction as beneficial for syngas production with ratio (H<sub>2</sub>/CO=1) or below 1. A side reaction of the RWGS reaction is the formation of carbon which is the main factor beyond the rapid deactivation. The carbon formation happened in in tow reaction which is methane decomposition and boudouard reaction as shown in Equation 2.6 (Jang, et al., 2016, 2018).



Dry reforming performance varies by many factors, and it depends mainly on the primary fuels used in the reforming process. Natural gas (methane) is preferred in dry reforming process than the liquid hydrocarbon, such as diesel and gasoline. This is because natural gas dry reforming requires a lower temperature and the catalyst activity is considered better due to the higher number of carbon atoms in the case of the liquid hydrocarbons (D. Fennell, et al., 2015; Golunski, 2010; Tartakovsky, et al., 2018).

Dry reforming of natural gas is an extremely endothermic reversible reaction. Thus, the high temperature is required to achieve the desired conversion into syngas because of the high stability of CH<sub>4</sub> and CO<sub>2</sub> with the high dissociation energy: 435 (CH<sub>3</sub>-H) and 526 (CO-O) respectively. Several researchers suggested that, to reduce the high carbon formation and increase the conversion of CH<sub>4</sub> and CO<sub>2</sub>, a temperature above 850 °C, low pressure and ratio of (CO<sub>2</sub>/ CH<sub>4</sub>=1). The carbon formation is also dependent on the type of catalyst used in the process. The DRM has been investigated over various noble such as Rh/Pt/Ru/Pd-based and Non-noble metal such as Ni/CO-based. Noble based catalyst showed better performance and higher resistance than the non-noble

against the deactivation that caused by the carbon formation and the elevated temperature (Jang, et al., 2018; Kathiraser, et al., 2015; Liao, et al., 2017; Pakhare, et al., 2014; Y. Wang, Yao, Wang, Mao, et al., 2018; Y. Wang, Yao, Wang, Wang, et al., 2018; Yao, et al., 2017).

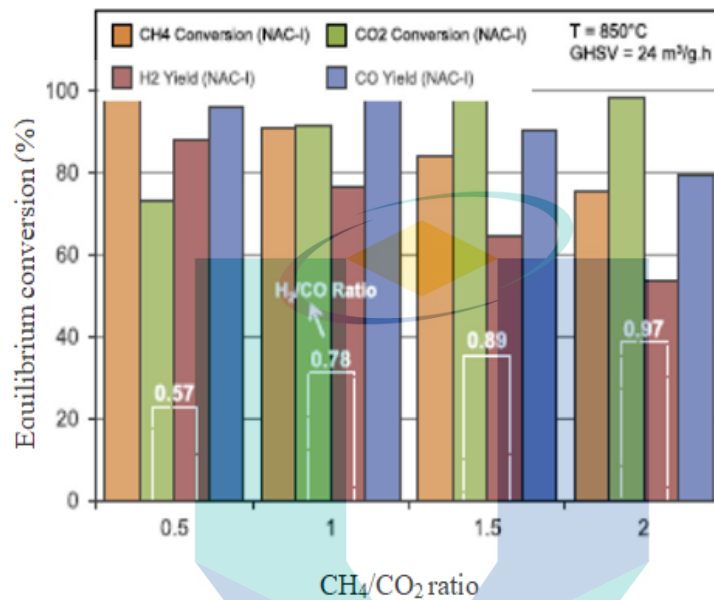
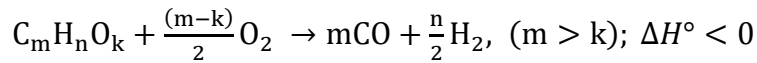


Figure 2.4 CH<sub>4</sub>/CO<sub>2</sub> ratio on conversion of CH<sub>4</sub> and CO<sub>2</sub> and yield of CO and H<sub>2</sub> at 850 °C and 1atm

Source: Abdullah, et al., (2017)

### 2.4.1.3 Partial Oxidation

Partial oxidation is a reaction between hydrocarbons and oxygen in the presence of a catalyst to produce hydrogen and carbon monoxide, as shown in Equation 2.7. The ideal conditions of the POX reaction for high consumption of hydrocarbons and oxygen at a temperature between 700-1000 K. This process is industrially used, and Shell has adapted the POX process for their Pearl GTL plant in Qatar, which is the largest in the world at a capacity of 140,000 Barrels per day of GTL production. The reaction occurs in a very short time once contact the precious metals in the reactor used in the process. This reaction can produce syngas with a ratio of H<sub>2</sub>: CO between 1 and 2 depending on the type of hydrocarbon used in this reaction (Baxter, et al., 2008a, 2008b; Keiski, et al., 2011; Ma, et al., 2019; Trimm, et al., 2011).



2.7

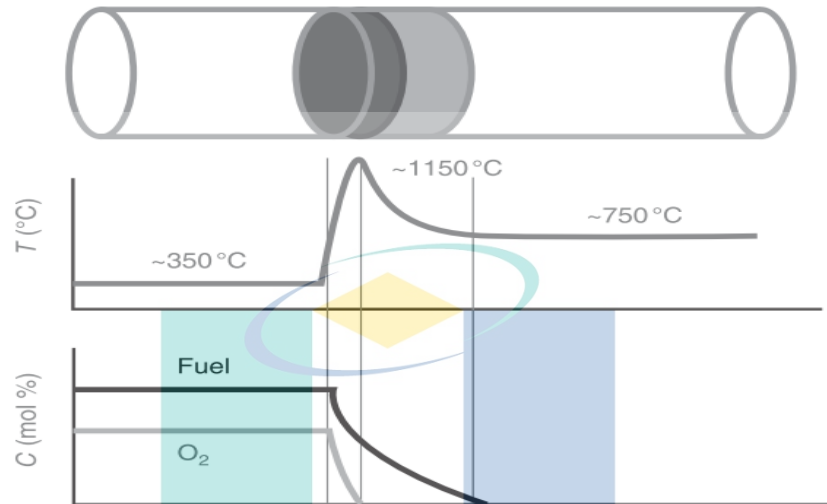


Figure 2.5 Typical temperature profile of a CPO reactor with concentration profiles of fuel and  $O_2$  along a COX catalyst bed

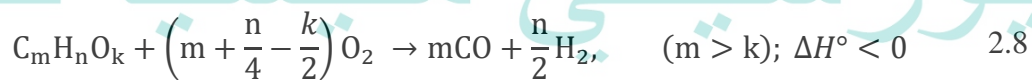
Source: Baxter, et al., (2008)

Natural gas ( $CH_4$ ) partial oxidation can produce syngas with a molar  $H_2/CO$  ratio of 2 with no need of steam in the feed composition. This advantage eases the reformer design because the complex system of steam management will not be required. The reaction of POX enhances the exhaust gas reforming process, due to the high heat release from the reaction which increase the reaction temperature. Therefore, the rate of the steam reforming rate will be higher resulting in higher hydrogen production. However, POX reaction has its own conditions, such as the very short contact, high temperature, molar C/O ratio around 1 and catalyst with extreme resistance against the high temperature release. The reformer construction materials should also have high thermal resistance to be capable of withstanding under the high temperature avoid any negative impact that may occur during the reforming process. Rh-based catalyst shows the highest activity among all the catalyst types in partial oxidation reactions. The use of the other catalyst showed poor activity and selectivity performance (Pt, Ir), deactivation as a result of aluminate formation (Ni, Co), coking (Pd), and difficulty in sustaining autothermal operation (Re, Ru, Fe). The geometric form of the catalyst support plays an important

role in the production of hydrogen by affecting the mass and heat transport. (Alvarez-Galvan, et al., 2019; Christian Enger, et al., 2008; Guo, et al., 2019; Schneider, et al., 2006; Smith, et al., 2011).

#### 2.4.1.4 Oxidative steam reforming OSR (Autothermal reforming)

Methane oxidative steam reforming is sequential in nature and begins with exothermic oxidation that releases the heat required to support endothermic steam reforming reactions. Nonetheless, the start of oxidation does not take place under environmental conditions, except for fuels such as methanol and hydrogen, which requires some energy. This process of the OSR is called "light-off" and is defined by the light-off temperature corresponding to the fuel conversion of 10% total oxidation (TOX) and is a function of the fuel form, C /O ratio and catalyst form. Methane is the most difficult alkane compared to ethane and propane and has the lowest light-off temperature. For all fuels, Pt delivers higher activity than Ni results in lower light-off temperatures. When the catalyst bed and reactants are heated, the oxidation is accelerated which leads to higher temperature dictated by the C/O ratio at the inlet. As the feed stream in OSR is lean in oxygen, its total conversion prevents oxidation and the remaining fuel is reformed by steam to hydrogen at high temperatures. Steam reforming then starts to show a significant effect on hydrogen generation, and the temperature declines at the downstream of the reactor and become constant. The composition products at the outlet is normally is characterized due to the thermodynamic of the steam reforming and water gas shift reaction (Ilsen Önsan, et al., 2011; Jiménez-González, et al., 2016).

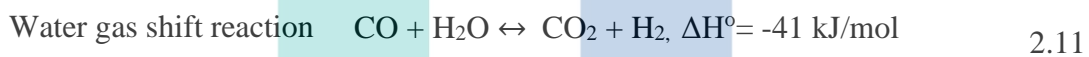


#### 2.5 Reaction Scheme and Kinetic of Exhaust Gas Reforming of Natural Gas

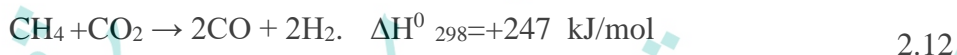
The conversion and utilization of methane-based on reforming processes for Hydrogen-rich syngas production by obtaining the desired H<sub>2</sub>/CO ratio. This process used in industrial applications, such as the utilization of the flue gas from power plants or the exhaust from an internal combustion engine to use its products support of the primary

fuel. Tri-reforming is a combination of steam reforming, dry reforming, partial and complete oxidation of methane (Dwivedi, et al., 2017; Gaber, et al., 2019)

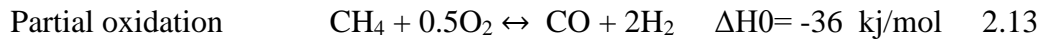
Steam reforming is considered as the most effective process for syngas production with a high amount of hydrogen in the syngas mixture. As mentioned in previous section, this process is a highly endothermic process, and it requires a high amount of energy to drive the related chemical reaction. The chemical reactions occurring during the steam reforming process are as following:



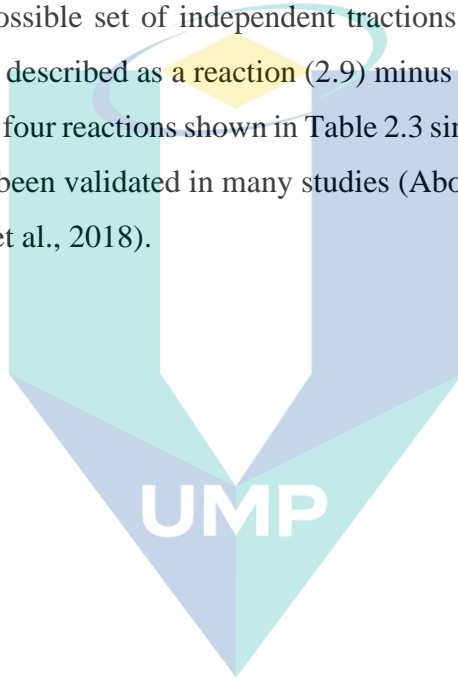
Dry reforming is the process that uses carbon dioxide as a reforming agent, as shown in Equation 2.12. Therefore, this reaction is attractive to understand its behaviour due to  $\text{CO}_2$  consumption. This process involves several disadvantages, such as the need of the high amount of energy, the fast catalyst deactivation and the low ratio of  $\text{H}_2/\text{CO}$  compared to steam reforming process. However, this disadvantage can be overcome by using auto-thermal reforming (Tartakovsky, et al., 2018).



The presence of oxygen in the reforming mixture has the advantage to overcome the demand of the high endothermic reactions due to the heat release from the partial oxidation and complete combustion reactions as shown in equations 2.11 and 2.12. Therefore, there is no need for external energy. The presence of  $\text{O}_2$  and  $\text{H}_2\text{O}$  in the reforming mixture also has advantages to contribute in the reduction of the coke formation on the catalyst which will result in the improvement of the catalyst stability (Dwivedi, et al., 2017; Gaber, et al., 2019).



As mentioned above, exhaust gas reforming process is a combination of steam reforming, water gas shift reaction dry reforming, partial and complete oxidation as shown in Table 2.1. In this process, four reactions shown in Table 2.3 are used to describe the auto-thermal exhaust gas reactions. Reactions (equation 2.9), (equation 2.10) and equation 2.12 are a possible set of independent reactions. For instance, DRM reaction (equation 2.12) can be described as a reaction (2.9) minus reaction (2.11). However, it is an advantage to use all four reactions shown in Table 2.3 since the kinetic rate expressions of these reactions has been validated in many studies (Aboosadi, et al., 2011; Fekri Lari, et al., 2019; Sadeghi, et al., 2018).



اونيورسيتي ملايسيا قهغ

UNIVERSITI MALAYSIA PAHANG

Table 2.2 The kinetic rate equations based on the mentioned models for the tri-reforming process

No	Detailed reaction	Reaction formula	Rate equation
1	Steam reforming <sup>1</sup>	$\text{CH}_4 + \text{H}_2\text{O} \leftrightarrow \text{CO} + 3\text{H}_2$	$R_1 = \frac{k_1}{P_{\text{H}_2}^{2.5}} \left( P_{\text{CH}_4} P_{\text{H}_2\text{O}} - \frac{P_{\text{H}_2}^3 P_{\text{CO}}}{K_I} \right) X \frac{1}{\phi^2}$
2	Steam reforming <sup>2</sup>	$\text{CH}_4 + 2\text{H}_2\text{O} \leftrightarrow \text{CO}_2 + 4\text{H}_2$	$R_2 = \frac{k_2}{P_{\text{H}_2}^{3.5}} \left( P_{\text{CH}_4} P_{\text{H}_2\text{O}}^2 - \frac{P_{\text{H}_2}^4 P_{\text{CO}_2}}{K_{II}} \right) X \frac{1}{\phi^2}$
3	Complete oxidation	$\text{CH}_4 + 2\text{O}_2 \leftrightarrow \text{CO}_2 + 2\text{H}_2\text{O}$	$R_3 = \frac{k_3}{P_{\text{H}_2}} \left( P_{\text{CO}} P_{\text{H}_2\text{O}} - \frac{P_{\text{H}_2} P_{\text{CO}_2}}{K_{III}} \right) X \frac{1}{\phi^2}$
4	Water gas shift reaction	$\text{CO} + \text{H}_2\text{O} \leftrightarrow \text{CO}_2 + \text{H}_2$	$R_4 = \frac{k_{4a} P_{\text{CH}_4} P_{\text{O}_2}}{(1 + K^C_{\text{CH}_4} P_{\text{CH}_4} + K^C_{\text{O}_2} P_{\text{O}_2})^2} + \frac{k_{4b} P_{\text{CH}_4} P_{\text{O}_2}}{(1 + K^C_{\text{CH}_4} P_{\text{CH}_4} + K^C_{\text{O}_2} P_{\text{O}_2})}$

$$\phi = 1 + K_{\text{CO}} P_{\text{CO}} + K_{\text{H}_2} P_{\text{H}_2} + K_{\text{CH}_4} P_{\text{CH}_4} + K_{\text{H}_2\text{O}} \frac{P_{\text{H}_2\text{O}}}{P_{\text{H}_2}}$$

Source: Aboosadi, et al., (2011); Fekri Lari, et al., (2019); Sadeghi, et al., (2018)

The kinetic model used in equations (1), (2), and (4) in Table 2.2 is a famous model developed by Xu and Forment over Ni-based catalyst, and this model can be adjusted to be used for the demanded catalyst. This model has been extensively tested under lab-scale conditions. The kinetic model of Trimm and Lam is considered as a rigorous study for methane combustion (reaction (3) in table 2.3 (Trimm, et al., 1980). However, since it was derived over supported Pt-based catalyst, the model adsorption parameters are adjusted any catalyst.

However, this kinetic model is intensively used by researchers to describe the reforming process mathematically. The consumption and generation of the species are expressed by using the rate expression of the auto-thermal reactions occurring in Tri-reforming, such as the exhaust gas fuel reforming.

Sadeghi et al. (Sadeghi, et al., 2018) performed one-dimensional homogenous modelling by using the chemical kinetic shown in Table 2.3 for methane tri-reforming process in a fixed bed reactor. This study was conducted to determine the demanded volume of the reactor that can be used for hydrogen-rich syngas production with desired H<sub>2</sub>/CO ratio. The mathematical modeling was validated with an experimental study, and it showed great consistency between the modeling results and experiments data. It was noticed that, as the concentration of CO<sub>2</sub> increased in the feeding mixture caused a reduction in the amount of H<sub>2</sub> in the reforming products. This reduction is due to the low value of energy efficiency compared to the required energy to consume the CO<sub>2</sub> in through the dry reforming reaction. It was also found that, as the amount of the steam concentration is higher in the feeding mixture, more hydrogen is produced due to the exergy efficiency enhancement. It was observed that the combustion of methane (reaction 3) led to higher reaction temperature along the reactor and higher H<sub>2</sub> and CO concentration in the reforming product.

Fekri (Fekri Lari, et al., 2019) conducted a study using the kinetic model in Table 2.2 to investigate the effect of the conventional reactor modification on the idea production of syngas to be used in methanol and Fischer–Tropsch synthesis units. The tri-reforming reactor was divided into three equal beds in series, and steam, carbon dioxide, and oxygen were distributed between beds. The results of the mathematical modeling were validated with experimental data, and the relative error was lower than 5% in all the cases. It was proven that the single fixed bed reactor was the most effective model for hydrogen production and the amount of hydrogen produced was higher than conventional and multi-bed by 2.93%, and the ratio of H<sub>2</sub>/CO was lower by 0.38.

Fekri (Fekri Lari, et al., 2019) performed a simulation study of catalytic conversion of flue gas to methanol by using the tri-reforming of methane. This simulation was conducted by the chemical kinetic models in the Table 2.2 and the, and it showed a

great accuracy between the experimental data and simulation results with relative error less than 5% in all the cases. In this study, two types of fixed bed reactor were used, which are single and multi-bed reactor. This study focused on the possibility of CO<sub>2</sub>. It was found that the conversion of CO<sub>2</sub> in the case of the multi-bed was higher than the single bed by 5%. Typically, the auto thermal condition, high CO<sub>2</sub> conversion, flexibility and production of high-quality syngas were the main advantages of the multi-bed tri-reformer against the single-bed reactor. The methane conversion in the single-bed and multi-bed tri-reformers was 84.62% and 99.91%, respectively. In addition, the higher CO<sub>2</sub> conversion to methanol in the methanol synthesis reactor was one of the main benefits of modified configuration compared to the conventional process.

## 2.6 Catalyst

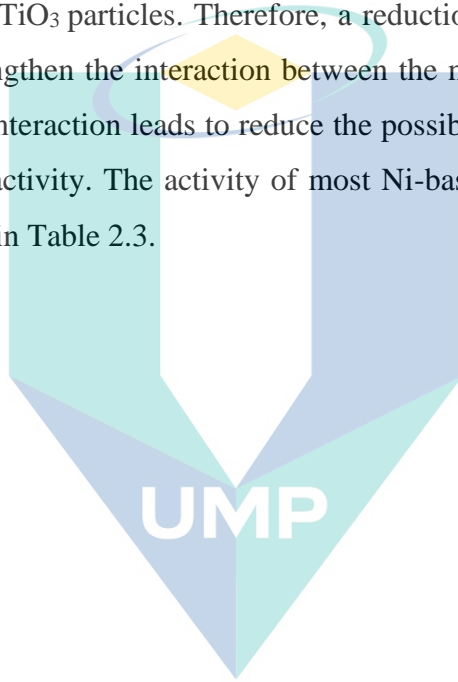
Catalysts are normally used to increase the reaction speed. In the reforming process, the catalyst plays an essential role in the reforming performance by affecting the reforming products and reaction path.

### 2.6.1 Catalyst Performance in Reforming Process

One of the main obstacles of the utilization of the exhaust gas fuel reforming process in industrial applications is the low effectiveness of the catalysts. Thus, due to the rapid deactivation of the catalyst used in the DRM process because of the high carbon deposition. Many attempts and huge investigations have been made to develop a new catalyst can achieve high activation of CH<sub>4</sub> and CO<sub>2</sub> at low temperature. Ni-based is the most common type of catalyst used in the DRM process due to its availability and reasonable cost. They showed acceptable activity, but they deactivated rapidly due to the high carbon formation during the reaction. Novel metals (Rh, Pd, Ru, Pt and Ir) have the highest activity for DRM process is resisting to the formation of carbon, but they are not used significantly due to their cost ineffectiveness (Richardson, et al., 2003).

Current studies attempt to perform a mechanistic investigation on the interaction between nickel and different supports. To modify the interaction of the Ni and their supports, carrier of composites was used to achieve higher activity at a lower temperature. Li et al. (Li, et al., 2012) arranged a catalyst series from Ni/BaTiO<sub>3</sub>-AL<sub>2</sub>O<sub>3</sub> with various

contents of  $\text{BaTiO}_3$  for DRM at low temperature. It was found that the  $\text{Ni}/32.4 \text{ BaTiO}_3\text{-AL}_2\text{O}_3$  had the highest activity and it was stable during 50 h on the reactants stream. It was considered that  $\text{BaTiO}_3$  enhanced the dispersion of the active nickel and species of  $\text{NiO}_x$  with the intensity of electronic donor and then improved the catalyst stability. The equilibrium conversion of  $\text{CH}_4$  on the following catalyst support  $\text{Ni}/32.4 \text{ BaTiO}_3\text{-AL}_2\text{O}_3$ ,  $\text{Ni}/\text{BaTiO}_3$  and  $\text{Ni}/\text{AL}_2\text{O}_3$  was 88%, 80% and 86% respectively. The enhancement of catalyst was due to the addition of  $\text{BaTiO}_3$  to  $\text{AL}_2\text{O}_3$  as a result of intermittent dispersion of the particles of  $\text{BaTiO}_3$  on the surface of  $\text{AL}_2\text{O}_3$ . The dispersion of  $\text{BaTiO}_3$  formed individual isolated  $\text{BaTiO}_3$  particles. Therefore, a reduction in the  $\text{Ni-AL}_2\text{O}_4$  formation and that helps to strengthen the interaction between the nickel-based and the supports. The enhancement of interaction leads to reduce the possibility of carbon deposition and improve the catalyst activity. The activity of most Ni-based catalysts for DRM at low temperature is shown in Table 2.3.



اونيورسيتي مليسيا قهغ

UNIVERSITI MALAYSIA PAHANG

Table 2.3 Properties of different catalyst at various temperature

Catalyst	Ni loading g %	Reaction conditions		Conversion %		H <sub>2</sub> /CO ratio	Ref
		Temperature °C	Feed ratio CH <sub>4</sub> /CO <sub>2</sub> / N	CH <sub>4</sub>	CO <sub>2</sub>		
Ni/AL <sub>2</sub> O <sub>3</sub> -CeO <sub>2</sub>	10	550	1:1:0	50	55	0.64	(Aghamohammadi, et al., 2017)
ZrO <sub>x</sub> /Ni-MnO <sub>x</sub> / SiO <sub>2</sub>	10	500	1:1:0	17.9	23.6	0.64	(Yao, et al., 2017)
NiSc/AL <sub>2</sub> O <sub>3</sub>	11	450	1:1:0	10	12	-	(Zhao, et al., 2017)
Ni-Zr/SiO <sub>2</sub>	10	450	1:1:0	6.5	9.1	0.61	(Yao, et al., 2016)
1.2%Ni/TiO	1.2	450	1:1:1.8	3.2	5.9	-	(Yao, et al., 2017)
Ni-Zr/SiO <sub>2</sub>	10	400	1:1:0	2.2	4.9	0.56	(Yao, et al., 2017)
1%Ni/10%La-ZrO <sub>2</sub>	10	150	1:1:2	74.5	85.3	0.83	(Yabe, et al., 2017)

## 2.6.2 Catalyst in Exhaust Gas Reforming

Catalyst selection plays a significant role in the activity and product selectivity of chemical reactions. Many metals have shown to be active for methane reforming such as Nickel (Ni), Cobalt (Co), Rhodium (Rh), Platinum (Pt), Palladium (Pd), and Ruthenium (Ru). In this section is primarily focused on Ni and Rh as reforming catalysts due to the ubiquity with which they appear in the literature.

The most common catalyst used for SMR in industrial processes is Ni (Abdullah, et al., 2017a). Ni is an attractive catalyst for large-scale processes because it has a high activity for steam reforming reactions and is relatively cheap compared to other reforming catalysts. There have been a large number of studies performed on Ni as a steam reforming catalyst. A well-known disadvantage of using Ni as a catalyst is the propensity for solid carbon (coke) to form and deactivate the catalyst (Yabe, et al., 2017). For this reason, industrial reformers typically add extra H<sub>2</sub>O into the reactor feed, which inhibits carbon formation on the catalyst surface. Typical S/C ratios are anywhere between 2 and 5 for industrial applications. While this helps to preserve the life of the catalyst, requires a non-trivial amount of additional energy to vaporize and heat the extra steam.

Rhodium is a promising catalyst for SMR due to very high catalyst activity and natural resistance to coke formation (Long, et al., 2018; Schmal, et al., 2018; Zhang, Jia, et al., 2017). Even though Rh is a more attractive option than Ni in many ways, the high cost prevents it from being used in the majority of industrial processes.

Nickel has been shown to be an active catalyst for oxidation reactions. However, as is the case for SMR, coke formation is a severe issue for nickel-based catalysts. Additional O<sub>2</sub> can be added to inhibit coke formation, although that shifts the products away from the desired composition. Rhodium has also been studied for CPOX applications with promising results. Rh is one of the most studied catalysts for partial oxidation applications (Zhang, Jia, et al., 2017). It is thought that Rh has a higher selectivity to hydrogen than other common CPOX catalysts such as Pt, Pd and Ni (Aramouni, et al., 2018b).

A study by G. Ji et al. (2018). suggested that Rh is the most effective catalyst for ATR reforming (Ji, et al., 2018). The study compared Pd, Pt, and Rh for ATR in a fixed bed reactor. Thermal analysis showed that the Rh catalyst inhibited hot-spot formation compared to Pd and Pt, which leads to higher methane conversion and more stable catalyst life. It is thought that the combustion and reforming zones overlap in the Rh catalyst, resulting in a lower catalyst temperature (Choi, et al., 2017a; Zhang, Jia, et al., 2017).

However, in this study, Rhodium is chosen for its high activity in the steam methane reforming reaction, as well as a natural resistance to coke formation. Ceria is used as a catalyst promoter, which has been shown to help prevent carbon buildup and sintering, improve active metal dispersion and increase catalyst activity. Alumina is chosen due to its high porosity as catalytic support (Zhang, et al., 2018, 2020; Zhang, Xie, et al., 2017).

## **2.7 Design of Exhaust Gas Fuel Reformer**

Correct design of a fuel reformer is critical for achieving maximal primary fuel conversion, the desired composition of the reforming products, efficient utilization of the exhaust gas energy, low backpressure, and negligible coke formation together with compact design and acceptable cost. We review the advantages and shortcomings of popular catalytic reactors like fixed beds, monoliths, and fibre-packed beds (Ilsen Önsan, et al., 2011).

The majority of the fuel reformer designs are based on fixed-bed reactors which is considered to be built and operated. Since fixed-bed reactors have lower vibration resistance undergo the mechanical attrition with the time compared to monoliths. One of the disadvantages of the fixed-bed reactors is the pressure drop, but it can be neglected in the lab-scale design. Fixed- bed reactor has advantages over the monolith reactor in the case of the laminar flow. Monolith reactor is more preferable than the fixed-bed reactor in the term of heat transfer. Because, the heat is transferred to the wall of the Monolith reactor, which is coated by a catalyst and lead to increase the catalyst temperature that will result to higher consumption and formation rate of the reactants. But, with the time the coke formation in the monolith reactor is higher than the fixed-bed

reactor, which caused to faster catalyst deactivation. Therefore, the fixed-bed reactor is more favoured for the longer period use syngas (Ilsen Önsan, et al., 2011; Tartakovsky, et al., 2018).

Many studies suggested that shell and tube design is the ideal design. Thus, due to the higher heat transfer between the reaction zone (tube) and the shell. This heat transfer contributes to higher fuel and exhaust conversion to hydrogen-rich syngas (Ilsen Önsan, et al., 2011; Tartakovsky, et al., 2018).

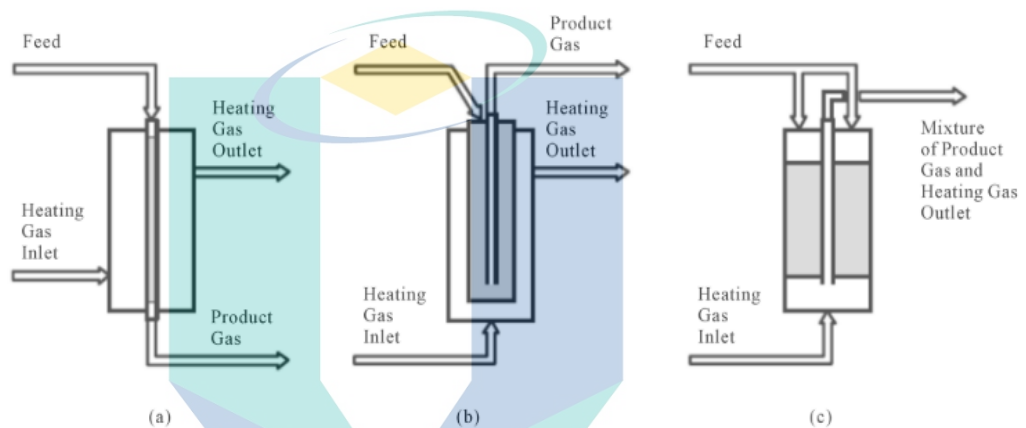


Figure 2.6 Different kinds of heat exchange reformers

Source: Ghoneim, et al.,(2016)

## 2.8 Exhaust Gas Reforming F Natural Gas in an Internal Combustion Engine (Si Engine)

### 2.8.1 Overall Performance

Reforming process of exhaust gas recirculated (EGR) and natural gas is a promising technology to enhance the combustion stability and performance of the natural gas engine and thereby lowering the combustion born emissions. Exhaust gas reforming is conducted in a catalytic reactor which acts as a space for the reaction between the exhaust gas composition and natural gas.

Exhaust gas mainly is composed of steam, CO<sub>2</sub>, O<sub>2</sub>, N<sub>2</sub> and a trace amount of CO and some unburned hydrocarbons (Long, et al., 2018; Zhang, et al., 2020; Zhang, Jia, et al., 2017). With CNG as a fuel, the content of unburned hydrocarbon is negligible. The

exhaust gas reforming trends include steam reforming, dry reforming, and oxidation reforming, as shown in Table 2.4. Exhaust gas reforming is a combination of endothermic and exothermic reactions; the oxidative reactions are a highly exothermic reaction that occurs in a short time; however, they can start up at low temperature. Whereas, steam and dry reforming are endothermic reaction and reaction that needs a high amount of heat to achieve the desired conversion of methane and carbon dioxide delivering a higher amount of the hydrogen combustion in the produced syngas (Zhang, et al., 2018).

Table 2.4 Main reaction in the reforming process of methane

No	Detailed reaction	Reaction formula	$\Delta H^\circ$ kJ/mol
1	Steam reforming <sup>1</sup>	$\text{CH}_4 + \text{H}_2\text{O} \leftrightarrow \text{CO} + 3\text{H}_2$	+206
2	Steam reforming <sup>2</sup>	$\text{CH}_4 + 2\text{H}_2\text{O} \leftrightarrow \text{CO} + 4\text{H}_2$	+165
3	Partial Oxidation	$\text{CH}_4 + 0.5\text{O}_2 \leftrightarrow \text{CO} + 2\text{H}_2$	- 36
4	Complete oxidation	$\text{CH}_4 + 2\text{O}_2 \leftrightarrow \text{CO}_2 + 2\text{H}_2\text{O}$	-802.7
5	Carbon dioxide reforming (DRM)	$\text{CH}_4 + \text{CO}_2 \leftrightarrow 2\text{CO} + 2\text{H}_2$	+247
6	Water-gas shift reaction	$\text{CO} + \text{H}_2\text{O} \leftrightarrow \text{CO}_2 + \text{H}_2$	-41

Source: Halabi, et al., 2008; Zhang, Jia, et al., (2017)

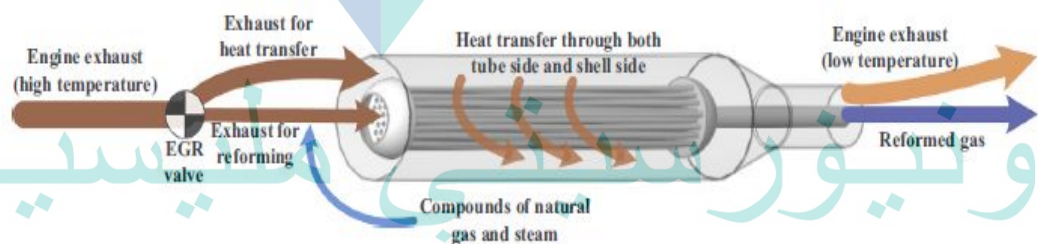


Figure 2.7 Principle of the exhaust reforming process

Source: Zhang, Jia, et al., (2017)

Exhaust gas reforming of natural gas in the catalytic reactor has been simulated by a few researchers using the reaction model of Langmuir-Hinshelwood-Hougen-Watson (LHHW). Bulutoglu has performed a numerical study of exhaust reforming of natural gas in microchannel reactor at different feed molar ratio and temperature in the presence of Rh/Al<sub>2</sub>O<sub>3</sub> as a catalyst. This study has shown that, as the feed temperature and the

amount of steam in the feed increased, the rate of  $H_2$  production is enhanced. It was also found that; the conversion of methane is more preferable at higher  $O_2/C$  ratio due to the higher temperature produced from the complete and partial oxidation reactions (Bulutoglu, et al., 2015).

Zhang, Jia, et al. have conducted a numerical study of the characteristics of exhaust gas reforming on the production rate of hydrogen in LNG marine engine. In their study, it was noticed that the oxidative reaction occurs before the first half of the tube. Moreover, methane is mostly converted by steam reforming, which leads to higher syngas ratio ( $H_2:CO$ ). Therefore, the reforming process is more preferable to achieve higher performance (Zhang, Jia, et al., 2017).

Another simulation study was performed by (Zhang, et al., 2018) by using a porous medium to describe the mechanism of exhaust gas reforming in a catalytic fixed bed reactor. It was observed that methane oxidation spent a short time at the beginning of the reaction before the middle of the tube. Oxidation reaction has increased the reaction temperature, which leads to higher consumption and conversion of methane through the reaction of the steam reforming. In this reaction, the dry reforming rarely occurs due to the low concentration of the  $CO_2$  in the feed composition.

Zhang (Zhang, et al., 2020). performed a 3D CFD simulation of porous medium model with the detailed mechanism of surface catalytic reaction to describe the exhaust gas reforming of natural gas in a tubular type fixed-bed catalytic reactor. It was found that the exhaust gas that surrounds the reaction tube affected the reforming characteristics in the reaction zone because it provides a preheating which contribute to the rise of the mixture heat. This preheating is beneficial to enhance the reforming performance. It was also observed that, in the entry of the reaction zone, the oxidation reaction releases a heat that benefits the consumption and generation rate of species. Therefore, the Hydrogen is mainly produced from the partial oxidation reaction and the steam reforming reaction. It was noticed that the rise of the EGR ratio led to higher hydrogen production regardless of the excess air coefficients. The simulation results also showed that with all other parameters fixed, there is an optimum amount of steam addition to achieving the maximum hydrogen production, which occurs when  $W/M$  is about 1.25 .

### 2.8.2 Rate of exhaust gas recirculation

The EGR valve shown in Figure 2.7 is important to control the amount of the exhaust gas that will be recirculated and reformed in the catalytic fixed bed reactor. In this study, the maximum EGR rate used is 25%. However, higher EGR levels increase cycle-to-cycle variability and decrease the level of improvement in fuel consumption. High-level homogeneous EGR causes reduction of burning speed, increase of cycle to cycle variation, and even misfire so that the steady-state combustion is difficult to achieve (Fontana, et al., 2010). As reported in the research of (Long, et al., 2018), the engine can only get the smooth operation up to 25% EGR, and the coefficient of variation in IMEP is beyond the acceptable limit (5%) at high EGR rate. Similar results were also obtained from research (Bogarra, et al., 2017; Choi, et al., 2017b). The most significant factor is the substantial decrease in the flame speed that occurs with EGR, as reported by (Tartakovsky, et al., 2018). The reduction of mixture flame speed results in significantly increased combustion initiation periods and burn durations. In the literature review by (Golunski, 2010; Lu, et al., 2016), it is shown that flame speed effects on combustion stability are related to the early flame kernel development. Fuels with high flame speed complete the early flame kernel development process faster, making them less susceptible to the stochastic cycle-to-cycle differences in turbulence, and ultimately providing more stable combustion. Also, the technical challenges of EGR dilution limit need an investigation to get more benefits from high levels of EGR.

### 2.9 Effect of Hydrogen-Rich Syngas on Combustion Characteristics, Performance, and Emission of SI Engine Fuelled by Natural Gas

The employment of natural gas to substitute the feasible fuels in an internal combustion engine has become an attractive method throughout the world. The acceptance of natural gas to replace the fossil fuel in diesel and gasoline engine due to its great environmental, availability, economic advantages. Natural gas utilization in internal combustion engines faces various like difficulties ignitability of methane and low flame speed. The lower efficiency of natural gas is due to its natural combustion properties. Therefore, to enhance natural gas properties, it is needed to be mixed with another gas which can increase the lower thermal properties of natural gas (Alrazen, et al., 2018).

However, mixing hydrogen with natural gas started to receive major interest in recent years. According to many previous studies, adding hydrogen natural showed great enhancement of internal combustion engines due to the thermal properties of hydrogen. Since, hydrogen has higher burning velocity, lower ignition energy and satisfied lean-burn capability, the combustion was more efficient, and the emission was lower (Alrazen, et al., 2018).

Since, the unsafe storage of hydrogen and the unavailable infrastructure of hydrogen, the recent studies started to examine the syngas mixture ( $H_2:CO$ ). The use of syngas in the internal gas engine fueled by natural gas is performed through a dual fueling system because it cannot be used as standalone fuel to replace the primary fuels.

Hagos et al. performed an experimental investigation to evaluate the effect of syngas utilization in a DISI engine as a potential alternative for fossil fuels. The experimental study aimed to test the influence of syngas addition on the combustion, performance and emissions characteristics of syngas in DISI engines, compared to baseline data for CNG. Syngas was shown to have a higher peak cylinder pressure, higher heat release rate and faster combustion duration than CNG at all operating speeds and loads. This was attributed to the fast flame propagation of the hydrogen species in the syngas fuel. The ignition advance for the MBT of syngas was observed to become delayed near TDC. The  $COV_{IMEP}$  of syngas was also smaller than that of CNG at all operation loads and speeds. The BTE of the syngas was reported to be lower than that of CNG, especially at lower engine loads. With increasing speed, the difference was decreased. Similarly, the BSFC of syngas was higher than that of CNG. This was mainly attributed to the low calorific value nature of syngas. Reduced CO emissions were observed at higher loads, whereas they were increased at lower loads compared to CNG at all engine speeds. The NO<sub>x</sub> emission was higher than that of CNG at all load and speed conditions. The THC emission was also improved significantly with syngas at all engine loads and speeds. Therefore, this fuel proves to be a good substitute for gaseous fossil fuels in DISI engines without requiring major alterations to the engine (Hagos, et al., 2014a).

He et al. experimentally evaluated the effect of effects of H<sub>2</sub> and CO enrichment on the combustion, emission and performance characteristics of spark ignition natural gas engine. It was found that Both H<sub>2</sub> and CO increase the peak of cylinder pressure and heat release rate and advance their phases. In addition, when H<sub>2</sub> or CO is inducted, heat release traces get more centralized. With the increase of H<sub>2</sub> content in H<sub>2</sub>-CO blends, both the peaks of in-cylinder pressure and heat release rate increase. Also, the addition of H<sub>2</sub> and CO shortens flame development duration and rapid combustion duration. Besides, H<sub>2</sub> and CO also lower COV<sub>IMEP</sub> of the engine, indicating a smoother engine operation. In compare, H<sub>2</sub> is more effective than CO. With the increase of H<sub>2</sub> percentage in H<sub>2</sub>-CO blends, flame development duration and rapid combustion duration as well as COV<sub>IMEP</sub> decreased. Both H<sub>2</sub> and CO help to lower THC emission and enhance engine effective thermal efficiency. With the increase of H<sub>2</sub> percentage in H<sub>2</sub>-CO blends, THC emission decreases. However, their effects on CO emission are different due to different mechanisms. H<sub>2</sub> addition slightly affects CO emission while CO addition remarkably increases CO emission because of incomplete combustion (mainly by quenching and crevice effect). Both H<sub>2</sub> and CO addition worsen engine NO<sub>x</sub> emission while improving engine thermal efficiency (Liu, et al., 2018).

Liu et al. (2018) conducted an experimental study to evaluate the knock tendency and lean limit of the natural gas engine after adding H<sub>2</sub>/CO into the cylinder. It was found that H<sub>2</sub>/CO addition increases the knock tendency and intensity in the natural gas engine. The reasons relied on two aspects are the addition of H<sub>2</sub>/CO increases the energy density of in-cylinder mixture, which is increased by 1.35% and 4.5% with 1% and 2% H<sub>2</sub>/CO addition respectively; and the addition of H<sub>2</sub>/CO promotes the mixture flame speeds due to hydrogen's high reactivity and higher propagation speed so that the temperature and pressure in end gas region is higher due to lower heat loss. H<sub>2</sub>/CO addition extends the lean limit and stabilizes the combustion. At 1.2MPa load, the lean limits are extended from  $\lambda=1.5$  to  $\lambda=1.57$  and  $\lambda=1.65$  respectively, with 1% and 2% H<sub>2</sub>/CO addition which implies that the engine could be operated on even leaner air/fuel mixtures after H<sub>2</sub>/CO addition with the same limiting factor imposed on a lean burn. The maximum thermal efficiencies with H<sub>2</sub>/CO addition are slightly higher than a pure natural gas combustion. H<sub>2</sub>/CO addition could slightly increase the NO<sub>x</sub> emission, but significantly decrease THC

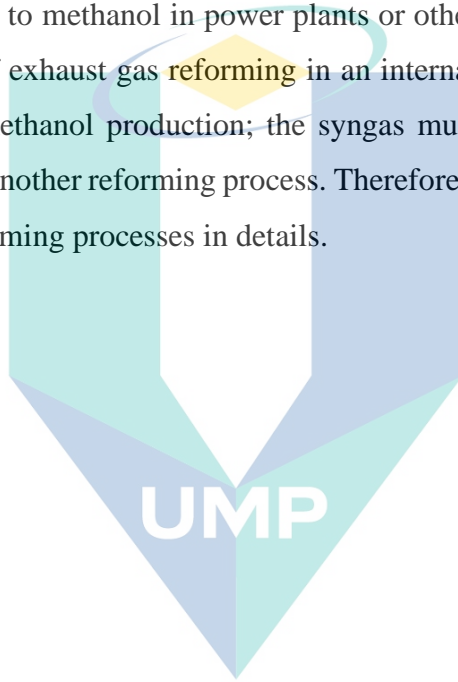
and CO emissions. Knock intensity increases linearly as knock onset angle is advanced towards to TDC. H<sub>2</sub>/CO addition significantly shortens the ignition lag due to its promotion on flame speed in an early stage of combustion. The increase in knock intensity caused by H<sub>2</sub>/CO addition is closely related to faster flame propagation speed. The increase in knock intensity with H<sub>2</sub>/CO addition is mainly related to more rapid flame propagation. The sensitivity analysis reveals the main reason for faster flame speed is that H<sub>2</sub> increases the reaction rate of the branching reaction  $H+O_2=O+OH$ . The reaction rates of the other two dominating reactions  $CH_3+HO_2=CH_3O+OH$  and  $CO+OH=CO_2+H$  become much faster due to the presence of H<sub>2</sub>/CO. Besides, 1% and 2% H<sub>2</sub>/CO addition extend lower equivalence ratio limits by 14% and 26%, which is beneficial for further efficiency improvement and emission reduction (Changpeng Liu, et al., 2018).

## 2.10 Summary

This chapter has reviewed the methods that are used in syngas production, and it started with the background of syngas and its applications. Syngas has various applications, and this study showed some of them, such as fuel cells and syngas utilization in ICE. Nowadays, syngas has the interest to be used in an internal combustion engine and produce it inline through exhaust gas fuel reforming. The reforming processes in industry are similar to the reforming process used in an internal combustion engine, such as methane reforming.

Exhaust gas reforming is a complex method of fuel conversions because it involves a different type of reforming reactions, steam reforming, dry reforming, and oxidation reactions. Therefore, it was essential to perform a comprehensive literature review of each reaction in the exhaust gas reforming process. The review study focused on the behaviour of each reaction and each factor that plays an important role in hydrogen-rich syngas production, such as, thermodynamic analysis, catalysts, chemical kinetic and reformer design. It was shown that steam reforming reaction is the favoured one for methane conversion and hydrogen production. Whereas, dry reforming is the most difficult reaction for methane consumption and syngas generation due to the high demanded temperature to increase the rate reaction. Meanwhile, oxidation reaction releases high temperature, which can enhance the reforming performance. The effect of

the feed composition components on the methane conversion and hydrogen production were discussed, and it was found that, as the amount of steam is high in the feeding components, rise in reforming performance is achieved. The review study also discussed the effect of hydrogen-rich syngas on the combustion characteristics of the SI engine. It was found that the addition of syngas can enhance combustion efficiency and engine performance due to the high energy generation from hydrogen combustion. And before, discussing the production methods of syngas in the internal combustion engine, it was essential to review the ways that are being used in the industrial application such, as the conversion of flue gas to methanol in power plants or other industries. This process has the same principles of exhaust gas reforming in an internal combustion engine because before the stage of methanol production; the syngas must be produced through auto-thermal reforming or another reforming process. Therefore, this literature review focused on these types of reforming processes in details.



اونيورسيتي ملايسيا قهغ

UNIVERSITI MALAYSIA PAHANG

## CHAPTER 3

### METHODOLOGY

#### 3.1 Overview

This chapter discusses the methods that are followed in this research to achieve the research objectives discussed in Chapter 1. Figure 3.1 shows the detail schematics of the methodology flowchart. It starts with the thermodynamics analysis, which is essential in this study. Thermodynamics analysis involved the mixture temperature, pressure, mixture flow rate, exhaust components, and the thermodynamic properties of the mixture. Thermodynamic characteristics depend on the engine condition, such the engine speed, injection timing and the air-fuel ratio to determine the flow rate of the exhaust mixture, the exhaust compositions and thermodynamic properties which varies with the temperature of the exhaust mixture. Based on the thermodynamics analysis, the catalyst is selected because it must be capable of withstanding under the stream temperature and the mixture components of the flow. The chemical kinetics is essential to determine the reaction path along the plug flow fixed bed reactor and calculate the consumption and the formation rate of the species at the outlet of the reactor. It also determines the required amount of catalyst and the methane flow rate to achieve the maximum methane conversion and the produced syngas ( $H_2+CO$ ) at each engine speed. The formation and consumption rate of the species is conducted through 1D modelling using the reactor design algorithms of the fixed-bed reactor. The reforming characteristics which is determined from the 1D modelling vary with the engine speed. Each engine speed has a different amount of catalyst and methane flow rate from the other speeds. The amount of catalyst is important because it determines the size of the reactor, and the methane flow needs to be lower than the fuel rate used in the engine combustion. In order to have one catalyst weight and methane flow rate for all the engine speeds, RSM optimization study is conducted to have the maximum methane conversion and syngas production at one minimum methane flow rate and catalyst weight. After finding the catalyst weight, the

size of the reformer is selected, and the 2D CFD model is developed to verify the 1D mathematical modelling. 2D CFD modelling is used to determine the effect of the engine speed and other parameters on the reforming characteristics. Finally, the reforming characteristics are studied, and the reformed gas components are determined, the 3D CFD model is used to study the effect of the reformed gas on the combustion characteristics. The 3D CFD model is used to compare the combustion characteristics of the CNG, and CNG added with reformed gas in SI engine.

Figure 3.1 shows the research flow chart. The research methodology starts with the thermodynamic analysis. In this step, the thermodynamic properties were calculated using the temperature equation dependent. Besides, the exhaust gas flow rate calculation at each engine speed. In the chemical kinetic model step, the reaction rate of species consumption and formation was developed. Then 1D Modeling was used to determine the amount of catalyst mass, and the natural gas flow rate needed to achieve maximum syngas production and methane conversion at each engine speed. 1D Modeling is conducted based on plug flow reactor design algorithm, which is commonly used in chemical reactor design processes. In validation step, the 1D Modeling was compared with published experimental results to ensure that the model can predict the reaction results by using the average error which supposed to be less than 10% in the overall validation. RSM CCD optimization was used to optimize the one minimum amount of catalyst mass and natural gas flow rate for all the engine speeds used. From RSM optimization, the reformer size was selected based on the catalyst mass. Then, the 2D CFD porous medium model was used to test the sized reformer performance at various conditions and to verify it with 1D Modeling for advance model confirmation. The 2D CFD also was validated with experimental results was published in high impact factor journals, and the average error supposed to be less than 10%. Finally, to test the effect of the reforming products on combustion characteristics, 3D CFD combustion model was used as shown in a flow chart, and the overall validation should be less than 10 % with experimental results which was collected from previous works was conducted by the research group.

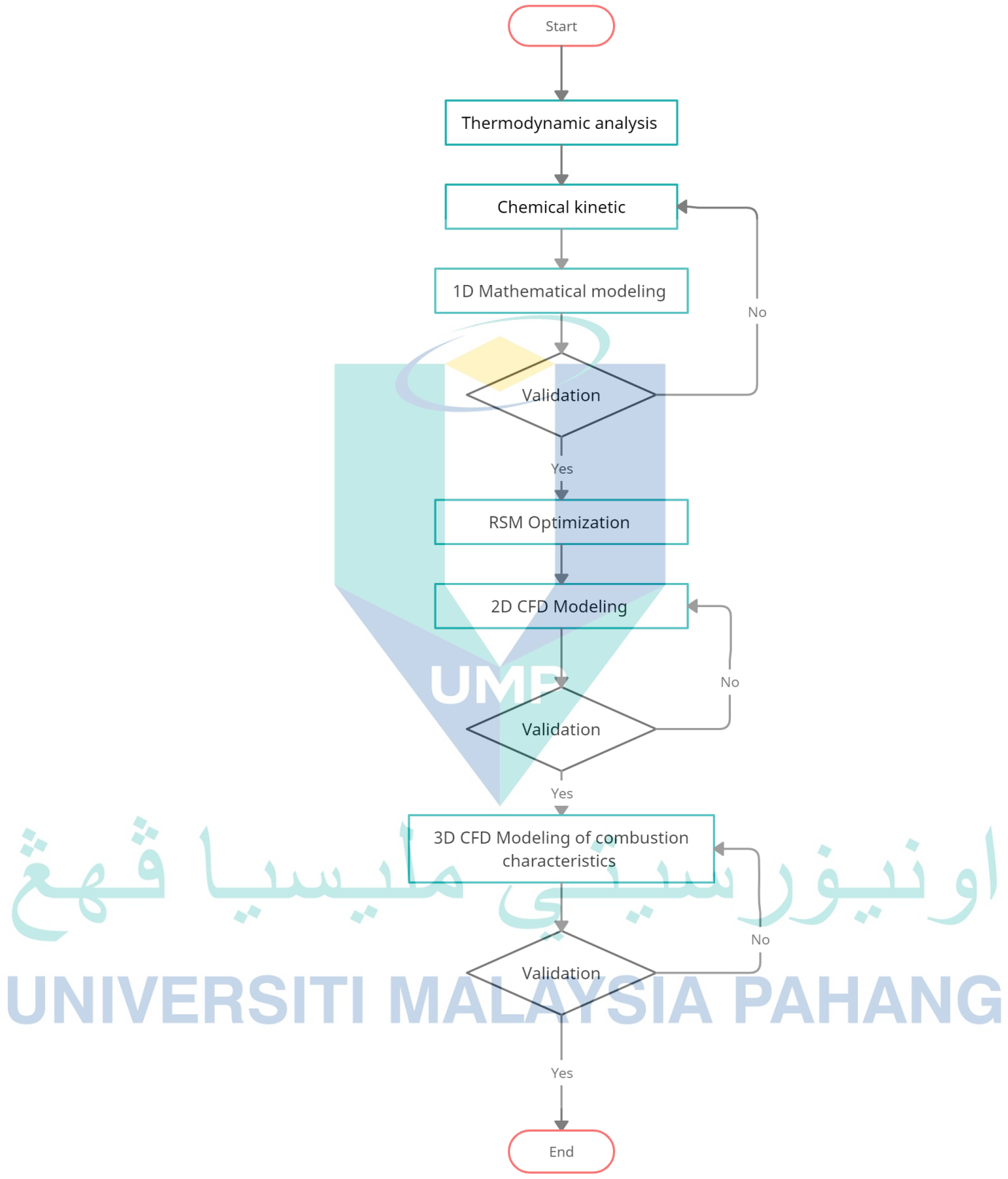


Figure 3.1 Flow chart of the research

### 3.2 Thermodynamics Analysis

Thermodynamics analysis mainly depends on the engine conditions, especially the engine speed, which will determine the exhaust component and the thermodynamics properties.

#### 3.2.1 The Engine Specifications and Conditions

In this study, the data are collected at full engine load (100%), and engine speed varied from 1200 to 3000 revolutions per minute (rpm) with an interval of 300 rpm. The range of low and higher engine speeds are selected. This is because the main aim of this study is to investigate the reforming characteristics at these conditions due to the lower performance of the natural gas engines at the lower engine speed and higher engine loads. In this study, the exhaust data is collected experimentally and recalculated from a compressed natural gas (CNG) direct-injection (DI) SI with its specification as shown in Table 3.1.

Table 3.1 Engine specifications.

Engine parameters	Specifications
Engine type	DISI
Compression ratio	14
Displacement volume	399.25 cm <sup>2</sup>
Cylinder bore	76.0 mm
Cylinder stroke	88.0 mm
Number of valves	4
Inlet valve open (IVO)	BTDC 12°
Inlet valve closed (IVC)	ABDC 48°
Exhaust valve open (EVO)	BTDC 45°
Exhaust valve closed (EVC)	ATDC 10°

Figure 3.2 shows the mechanism of exhaust gas reforming. The exhaust gas mixture and the natural gas are reacted in the tube in the presence of the pellets of catalyst. The remaining exhaust is used to provide additional heat to enhance the reforming process inside the container. The produced syngas will be delivered to the combustion chamber during the air intake manifold. This process will be simulated in this study using 1D modelling to design the reforming tube (EGR reformer) and will be tested by using the 2D CFD simulation. Finally, the effect of produced syngas addition on the combustion characteristics will be simulated using 3D CFD combustion model.

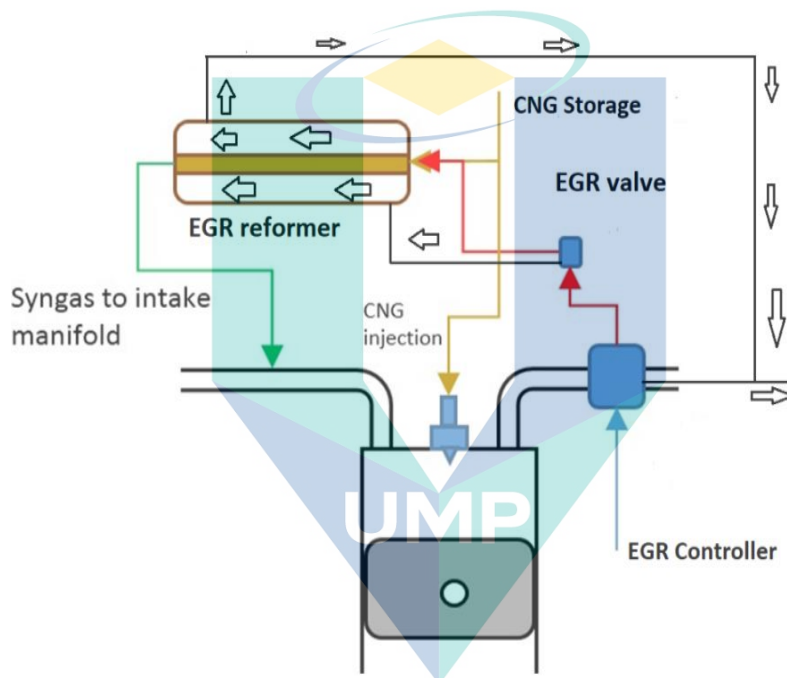


Figure 3.2 Schematics of exhaust gas reforming mechanism

### 3.2.2 Injection Timing

The injection timing in this study was taken at  $180^\circ$  BTDC because this study is conducted at the full engine load. The in-cylinder pressure is proven experimentally to have better combustion characteristics than  $120^\circ$  BTDC. The starting of combustion at  $180^\circ$  BTDC occurred before  $120^\circ$  BTDC. Therefore, the in-cylinder pressure at  $180^\circ$  BTDC is higher than  $120^\circ$  BTDC, and the burning rate of the fuel is also faster which make it more convenient to be selected at the full load (100%). However, the performance

of the engine at 180° BTDC is high compared to 300° and 120° BTDC (Hagos, et al., 2014a).

Figure 3.3 indicates the injection timing and combustion duration of different crank angle. It is shown that 180 BTDC has enough time for mixing the primary fuel (natural gas), secondary fuel (syngas) and the air. Therefore, this enough time of mixing provides the desired condition for the combustion process, which can result in higher energy generation and better combustion stability, especially at full load condition.

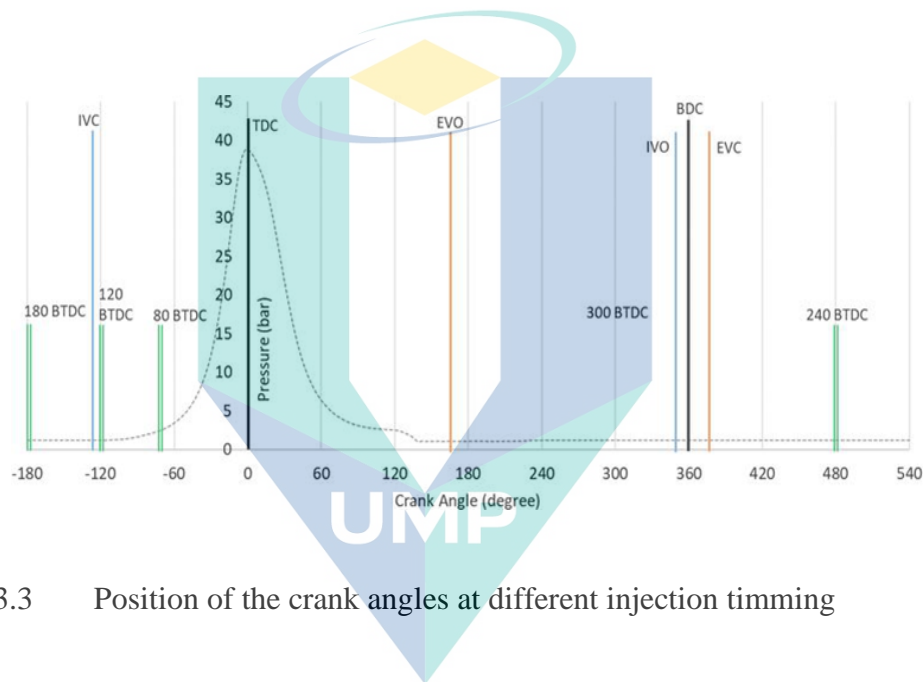
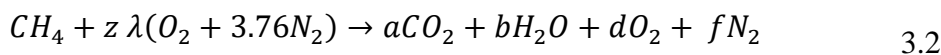
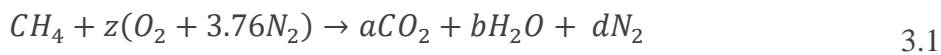


Figure 3.3 Position of the crank angles at different injection timing

### 3.2.3 Exhaust Gas Calculation

This section describes the measurement and calculation of the exhaust gas flow rate and concentration of each component. The exhaust flow rate is measured experimentally, and to find each component flow rate, Equations 3.1 and 3.2 are used.



where  $z$  and  $\lambda$  are the haze and air-to-fuel ratio, respectively,  $a, b, d$  and  $f$  are exhaust concentrations. At each engine speed, different inlet fuel rate is used as shown in Table 3.2.

Table 3.2 Inlet fuel rate, air-fuel ratio and exhaust gas flow rate at each engine speed

Engine speed (rpm)	Air-fuel ratio $\lambda$	Fuel rate g/s	Total Exhaust flow rate Mol/hr	Temperature K
1,200	1.0156	0.2380	571.440	761
1,500	1.0158	0.2970	713.130	791
1,800	1.1011	0.3603	779.084	816
2,100	1.103	0.4049	838.00	847
2,400	1.202	0.4786	1021.807	865
2,700	1.2036	0.5148	1442.916	882
3,000	1.2046	0.5587	1567.311	888

The exhaust concentration is calculated at each engine speed at each flow rate using Equations 3.1 and 3.2 and the results were as shown in Table 3.3. Table 3.4 shows the calculated exhaust gas mole fraction for a speed of 1,800 rpm with the EGR varying from 5-25%.

اونيورسيتي ملايسيا قهغ

UNIVERSITI MALAYSIA PAHANG

Table 3.3 Exhaust gas volume fraction at 25% EGR

Engine speed rpm	Exhaust gas flow rate <i>Mol/hr</i>	Exhaust gas mole fraction			
		$CO_2$	$H_2O$	$O_2$	$N_2$
1,200	142.861	0.0936	0.1875	0.0029	0.7158
1,500	178.34	0.0938	0.1875	0.0029	0.7159
1,800	194.776	0.1041	0.2081	0.0210	0.6667
2,100	209.525	0.1087	0.2174	0.0224	0.6514
2,400	255.451	0.1054	0.2108	0.0425	0.6412
2,700	360.732	0.0803	0.1605	0.0326	0.7264
3,000	391.825	0.0802	0.1604	0.0328	0.7265

Table 3.4 Exhaust gas volume fraction at 1,800 rpm at various EGR rates

EGR rate	Exhaust gas flow rate <i>Mol/hr</i>	Exhaust gas mole fraction			
		$CO_2$	$H_2O$	$O_2$	$N_2$
5	38.954	0.104	0.210	0.0210	0.665
10	77.908	0.104	0.210	0.0210	0.665
15	116.862	0.104	0.210	0.0210	0.665
20	155.816	0.104	0.210	0.0210	0.665
25	194.771	0.104	0.210	0.0210	0.665

### 3.2.4 Natural Gas Flow Rate

It is important to determine the amount of the demanded natural gas (Methane) to achieve the desired reforming performance. The amount of natural gas that is being supplied to the reformer to produce syngas must be less than the amount of the primary fuel rate to avoid the higher fuel consumption rate. Therefore, several natural gas flow rates are tested in this study by taking various ratios of the exhaust to methane at each speed as shown in Table 3.5.

Table 3.5 Molar flow rate of natural gas at each engine speed based on the exhaust flow rate.

$F_{exhaust}$ $/F_{CH_4}$ Ratio	Natural gas flow rate (Mol/hr) at various engine speeds (rpm)						
	1200	1500	1800	2100	2400	2700	3000
0.1	14.313	17.830	19.484	20.951	25.544	36.073	39.207
0.15	21.431	26.753	29.215	31.951	38.323	54.114	58.771
0.2	28.584	35.661	38.950	41.908	51.091	72.144	78.365
0.25	35.7286	44.570	48.705	52.384	63.860	90.181	97.953
0.3	42.870	53.508	58.431	62.861	76.630	108.223	117.551
0.4	57.161	71.321	77.910	83.803	102.186	144.308	156.732
0.5	71.456	891.152	97.401	104.763	127.735	180.368	195.921

### 3.2.5 Thermodynamic Properties for The Gas Mixtures

All gas streams in the models are assumed ideal and their physical properties are given as function of temperature, pressure, and composition.

#### 3.2.5.1 Density

The ideal gas law is used for estimating the gas density, which is reasonable considering the high temperatures. The mole weight of the mixture is found from the sum of the component mole weights,  $M_i$ , weighted on the component mole fractions,  $y_i$ . The density  $\rho_g$  of the gas mixture is then expressed by the equation (Companies, 1999):

$$\rho_g = \frac{P}{RT} \sum_{i=1}^n y_i M_i \quad 3.3$$

#### 3.2.5.2 Thermal Conductivity

Thermal conductivities of pure gases,  $K_g$ , are estimated by polynomial expressions given by (Bruce E. Poling, George H. Thomson, Daniel G. Friend, Richard

L. Rowley, 2008; Companies, 1999) shown in equation 3.4 , with constants as shown in Table 3.6.

$$K_i = A_i + B_iT + C_iT^2 + D_iT^3 \quad 3.4$$

The thermal conductivity of gas mixtures,  $K_g$  is calculated by equation 3.5 with the modification of Mason and Saxena (Bruce E. Poling, George H. Thomson, Daniel G. Friend, Richard L. Rowley, 2008; Companies, 1999):

$$K_g = \sum_{i=1}^n \frac{y_i K_i}{\sum_{i=1}^n y_i} \quad 3.5$$

Table 3.6 Constants for polynomial in Equation 3.4

	$CH_4$	$CO_2$	$H_2O$	$N_2$	$H_2$	$CO$
$A_i$	$-1.869 \times 10^{-3}$	$-7.215 \times 10^{-3}$	$7.341 \times 10^{-3}$	$0.392 \times 10^{-3}$	$8.099 \times 10^{-3}$	$0.506 \times 10^{-3}$
$B_i$	$8.727 \times 10^{-5}$	$8.015 \times 10^{-5}$	$-1.013 \times 10^{-5}$	$9.966 \times 10^{-5}$	$66.890 \times 10^{-5}$	$9.125 \times 10^{-5}$
$C_i$	$1.179 \times 10^{-7}$	$0.055 \times 10^{-7}$	$1.801 \times 10^{-7}$	$-0.506 \times 10^{-7}$	$-4.158 \times 10^{-7}$	$-0.352 \times 10^{-7}$
$D_i$	$-3.614 \times 10^{-11}$	$-1.053 \times 10^{-11}$	$-9.100 \times 10^{-11}$	$-1.504 \times 10^{-11}$	$15.620 \times 10^{-11}$	$-0.819 \times 10^{-11}$

Source: Bruce E. Poling, George H. Thomson, Daniel G. Friend, Richard L. Rowley (2008); Companies (1999)

### 3.2.5.3 Specific Heat Capacity

The specific heat capacity of pure gases,  $CP_i$  is calculated as given by (Bruce E. Poling, George H. Thomson, Daniel G. Friend, Richard L. Rowley 2008; Companies 1999) in equation 3.6, with the correlation constants cited in Table 3.7. The equation is defined as a function of the gas constant,  $R$ , and is here converted from model basis to mass basis:

$$C_{p,i} = \frac{R}{M_i} (a_{0,i} + a_{1,i}T + a_{2,i}T^2 + a_{3,i}T^3 + a_{4,i}T^4) \quad 3.6$$

The specific heat capacity of the gas mixture is dependent on the gas composition and is here weighted with the mole fractions:

$$C_{p,g} = \frac{\sum_{i=1}^n y_i M_i C_{p,i}}{\sum_{i=1}^n y_i M_i} \quad 3.7$$

Table 3.7 Constants for calculation of  $C_{p,i}$

	$CH_4$	$CO_2$	$H_2O$	$N_2$	$H_2$	$CO$
$a_{0,i}$	4.568	3.259	4.395	3.539	2.883	3.912
$a_{1,i}$	$-8.975 \times 10^{-3}$	$1.356 \times 10^{-3}$	$-4.186 \times 10^{-3}$	$-2.610 \times 10^{-4}$	$3.681 \times 10^{-3}$	$-3.913 \times 10^{-3}$
$a_{2,i}$	$3.631 \times 10^{-5}$	$3.631 \times 10^{-5}$	$1.405 \times 10^{-5}$	$7.00 \times 10^{-8}$	$-7.720 \times 10^{-6}$	$1.182 \times 10^{-5}$
$a_{3,i}$	$-3.407 \times 10^{-8}$	$-2.374 \times 10^{-8}$	$-1.564 \times 10^{-8}$	$1.570 \times 10^{-9}$	$6.920 \times 10^{-8}$	$-1.302 \times 10^{-8}$
$a_{4,i}$	$1.091 \times 10^{-11}$	$1.056 \times 10^{-11}$	$6.320 \times 10^{-12}$	$-9.900 \times 10^{-13}$	$5.150 \times 10^{-12}$	$6.320 \times 10^{-12}$

Source: Bruce E. Poling, George H. Thomson, Daniel G. Friend, Richard L. Rowley (2008); Companies (1999)

Among the properties temperature-dependent models, the above equations (3.4-3.7) were selected because it provides the constant factors of the chemical species in this study. Therefore, the accuracy of this model can be achieved more than the other models.

### 3.3 Catalyst Selection

As shown in section 2.5.2, the favoured catalyst for exhaust gas reforming is  $Rh - AL_2O_3$  due to many reasons, such as:

- Its resistance to the high temperature due to the high heat release from the oxidation reactions.
- Its longer activity under the stream of the exhaust which contain of carbon dioxide which is considered one of the main reasons beyond the coke formation.
- High resistance against the methane decomposition.
- Higher methane conversion compared to Pd and Pt.
- Rh has a higher selectivity to hydrogen than other common CPOX catalysts such as Pt, Pd and Ni-based.

Table 3.8 Catalyst properties

Parameters	Value
Specific heat (J/kg.K)	850
Thermal conductivity (w/(m.K)	12.6
Number of catalyst active site kmol/m <sup>2</sup>	$2.7 \times 10^{-5}$
Pellet diameters	0.005
Porosity ( $\epsilon$ )	0.5

### 3.4 Chemical Kinetic and Mathematical Modelling

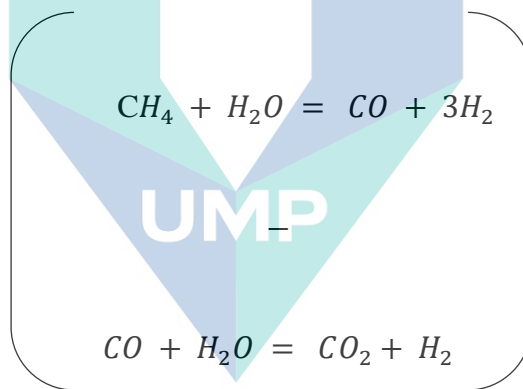
#### 3.4.1 Chemical kinetic

Exhaust gas reforming is a combination of steam reforming, dry reforming, partial and complete oxidation, as shown in Table 3.9 of the six reactions (1-6). Reactions (1), (2) and (5) can be set as independent reactions. For instance, dry reforming of methane (DRM) reaction (5) can be described as reaction (1) minus reaction (6) as shown in the mathematical description. However, the four reactions (1), (2), (4) and (6) are used to describe the exhaust gas reforming. Xu and Forment model over Ni-based catalyst is used for reactions (1), (2) and (6). Trimm and Lam model, which derived over Pt-based catalyst, is considered as a rate expression for methane combustion (reaction (6)). These kinetic models are commonly used by many researchers today for the reforming processes that involve steam reforming, dry reforming, partial and complete oxidation such as tri and auto-thermal reforming, as seen in Chapter 2.

Table 3.9 Main reactions in the exhaust gas reforming process

No	Detailed reaction	Reaction formula	$\Delta H^\circ$ kJ/mol
1	Steam reforming	$CH_4 + H_2O \leftrightarrow CO + 3H_2$	+206
2	Steam reforming	$CH_4 + 2H_2O \leftrightarrow CO_2 + 4H_2$	+165
3	Partial Oxidation	$CH_4 + 0.5O_2 \leftrightarrow CO + 2H_2$	-36
4	Complete oxidation	$CH_4 + 2O_2 \leftrightarrow CO_2 + 2H_2O$	-802.7
5	Carbon dioxide reforming (DRM)	$CH_4 + CO_2 \leftrightarrow 2CO + 2H_2$	+247
6	Water-gas shift reaction	$CO + H_2O \leftrightarrow CO_2 + H_2$	-41

Mathematical description of dry reforming reaction:



$$R_1 = \frac{k_1}{P_{H_2}^{2.5}} \left( P_{CH_4} P_{H_2O} - \frac{P_{H_2}^3 P_{CO}}{K_I} \right) X \frac{1}{\phi^2} \quad 3.8$$

$$R_2 = \frac{k_2}{P_{H_2}^{3.5}} \left( P_{CH_4} P_{H_2O}^2 - \frac{P_{H_2}^4 P_{CO_2}}{K_{II}} \right) X \frac{1}{\phi^2} \quad 3.9$$

$$R_3 = \frac{k_3}{P_{H_2}} \left( P_{CO} P_{H_2O} - \frac{P_{H_2} P_{CO_2}}{K_{III}} \right) X \frac{1}{\phi^2} \quad 3.10$$

$$R_4 = \frac{k_{4a} P_{CH_4} P_{O_2}}{(1 + K^C_{CH_4} P_{CH_4} + K^C_{O_2} P_{O_2})^2} + \frac{k_{4b} P_{CH_4} P_{O_2}}{(1 + K^C_{CH_4} P_{CH_4} + K^C_{O_2} P_{O_2})} \quad 3.11$$

$$\phi = 1 + K_{CO} P_{CO} + K_{H_2} P_{H_2} + K_{CH_4} P_{CH_4} + K_{H_2O} \frac{P_{H_2O}}{P_{H_2}} \quad 3.12$$

The equilibrium constant and Arrhenius kinetic parameters are indicated in Table 3.10. The parameters of Van't Hoff for the adsorption species are listed in Table 3.11.

Table 3.10 Equilibrium constant and Arrhenius kinetic coefficient

No	Equilibrium constant	A (mol/kg <sub>cat</sub> .s)	E <sub>j</sub> (J/mol)
R <sub>1</sub>	$K_I = \exp\left(\frac{-26830}{T_s} + 30.114\right)$ (bar <sup>2</sup> )	$1.17 \times 10^{15} \text{ bar}^{0.5}$	240,100
R <sub>2</sub>	$K_{II} = K_I \cdot K_{III}$ (bar <sup>2</sup> )	$2.83 \times 10^{14} \text{ bar}^{0.5}$	243900
R <sub>3</sub>	$K_{III} = \exp\left(\frac{4400}{T_s} - 4.036\right)$	$5.43 \times 10^5 \text{ bar}^2$	67130
R <sub>4</sub>		$8.11 \times 10^5 \text{ bar}^{-2}$ $6.82 \times 10^5 \text{ bar}^{-2}$	86000 86000

$$k_j = A X \exp\left(\frac{-E_j}{RT}\right)$$

Table 3.11 Equilibrium constant and Arrhenius kinetic coefficient

Reactants	K <sub>oj</sub> (bar <sup>-1</sup> )	ΔH <sub>j</sub> (J/mol)	K <sub>oj</sub> <sup>C</sup> (bar <sup>-1</sup> )	ΔH <sub>j</sub> <sup>C</sup> (J/mol)
CH <sub>4</sub>	$6.65 \times 10^{-4}$	-38,280		
CO	$8.23 \times 10^{-5}$	-70,650		
H <sub>2</sub>	$6.12 \times 10^{-9}$	-82,900		
H <sub>2</sub> O	$1.77 \times 10^5$ bar	88,680		
CH <sub>4</sub> (Combustion)			$1.26 \times 10^{-1}$	-27,300

Table 3.11 Continued

Reactants	$K_{oj}$ (bar <sup>-1</sup> )	$\Delta H_j$ (J/mol)	$K_{oj}^C$ (bar <sup>-1</sup> )	$\Delta H_j^C$ (J/mol)
O <sub>2</sub> (Combustion)			$7.78 \times 10^{-7}$	-92,800

$$K_j = K_{oj} X \exp\left(\frac{-\Delta H_j}{RT}\right)$$

$$K_j^C = K_{oj}^C X \exp\left(\frac{-\Delta H_j}{RT}\right)$$

Table 3.12 Heat transfer coefficient

No	Parameter	Equation	Ref
1	Coefficient of overall heat transfer between the wall of the EGR reformer and the gas phase inside the tube	$\frac{1}{U} = \frac{1}{h_i} + \frac{A_a \ln\left(\frac{D_o}{D_i}\right)}{2\pi L K_w}$	
2	Heat transfer coefficient between the wall of the reactor and gas phase	$\frac{h_i}{CP\rho\mu} \left(\frac{CP}{k}\right)^{\frac{2}{3}}$ $= \frac{0.458}{\varepsilon_B} \left(\frac{\rho u d_p}{\mu}\right)^{-0.407}$	(Halabi, et al., 2008)
3	Heat exchange area per unit volume	$a = \frac{4}{D}$	

The consumption rate of species formation  $i$ ,  $r_i$  (mol/kgcat.s) is determined by summing up the reaction rates of each species as shown in Equations 3.13 – 3.18 as:

$$r_{CH_4} = -\eta_1 R_1 - \eta_2 R_2 - \eta_4 R_4 \quad 3.13$$

$$r_{O_2} = -2 R_4 \quad 3.14$$

$$r_{H_2O} = -\eta_1 R_1 - 2\eta_2 R_2 - \eta_3 R_3 + 2\eta_4 R_4 \quad 3.15$$

$$r_{CO_2} = \eta_2 R_2 + \eta_3 R_3 + \eta_4 R_4 \quad 3.16$$

$$r_{H_2} = \eta_1 R_1 + \eta_2 R_2 + \eta_3 R_3 \quad 3.17$$

$$r_{CO} = \eta_1 R_1 - \eta_3 R_3 \quad 3.18$$

$$\eta_1 = 0.07, \eta_2 = 0.06, \eta_3 = 0.7, \eta_4 = 0.05 \text{ (Gosiewski, et al., 1999)}$$

### 3.4.2 Mathematical Modelling

The model of a fixed bed reactor with heat and mass transfer has been developed to determine the conversion of reactant species and the distribution of temperature inside the reactor. The following assumptions are used in the development of the model:

- i. The gas-phase is in ideal condition.
- ii. The fluid flow is considered to be incompressible and in a steady-state condition.
- iii. Axial diffusion is neglected.
- iv. The porosity of the fixed bed reactor is uniform.
- v. Surrounding heat loss is neglected.
- vi. Wall temperature is constant.
- vii. The radiation heat transfer is ignored.
- viii. Pressure drop is neglected.
- ix. Natural gas is represented by pure methane.

In order to model the process of EGR reforming mathematically, a one-dimensional single phase plug flow reactor is divided into differential equations, mass and energy balance as expressed in Equations 3.19 to 3.25

$$\frac{dF_{CH_4}}{dW} = \eta_1 R_1 - \eta_2 R_2 - \eta_4 R_4 \quad 3.19$$

$$\frac{dF_{H_2O}}{dW} = -\eta_1 R_1 - 2\eta_2 R_2 - \eta_3 R_3 + 2\eta_4 R_4 \quad 3.20$$

$$\frac{dF_{O_2}}{dW} = -2 R_4 \quad 3.21$$

$$\frac{dF_{CO_2}}{dW} = \eta_2 R_2 + \eta_3 R_3 + \eta_4 R_4 \quad 3.22$$

$$\frac{dF_{H_2}}{dW} = \eta_1 R_1 + \eta_2 R_2 + \eta_3 R_3 \quad 3.23$$

$$\frac{dF_{CO}}{dW} = \eta_1 R_1 - \eta_3 R_3 \quad 3.24$$

$$\frac{dT}{dW} = \frac{Ua(T_w - T) + \sum_i^q (-r_i) [\Delta H_{Rxi} R_i(T)]}{\sum_j^m F_j C_{Pj}} \quad 3.25$$

where  $F_j$  and  $r_i$  indicate the molar flow rates and rate of consumption or formation of component  $i$ , respectively and  $W$  represents the catalyst mass. Equation 3.25 is the energy balance, and  $U$  and  $a$  are overall heat transfer coefficient and heat exchange area of the reactor per unit volume.  $\Delta H_{Rxi}$  shows the heat of the reaction and  $R_i$  is the rate of reaction, as shown in Equations (3.8-3.12).  $F_j$  and  $C_{Pj}$  illustrate the molar flow rates and specific heat of each species inside the reactor.

Equations 3.19-3.25 are the mass balance of each species, whereas Equation 3.25 is developed for energy balance along the reactor, respectively. These equations formed a system of differential equations that involve six equations of mass balance and one energy balance equation. To solve the differential equation system, Runge Kutta method in POLYMATH software was applied.

### 3.4.3 Boundary Conditions

The inlet flow rate, the feed composition of the gas, the inlet temperature and inlet pressure at the reactor entrance are known. However, the boundary condition can be considered as follows:

Inlet:  $W_i = 0$  ,  $F_i = F_{i0}$  ,  $T = T_0$  ,  $T_w = T_0$  ,  $P = P_0$

Outlet:  $W_f = 1000g$  ,  $F_i = \frac{dF_i}{dW}$  ,  $T = \frac{dT}{dW}$  ,  $T_w = T_0$  ,  $P = P_0$

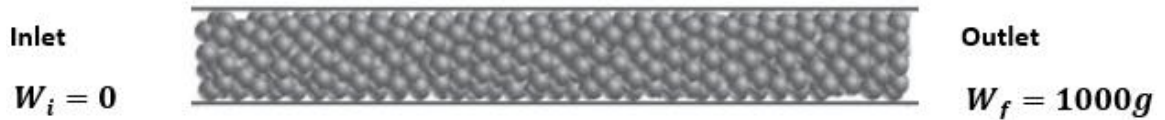


Figure 3.4 Catalytic fixed bed tube

$$\text{Methane conversion} = \frac{CH_{4in} - CH_{4out}}{CH_{4in}} \times 100\%$$

### 3.4.4 Model of Validation

The model is validated with a published experimental study, as shown in Tables 3.20 and 3.21. To validate the 1D modeling, the differential equations (3.19-3.25) are modified to be dependent on the length instead of the catalyst mass as shown in equations (3.27 and 3.28):

$$\rho = \frac{W}{L} \Rightarrow L = \frac{W}{\rho} \quad 3.26$$

$$\frac{dF_j}{dL} = \rho_{cat} \times A_a \times r_i \quad 3.27$$

$$\frac{dT}{dL} = \rho_{cat} \times A_a \frac{Ua(T_w - T) + \sum_i^q (-r_i) [\Delta H_{Rxi} R_i(T)]}{\sum_j^m F_j C_{pj}} \quad 3.28$$

Where,  $r_i$  is the rate Reaction rate of component  $j$ . Validation results are shown in Section 3.6.6.

### 3.5 Optimization by Response Surface Method (RSM)

In the 1D kinetic modelling, the demanded amount of catalyst weight and natural gas flow rate are determined at each engine speed. Then, the optimization study is needed to choose the possible minimum natural gas flow rate and catalyst weight to achieve the maximum methane conversion and syngas quantity in the reformed gas. Therefore, the central composite design (CCD) which is one the most popular response surface method (RSM) that is well suited for fitting these kinds of systems. Central composite design

(CCD) with multi objectives is used to find out the relations between independent factors and the responses. The statistical study is very effective to obtain the best possible responses by decreasing the number of modelling runs. The steps of the CCD RSM optimization are shown in Figure 3.5. The RSM optimization was conducted by Design-Expert software to study the regression analysis of the 1D modelling data.

Figure 3.5 Starts with the factors selections, which will be used to determine the demanded factors to conduct the CCD design. The factors are engine speeds, natural gas flow rate, catalyst mass, syngas production and methane conversion. In the second steps, the variables and response were selected. The main variables used in this study are engine speeds, natural gas flow rate and catalyst mass. Whereas, the responses are the amount of syngas produced, which will be represented by the percentage of hydrogen and carbon monoxide in the reforming products besides the methane conversion percentage.

Natural gas flow rate and catalyst mass at each engine speeds were calculated by using 1D mathematical modelling. After that, the transform model was selected, and the optimization was conducted, and the model significance of the model was tested using ANOVA analysis. Then, the regression model equations of syngas production and methane conversion were obtained and validated with the results of the 1D modelling, and if the average validation were less than 10%, it could be ensured that the optimization objective is achieved. Finally, the numerical optimization was performed to select the main variables which are required minimum natural gas flow rate and catalyst mass to achieve the maximum methane conversion and syngas production.

اونيورسيتي ملايسيا قهق

UNIVERSITI MALAYSIA PAHANG

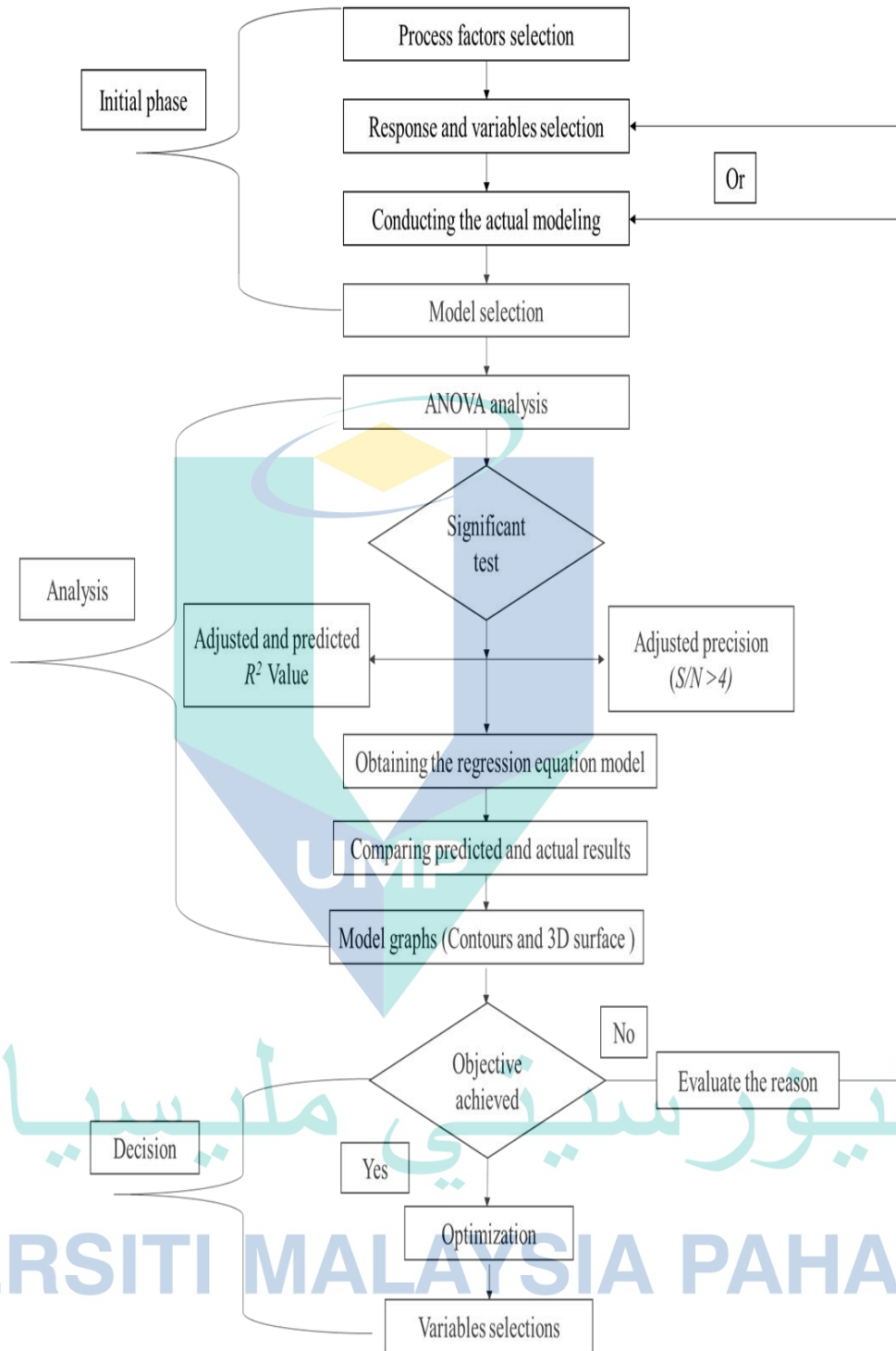


Figure 3.5 CCD RSM optimization steps

### 3.5.1 Independent Variables and Response Determination

The effect of the independent variables is given in Table 3.13, engine speed, catalyst weight and natural gas flow rate. Whereas, the responses are represented by methane conversion and the amount of produced syngas at each engine speed.

Table 3.13 Independent variables and responses

Independent variables			Responses	
Engine speed (rpm)	Catalyst weight (g)	CH <sub>4</sub> Flow rate (Mol/hr)	CH <sub>4</sub> Conversion (%)	Syngas (%)
1200	900	21.43	40.410	22.015
1500	800	26.745	45.090	23.017
1800	700	38.954	48.00	25.75
2100	600	41.904	52.650	26.013
2400	550	51.090	55.30	25.8804
2700	450	54.110	58.671	22.45
3000	350	62.850	61.730	22.300

It is shown that the maximum methane conversion and syngas percentages are 61.73% and 26.013%, respectively. The conversion of methane has increased with the rise of the engine speed. While the syngas percentage has increased at first with the engine speed up to 1,200 rpm, it started to decline from 2,400 rpm to 3,000 rpm. Therefore, the aim of the optimization study is to obtain the maximum conversion rate and syngas.

However, the design layout is constructed, as shown in Table 3.14. Since there are three variables, 20 runs are conducted by 1D modelling according to the faced centred option. Thus, all the modelling runs are varied between their minimum and maximum values, not lower nor higher.

Table 3.14 Design layout of the CCD model design for the process optimization and the corresponding responses

Run	Independent variables			Responses	
	Engine speed (rpm)	Catalyst mass (g)	Molar flow rate (Mol/hr)	Syngas (%)	Conversion (%)
1	2100	675	40.100	26.042	52.828
2	1200	675	40.100	5.660	6.873
3	1200	350	58.770	3.014	2.844
4	2100	675	58.770	21.721	36.184
5	2100	675	40.100	26.042	52.827
6	3000	350	58.770	22.300	61.730
7	2100	675	40.100	26.042	52.827
8	1200	1000	58.770	20.283	19.468
9	3000	350	21.430	11.719	89.793
10	3000	675	40.100	18.347	67.171
11	2100	675	40.100	26.042	52.827
12	2100	675	21.430	20.540	66.003
13	2100	675	40.100	26.042	52.828
14	3000	1000	58.770	22.300	61.730
15	2100	1000	40.100	26.043	52.828
16	1200	350	21.430	2.567	5.789
17	2100	350	40.100	13.460	24.769
18	1200	1000	21.430	22.015	40.410
19	3000	1000	21.430	11.719	89.794
20	2100	675	40.100	26.043	52.828

### 3.5.2 Statistical Analysis

The statistical analysis is important for the consistency of optimization modelling. The statistical analysis is developed by a few steps. Firstly, the response transformation is selected and evaluated. Secondly, the fit summary is evaluated to select the  $f_x$ . Then, the ANOVA table is constructed and evaluated by seeing whether the model is significant

or not. Finally, the model is evaluated by comparing the predicted results and the actual modelling results.

### 3.5.2.1 Transform ( $Y^\lambda$ ) selection

Normally in design expert, there are eight transformation models as shown in the following equations equations (3.29-3.34)

- Non model:  $y = y$  3.29

- Square root model:  $y^\lambda = \sqrt{y + k}$ , where ( $\lambda = 0.5$ ) 3.30

- Natural log model:  $y^\lambda = \ln(y + k)$ , where ( $\lambda = 0$ ) 3.31

- Base 10 log:  $y^\lambda = \log_{10}(y + k)$ , where ( $\lambda = 0$ ) 3.32

- Inverse square root:  $y^\lambda = \frac{1}{\sqrt{y+k}}$ , where ( $\lambda = -0.5$ ) 3.33

- Inverse:  $y^\lambda = \frac{1}{y+k}$ , where ( $\lambda = -1$ ) 3.34

The transform models of methane conversion and syngas were selected by testing each one and compare the predicted and the actual modelling data and the average error of all the data as shown in Figure 4.9 and Figure 4.10.

## 3.6 2D CFD Modeling of The Reforming Characteristics

The 2D CFD modelling is used to test the reforming characteristics of the reformer to verify 1D modelling. Besides, the 2D CFD modelling has the advantage of giving higher accuracy of the reforming performance along the reactor. CFD modelling is conducted by ANSYS-FLUENT solver. The fixed bed reactor is represented by the 2D porous medium model due to the complex arrangement of the random catalytic pellets, which make very complex to generate a three-dimensional model because of the irregular porous structure and contact region between the catalytic pellets and the reactor. Figure 3.6 shows the physical domain of the fixed bed of exhaust gas reformer.

However, the first step before CFD modelling is determining the dimensions and of the reactor using the catalysts characteristics and its demanded amount.

### 3.6.1 Reactor Sizing

From RSM optimization, it is found that the minimum catalyst weight to achieve the maximum syngas production and methane conversion is 850 g; therefore, to determine the size of the reactor, the density equation 3.35 is used. The physical domain of the fixed bed reactor considered in this study is shown in figure 3.6.

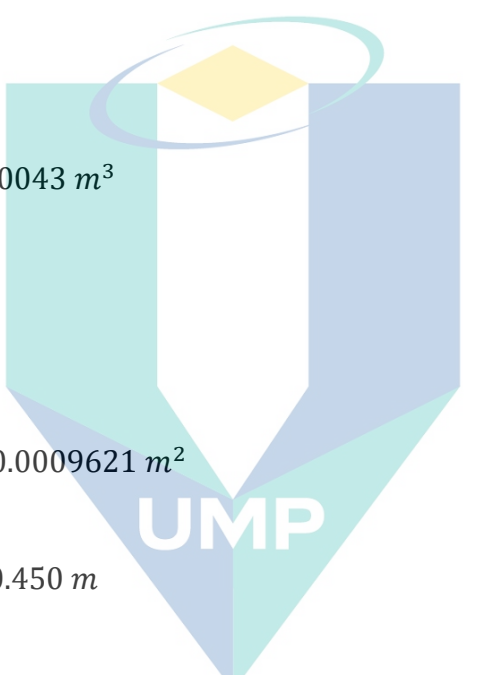
$$\rho = \frac{W}{V} \quad 3.35$$

$$V = \frac{W}{\rho} = 0.00043 \text{ m}^3 \quad 3.36$$

$$V = A \times L \quad 3.37$$

$$D = 0.035 \text{ m}$$

$$A = \frac{\pi}{4} D^2 = 0.0009621 \text{ m}^2 \quad 3.38$$

$$L = \frac{V}{A} = 0.447 \cong 0.450 \text{ m} \quad 3.39$$


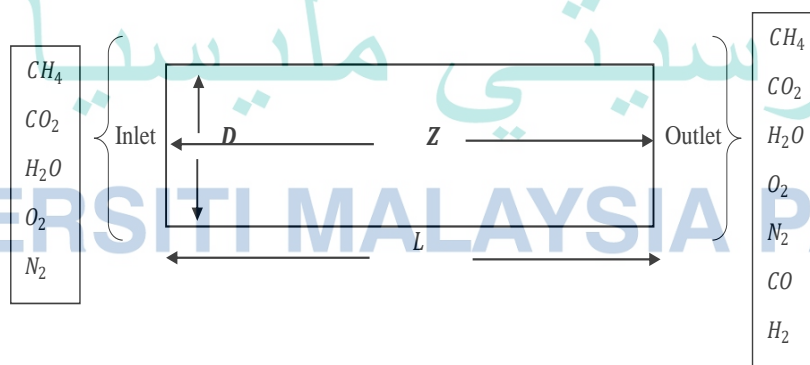


Figure 3.6 Physical domain of fixed bed of exhaust gas reformer

### 3.6.2 Boundary conditions

The boundary conditions of the 2D CFD model are the same with the boundary conditions of the 1D modelling except for the pressure change. In 2D CFD modelling, the porous medium model is used to simulate the catalytic fixed bed reactor, and the pressure drop can not be neglected despite its low value. Therefore, the pressure drop is considered using the Ergun pressure drop equation. The assumptions were also same with the 1D modelling.

$$\text{Inlet: } L_i = 0, F_i = F_{i0}, T = T_0, T_W = T_0, P = P_0$$

$$\text{Outlet: } L_f = Z, F_i = \frac{dF_i}{dW}, T = \frac{dT}{dZ}, T_W = T_0, P = \frac{dP}{dZ}$$

$$\frac{dP}{dZ} = 150 \left( \frac{(1 - \varepsilon)^2 \mu \mu_g}{\varepsilon^3 d_p^2} + 1.75 \frac{(1 - \varepsilon) \mu_g^2 \rho}{\varepsilon^3 d_p} \right) \quad 3.40$$

Before the model development, the flow region is essential to be determined. Therefore, Reynolds number is calculated by using Equation 3.41 at each flow engine speed, as shown in Table 3.15. The natural gas flow rate was constant (35 Mol/hr) at all the engine speed.

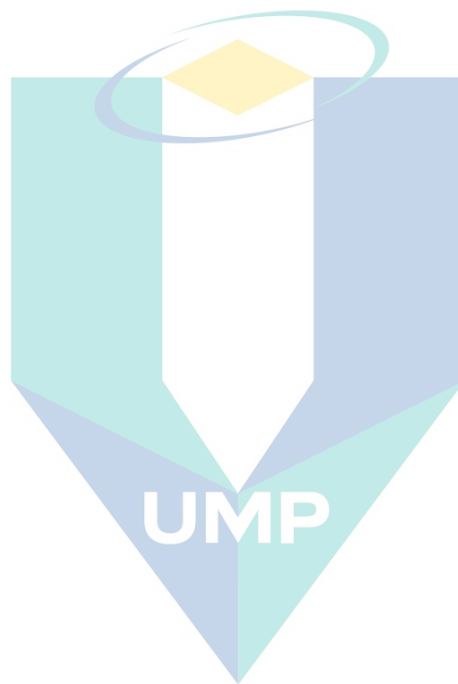
$$Re = \frac{\rho V D}{\mu} \quad 3.41$$

Equations 3.42 and 3.43 are used to convert the Mol/hr to g/s the in order to determine the flow speed in m/s:

$$m_g = \sum_{i=1}^{i=n} F_j y_i M_i \quad 3.42$$

$$m_g = \rho V A \Rightarrow V = \frac{m_g}{V A} \quad 3.43$$

As shown in Table 3.18, the flow of the gas mixture is laminar at the lower engine speed (1200-2100 rpm) and turbulent at the higher engine speed (2400-3000 rpm). Therefore, the turbulent model is considered for the higher speed, as shown in the governing equations.



اونيورسيتي مليسيا قهغ

UNIVERSITI MALAYSIA PAHANG

Table 3.15 The mixture volume fractions and flow region at engine speed

Engine speed rpm	Exhaust flow rate Mol/hr	Gas mixture volume fractions					Exhaust Flow g/s	Reynold Number	Flow region
		Natural gas CH <sub>4</sub>	Exhaust gas mixture						
			CO <sub>2</sub>	H <sub>2</sub> O	O <sub>2</sub>	N <sub>2</sub>			
1200	177.86	0.1967	0.0751	0.1506	0.00234	0.5749	1.2524	1720.265	Laminar
1500	213.3	0.1640	0.0784	0.1567	0.00247	0.5984	1.5249	2041.118	Laminar
1800	229.77	0.1523	0.0882	0.17640	0.01780	0.5651	1.6528	2149.513	Laminar
2100	244.52	0.1431	0.0931	0.1862	0.0192	0.5581	1.7654	2230.24	Laminar
2400	290.45	0.1205	0.0926	0.1853	0.0374	0.5639	2.1250	2660.784	Turbulent
2700	395.73	0.0884	0.0731	0.1463	0.0297	0.6621	2.9425	3520.548	Turbulent
3000	426.825	0.0820	0.0736	0.1472	0.0301	0.6669	3.1828	3757.279	Turbulent

اونيور سيئي ملايسيا قهغ

UNIVERSITI MALAYSIA PAHANG

### 3.6.3 Governing Equations

#### 3.6.3.1 Governing Equation in The Laminar Flow Region

The Equations 3.44, 3.45, 3.48 and 3.51 are solved simultaneously to model the flow and reactions of the reforming process along the packed-bed reactor:

The continuity equation:

$$\frac{\partial(\varepsilon\rho u_i)}{\partial Z_i} = 0 \quad 3.44$$

The momentum conservation equation:

$$\begin{aligned} \frac{\partial(\varepsilon\rho u_i u_j)}{\partial Z_i} = & -\varepsilon \frac{\partial P}{\partial Z_j} + \frac{\partial}{\partial Z_j} \left( \varepsilon\mu \frac{\partial u_k}{\partial Z_k} \right) + \frac{\partial}{\partial Z_i} \left( \varepsilon\mu \left( \frac{\partial u_i}{\partial Z_j} + \frac{\partial u_j}{\partial Z_i} \right) \right) \\ & - \left( \frac{\varepsilon^2\mu}{K} u_j - \frac{\varepsilon^2 C_2}{2} |v_i| v_i \right) \end{aligned} \quad 3.45$$

where  $\mu$  is the viscosity of the fluid mixture, and it is determined by using ideal mixing law,  $\varepsilon$  is the fixed-bed reactor porosity,  $K$  denotes the coefficient of the permeability and  $C_2$  is the factor of inertial resistance coefficient, which can be calculated by using Ergun formula.

$$K = \frac{d_p^2}{150} \frac{\varepsilon^3}{(1-\varepsilon)^2} \quad 3.46$$

$$C_2 = \frac{3.5(1-\varepsilon)}{d_p} \frac{1}{\varepsilon^3} \quad 3.47$$

where,  $d_p$  is the catalytic pellets diameter.

Species conversion equation:

$$\frac{\partial(\varepsilon\rho u_j Y_i)}{\partial x_j} + \frac{\partial(J_{ij})}{\partial x_j} = R_i \quad 3.48$$

where  $Y_i$  is the species mass fraction and  $J_{ij}$  is the mass flux diffusion and it is determined as follows:

$$J_{ij} = -D_{i,m} \frac{\partial Y_i}{\partial Z_j} - \frac{D_{T,i}}{T} \frac{\partial T}{\partial Z_j} \quad 3.49$$

$$R_i = S_V M_i S_i \quad 3.50$$

Energy equation:

$$\frac{\partial(\varepsilon\rho u_i u_j h_f)}{\partial Z_j} = \varepsilon u_j \frac{\partial P}{\partial Z_j} + \frac{\partial}{\partial Z_j} \left( k_{eff} \frac{\partial T}{\partial Z_j} - \sum_{i=1}^{N_g} h_i J_{i,j} \right) \quad 3.51$$

where  $h_i$  indicates the explicit enthalpy,  $h_f$  is the specific enthalpy of the flow mixture and  $k_{eff}$  denotes the effective thermal conductivity in the porous medium, and they were determined through the following equation:

$$h_f = \sum_{i=1}^{N_g} Y_i h_i \quad 3.52$$

$$k_{eff} = k_f + (1 - \varepsilon)k_s \quad 3.53$$

### 3.6.3.2 Governing Equation in The Turbulent Flow Region

The reformer is modelled in the turbulent region based on the following continuity, momentum equations and energy equations.

Continuity equation:

$$\frac{\partial(u_i)}{\partial z_i} = 0 \quad 3.54$$

Momentum equation:

$$\frac{\partial}{\partial z_i} (\rho u_i u_j) = -\frac{\partial p}{\partial z_i} + \frac{\partial}{\partial z_j} \left( \mu \frac{\partial u_i}{\partial z_i} - \rho u_i u_j \right) \quad 3.55$$

Energy equation:

$$\frac{\partial}{\partial z_i} (\rho u_j T) = \frac{\partial}{\partial z_j} \left( \Gamma \frac{\partial T}{\partial z_i} - \rho u_j T' \right) \quad 3.56$$

where,  $\mu$ ,  $P$ , and  $T$  were the molecular viscosity, pressure, and temperature of the mixture, which are obtained through the ideal-mixing law in FLUENT solver. The Reynold number-averaging equations are applied to deal with the turbulence, where  $-\rho u_j T'$  is the Reynold stress generated by instantaneous pulsating flow  $-\rho u_j T'$  is an additional term of turbulence pulsation of temperature. The Reynolds stress is related to the average velocity gradient using vortex viscosity coefficient:

$$-\rho u_j T' = \tau_{ij} = \mu_t \left( 2S_{ij} - \frac{2}{3} \frac{\partial u_i}{\partial z_i} \delta_{ij} \right) - \frac{2}{3} \rho k \delta_{ij} \quad 3.57$$

The temperature estimated by the turbulence pulsation can be related to the time averaging parameters through the following equations

$$-\rho u_j T' = \Gamma_t \frac{\partial T}{\partial z_i} \quad 3.58$$

Among them,  $\mu_t$  is the turbulent viscous coefficient, and  $\Gamma_t$  is the turbulent diffusion coefficient.

Turbulent kinetic energy equation:

$$\rho \frac{\partial k}{\partial t} = \rho u_j \frac{\partial k}{\partial z_i} = \frac{\partial}{\partial z_i} \left[ \left( \mu + \frac{\mu_t}{\sigma_\epsilon} \right) \frac{\partial k}{\partial z_i} \right] + \mu_t \frac{\partial \mu_i}{\partial z_i} \left( \frac{\partial \mu_i}{\partial z_i} + \frac{\partial \mu_i}{\partial z_j} \right) - \rho \epsilon \quad 3.59$$

Turbulent dissipation equation:

$$\rho u_k \frac{\partial \varepsilon}{\partial z_i} = \frac{\partial}{\partial z_i} \left[ \left( \mu + \frac{\mu_t}{\sigma_\varepsilon} \right) \frac{\partial \varepsilon}{\partial z_i} \right] + \frac{c_1 \varepsilon}{k} \mu_t \left( \frac{\partial \mu_i}{\partial z_i} + \frac{\partial \mu_i}{\partial z_j} \right) - c_2 \rho \frac{\varepsilon^2}{k} \quad 3.60$$

Turbulent viscosity and turbulent diffusion coefficient are evaluated from the Equations 3.61 and 3.62, respectively:

$$\mu_t = \rho C_\mu \frac{k^2}{\varepsilon} \quad 3.61$$

$$\Gamma = \frac{\mu}{Pr} + \frac{\mu_t}{\sigma_t} \quad 3.62$$

where  $\sigma_t$  is the turbulent  $Pr$  number related to the temperature field,  $\frac{\mu}{Pr}$  is caused by molecular diffusion, while  $\frac{\mu_t}{\sigma_t}$  is due to the turbulent fluctuation. The model coefficient and constants values are:  $c_1 = 1.44$ ,  $c_2 = 1.92$ ,  $C_\mu = 0.09$ ,  $\sigma_k = 1.0$ ,  $\sigma_\varepsilon = 1.3$ ,  $\sigma_t = 0.94$  (Janardhanan, et al., 2011; O. Deutschmann, 2008; Zhang, et al., 2020; Zhang, Jia, et al., 2017). The  $k - \varepsilon$  model is most widely used for modelling the Reynold stresses which add to additional differential equations as shown in equations (3.63- 3.64). Thus, this model was used in this study due to its ability to predict the results of the flow in the fully developed region besides its simplicity to achieve early convergence. (O. Deutschmann, 2008).

### 3.6.3.3 Scheme of Heterogeneous Chemical Reaction

The mechanism of surface reactions was presented by Schwiedernoch et al. (2003) (Schwiedernoch, et al., 2003), as shown in Table 3.16. This mechanism has shown the steps of hydrogen production from the reforming of methane, and it consisted of 38 reactions, 12 surface and six gas-phase species. The rate of consumption or formation of adsorbed species can be defined as:

$$S_i = \sum_{n=1}^{K_S} v_{i,n} k_{f,n} \prod_{f=1}^{N_g+N_s} [C_j]^{v_{j,n}} \quad 3.63$$

where  $K_S$  is the number of reactions including the component  $i$  and  $C_j$  is the concentration of the species in the reactor whereas the  $v$  is the stoichiometric coefficient of the reactant species. The reaction rate of the catalytic surface reaction can be expressed as shown in the following equation:

$$k_n = AT^{a,n} \exp\left(\frac{-E_{a,n}}{RT}\right) \prod_{i=1}^{N_s} \theta_i^\varphi \exp\left(\frac{\xi_{i,n}\theta_i}{RT}\right) \quad 3.64$$

The rate of the catalytic surface reaction is dependent on the coverage of the particle surface which is indicated by  $\theta_i$ . And the two parameters  $\varphi$  and  $\xi_{i,n}$  gives the coverage dependence of the reaction rate. The rate of the adsorption reaction can be expressed as:

$$k_n = \frac{\gamma}{\Gamma^\tau} \sqrt{\frac{RT}{2\pi M_i}} \quad 3.65$$

where  $\tau$  is the sum of stichometry of the surface reaction component which is expressed by:

$$\tau = \sum_{j=1}^{N_s} v_n$$

Table 3.16 Catalytic reaction scheme

Z	Equation	A	b	E
<i>1. Adsorption reaction</i>				
R1	$CH_4 + * (s) \rightarrow CH_4(s)$	0.008	0.0	0.0
R2	$O_2 + 2 * (s) \rightarrow 2O(s)$	0.01	0.0	0.0
R3	$H_2 + 2 * (s) \rightarrow 2H(s)$	0.01	0.0	0.0
R4	$H_2O + * (s) \rightarrow H_2O (s)$	0.01	0.0	0.0
R5	$CO_2 + * (s) \rightarrow CO_2(s)$	$10^{-5}$	0.0	0.0
R6	$CO + * (s) \rightarrow CO (s)$	0.5	0.0	0.0
R7	$H + * (s) \rightarrow H(s)$	1.0	0.0	0.0
R8	$O + * (s) \rightarrow O(s)$	1.0	0.0	0.0
R9	$OH + * (s) \rightarrow OH(s)$	1.0	0.0	0.0
<i>2. Surface reaction</i>				
R10	$H(s) + O(s) \rightarrow OH(s) + * (s)$	$5.22 \times 10^{22}$	0.0	83.7
R11	$OH(s) + * (s) \rightarrow H(s) + O(s)$	$3.0 \times 10^{20}$	0.0	37.7
R12	$H(s) + OH(s) \rightarrow H_2O(s) + * (s)$	$3.0 \times 10^{20}$	0.0	33.5
R13	$H_2O(s) + * (s) \rightarrow H(s) + O(s)$	$3.0 \times 10^{20}$	0.0	106.4
R14	$OH(s) + OH(s) \rightarrow H_2O(s) + O(s)$	$5.22 \times 10^{22}$	0.0	100.8
R15	$H_2O(s) + O(s) \rightarrow H(s) + OH(s)$	$3.0 \times 10^{21}$	0.0	224.2
R16	$C(s) + O(s) \rightarrow CO (s) + * (s)$	$3.0 \times 10^{21}$	0.0	97.9
R17	$CO (s) + * (s) \rightarrow C(s) + O(s)$	$3.0 \times 10^{22}$	0.0	169.0
R18	$CO (s) + O(s) \rightarrow CO_2 (s) + * (s)$	$1.4 \times 10^{20}$	0.0	121.6
R19	$CO_2 (s) + + * (s) \rightarrow CO (s) + O(s)$	$3.0 \times 10^{21}$	0.0	115.3
R20	$CH_4(s) + * (s) \rightarrow CH_3(s) + H(s)$	$3.7 \times 10^{21}$	0.0	61.0
R21	$CH_3(s) + H(s) \rightarrow CH_4(s) + * (s)$	$3.7 \times 10^{21}$	0.0	51.0
R22	$CH_3(s) + * (s) \rightarrow CH_2(s) + H(s)$	$3.7 \times 10^{24}$	0.0	103.0
R23	$CH_2(s) + H(s) \rightarrow CH_3(s) + * (s)$	$3.7 \times 10^{21}$	0.0	44.0
R24	$CH_2(s) + * (s) \rightarrow CH(s) + H(s)$	$3.7 \times 10^{24}$	0.0	100.0
R25	$CH(s) + H(s) \rightarrow CH_2(s) + * (s)$	$3.7 \times 10^{21}$	0.0	21.0
R26	$CH(s) + * (s) \rightarrow C(s) + H(s)$	$3.7 \times 10^{21}$	0.0	97.9

Table 3.16 Continued

Z	Equation	A	b	E
R27	$C(s) + H(s) \rightarrow CH(s) + * (s)$	$3.7 \times 10^{21}$	0.0	172.8
R28	$CH_4(s) + O(s) \rightarrow CH_3(s) + OH(s)$	$1.7 \times 10^{24}$	0.0	80.3
R29	$CH_3(s) + O(s) \rightarrow CH_4(s) + O(s)$	$3.7 \times 10^{21}$	0.0	24.3
R30	$CH_3(s) + O(s) \rightarrow CH_2(s) + OH(s)$	$3.7 \times 10^{21}$	0.0	120.3
R31	$CH_2(s) + OH(s) \rightarrow CH_3(s) + O(s)$	$3.7 \times 10^{24}$	0.0	15.1
R32	$CH_2(s) + O(s) \rightarrow CH(s) + OH(s)$	$3.7 \times 10^{24}$	0.0	158.4
R33	$CH(s) + OH(s) \rightarrow CH_2(s) + O(s)$	$3.7 \times 10^{21}$	0.0	36.8
R34	$CH(s) + O(s) \rightarrow C(s) + OH(s)$	$3.7 \times 10^{21}$	0.0	30.1
R35	$C(s) + OH(s) \rightarrow CH(s) + O(s)$	$3.7 \times 10^{21}$	0.0	145.5
3. Desorption reaction				
R36	$2H(s) \rightarrow H_2 + 2 * (s)$	$3.0 \times 10^{21}$	0.0	77.8
R37	$2O(s) \rightarrow O_2 + 2 * (s)$	$1.3 \times 10^{22}$	0.0	$355.2-280\theta_o$
R38	$H_2O(s) \rightarrow H_2O + 2 * (s)$	$3.0 \times 10^{13}$	0.0	45.0
R39	$CO(s) \rightarrow CO + * (s)$	$3.5 \times 10^{13}$	0.0	$133.4-15\theta_{CO}$
R40	$CO_2(s) \rightarrow CO_2 + * (s)$	$1.0 \times 10^{13}$	0.0	21.7
R41	$CH_4(s) \rightarrow CH_4 + * (s)$	$1.0 \times 10^{13}$	0.0	25.1
R42	$OH(s) \rightarrow OH + * (s)$	$8.1 \times 10^{11}$	0.0	142.2

### 3.6.4 Solution Procedure

The numerical simulation is used to verify the 1D mathematical model in 2D geometry, and it is conducted using ANSYS Fluent 18.1. To describe the behaviour of the flow, the laminar model is used, and the viscous heating is negligible. The laminar finite rate model is used to solve the surface catalytic reaction by using finite volume method. Ideal mixing gas law is used to calculate the physical parameters of the mixed gas such as specific heat, thermal conductivity and viscosity. In this study, axisymmetric geometry property is applied to the reforming tube as shown in Figure 3.7 (Inc., 2016).

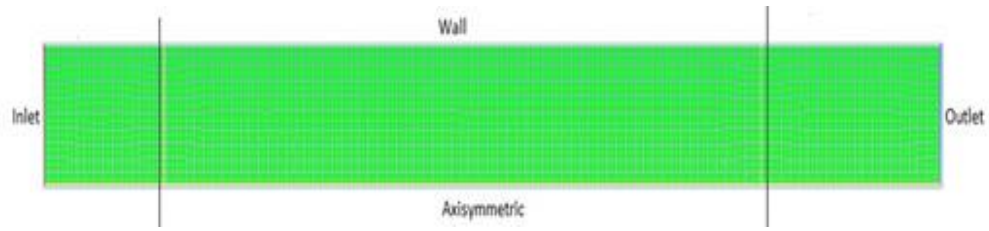


Figure 3.7 Model of the single fixed bed reactor tube.

### 3.6.5 Grid Independency Test

To check the consistency of the solution on the mesh, a study of grid independency test is followed. Six meshes are developed with a different number of elements and nodes. The mole fraction of methane at the outlet of EGR reformer is selected to evaluate the independence of the grid and check either the solution is independent or it demands advanced refinement. It can be noticed in Figure 3.8 that at the coarse mesh, the value of mole fraction of methane is high compared to the fine mesh. As the mesh is refined, the difference between the molar fractions became lower and reached a constant value. Therefore, mesh number 6 with 10,500 elements and 10,881 nodes are selected to conduct the simulation and generate all the 2D model results in this study.

Table 3.17 Meshing details

Mesh No	No of elements	No of nodes
1	656	747
2	800	909
3	1680	1833
4	2816	3009
5	4680	4935
6	10500	10881

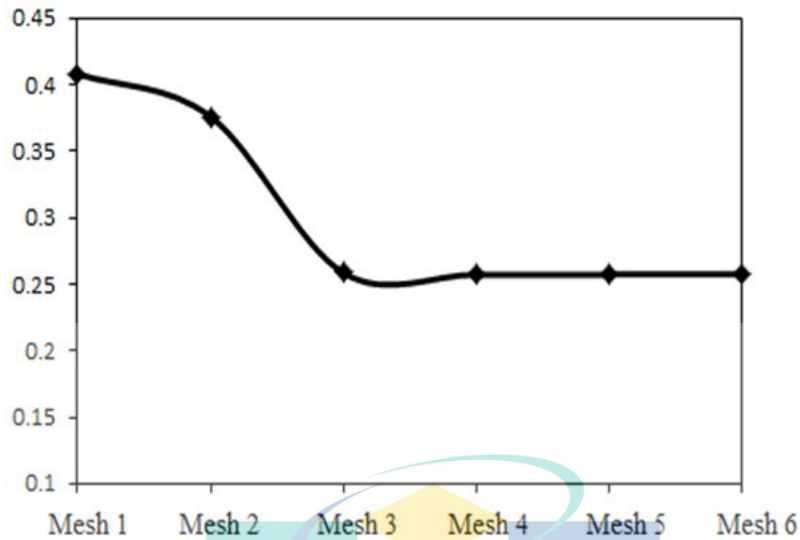


Figure 3.8 Variation of the molar fraction of methane with the size of the mesh

### 3.6.6 Model Validation

The model is verified with the 1D modelling and the empirical regression model. While it is also validated with a published experimental work is also conducted in the same area of reforming. It is validated with two different experimental studies.

Since there are a few studies of exhaust gas reforming of the natural gas engine that is conducted numerically not experimentally, the model's reliability is validated with an experimental data of catalytic partial-oxidation of  $\text{CH}_4/\text{O}_2$  mixtures diluted with  $\text{H}_2\text{O}$  and  $\text{CO}_2$  in a short contact time reactor by Schneider et al (Schneider, et al., 2006). The inlet gas was a mixture of  $\text{CH}_4$ ,  $\text{O}_2$ ,  $\text{H}_2\text{O}$  and  $\text{CO}_2$  and the molar fraction of the mixture species was 0.204: 0.102: 0.462: 0.231. The inlet velocity and temperature of the gas mixture were 5.1 m/s and 623 K, respectively, with an adiabatic wall surface considered. The inner surface of the reactor was coated by Rh, and the support material was  $\text{ZrO}_2$ . The reactor used to perform this experiment has a length and diameter of 75 mm and 1.2592 mm, respectively. The mass fraction of each component at the outlet and values obtained from the mathematical modelling and CFD simulation are shown in Table 3.18. It can be noticed a consistency between the experimental, 1D modelling and

2D numerical values. Therefore, the model can be used to describe the process the exhaust gas reforming reactions for syngas production.

Table 3.18 Comparison between experimental, 1D and 2D modelling mole fractions values

Species	CH <sub>4</sub>	O <sub>2</sub>	H <sub>2</sub> O	CO <sub>2</sub>	CO	H <sub>2</sub>
Experimental value	0.074	0.001	0.420	0.228	0.0830	0.1930
1D Model	0.06916	0.00096	0.468	0.210	0.0709	0.1804
2D Model	0.0710	0.00105	0.4356	0.2316	0.0741	0.1927
Relative error <sup>1</sup> %	6.5	4.3	11.4	7.850	14.50	6.50
Relative error <sup>2</sup> %	4.0	4.5	4.0	1.50	10.5	0

The 1D modelling and CFD simulation were also validated with was validated with a numerical investigation study of a tubular exhaust gas reformer with thermochemical recuperation for LNG engine (Zhang, et al., 2020). In this study, an experimental investigation was developed to validate the numerical data as shown in Figure 3.11. The fixed bed reactor has a length and diameter of 300 mm and 44 mm, respectively. The validation between the experimental data and the current study was as shown in Table 3.19. The validation is conducted at 2:1 ratio of methane to oxygen.

Table 3.19 Comparison between experimental, 1D modelling and 2D simulation of Hydrogen and methane mole fraction

Mole fractions at the reactor outlet	Experimental data	1D modelling	Relative error <sup>1</sup>	2D Simulation	Relative error <sup>2</sup>
H <sub>2</sub>	0.107	0.0957	11%	0.105	2%
CH <sub>4</sub>	0.065	0.0695	6%	0.072	9%

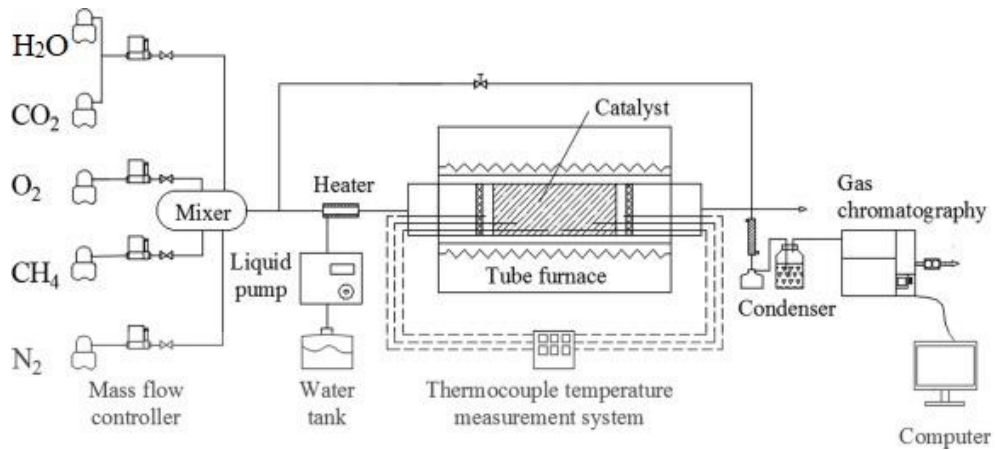


Figure 3.9 Schematic diagram of the single tube reforming test bench system  
 Source: Zhang, et al., (2020)

### 3.7 3D CFD Simulation of the Combustion Characteristics of The SI Engine Fueled by Natural Gas with the Addition of Reforming Products in Dual Fueling System

This section shows, the 3D CFD simulation of the combustion of the engine fueled by natural gas and the reforming product. This study aims to evaluate the effect of reformed gas addition on the combustion characteristics compared with the natural gas ( $CH_4$ ). There are two types of simulation used in this study. The cold flow is used to observe the flow of the air without the combustion reactions. The combustion simulation is used to determine the energy released from the combustion and its effect on the engine combustion efficiency. The simulation is conducted at 1800 rpm as the operating speed and the throttle wide open to considering full load condition.

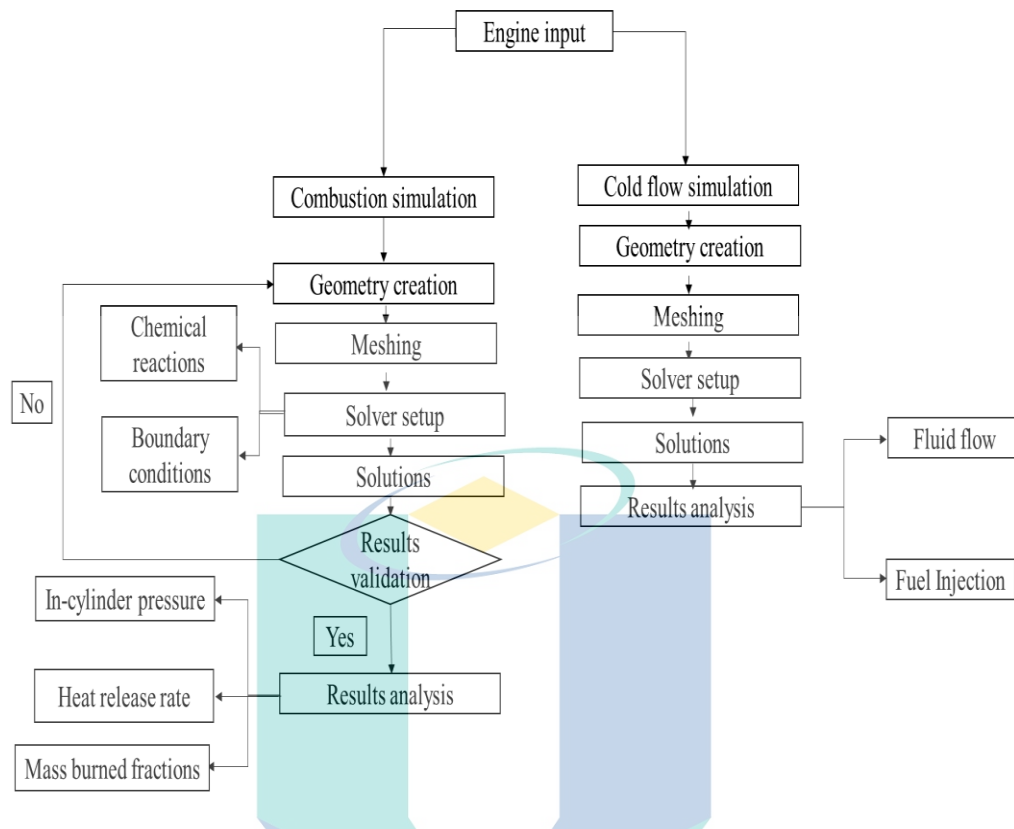


Figure 3.10 Engine simulation steps

### 3.7.1 Model Design

This modelling is conducted in a four-stroke, single-cylinder, direct-injection spark-ignition research engine developed in a comprehensive IC engine flow and combustion simulation of Ansys with a compression ratio of 14. The crankshaft is one rotation which is  $360^\circ$  of crank angle (CA). The simulation process starts with the Inlet Valve Opening (IVO), which is  $168^\circ$  CA which is equivalent to  $12^\circ$  BTDC. The reformate gas is injected by the second injector in the port and CNG is injected by direct injection, which is shown in schematic diagram Figure 3, and the engine specifications are listed in Table 3.1. Figure 3.11 indicates the model of the dual fueling system that will be used to test the combustion of the natural gas and added reformed gas

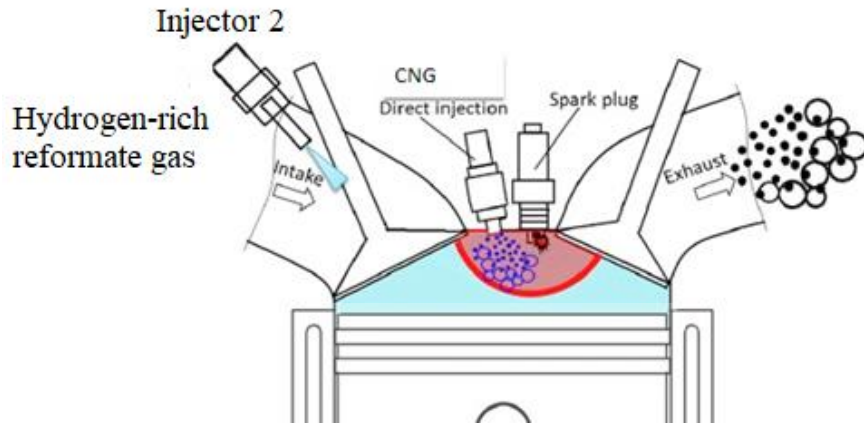
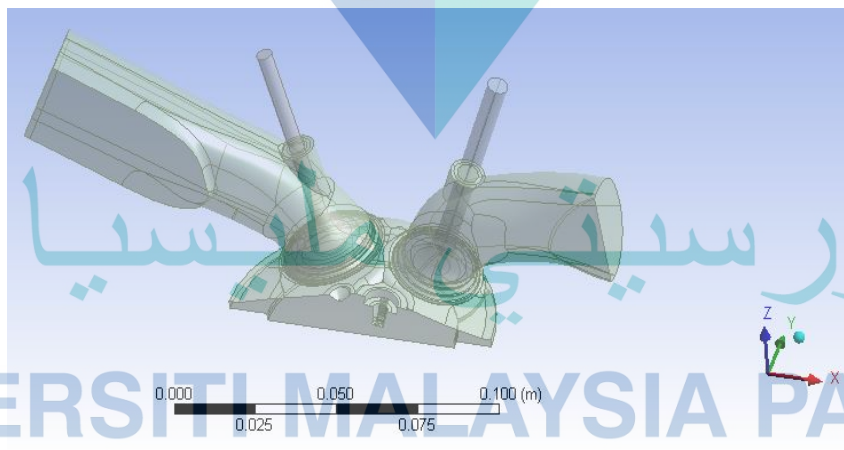


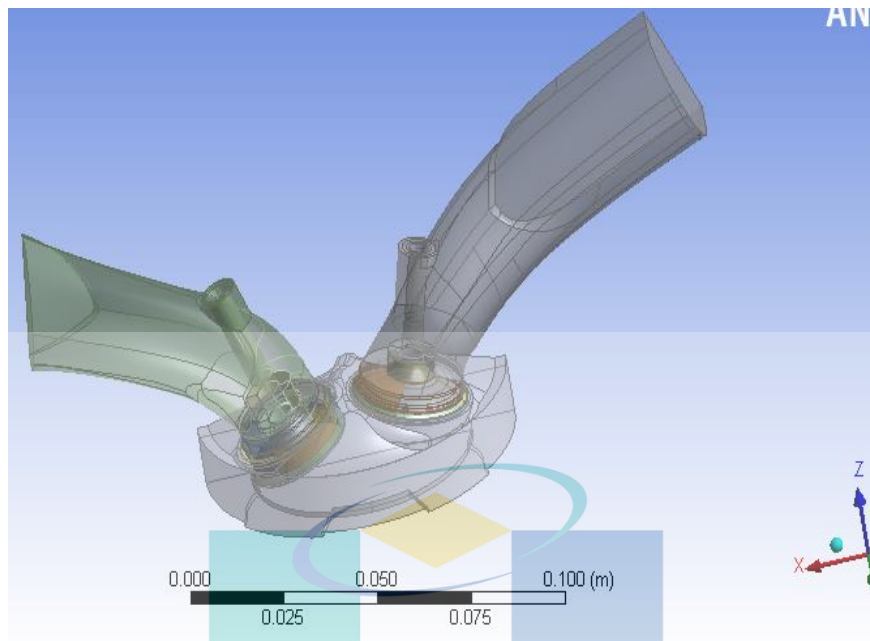
Figure 3.11 Schematic diagram of direct-injection spark-ignition engine

The geometry of the model is then generated using the IC Engine (ANSYS-FLUENT) as shown in Figure 3.12 (a and b). The geometry of the model is generated using IC Engine ANSYS-FLUENT) as shown in Figure3.12a. The geometry is designed as symmetry body since it is a four-strokes engine to reduce computational time. The geometry is then decomposed to generate hexahedral mesh for three-dimensional solid and to simulate the engine with real engine specifications. The decomposed geometry is shown in Figure3.12b



(a) before decomposition

Figure 3.12 Engine geometry



(b) decomposed geometry

Figure 3.12 Continued

### 3.7.2 Mesh Geometry

In order to keep the calculation time within reasonable limits, the type of mesh used in this simulation is default mesh which is coarse meshing with a reference size of 1.395 mm. With these restrictions, the 52,6567 nodes and 1,375,615 nodes are generated. Further refinement of mesh might help to achieve better results, which in turn might slow the computation speed to unacceptable levels. The mesh generated for DISI engine model is shown in Figure 3.13.

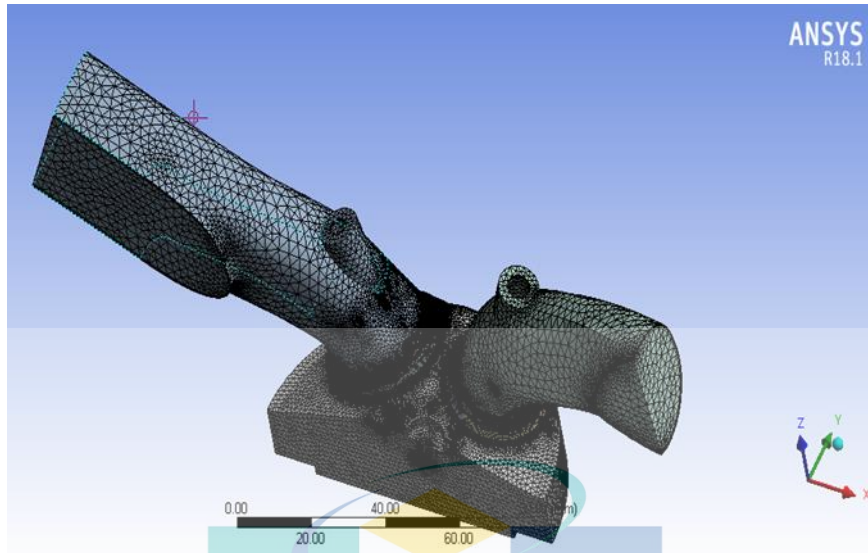


Figure 3.13 A generated mesh of the geometry

### 3.7.3 Cold Flow Simulation

Cold flow analysis involves the simulation of airflow in the transient engine without any reactions taking place. There is not any injection and combustion process during the cold flow analysis. The goal is to observe the airflow and streamline in the engine when the opening and closing of the intake and exhaust valves. Before getting into meshing, the geometry is labelled with the input manager to be selected for cold flow model. The dynamic mesh is generated automatically by the software and it is shown in Apeendix D

#### 3.7.3.1 Boundary Conditions

The simulation continues with the edit solver settings. The engine speed is set at engine speed which is 1,800 rpm, and the number of crank angle is 360°. The boundary condition setting is shown in Table 3.20.

Table 3.20 Boundary condition for cold flow simulation

Zones	Temperature (K)	Pressure (kPa)
ice-outlet-exvalve-1port	333	100
ice-inlet-invalve-1port	313	80
cyl-head	348	
cyl-tri	318	
piston	318	

After setting up the boundary condition, the next step is to run the solution. The double-precision is enabled to increase the accuracy of the solution. The processing option can be changed as high as possible to increase the calculation speed. The ANSYS Fluent initialized the mesh file and patching the solution. Under Run Calculation navigation plane, the Number of Time Steps is set to 2,940, which is calculated from the number of CA to Run set in the Basic Settings dialogue box. The results and data are then collected and analyzed.

### 3.7.4 Combustion Simulation

Combustion simulation involves the simulation of the power stroke during the engine cycle. In this study, two combustion simulation combustion is conducted. One is a simulation with direct-injected natural gas to be validated with the experimental data and the second, to evaluate the effect of the hydrogen-rich reformat on the combustion characteristics compared with the purely natural gas. In this simulation, the EGR rate is set at 25% to use the exhaust gas as much as possible. The combustion is simulation according to the following assumptions.

- The flow used in this study is unsteady.
- The injection timing is at 180° CA.
- The simulation is conducted the ambient pressure and temperature.
- The hydrogen-rich reformat is assumed to be cooled down to the room temperature 300K
- The concentration of the water moisture in the reformat mixture is assumed to be trapped by a moisture trap.

- The radiation heat transfer is ignored.
- The crank angle interval is between 0° and 720°.

### 3.7.4.1 Combustion Simulation of Natural Gas and Boundary Conditions

Before getting into meshing the geometry is labelled with the spark point, beam point, footprint and finally input manager. The coordinate of spark point is 5.5096 mm, 0.94526 mm, -1.6782 mm. The coordinate of beam point is -6 mm, 0 mm, 8.58 mm. The footprint generated with the coordinates file as shown in Figure 3.14 The footprints simulate the real spark points in the combustion chamber of the engine used in this study.

After labelled all the points, the input manager is generated, the spray cone of injection after decomposing, as shown in Figure 3.15. and Figure 3.15.

Table 3.21 Boundary condition for combustion simulation CNG fuel

Part	Zones	Temperature
Head	cyl-head, Invalve1-ch, exvalve1-ch	485 K
Piston	piston	485 K
Liner	cyl-tri	500 K
Exhaust valve	exvalve-lb, exvalve1-ob, exvalve1-stem	777 K
Exhaust port	exvalve1-port, exvalve1-seat	485 K
Intake valve	Invalve1-lb, Invalve1-ob, Invalve1-stem	400 K
Intake port	Invalve1-port, Invalve1-seat	313 K

After setting up the boundary condition, the next step is to run the solution. The double-precision is enabled to increase the accuracy of the solution. The processing option can be changed as high as possible to increase the calculation speed The ANSYS Fluent initialized the mesh file and patching the solution. Under Run Calculation navigation plane, the Number of Time Steps is set to 3,281, which is calculated from the Number of CA to Run set in the Basic Settings dialogue box

```
footprint CNG - Notepad
File Edit Format View Help
# List of Point Coordinates
# Format is: integer Group, integer ID, X, Y, Z
# all delimited by spaces, with nothing after the Z value.
# Group 1
1      1      -9.5   9      -30
1      2       5.3  18     -30
1      3      10     9     -30
```

Figure 3.14 Variation Coordinates file of footprint CNG injection

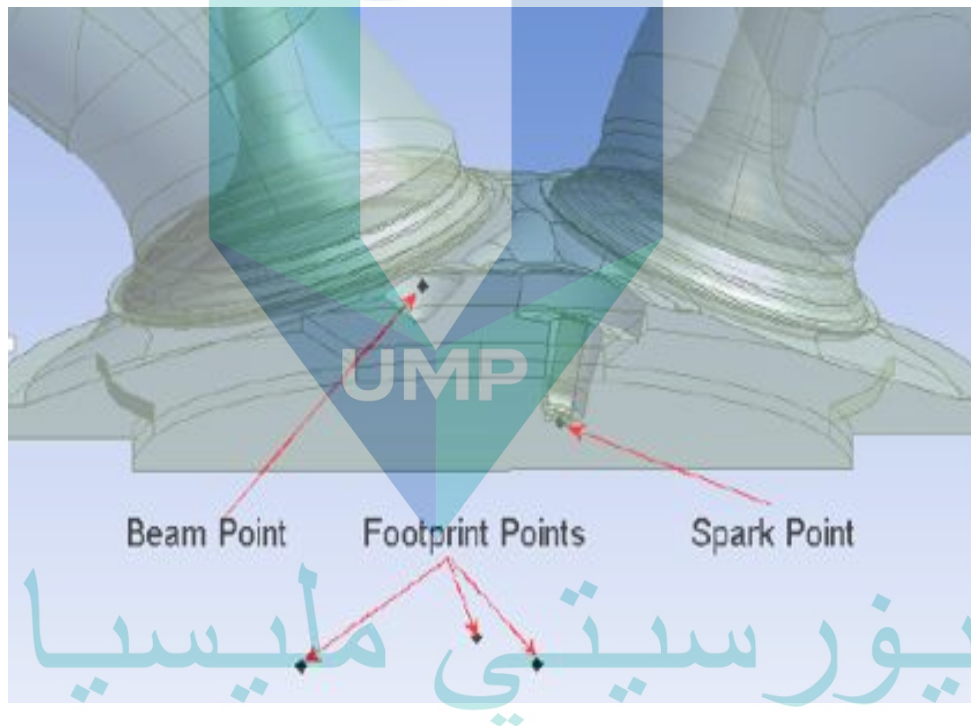


Figure 3.15 Variation Labelled beam, spark, and footprint point

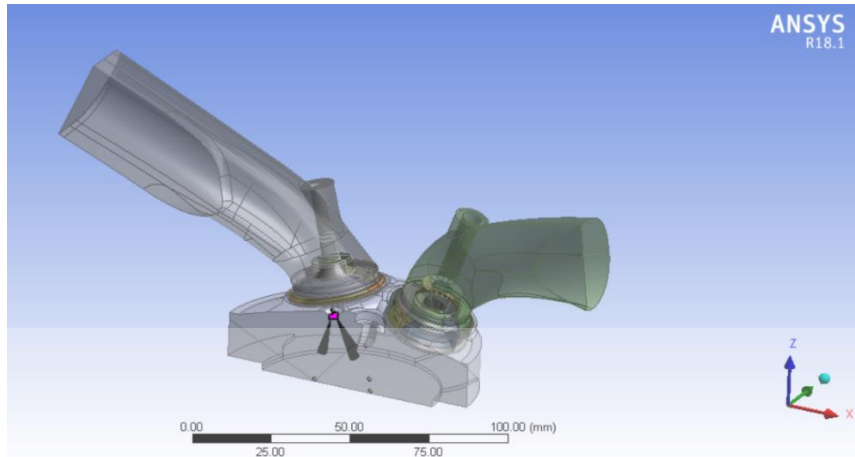


Figure 3.16 Decomposed geometry with spray cone

### 3.7.4.2 Combustion of Natural Gas with The Addition of Hydrogen-Rich Reformate

After the validation of simulation data of natural gas with the experimental data, the simulation is continued with the port-injection of EGR reformed-gas and direct-injection of the natural gas. The step of preparing this simulation is almost similar as in Section 3.7.4.1. The only difference is that a separate port injection is added to the geometry. The coordinate of EGR beam point is -45 mm, 8 mm, 53.58 mm. The footprint of EGR beam is generated with the coordinates file as shown in Figure 3.17. and the labelled points In Figure 3.18.

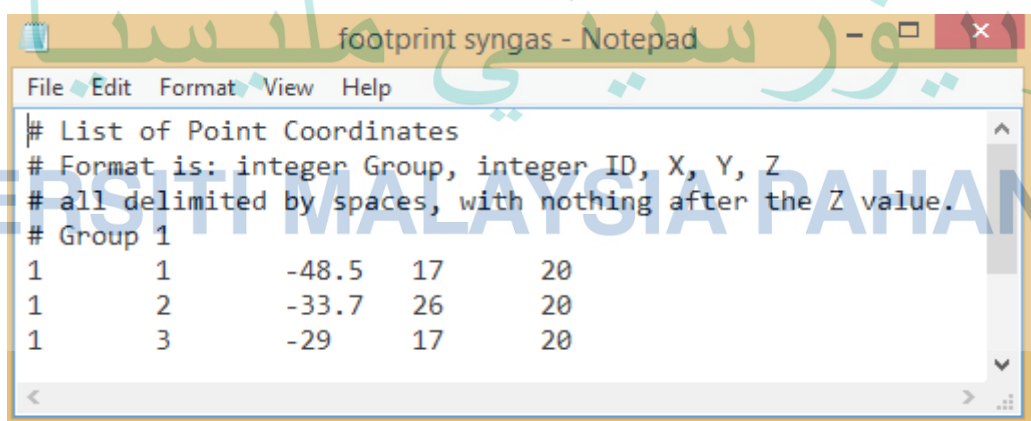


Figure 3.17 Coordinates file of footprint reformat injection

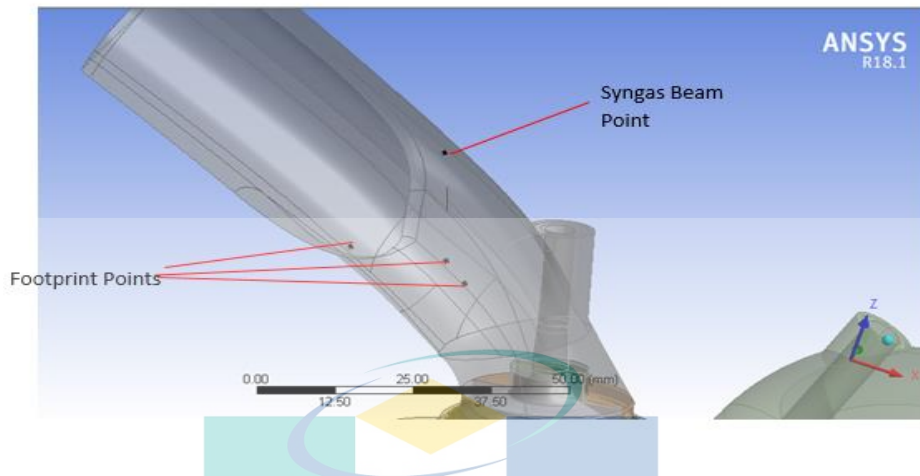


Figure 3.18 Labelled EGR beam point and footprint

The simulation continues with the edit solver settings. The combustion simulation type is Full Engine Full Cycle. The engine speed is set at 1,800 rpm and the number of crank angles to run is 720°. For the physical setting, the engine type is an SI engine with a partially premixed species model since it is turbulence flow.

### 3.7.5 Mathematical Model and Numerical Solution

The unsteady CFD 3D model is developed using the commercial CFD software ANSYS 18.1- IC Engine-FLUENT. This software can solve both the full unsteady RANS equations and the LES equations, thus providing accurate flame propagation models with specific turbulent flame interactions. The following transport equation for the conservation of mass, momentum, energy and turbulence properties is solved:

$$\frac{\partial(\rho\phi)}{\partial t} + \nabla \cdot (\rho u\phi) = \nabla \cdot (\Gamma_{\phi} \nabla (\phi)) + S_{\phi} \quad 3.66$$

where  $\phi$  is the generic transported variable,  $\Gamma_{\phi}$  is the convection term, and  $S_{\phi}$  is the source term

The conservation equation for the chemical species  $k$  is:

$$\frac{\partial \rho_k}{\partial t} + \nabla \cdot (\rho_k u) = \nabla \left[ \rho D_t \nabla \left( \frac{\rho_k}{\rho} \right) \right] + \rho_k^c + \rho_k^s \quad 3.67$$

(k=1,...K)

where  $\rho$  is the density, subscript  $k$  is the species index,  $K$  is the total number of species and  $u$  is the flow velocity vector.

The unsteady-RANS re-normalized group (RNG)  $k$ - $\varepsilon$  model is used for turbulence modelling. The RNG theory for turbulence calculations considers velocity dilatation in the  $\varepsilon$ -equation and spray-induced source terms for both  $k$  and  $\varepsilon$  equations:

$$\frac{\partial \rho k}{\partial t} + \nabla (\rho k u) \quad 3.68$$

$$= -\frac{2}{3} \rho k \nabla \cdot u (\sigma - \Gamma) : \nabla u + \nabla \cdot \left[ \frac{(\mu + \mu_k)}{Pr_k} \nabla k \right] - \rho \varepsilon + W^s$$

$$\frac{\partial \rho \varepsilon}{\partial t} + \nabla (\rho u \varepsilon) \quad 3.69$$

$$= -\left( \frac{2}{3} C_{\varepsilon 1} - C_{\varepsilon 3} \right) \rho \varepsilon \nabla \cdot u + \nabla \cdot \left[ \frac{(v + v_k)}{Pr_k} \nabla \varepsilon \right] + \frac{\varepsilon}{k} (C_{\varepsilon 1} (\sigma - \Gamma) : \nabla u - C_{\varepsilon 2} \rho \varepsilon + C_s W^s)$$

In Equations 3.68 and 3.69,  $C_\varepsilon$  are model constants  $W_s$  is the negative of the rate at which the turbulent eddies are doing work in dispersing the spray droplets and  $C_\varepsilon$  was suggested by Amsden based on the postulate of length scale conservation in spray/turbulence interactions.

The initial turbulent boundary conditions were estimated based on Heywood suggestions, according to the following formulas:

$$k_t = \frac{1}{2} \left[ \frac{2 \cdot \text{strok} \cdot n}{60} \right]^2 \quad 3.70$$

$$\varepsilon = C_\mu k_t^{\frac{3}{2}} L \quad 3.71$$

where  $k_t$  is the initial turbulent kinetic energy,  $n$  is the engine rotational speed,  $C_\mu$  is a model constant equal to 0.0845,  $\varepsilon$  is the dissipation rate, and  $L$  is the turbulent length scale.

The complex chemical reactions, which occur during the combustion process, are described by chemical kinetic mechanisms. These mechanisms define the reaction pathways and the associated reaction rates, thus leading to the change in species concentrations. The ANSYS Fluent solver, coupled with the advanced chemistry solver CHEMKIN-PRO, allows for the modelling of the chemical kinetics of all the  $K$  species related to the combustion process. The Chemkin file used in this simulation is naturalGas\_methane\_MFL2016.cks, which is obtained from the Model Fuel library in ANSYS. The Chemkin file used for hydrogen-rich syngas combustion is naturalGas\_3-comp\_syngas\_chem\_MFL2016 as shown in Appendix B.

### 3.7.6 Flow Rates and Mole Fractions of The Fuels

The flow rate of the natural gas used in this study is 0.3603 g/s, and the air to fuel ratio is 1.1011. Whereas the flow rate of the reformat gas that is used in this study is the outlet flow from the reactor which is (1.414 EGR+0.3603 CNG) and the mole fraction is of the composition is as shown in Table 3.22:

Table 3.22 Mole fraction and flow rate of the reformat gas

Species	Mole fractions	Flow rate (Mol/hr)
$CH_4$	0.06235	13.9655
$H_2O$	0.160	35.83776
$CO_2$	0.08005	17.930
$O_2$	0.001408	0.31537
$H_2$	0.1616	36.1961
$CO$	0.07441	16.6667
$N_2$	0.46018	103.0738
Total flow rate		223.9860

The flow rate of the water steame in this study is negligible. However, the reformat flow rate is:

$$F_{reformat} = F_{total} - F_{steam} = 188.1482 \text{ Mol/hr} \quad 3.72$$

The mole fraction of the reformat gas is computed as shown in Table 3.23.

Table 3.23 Mole and mass fractions and molar and mass flow rate of the reformat gas

Species	Mole fractions	Flow rate (Mol/hr)	Mass fractions	Mass flow rate g/s
$CH_4$	0.07422	13.9655	0.0504	0.0622
$CO_2$	0.09530	17.930	0.1774	0.2192
$O_2$	0.0016761	0.31537	0.00227	0.002801
$H_2$	0.19238	36.1961	0.0164	0.02031
$CO$	0.08856	16.6667	0.10508	0.12967
$N_2$	0.5478	103.0738	0.648	0.802225
<b>Molar flow rate</b>		<b>188.1482</b>	<b>Mass flow rate</b>	<b>1.234</b>

### 3.7.7 Fuel Properties

The engine output is mainly dependent on the chemical energy of the combustion of the fuel injected into the combustion chamber. Combustion in ICE is influenced by the nature of the fuel, the oxidizer geometry of the chamber, among others. This section addresses the nature of the fuel used, the natural gas (methane) and the reformat gas. The details are shown in the following sub-sections.

#### 3.7.7.1 Molecular Weight

The molecular weight of the substance is the sum of the atomic mass of all the atoms in the molecule. The molecular weight of the reformat gas depends on the compositions of the constituent gases. Table 3.24 shows the characteristics features of different pure gases; the molecular weight is, among others. For the reformat gas, the molecular weight is calculated from the pure gas species as shown in Equation 3.73.

Table 3.24 Properties of the pure gases

Properties	CO	H <sub>2</sub>	CH <sub>4</sub>	N <sub>2</sub>	CO <sub>2</sub>
LHV (MJ/kg)	10.01	120.21	35.8	-	-
LHV MJ/Nm <sup>3</sup>	12.6	10.7	35.8	-	-
LFV (cm/s)	28.5	210	40	-	-
Flammability limit (% fuel in air)	12.5-74.2	4.0-74.2	5.0-15.0	-	-
Autoignition Temperature °C	609	500	580	-	-
Adiabatic flame temperature	2112	2110	1947	-	-
Molecular weight (g/mol)	28.01	2.02	16.04	28.02	44.01
Density (kg/m <sup>3</sup> ) at 1 atm	1.17	0.085	0.67	1.17	1.84

$$\begin{aligned}
 \text{Molecular weight } \left( \frac{\text{g}}{\text{mol}} \right) & \qquad \qquad \qquad 3.73 \\
 &= (0.07422 \times 16.04 + 0.09530 \times 44.01 \\
 &+ 0.0016761 \times 32 + 0.19238 \times 2.02 \\
 &+ 0.08856 \times 28.01 + 0.5478 \times 28.02 \\
 &= 23.577 \text{ g/mol}
 \end{aligned}$$

### 3.7.7.2 Density

The fuel injection system meters fuel in volume while the air-fuel ratio which affects the performance and emissions is determined by mass basis. Therefore, determining the density of the gas mixture is essential for the fuel quantity calculation and ignition quality analysis. The density of gases depends on temperature and pressure. For the mixture of the reformat gas, density depends on the constituent's gases density and the percentage composition in the mixture. Table 3.24 shows the different properties of the pure gases that major species of the reformat gas. The density of the reformat gas in kg/m<sup>3</sup> is calculated based on the density's at 20°C constituents' gases and 1 atm as shown in Equation 3.74.

$$M_{\text{reformat}} = \rho_{\text{CH}_4} y_{\text{CH}_4} + \rho_{\text{CO}_2} y_{\text{CO}_2} + \rho_{\text{H}_2} y_{\text{H}_2} + \rho_{\text{CO}} y_{\text{CO}} + \rho_{\text{O}_2} y_{\text{O}_2} + \rho_{\text{N}_2} y_{\text{N}_2} \quad 3.74$$

$$M_{\text{reformat}} = 1.26 \text{ kg/m}^3$$

Therefore, the density of the reformat gas at an ambient temperature and pressure is:

$$\rho_{\text{reformat}} = 1.26 \text{ kg/m}^3.$$

### 3.7.7.3 Calorific Value

The LHV for the gaseous fuels is calculated by the summation of the partial LHV of each individual combustible gas components in the gas mixture as shown in Equation 3.75, mathematically expressed as

$$LHV = \sum y_i LHV_i \quad 3.75$$

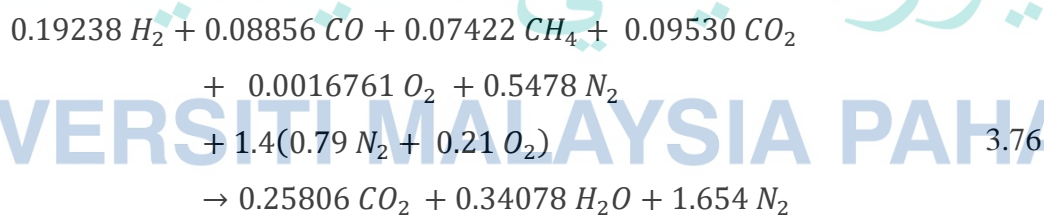
where  $y_i$  is the volume fraction of combustible gas components  $LHV$  is the volume basis and mass basis  $LHV$  of combustible gas components from Table 3.24 . The calorific value is calculated by Equation 3.75. The values of the calorific value of the reformat gas is as shown in the Table 3.25:

Table 3.25 Volume basis and mass basis LHV of the reformat gas

Fuel	Species of the reformat gas						$LHV$
	$H_2$	$CO$	$CH_4$	$CO_2$	$O_2$	$N_2$	
Volume	0.19238	0.08856	0.07422	0.09530	0.0016761	0.5478	5.83 MJ/Nm <sup>3</sup>
Mass	0.0164	0.10508	0.0504	0.1774	0.00227	0.648	5.54 MJ/kg

#### 3.7.7.4 Stoichiometric Air-Fuel Ratio

The reformat mixture contains combustible and non-combustible gases which affect the combustion reaction. Therefore, combustion of the reformat gas in ICE is unique in nature that requires a different approach. Apart of this, the air-fuel ratio is also an influential parameter as far as combustion is concerned. Combustion is considered to be stoichiometric if there is enough oxygen conversion of all the fuel into completely oxidized products. For the reformat gas, the complete combustion equilibrium reaction is



Calculating the stoichiometric air-fuel ratio, the mass flow rate of fuel (reformat gas) reactant was 23.64 g and that the air is 40.4 g. Therefore the mass basis and molar basis stoichiometric air-fuel ratio were calculated to be 1.71 and 1.4, respectively.

### 3.7.8 Combustion Characteristics Calculation

The cylinder pressure versus crank angle changes as a result of the cylinder volume changes, heat transfer to the chamber walls, flow into and out of the crevice regions and due to the leakage. Pressure due to cylinder volume changes and heat transfer to the chamber walls take the major share. The variation of the operating parameters on the heat release rate can be more understood by the zero-dimensional models. The combustion rate can be analyzed from the CFD pressure results based on the first thermodynamics using the simplest and most suitable model. Single and multi-zone models are used in the analysis of the combustion rate. In a single-zone model, the thermodynamic state of the cylinder content is treated to be uniform throughout, represented by an average value. Due to its simplicity, a single-zone model is widely used in the combustion rate analysis from pressure reading. A single-zone zero-dimensional model is preferred in the current study. Applying the first law of thermodynamics to an open-system boundary similar to a combustion chamber,

$$\delta Q - \delta W = dU - \sum_i h_i dm_i \quad 3.77$$

where  $dU$  is the internal energy changes of the mass in the system,  $\delta Q$  is the heat transfer to the system,  $\delta W$  is the work done by the system which is equal to  $PdV$  and  $\sum_i h_i dm_i$  is the enthalpy flux across the system boundary. Assumptions are taken in the analysis:

- Single zone model: in-cylinder contents are considered to be uniform throughout the chamber.
- Combustion is modelled as a heat energy release.
- The heat released is uniform throughout the chamber.
- The gas mixture is taken as an ideal gas.

The energy balance in Equation 3.78 depends on the accurate quantification of each term in the equation. The heat transferred to the system ( $\delta Q$ ) is equal to the heat

release from the chemical energy  $\delta Q_{ch}$  less the heat transfer to the chamber walls ( $\delta Q_{ht}$ ). The change in sensible energy as a function of temperature, given by  $mu(T)$ , where  $T$  is the mean change in temperature. By including the crevice effect and use of ideal gas law, the gross heat release rate is derived from the following equation:

$$Q_{ch} = \frac{1}{\gamma - 1} V dP + \frac{\gamma}{\gamma - 1} P dV + (h' - u + C_v T) dm_{cr} + \delta Q_{ht} \quad 3.78$$

where  $\gamma$  is the specific heat ratio and its value in this study is 1.33. Both the net and gross heat release rates can be calculated from Equation 3.71. The net heat release rate versus crank angle is calculated as follows:

$$\frac{dQ_{net}}{d\theta} = \frac{1}{\gamma - 1} V \frac{dP}{d\theta} + \frac{\gamma}{\gamma - 1} P \frac{dV}{d\theta} \quad 3.79$$

The MFB versus crank angle can be derived by integrating the net heat release rate in Equation 3.72, normalized to give unity at its maximum value,

$$X(\theta) = \frac{\int_{\theta_s}^{\theta} \frac{dQ_{net}}{d\theta} d\theta}{\int_{\theta_s}^{\theta_{EOC}} \frac{dQ_{net}}{d\theta} d\theta} \quad 3.80$$

### 3.8 Combustion validation

The combustion simulation is validated with an experimental data of the the in-cylinder pressure for the same engine specification of the engine used in this study. The validation was conducted with the experimental data, which was collected experimentally by (Hagos, et al., 2014a). The validation is performed using natural gas. It is found consistent between the simulation results and experimental. In some crank angles, the relative error reached 2%. The average error of the in-cylinder pressure at all the crank angles is 8%. The highest and lowest error along the crank angles was 18% and 2% respectively as shown in Figure 3.19

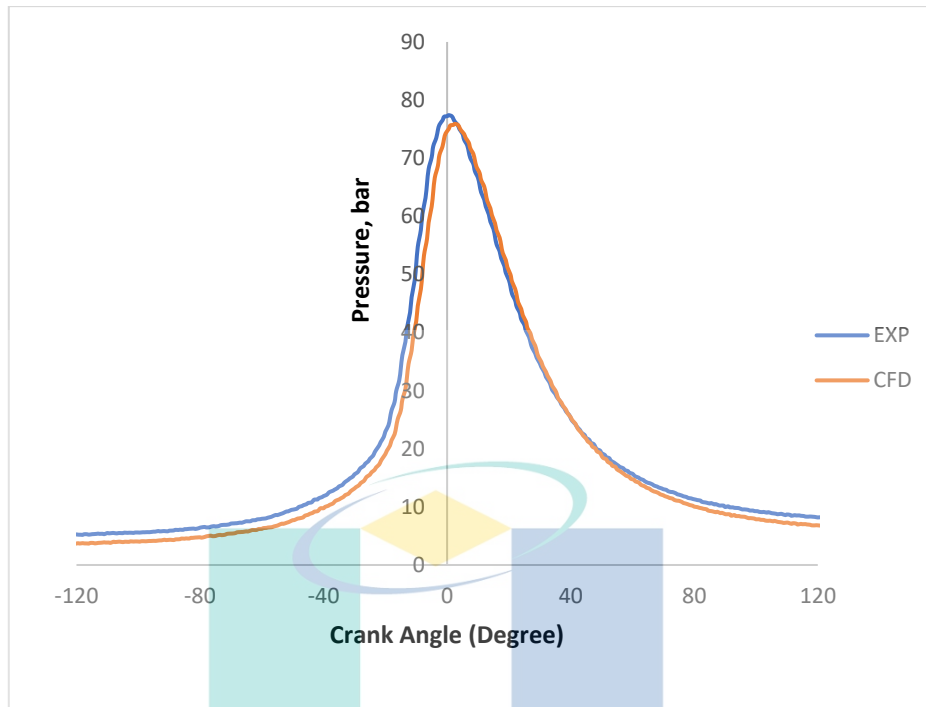


Figure 3.19 Comparison between experimental data and CFD simulation

UMP

اونيورسيتي ملايسيا قهغ

UNIVERSITI MALAYSIA PAHANG

## CHAPTER 4

### RESULTS AND DISCUSSION

#### 4.1 Introduction

The objective of this study was to investigate the process of hydrogen-rich syngas production through on-board exhaust gas reforming. Besides, the evaluation of the effect of the addition of reformat gas (hydrogen-rich syngas) produced from the exhaust gas reforming process on the combustion characteristics compared with natural gas combustion.

However, this chapter contains three parts. The first part shown in sections 4.2 shows the discussion of objective 1. It describes the reforming characteristics at the engine speeds used in this study. This section shows how the syngas production and methane conversion is affected by the variation of catalyst mass and natural gas flow rate, as shown in section 4.2.1. The aim of this investigation was to determine the natural gas flow rate and catalyst mass at each engine speed as shown section 4.2.2

Subsection 4.2.3. discusses the results of the RSM optimization. This part targets to determine the optimum syngas production and methane conversion at a minimum natural gas flow rate and catalyst mass. This section is necessary to determine a unified flow rate and catalyst mass for the engine speeds.

After optimizing the catalyst mass and natural gas flow rate, the reactor size was optimized and simulated by 1D and 2D modelling in the second part described in section 4.3 which presented objective 2. This section illustrates the reforming characteristics at different parameters. This section is important because its results can be used as a reference for reactor prototype design and fabrication.

The third part indicates the effect of reformat addition on the cold flow and combustion characteristics which is objective three discussions. The importance of this

section was to evaluate whether the addition of reformat can achieve any significant enhancement in the combustion of the SI engine compared with purely natural gas combustion.

#### **4.2 The Demanded Amount of Catalyst Mass, Natural Gas Flow Rate and The Effect of Engine Speed on Reforming Characteristics**

This section shows the variation of reforming characteristics with the change of methane flow rate and catalyst mass. The reforming characteristics are mainly described by methane conversion and syngas production.

##### **4.2.1 Variation of Natural Gas Flow and Catalyst Mass with the Engine speed**

The flow rates are determined by the ratio of methane to exhaust. The flow rate at each ratio for each speed is shown in Table 3.5.

Figure 4.1a shows the methane conversion at different natural gas flow rates at 1,200 rpm. It is found that as the ratio of natural gas to exhaust become higher than 0.15, the methane conversion and syngas started to decrease. This is because as the amount of methane is higher in the mixture, higher temperature and more steam is required to achieve higher conversion and syngas production.

Figure 4.1b shows the effect of reforming characteristics while the engine is operated at 1,200 rpm at different catalyst mass at the ratio of methane to exhaust of 0.15, which is equivalent to 21.43 mol/hr of methane flow rate. It is shown that the reforming performance increased with the rise of catalyst mass and became constant at 800 g. The temperature of the reaction increased from 761 to 850.4 K, this rise of temperature is due to the consumption of air which has led an oxidation reaction (reaction 4 in Table 3.9). It reached at its peak at 800 g because at this catalyst mass the consumption of air become 98%. This rise of temperature led to higher reforming performance in terms of methane conversion and hydrogen production because the steam reforming reaction is preferred at a higher temperature (Zhang, et al., 2018). Therefore, the rate of methane consumption and hydrogen production became higher at a higher temperature. Besides, the higher carbon dioxide consumption increased with the rise in temperature.

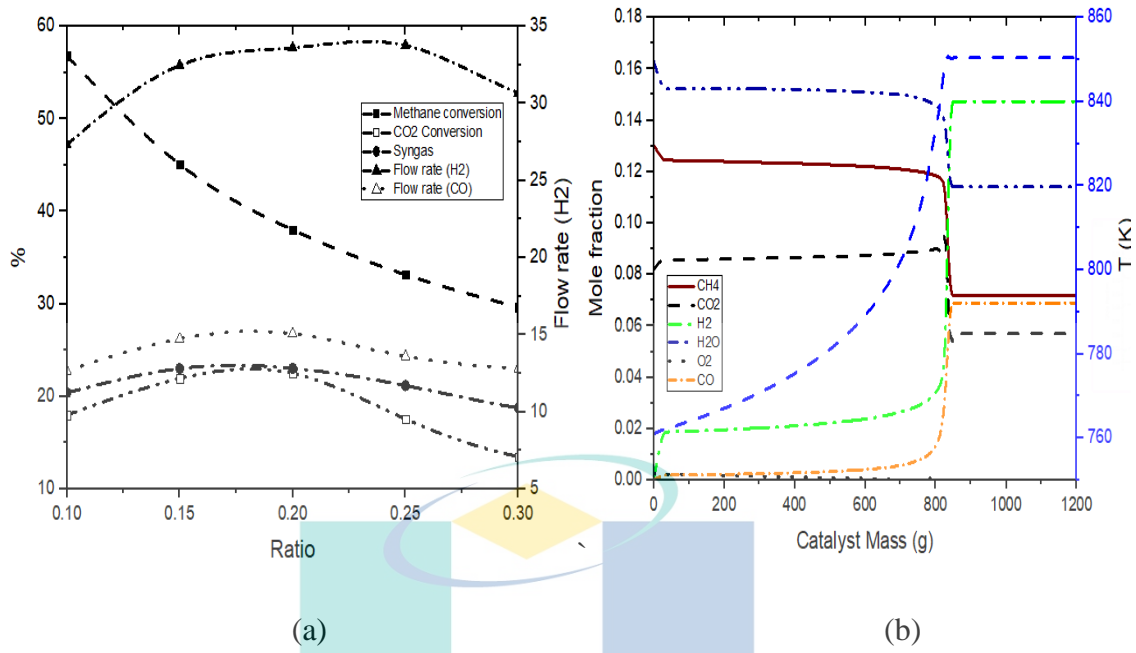


Figure 4.1 Methane conversion and syngas percentage at different ratio of methane flow rate to exhaust gas flow rate (a) reforming characteristics at 1,200 rpm at 0.15 ratio of methane to exhaust (b).

Figure 4.2 (a) shows the reforming performance represented by methane conversion and syngas production ( $H_2+CO$ ) at different methane to exhaust ratio at 1,500 rpm. The maximum methane conversion and syngas production is achieved at a ratio of 0.1 and 0.15, respectively. The higher methane conversion at 0.1 is due to the higher ratio of steam to natural gas which is 1.87 and 1.25 at 0.15 methane to exhaust ratio. Thus, because as the amount of methane increased in the reforming reactants, more steam is needed (Baxter, et al., 2008a). Therefore, the flow rate of natural gas at the ratio of 0.15, which is 26.745 mol/hr is selected.

Figure 4.2 (b) illustrates the reforming characteristics of natural gas at different amount of catalyst at 26.745 mol/hr natural gas flow rate. As the amount of catalyst increased, the reforming efficiency gets higher. Thus, due to the rise of the reaction rate as the catalyst increased. Thus, the reforming consumption and formation of all reactant became constant at approximately 700 g because, to achieve more conversion and syngas production, the mixture of the reactant must be changed, or more heat needs to be added.

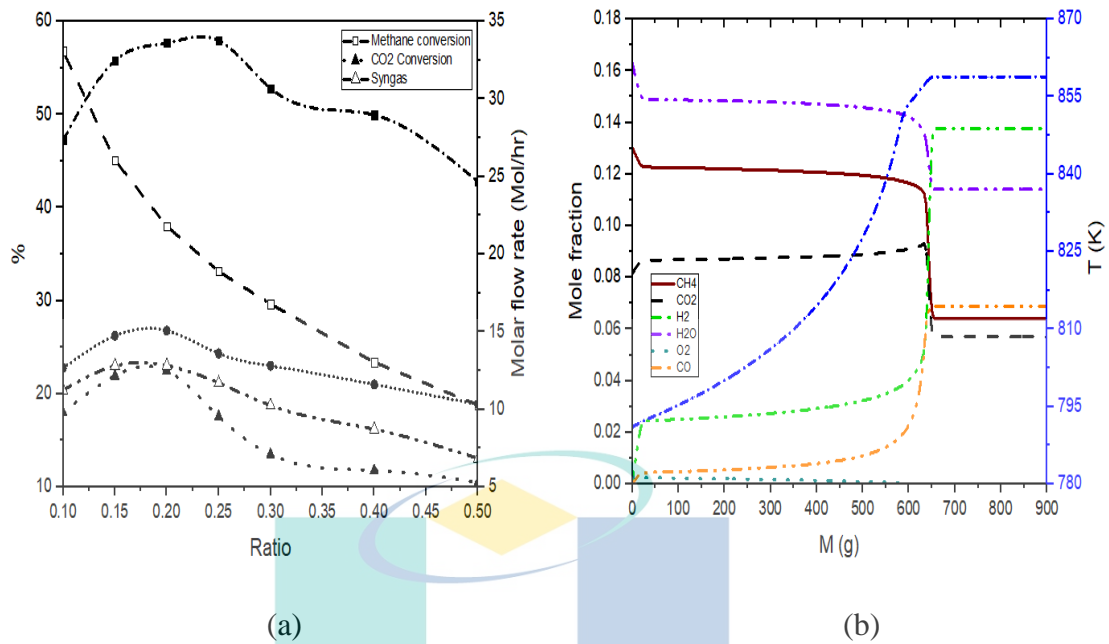


Figure 4.2 Methane conversion and syngas percentage 15,00 rpm at different ratio of methane flow rate to exhaust gas flow rate (a) reforming characteristics at 0.15 ratio of CH<sub>4</sub> to exhaust (b).

Figure 4.3 shows the reforming process at 1,800 rpm. The reforming performance at different natural gas (CH<sub>4</sub>) flow rates represented by the ratio of methane to exhaust gas is shown in Figure 4.3a. It is shown that the reforming performance is tested at five different methane flow rate (ratios). The methane conversion achieved its peak value (59%) at 0.1 ratio of methane to exhaust, which is 19.48 mol/hr due to the higher ratio of steam to methane. This rise contributes to the increasing of the rate of steam reforming rate. At the same flow rate, the syngas fraction is 20.1%. The maximum syngas production is obtained at 0.2 ratio methane to exhaust, which is 25.75%. The syngas achieved its peak at this ratio due to the rise of the hydrogen and carbon monoxide with the rise of the ratio from 0.1 to 0.2. The maximum conversion of carbon dioxide was 15.1% at the 0.25 methane to exhaust ratio (48.7 mol/hr) because of the rise of methane in the reactant mixture led to higher combustion reaction rate (reaction 4 in Table 3.9). This rise of reaction rate produces more heat, and carbon dioxide became more desired as the reaction temperature increased (Zhang, et al., 2018). The reforming performance in this study depends mainly on the amount of syngas production (H<sub>2</sub>+CO). However, the flow rate of natural gas (38.954 mol/hr) at 0.2 ratio of methane to exhaust is selected at this speed.

Figure 4.3b shows the variation of reforming characteristics with the amount of catalyst. It can be noticed that the rate of consumption and formation reach its maximum value at 550 g. This value is considered to be sufficient to achieve the maximum value. The amount of methane conversion, syngas production and carbon dioxide conversion has increased with the amount of catalyst. The rise of the amount of catalyst increased the reaction speed higher due to the rise of the reaction rate. Therefore, the complete oxidation reaction (methane combustion) occurred that lead to more heat addition and this heat is demanded to achieve more consumption of methane and carbon dioxide and more hydrogen generation (Ma, et al., 2019).

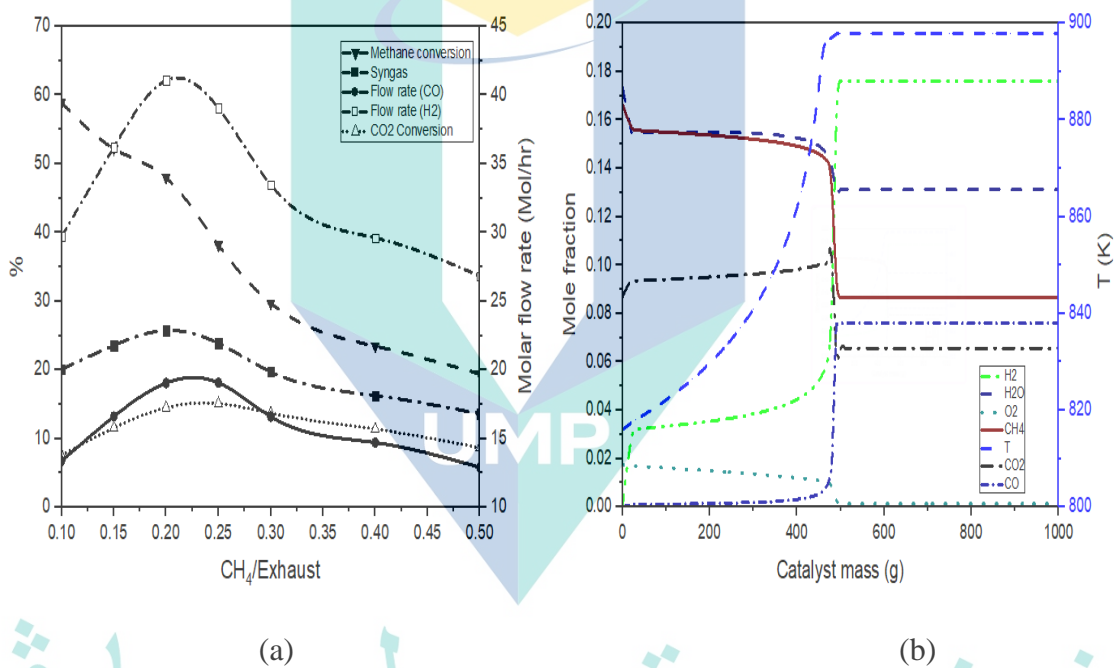


Figure 4.3 Reforming performance at different ratio of methane flow rate to exhaust gas flowrate (a) reforming characteristics at 1,800 rpm at 0.2 ratio of CH<sub>4</sub> to exhaust at 1,800 rpm (b).

The variation of reforming characteristics with the natural gas (CH<sub>4</sub>) flow rates and catalyst mass are at 2,100 rpm is shown in Figure 4.4. As shown in Figure 4.4a, the methane conversion has decreased as the amount of natural gas flow rates increased due to the rise of the ratio of steam to methane. Steam to methane ratio is 2.2 at 0.1 ratios of methane to exhaust and 0.435 at the maximum (0.5) ratio of methane to exhaust. Therefore, the methane conversion has decreased because to achieve more conversion, more steam or heat must be added. Whereas, the maximum syngas production is obtained

at 0.2 ratios of methane to exhaust, and it is 26.013% which has a natural gas flow rate of 41.904 mol/hr and the methane conversion at the same flow rate was 52.65%. The maximum syngas production is achieved at this flow rate due to the sufficient amount of methane compared to the other flow rates, which can be converted to hydrogen and carbon monoxide. Also, it is seen that carbon dioxide conversion has its maximum value at 0.25 and 0.2 ratios of methane to exhaust ratio, which is 14.45% and 13.61%, respectively. The carbon dioxide conversion has increased at these flow rates because the ratio of air to methane are more convenient than the others. The ratios of air to methane is 0.09 and 0.11 at 0.2 and 0.25 ratios of methane to exhaust, respectively. This slight rise of carbon dioxide conversion is due to the higher amount of methane that led to higher reaction temperature because DRM reaction is more desired at the elevated temperature (Sengodan, et al., 2018).

However, the flow rates of natural gas at 0.2 ratios of methane to exhaust ratio is selected at 2,100 rpm engine speed. The reforming characteristics at this flow rates with the change of mass catalyst is shown in Figure 4.4b. It is shown that the most desired reforming characteristics are obtained at catalyst mass of 500 g because as the amount of catalyst increased, reaction duration would be shortened due to the rise of reaction rate values. Besides, the higher consumption of oxygen which leads to more heat which increased the reaction temperature (Arku, et al., 2018).

اونيورسيتي ملايسيا قهغ

UNIVERSITI MALAYSIA PAHANG

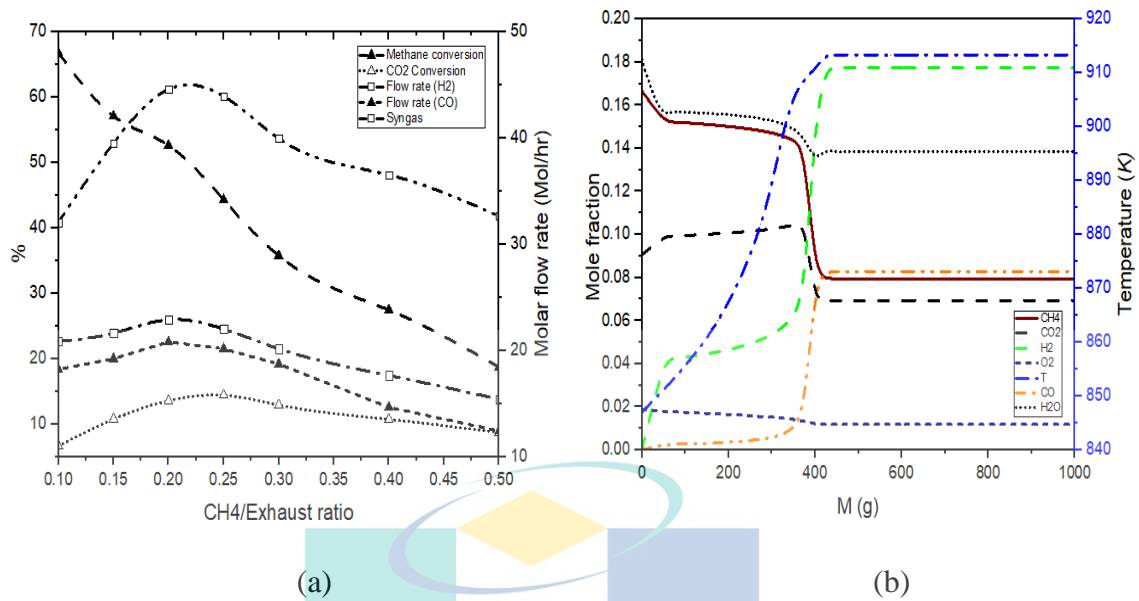


Figure 4.4 Reforming performance at different ratio of methane flow rate to exhaust gas flow rate (a) reforming characteristics at 2,100 rpm at 0.2 ratio of CH<sub>4</sub> to exhaust (b). (Continued)

Figure 4.5a shows the effect of natural gas flow rates on the reforming characteristics at 2,400 rpm. It is noticed that the maximum conversion occurred at 0.1 ratio due to the small amount of methane to the steam. Whereas the maximum syngas production is achieved at 0.25 and 0.2 with the value of 26.64% and 25.844%, respectively and the values of methane conversion are 44% and 55.3%, respectively. The higher amount of syngas at the ratio of 0.25 is due to the higher amount of methane which provides more heat release from the combustion reaction (complete oxidation). This heat increased the reaction temperature from 865 to 931 K. This rise of temperature cannot be achieved at the other natural gas flow rates because of the ratio of air to methane was less convience than 0.25 and 0.2 which are 0.170 and 0.213, respectively. These ratios of air to methane are considered to be more desired than the others as stated by Bulutoglu et al (Bulutoglu, et al., 2015). The carbon dioxide conversion rate has reached its peak at 0.25 ratios, and it is reported 4.47% and 3.967% at 0.2 ratios. This value is achieved due to the higher reaction temperature. In this case, the lower flow rates are selected because the flow rate of natural gas that enters the reformer must be lower as possible and the much higher methane conversion. Besides, the amount of produced syngas and carbon dioxide conversion at 0.2 and 0.25 are too close. Therefore, the flow rate at 0.2 ratios is selected.

Figure 4.5b shows the variation of reforming characteristics at different amount of catalysts at 2,400 rpm. It is shown that the reforming performance increased with the higher amount of catalyst. And the best performance is achieved at 550 g. After this value, the reforming performance became constant because the consumption and formation rates of species reached their maximum. In order to achieve more consumption or generation, the mixture of the reactants must be changed or more air, steam or heat must be added.

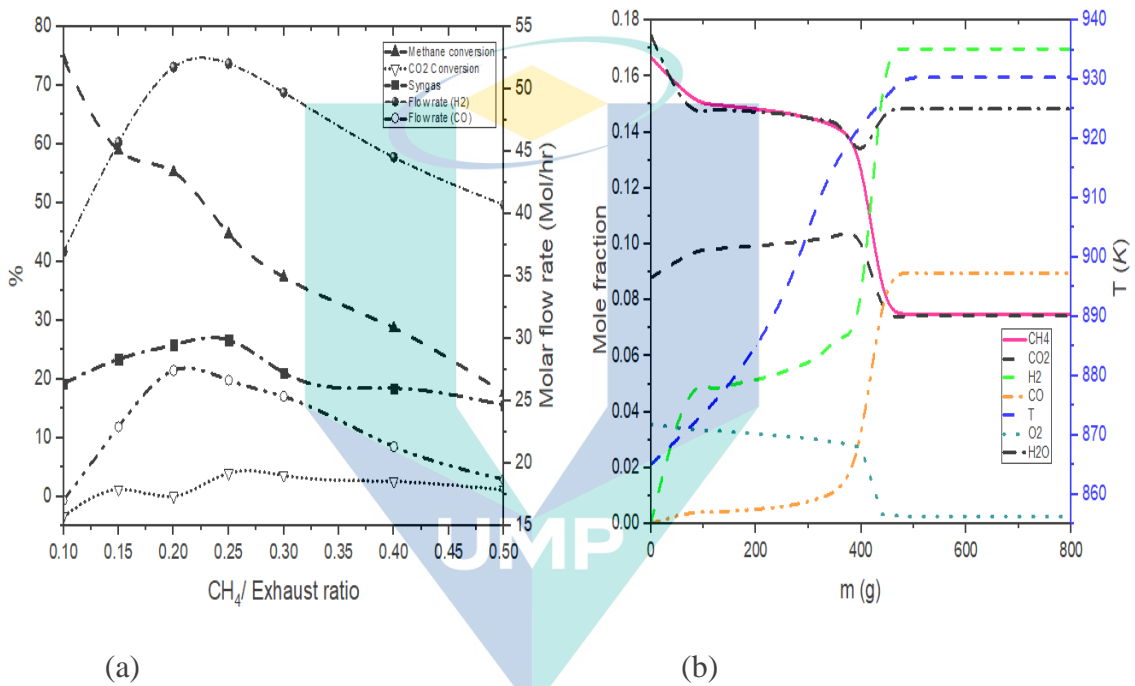


Figure 4.5 Reforming performance at different ratio of methane flow rate to exhaust gas flow rate (a), reforming characteristics at 2,400 rpm at 0.2 ratio of CH<sub>4</sub> to exhaust (b).

Figure 4.6 shows the effect of methane flow rate and catalyst mass on the reforming characteristics at 2,700 rpm. In Figure 4.6a, it is shown that methane conversion has decreased as the methane flow rate increased due to the high ratio of steam to methane that has increased the rate of methane consumption through steam reforming. The lowest value of syngas is found at the lowest natural gas flow rate because of the insufficient amount of methane that can be converted to hydrogen. The highest amount of hydrogen is produced at 0.15 and 0.2 ratio of methane to exhaust, which is equivalent to the methane flow rate of 54.11 mol/hr and 72.146. The syngas fraction at these ratios

are 22.445% and 22.662%, and methane conversion are 58.671% and 47.36%, respectively. Therefore, the natural gas flow rate at the ratio of 0.15 is selected due to the lower flow rate and the higher methane conversion.

Figure 4.6b shows the effect of catalyst mass on the reforming characteristics. The desired reforming characteristics are achieved at above 400 g, and it became constant after this amount of catalyst. This is because the sufficient amount of catalyst to increase the rate of combustion reaction to its maximum value, which is related to various variables such as, reaction temperature and the reactant compositions. Therefore, the temperature of the reaction increased with the higher amount of catalyst which has motivated the rates of consumption and generation of species to be increased.

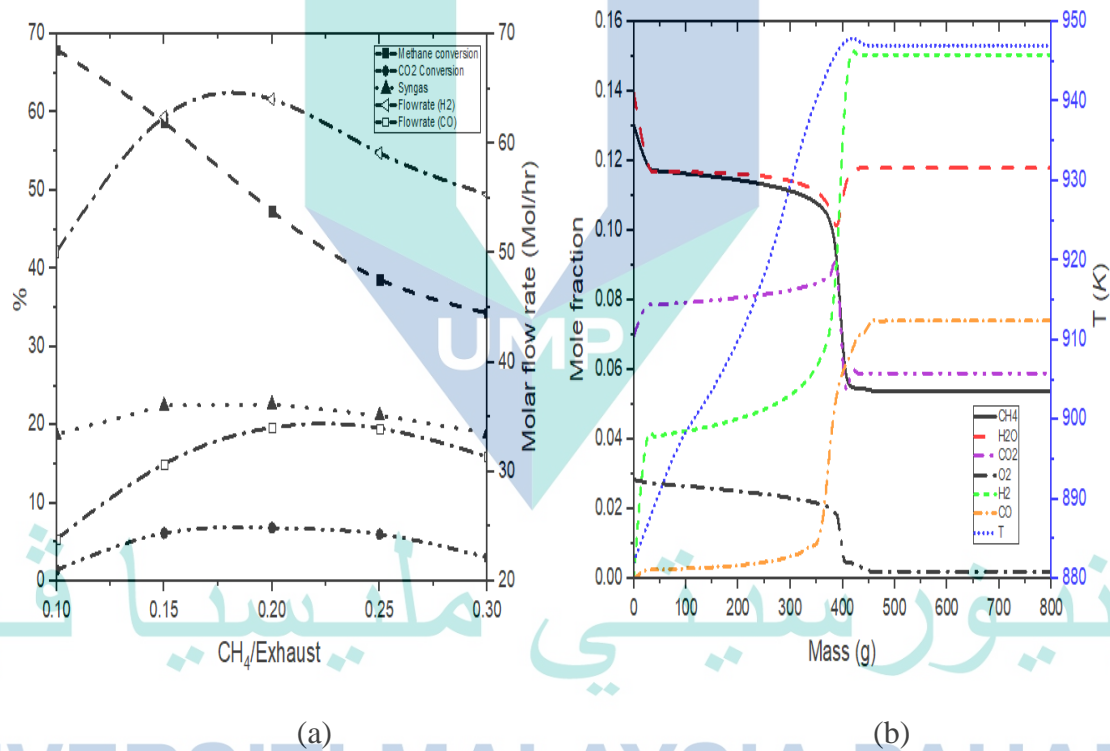


Figure 4.6 Reforming performance at different ratio of methane flow rate to exhaust gas flow rate (a) reforming characteristics at 2,700 rpm at 0.2 ratios of CH<sub>4</sub> to exhaust (b). (Continued)

Figure 4.7a shows the effect of the natural gas flow rate on the reforming performance, which is mainly evaluated by the amount of produced syngas and methane conversion. It is shown that the maximum methane conversion is obtained at the lowest natural gas flow rate (0.1 ratio of methane to exhaust) due to the higher of steam to

methane compared to the other ratios. Whereas the highest fraction values of syngas are obtained at ratio 0.15 and 0.2, respectively. The higher amount is due to the higher generation of hydrogen to carbon monoxide as shown in the trend of the H<sub>2</sub> and CO flow rate because of the higher consumption of carbon dioxide. Therefore, the flow rate at 0.15, which is 62.85 mol/hr.

Figure 4.7b illustrates the reforming characteristics at various catalyst mass. It is shown that the optimum reforming performance is achieved at 350 g due to the amount of heat release from the combustion reaction. This has led to higher consumption and formation rate of species. At the masses above this value became constant because to achieve more performance, the mixture of the reactants needs to be changed by adding or reducing the reactant fractions.

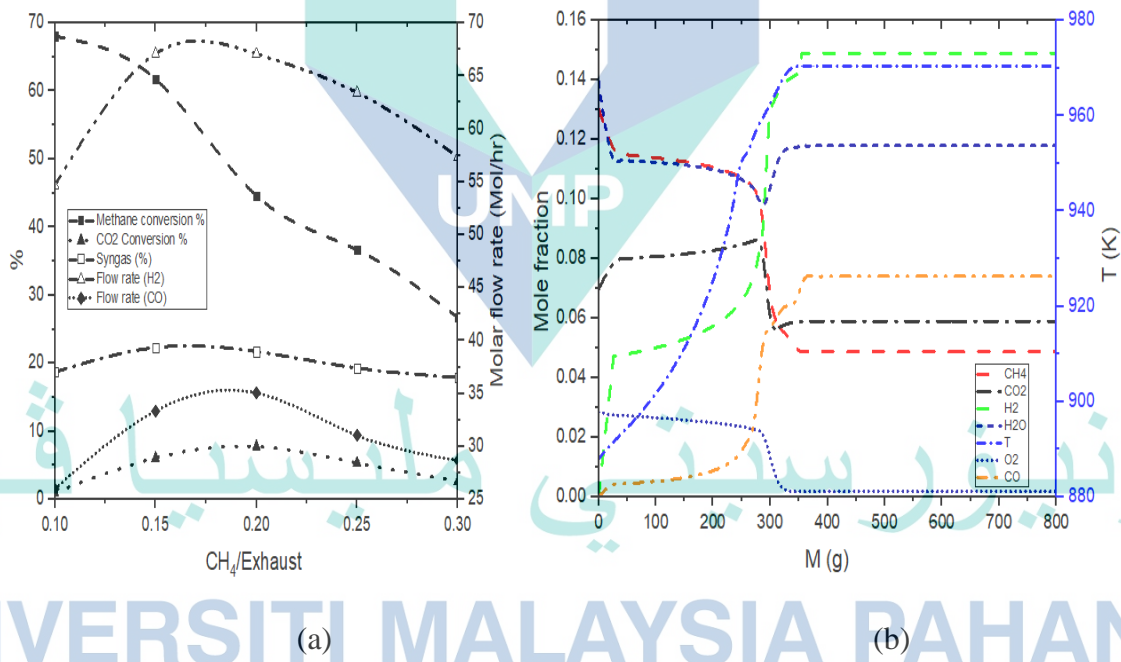


Figure 4.7 Reforming performance at different ratio of methane flow rate to exhaust gas flow rate (a) reforming characteristics at 0.2 ratio of CH<sub>4</sub> to exhaust (b). at at **3,000 rpm**

#### 4.2.2 Effect of Engine Speeds on Reforming Characteristics

Table 4.1 shows the selected catalyst mass and methane flow rate at each engine speed. It is illustrated that the catalyst mass decreases as the engine speed increased. This rise of catalyst mass is due to the higher amount of oxygen in the exhaust compositions as the engine speeds increased. Whereas the flow rate of methane increased as the engine speeds. Because to achieve higher performance of reforming the amount of natural gas must be identical as much as possible.

Table 4.1 Catalyst mass and methane flow rate at each engine speed.

Engine speed (rpm)	Catalyst mass (g)	CH <sub>4</sub> flow rate (Mol/hr)
1200	850	21.43
1500	800	26.745
1800	700	38.954
2100	600	41.904
2400	550	51.09
2700	450	54.11
3000	350	62.85

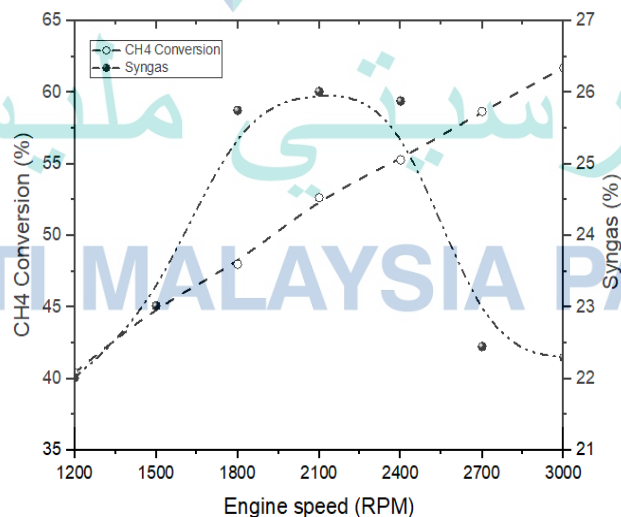


Figure 4.8 Effect of engine speed on methane conversion and syngas production

The effect of engine speed on the reforming characteristics at these parameters is shown in Figure 4.8. It is shown that the methane conversion has increased with higher engine speeds. This rise is mainly due to the higher temperature of the exhaust at the elevated engine speeds. The high temperature provides better circumstances to enhance reforming performance, especially increase the methane conversion. Syngas production has increased with the engine speed, and it has achieved the maximum produced amount at 2,100 rpm and then started to decline gradually from 26.013% at 2,100 rpm to 22.3% at 3,000 rpm. This reduction of produced syngas is due to the rise of carbon dioxide in the reactant mixture which requires a higher temperature and additional amount of steam to reduce the rate of steam-water gas shift reaction which releases more carbon dioxide.

#### **4.2.3 Optimization of The Amount of Demanded Natural Gas Flow Rate and Catalyst Mass**

RSM optimization results show the relationship between the reforming variables (speed, catalyst mass and natural gas flow rate) and their effects on the reforming characteristics (methane conversion and produced syngas). This optimization model is aimed to select one minimum catalyst mass and natural gas flow rate at all the engine speeds to achieve the possible maximum syngas. Since the optimization model is multi-objective, the results are divided into syngas production and methane conversion, as shown in the following subsections.

اونيورسيتي ملايسيا قهغ

UNIVERSITI MALAYSIA PAHANG

#### 4.2.4 Statistical Analysis

The transform models of methane conversion and syngas were selected by testing each one and compare the predicted and the actual modelling data and the average error of all the data as shown in Figure 4.9 and Figure 4.10

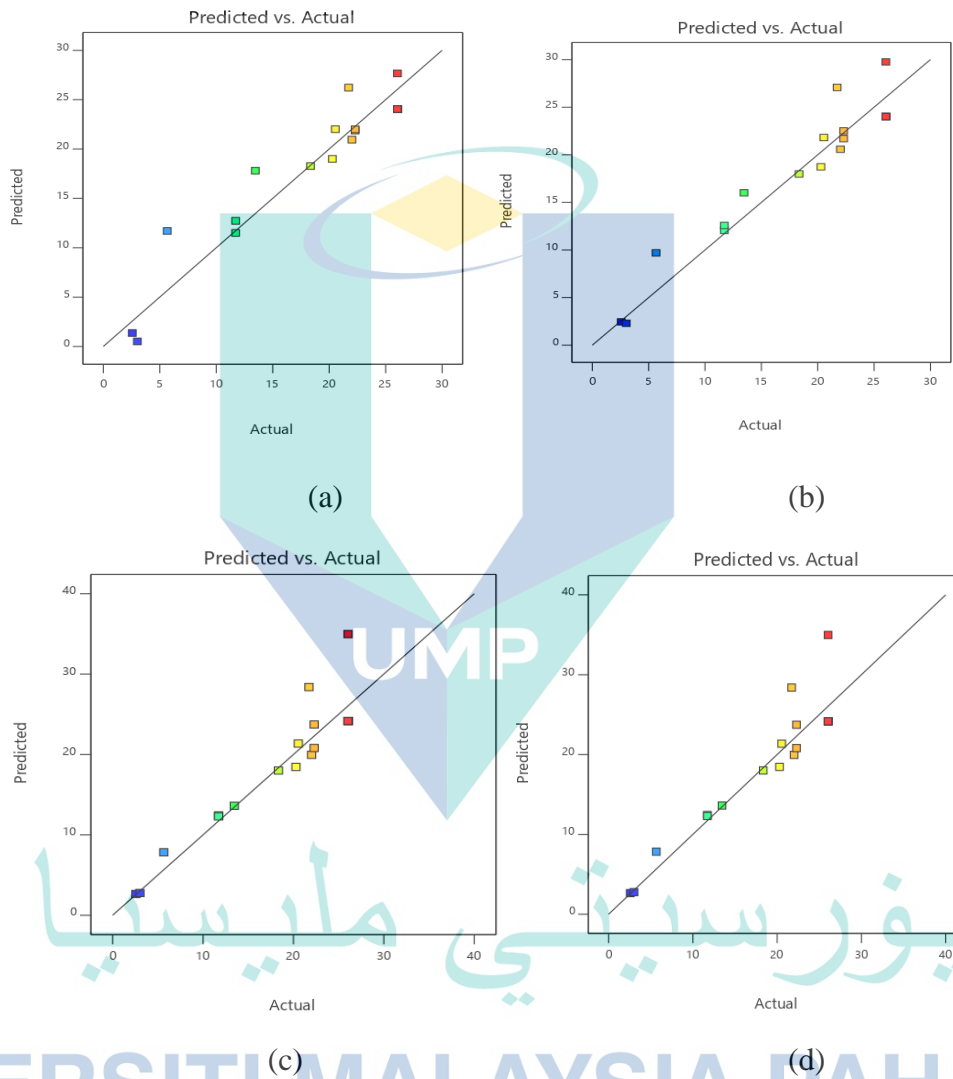


Figure 4.9 The predicted vs actual modeling using various transform models of syngas response, a) Non, b) square root, c) Natural log model, d) Inverse square root mode and e) Inverse model.

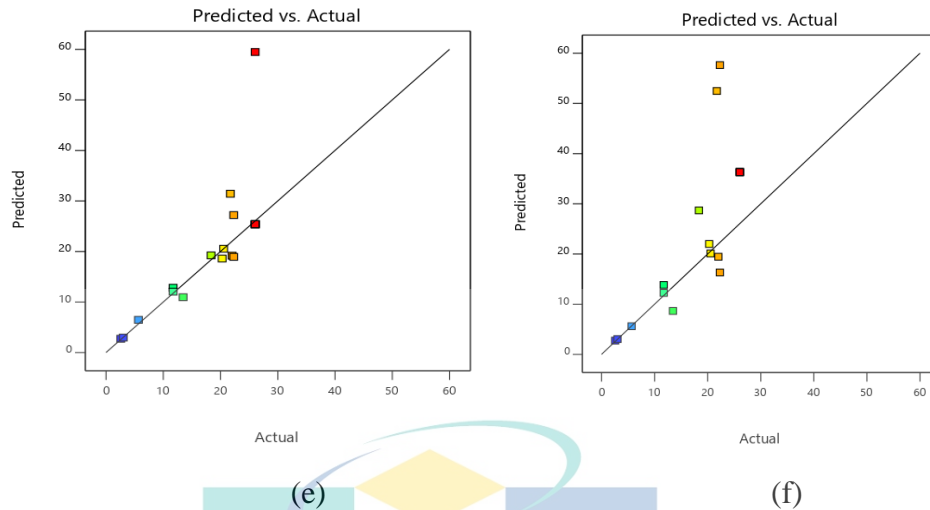
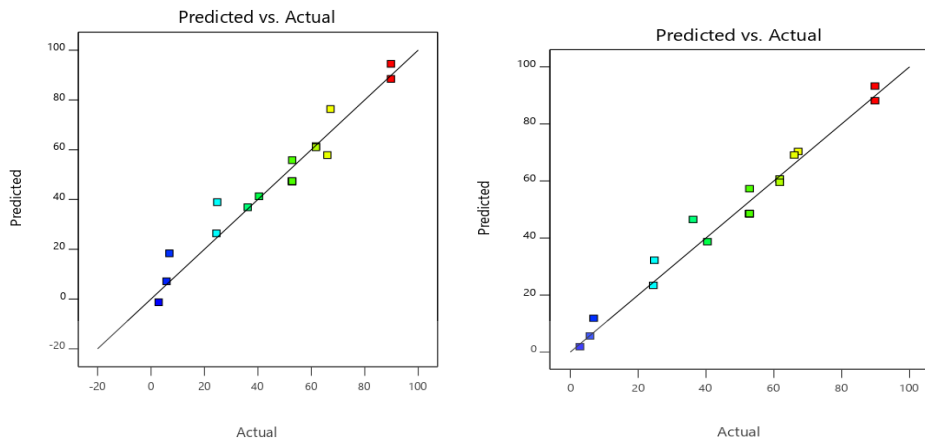


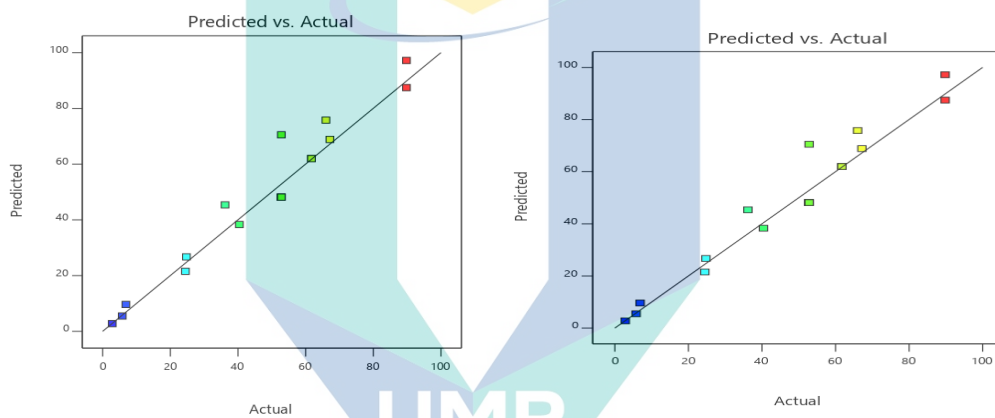
Figure 4.9 Continued

The best transformation response for syngas that has the closest results with the actual results is the none transform model and the square root model. Whereas, the none transform model is selected because it has a smaller average error than the square root model. The average error of the square root and none transform models are 10% and 5%, respectively.



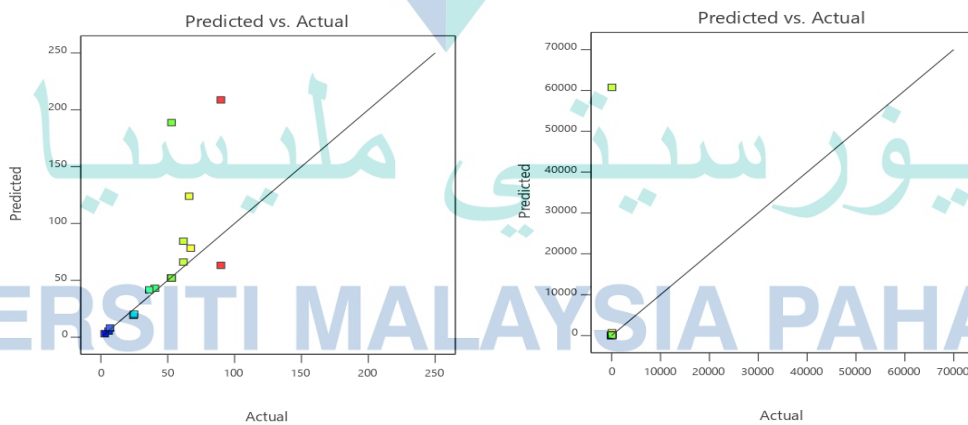
(a)

(b)



(c)

(d)



(e)

(f)

Figure 4.10 The predicted vs actual modelling using various transform models of methane conversion response, a) Non, b) square root, c) Natural log model, d) Inverse square root mode and e) Inverse model.

The closest predicted results to the actual modelling results for methane conversion model is achieved by square root and the non-transform models. Therefore, the square root transform model is selected because it has a lower average error which is 6% and an average error by the non-transform model is 11%.

#### 4.2.4.1 Analysis of Variance (ANOVA)

The models of syngas and methane conversion are significant as shown in Tables 4.2 and 4.3. Whereas, it is not shown that the lack of fit is not significant. Thus, in the modelling study, the repeated value plays an essential role to prevent the achievement of the not significant lack fit as shown in many previous studies (Hossain, et al., 2019; J. Kumar, et al., 2013; Qader, et al., 2019). In experimental studies, the repeated experiments have produced slight differences in the data, unlike the modelling, which always gives the same data repeated runs. Moreover, to fit a good model, the empirical regression models are validated with the actual modelling results, and it showed a small average error which was less than 10 % for both.

Table 4.2 Analysis of variance (ANOVA) for syngas response

Source	Sum of Squares	df	Mean Square	F-value	p-value	
Model	1113.79	9	123.75	10.66	0.0005	significant
A-SPEED	107.89	1	107.89	9.29	0.0123	
B-Catalyst mass	243.04	1	243.04	20.93	0.0010	
C-Flow	44.34	1	44.34	3.82	0.0792	
AB	168.51	1	168.51	14.51	0.0034	
AC	62.97	1	62.97	5.42	0.0421	
BC	0.5936	1	0.5936	0.0511	0.8257	
A <sup>2</sup>	225.79	1	225.79	19.44	0.0013	
B <sup>2</sup>	4.74	1	4.74	0.4084	0.5371	

Table 4.2 Continued

Source	Sum of Squares	df	Mean Square	F-value	p-value
C <sup>2</sup>	0.0121	1	0.0121	0.0010	0.9749
Residual	116.13	10	11.61		
Lack of Fit	116.13	5	23.23		
Pure Error	0.0000	5	0.0000		
Cor Total	1229.92	19			

Table 4.3 Analysis of variance (ANOVA) for Methane conversion response

Source	Sum of Squares	df	Mean Square	F-value	p-value	
Model	88.24	9	9.80	36.07	< 0.0001	significant
A-SPEED	61.72	1	61.72	227.07	< 0.0001	
B-Catalyst mass	9.03	1	9.03	33.22	0.0002	
C-Flow	5.59	1	5.59	20.57	0.0011	
AB	6.50	1	6.50	23.91	0.0006	
AC	0.1535	1	0.1535	0.5645	0.4697	
BC	0.0596	1	0.0596	0.2193	0.6496	
A <sup>2</sup>	3.10	1	3.10	11.41	0.0070	
B <sup>2</sup>	0.3334	1	0.3334	1.23	0.2940	
C <sup>2</sup>	0.9867	1	0.9867	3.63	0.0859	
Residual	2.72	10	0.2718			
Lack of Fit	2.72	5	0.5436			
Pure Error	0.0000	5	0.0000			
Cor Total	90.96	19				

The empirical regression models are represented by the following equation (4.3 and 4.4) where  $A$ ,  $B$  and  $C$  are engine speed, catalyst mass and molar flow rate, respectively:

Syngas (%):

$$Y_1(\%) = -62.4625 + 0.05453A + 0.066705B - 0.222835C - 1.569067e - 05 AB + 0.000166974 AC - 4.489211e - 05 BC - 1.1186788e - 05 A^2 - 1.2433671e - 05 B^2 + 0.00019042 C^2 \quad 4.1$$

Methane conversion (%):

$$Y_2(\%) = (-9.18319 + 0.010677851 A + 0.0144155 B - 0.1509584 C - 3.0815464e - 06 AB - 8.24251e - 06 AC - 1.4226071e - 05 BC - 1.3111581e - 06 A^2 - 3.29632e - 06 B^2 + 0.00171846 C^2) \quad 4.2$$

Table 4.4 Actual modeling and empirical regression model validation of Syngas

Engine speed (rpm)	Catalyst weight (g)	CH <sub>4</sub> Flow rate (Mol/hr)	Actual Syngas (%)	Predicted Syngas (%)	Error (%)
1200	1000	21.430	22.015	20.950	5
1500	800	26.745	23.017	20.653	10
1800	700	38.954	25.750	22.368	13
2100	600	41.904	26.013	23.054	11
2400	550	51.090	25.880	24.512	5
2700	450	54.110	22.450	23.452	4
3000	350	62.850	22.300	23.036	3
Average error					7%

Table 4.5 Actual modelling and empirical regression model validation of Methane conversion

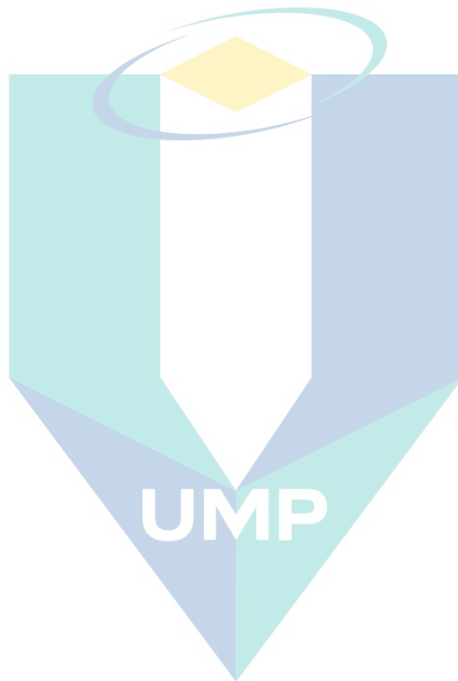
Engine speed (rpm)	Catalyst weight (g)	CH <sub>4</sub> Flow rate (Mol/hr)	CH <sub>4</sub> Conversion (%)	Predicted CH <sub>4</sub> conversion (%)	Error (%)
1200	1000	21.43	37.410	38.450	3
1500	800	26.745	41.090	38.009	7
1800	700	38.954	44.00	37.736	16
2100	600	41.904	48.650	44.178	9
2400	550	51.090	55.300	50.662	8
2700	450	54.110	58.671	55.898	5
3000	350	62.850	61.730	62.240	1
<b>Average error</b>					<b>7%</b>

From Tables 4.4 and 4.5, it can be seen that the small average error between the predicted data that is generated by the empirical regression models and the actual modelling results. Therefore, the models can be used to select the amount of catalyst and natural gas flow rate to achieve the optimum reforming performance.

#### 4.2.5 Syngas Production

RSM optimization model was used to study the 3D response plots, which is generated from the effect of the variables (speed, catalyst mass and natural gas flow rate) on the syngas production. Figure 4.11 (a) to (g) demonstrate the interactions between the variables in three-dimensional response surface plots. The value of the axis in all the figures are calculated using the 1D model through the equations 3.19-3.25. The plots have shown the combined effect of catalyst mass and natural gas on the syngas production (H<sub>2</sub>+CO) at each engine speeds. It is noticed that at each engine speed as the amount of catalyst and natural gas flow rate increased, more syngas production is achieved. This rise is due to the higher rate of hydrogen and carbon monoxide generation, which is motivated by a higher amount of catalysts. Besides, the higher amount of natural gas flowrate (CH<sub>4</sub>), which is consumed by steam reforming (reactions 1,2 in Table 3.9), dry reforming and oxidations reactions. This consumption of methane has led to more generation of syngas and reduce the production of carbon dioxide. Because, if the amount

of methane is too low compared to the other reactant, more methane is achieved while less hydrogen produced. This less production is due to low methane which has motivated reaction 2 and 4 in Table 3.9 to generate more carbon dioxide beside the re-consumption of carbon monoxide by water-gas shift WGS reaction (Ilsen Önsan, et al., 2011). Whereas, if the amount of syngas is sufficient and identical with the amount of exhaust, the steam would be consumed by reaction 1 and 2 in Table 3.9, and less amount would be used in WGS reaction. Therefore, the consumption of produced carbon dioxide would be lower and leading to an increase to the amount of syngas ( $H_2+CO$ ) in the produced components.



اونيور سيطي مليسيا قهغ

UNIVERSITI MALAYSIA PAHANG

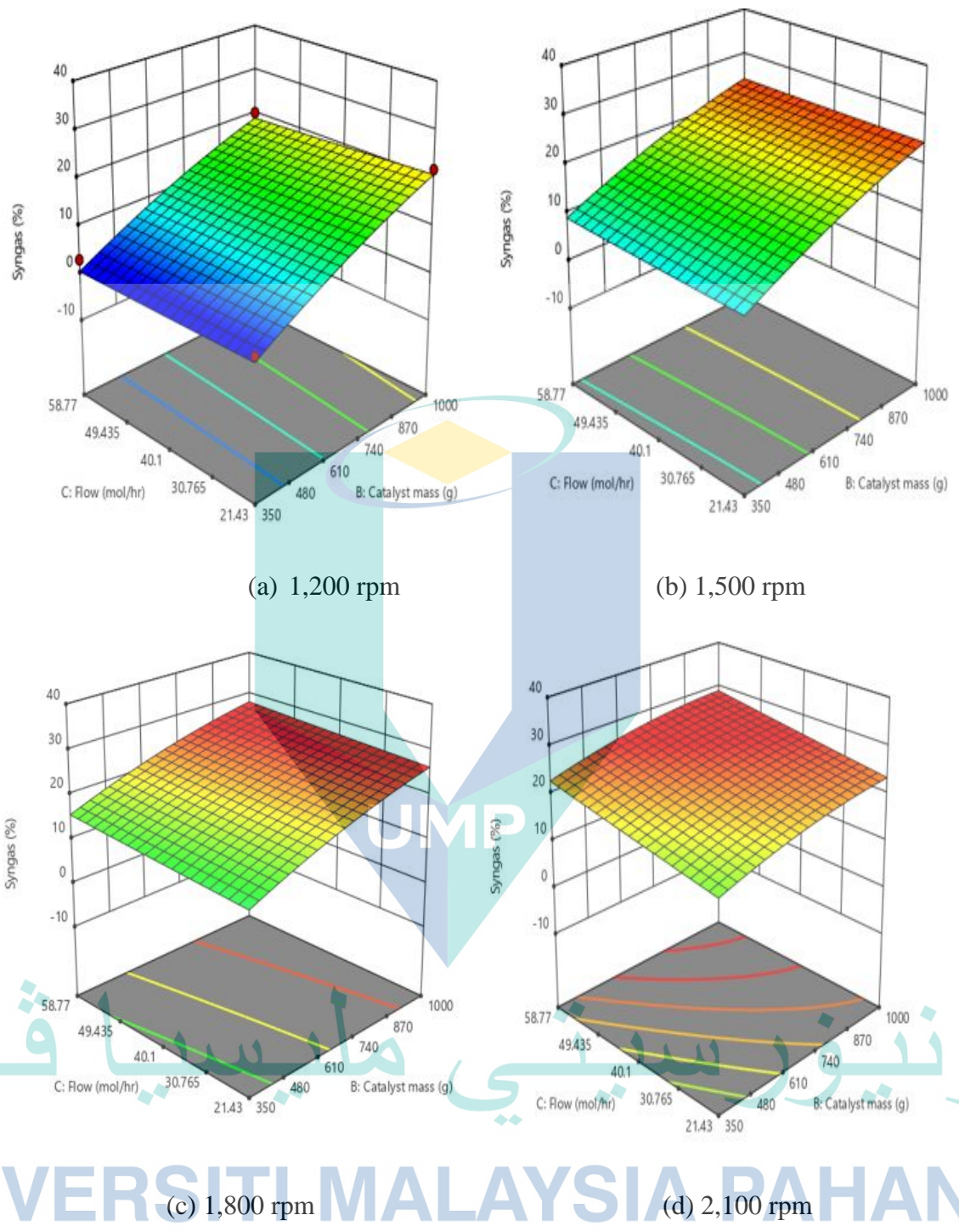


Figure 4.11 3D Surface of syngas production at each engine speed with the various catalyst mass and methane flow rate.

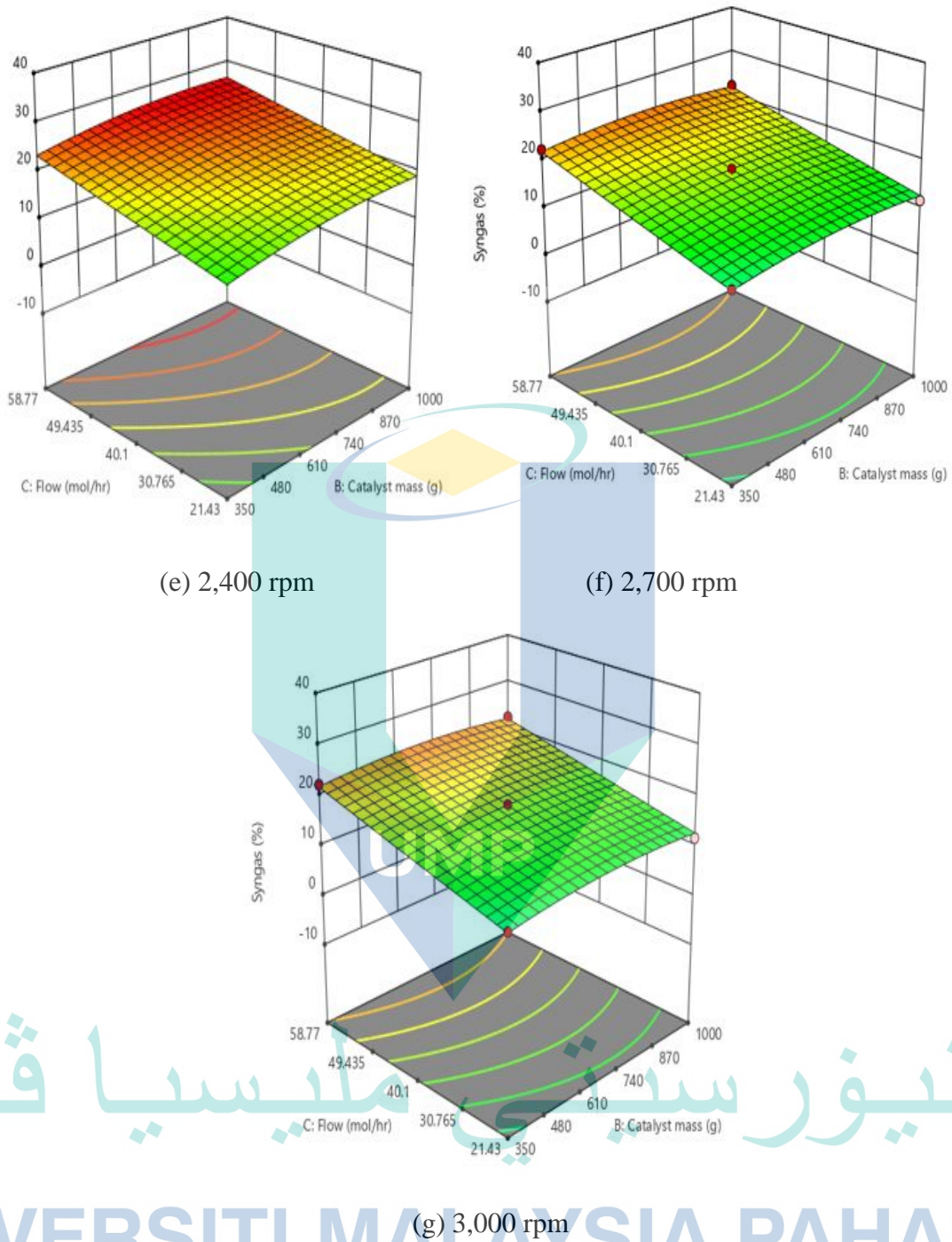
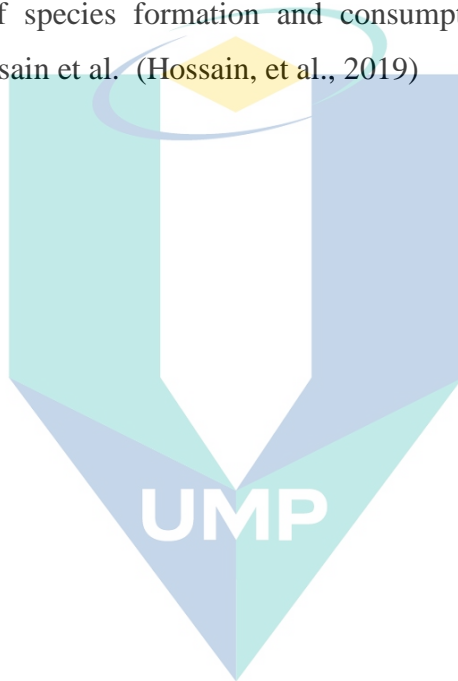


Figure 4.11 Continued

#### 4.2.6 Methane Conversion

Figure 4.12 demonstrates the interaction between flow rates and catalyst mass and their effects on methane conversion at each engine speed. It is shown that methane

conversion has decreased as the flow rate increases and the catalyst mass reduced. Because, as the amount of methane increased, other parameters such as the amount of the steam, temperature and air should be added. To achieve higher conversion, the rate of methane consumption should be increased. The rate of methane consumption can be increased by motivating the steam reforming reactions to increase besides the reaction temperature, which can be raised by adding heat addition or air to enhance the combustion reaction rate. Therefore, the conversion of methane increased with the rise of catalyst mass. This increases in catalyst mass contribute to the shorten the reaction time and increase the speed of species formation and consumption. Similar outcomes were obtained by M.A. Hossain et al. (Hossain, et al., 2019)



اونيورسيتي ملايسيا قهغ

UNIVERSITI MALAYSIA PAHANG

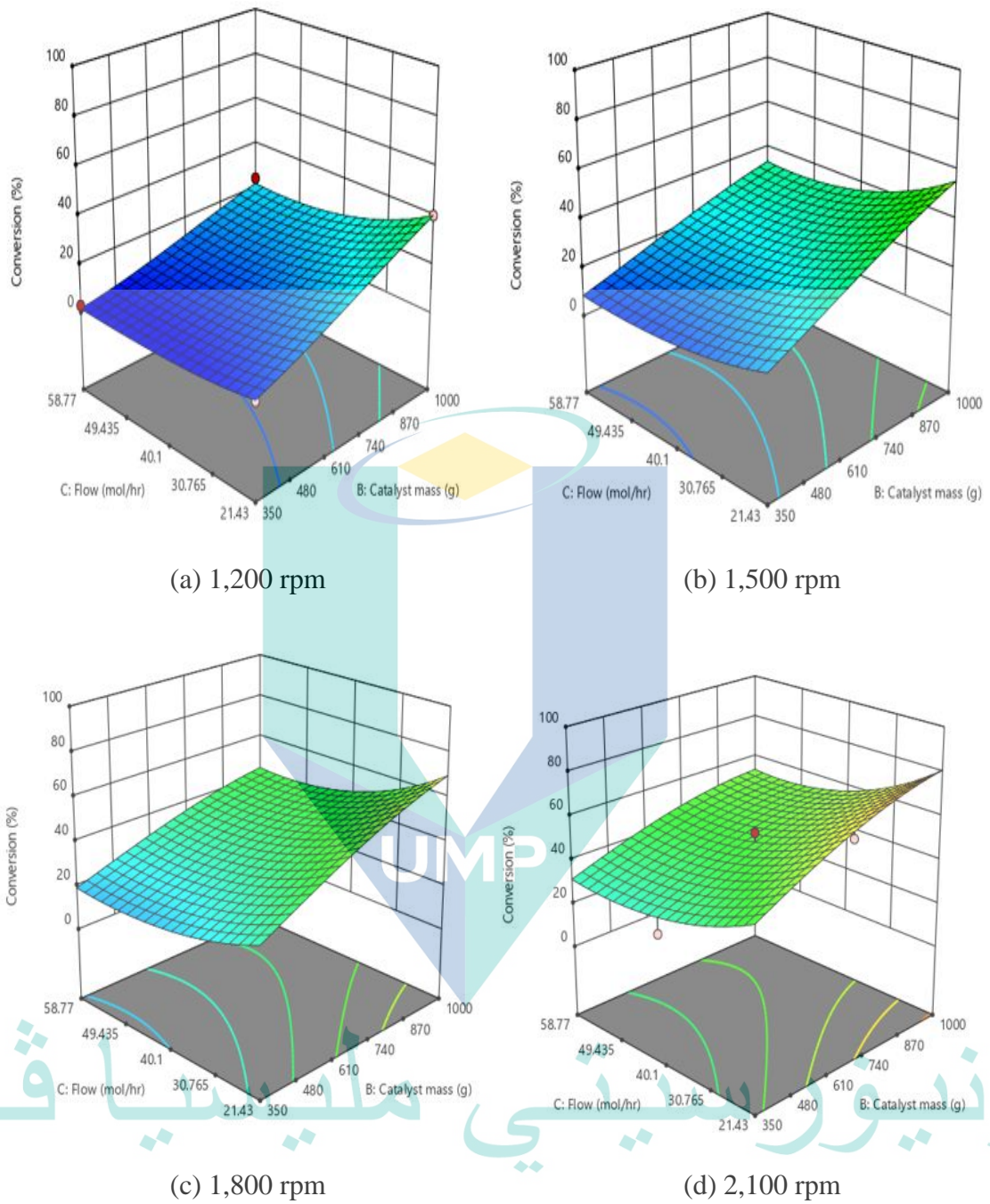


Figure 4.12 3D surface of variation of catalyst mass and flow rate and their effect on the methane conversion at each engine speed.

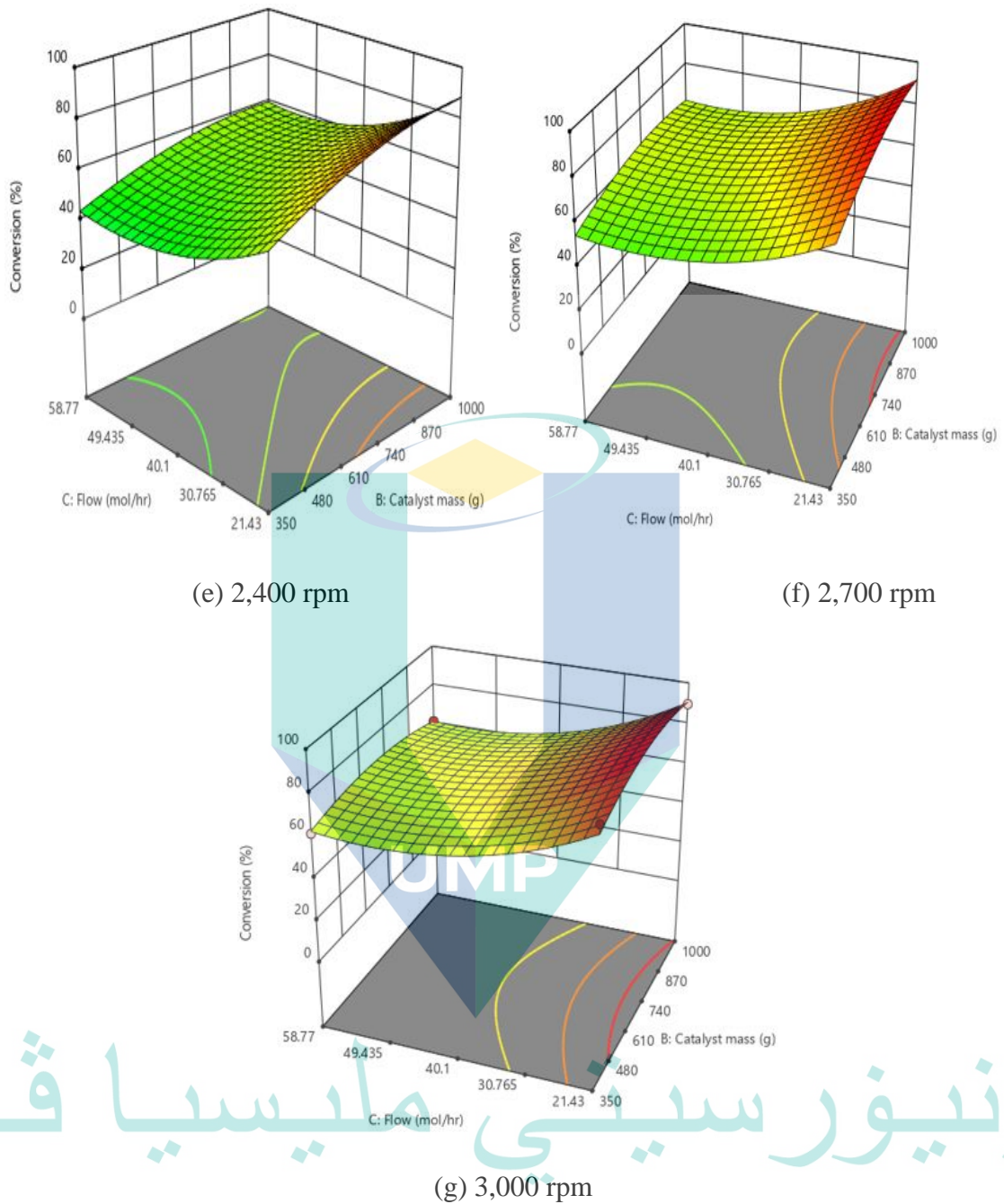


Figure 4.12 Continued

#### 4.2.7 Selection of catalyst mass and natural gas (CH<sub>4</sub>) flow rate

The RSM optimization aimed to select one minimum value of catalyst mass and methane flow rate. Therefore, in numerical optimization, the values of catalyst mass and flow rate were minimized. Meanwhile, the values of syngas production and methane

conversion were maximized. Whereas the engine speeds were selected to be in the range from 1,200 to 3,000 rpm Figure 4.13 shows the optimal conditions of maximum syngas production and methane conversion. The maximum syngas production and methane conversion were achieved at 2,100 rpm, and their values were 25.3023% and 64.652% respectively. These values were obtained at 850 g catalyst mass, and 35 mol/hr of natural gas flow rate with the desirability of 0.965 which was the highest values among all the 11 runs and the desirability variation of all the solutions are shown in Figure 4.14, and the desirability bar graphs of each solution are shown in . From Figure 4.14, the solution 1 were elected because it has the highest value of desirability, which represents the minimum catalyst mass and flow rate, as shown in Figure 4.14.

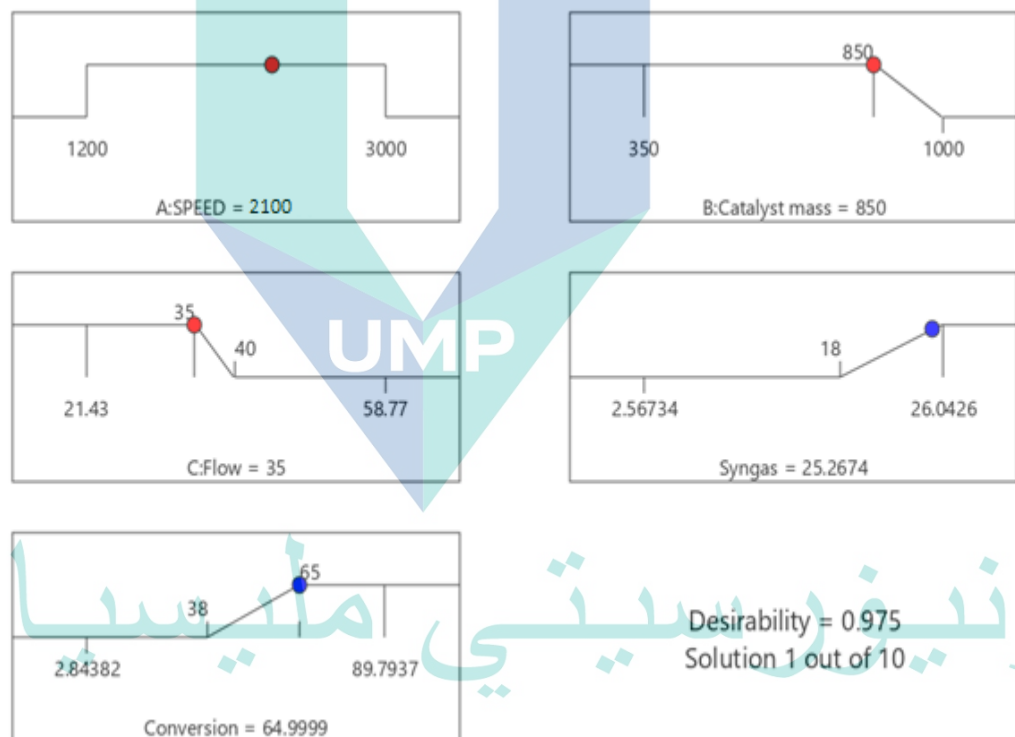


Figure 4.13 Optimal numerical solutions

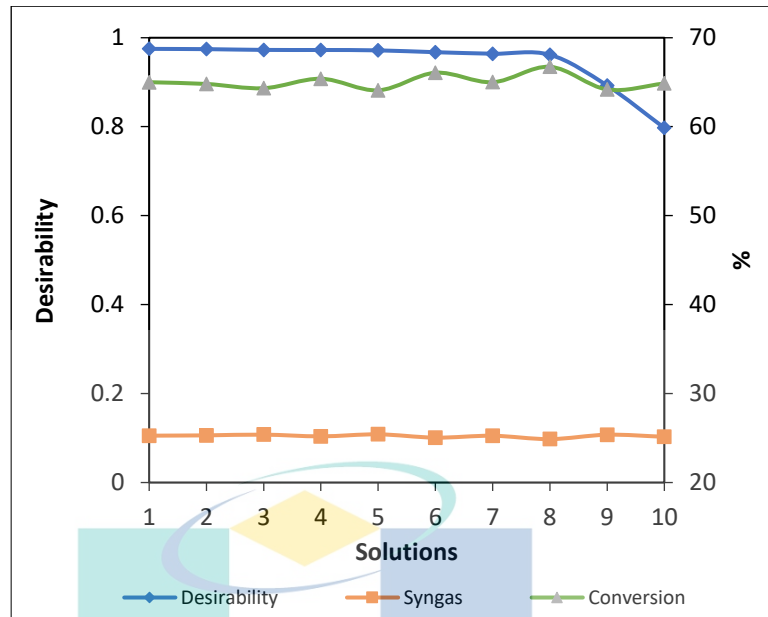


Figure 4.14 Desirability of the numerical solutions with syngas production and methane conversion.

#### 4.2.8 Syngas Production and Methane Conversion at The Selected Methane Flow Rate and Catalyst Mass

This section discusses the amount of natural gas flow rate and catalyst mass needed to produce the optimum amount of syngas mixture and convert the maximum possible amount of methane.

##### 4.2.8.1 Syngas Production

Figure 4.15 shows the 3D surface and contour of syngas production with the variation of engine speed and catalyst mass at 35 mol/hr of methane flow rate. It is noticed that the syngas production has started to increase at the higher engine speeds and reached its maximum value at 2,100 rpm. This rise of syngas production ( $H_2+CO$ ) is because of the rise of the amount of steam, air and heat with the rise of the engine speeds. The higher amount of steam has enhanced the steam reforming reaction rate. The higher amount of air led to faster combustion reaction, which leads to higher heat amount from the oxidation reaction. Increasing the engine speed after 2,100 rpm, the syngas production has decreased from 25.26% at 2,100 rpm to 16.78 % at 3,000 rpm. This reduction is

because of the much higher ratio of the exhaust to methane ratio. The ratio of steam to methane becomes higher, and as the ratio gets too high, the methane conversion increases. Meanwhile, the amount of hydrogen and carbon monoxide generation reduces due to the rise of the WGS reaction rate (Zhang, Jia, et al., 2017).

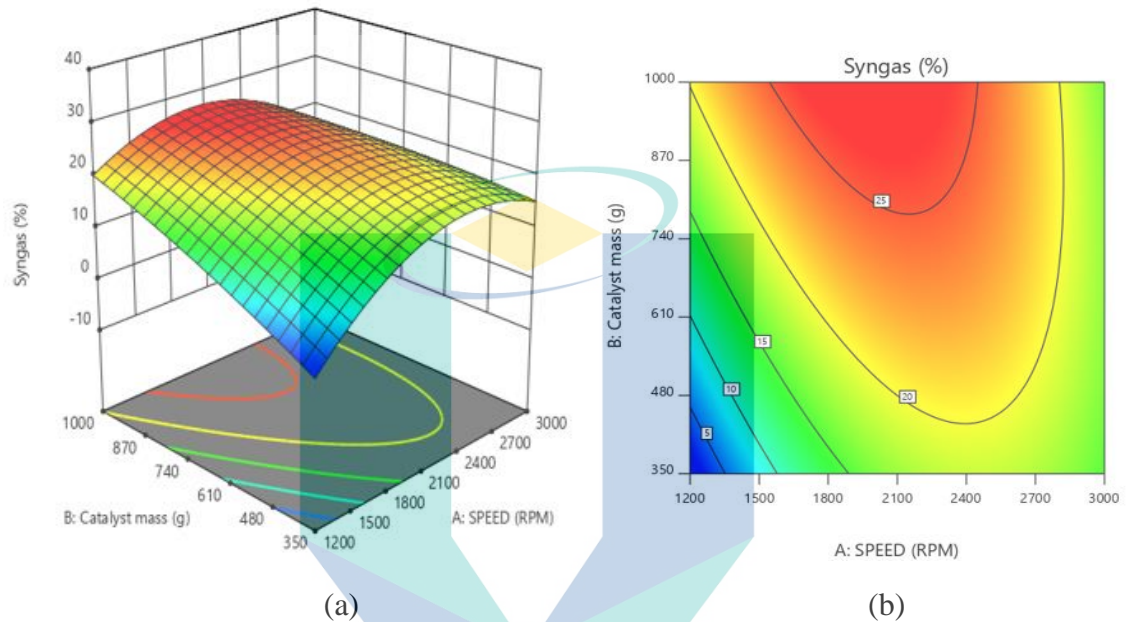


Figure 4.15 Syngas production in 3D surface (a) and 2D contour (b) at different engine speed and catalyst mass at 35 mol/hr

#### 4.2.8.2 Methane Conversion

Figure 4.16 illustrated the effect of engine speed and catalyst mass on the methane conversion at 35 mol/hr flow rate. The 850 g catalyst mass is selected to observe the change of methane conversion with the engine speed. It is shown that as the engine speed increased, more methane conversion is achieved. The higher methane conversion is due to the rise of steam, air and the exhaust temperature. The rise of these parameters led to motivate the methane consumption rate to increase. The higher steam in the reactant component has caused a rise in the rate of steam reforming reaction. And the higher air, led to more heat release from the oxidation reaction and as methane conversion is more desired at as the reaction temperature increased.

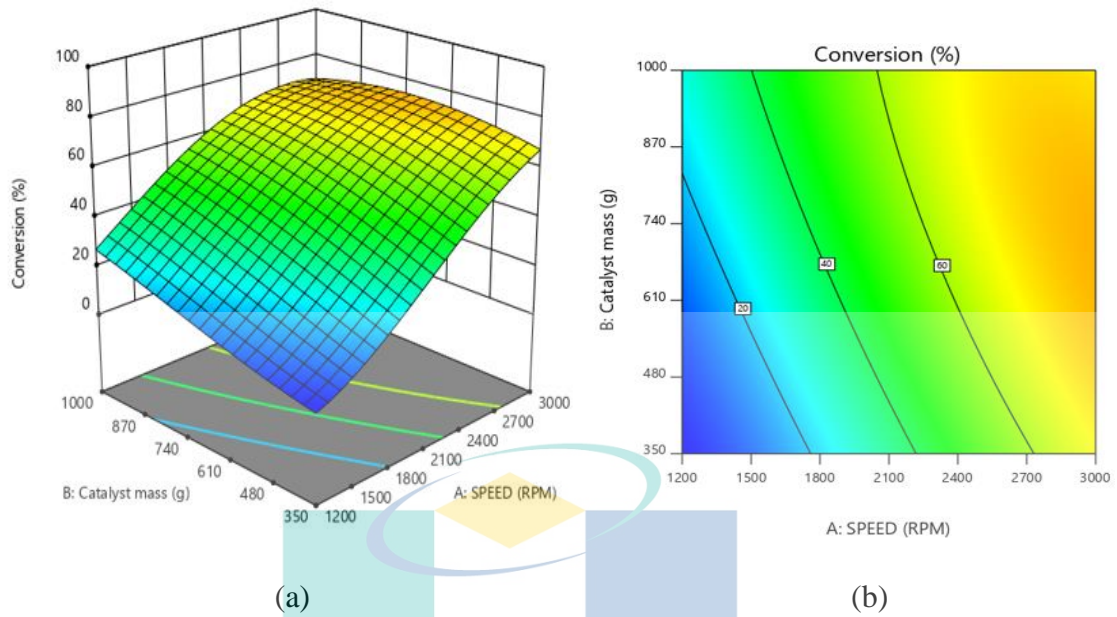


Figure 4.16 Effect of engine speed and catalyst mass on methane conversion at 35 mol/hr in 3D surface (a) and contour 2D (b)

### 4.3 Reforming Characteristics of The Optimized Model (Sized Model) At Different Parameters

2D CFD simulation is conducted to investigate the reforming characteristics of the reformer with the selected size. The simulation has shown the performance of the reformer at different speeds, steam to methane ratio, air to methane ratio, EGR ratios and wall temperature. The 2D CFD evaluated the reforming performance by methane conversion and produced syngas. In this section the 2D CFD was verified with 1D modelling and the error was lower than 15% in all results.

#### 4.3.1 Effect of Engine Speed on Reforming Characteristics

The effect of engine speed on the reforming characteristics such as temperature, the methane conversion and syngas concentration are studied over an operation speed of 1,200 to 3,000 rpm with an interval of 300 rpm.

#### 4.3.1.1 Effect of Engine Speed on The Temperature Profile

Feed temperature varies with engine behaviour, and in this study, it depends on the engine speed. The effect of engine speed variation on temperature profile along the reactor is shown in Figure 4.17. It is shown that the highest increment in temperature is observed at the lowest speed (1,200 rpm), which has the lowest feed temperature (772 K). In contrast, the lowest increase is at the highest speed, which has the maximum feed temperature (896 K). Thus, the reaction rate of steam reforming is preferred at an elevated temperature. Steam reforming and oxidation reactions are faster at elevated temperature, but the amount of heat used up by steam reforming reduces the possibility of the further increase in the temperature. As the rate of steam reforming reaction increases, more temperature is consumed by steam reforming reaction, which resulted in less temperature distribution along the reactor. Similar results were reported by Bulutoglu et al. (Bulutoglu, et al., 2015).

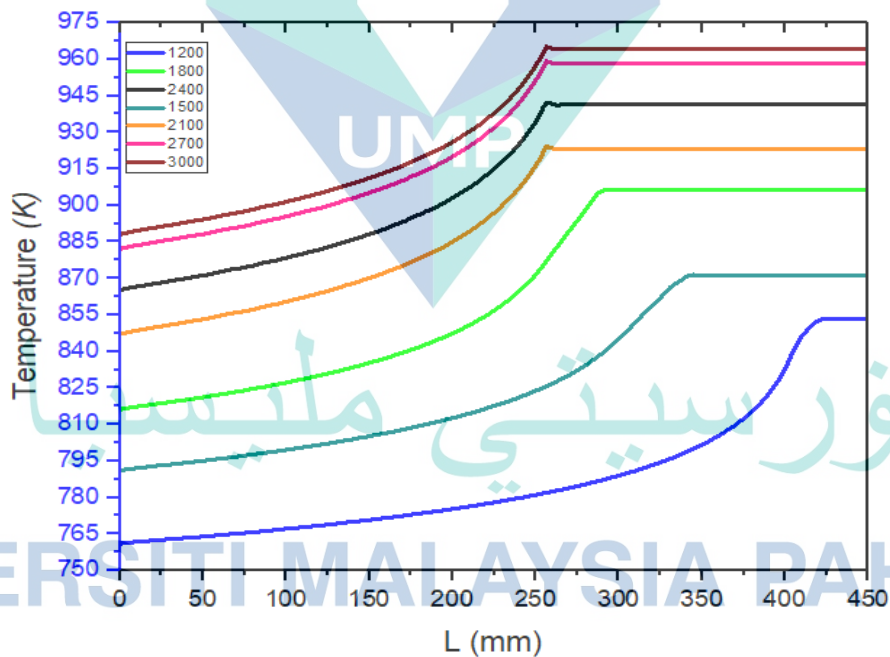
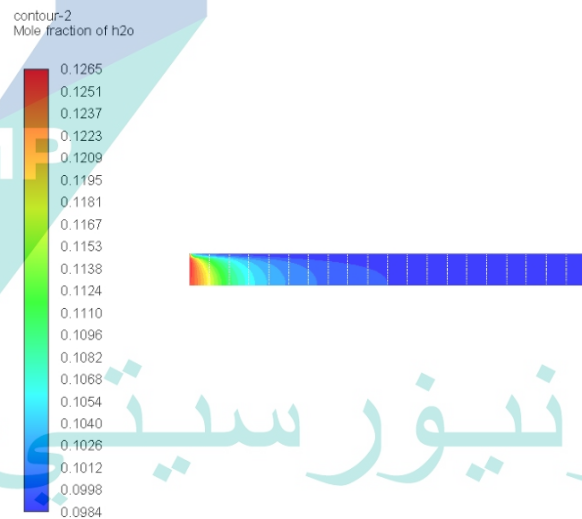
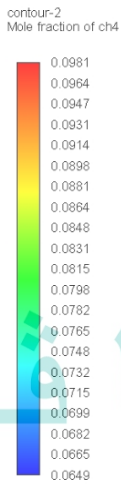
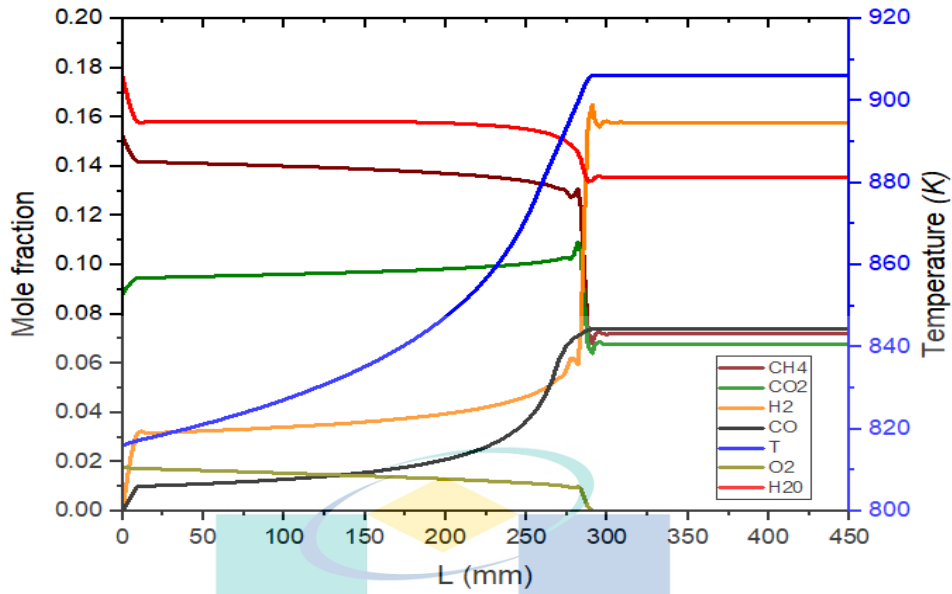


Figure 4.17 Effect of engine speed on temperature profile along the reactor with EGR rate of 25%.

#### 4.3.1.2 Axial Reforming Characteristics

Figure 4.18 shows the mole fraction conversion of natural gas ( $\text{CH}_4$ ) and exhaust gas components and the temperature profile along the axial direction of the EGR reformer. It can be noticed that immediate catalyzation of methane once the flow contacted with catalytic particles. The graph also indicates that at the point of maximum consumption of  $\text{O}_2$  ( $x = 293.34$  mm), the temperature increased sharply to its maximum value of 906.22 K. As a result of temperature increase, about 46.67% of methane conversion is achieved and the mole fraction of  $\text{CO}_2$  dropped sharply after slight increasing at the tube upstream. Also, the mole fraction of  $\text{H}_2$  and  $\text{CO}$  have increased sharply to their highest values due to the high-temperature release from  $\text{O}_2$  consumption by a complete oxidation reaction. The amount of  $\text{CO}$  is lower than  $\text{H}_2$  because of water gas shift reaction, which has consumed some amount of produced  $\text{CO}$ . The amount of steam has increased slightly after a small reduction due to the amount of steam produced from the complete oxidation reaction. The  $\text{CO}_2$  conversion is achieved at the maximum temperature. Still, due to the amount of  $\text{CO}_2$  produced from steam reforming reaction (2), water gas shift reaction (3) and complete oxidation reaction (4) in Table 3.9, the  $\text{CO}_2$  consumption has stopped and continue steadily.



UNIVERSITI MALAYSIA PAHANG

Figure 4.18 Mole fraction of natural gas and exhaust gas components disruption and temperature profile in the EGR reformer at 1800 rpm and EGR rate of 25% of 1D and 2D modelling. (a) 1D modeling, (b) CH<sub>4</sub> contours, (c) H<sub>2</sub>O contours, (d) CO<sub>2</sub> contours and (e) CO contour (f) H<sub>2</sub> contour (g) temperature contour

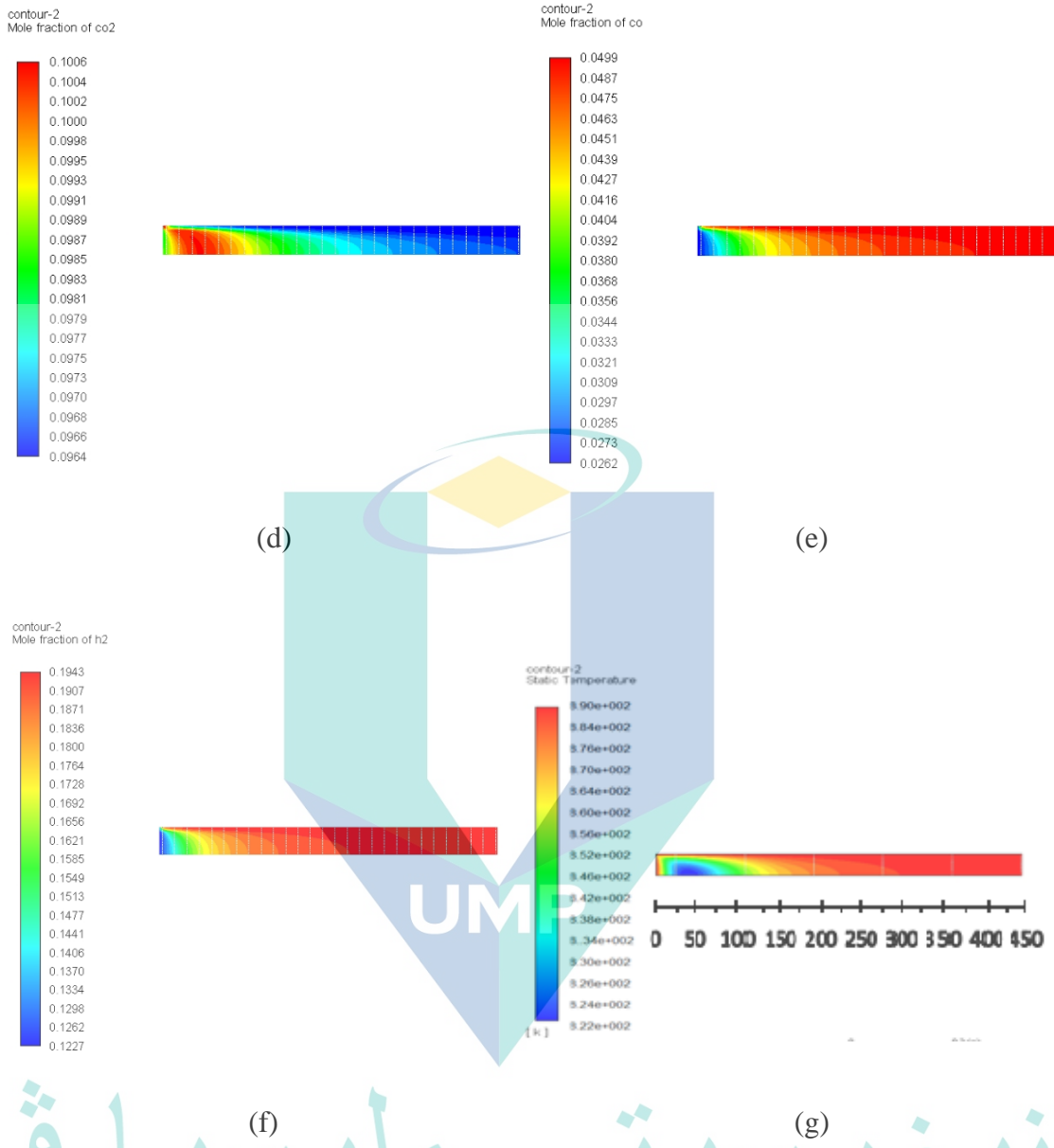


Figure 4.18 Continued

## اونیورسیتی ملیسیا قهغ

# UNIVERSITI MALAYSIA PAHANG

### 4.3.1.3 Effect of Engine Speed on Methane Conversion and Syngas

Figure 4.19 indicates the effect of engine speed on the reforming performance, which is represented by methane conversion and the amount of produced syngas ( $H_2+CO$ ). It is noticed that as the engine speed increased, more methane conversion is observed. This increment is because of the rise of temperature at higher speeds and as the feed temperature is higher, more methane is consumed by steam reforming and oxidation

reactions. Thus, the amount of CO and H<sub>2</sub> has increased with engine speeds due to the higher feed temperature at the higher speeds which increased the methane conversion efficiency (Bulutoglu, et al., 2015). This increasing formation of syngas is mainly due to the exponential increase in the rate of steam reforming and oxidations reactions. Besides, the increase of the oxygen in the exhaust gas components where the ratio of oxygen to methane (O/C) at 3,000 rpm is 0.3674 and 0.0119 at 1,200 rpm. The rise of the amount of oxygen at higher feed temperature has caused more consumption of oxygen which has released higher temperature, and this temperature has increased the rate of reforming reactions, consumption of methane and formation of H<sub>2</sub> and CO as well is up to 2,100 rpm. Increasing the engine speed after 2100 rpm, the amount of syngas in the reactor outlet records less than the lower speeds. This decline is due to the rise of carbon dioxide in the exhaust mixture. The ratio of CO<sub>2</sub>/CH<sub>4</sub> at 1,200 rpm is 0.3830 and 0.8991 at 3000 rpm. This higher amount of carbon dioxide needs a higher temperature than the reaction temperature to enhance the consumption rate of the carbon dioxide (Deposition, 2017). Therefore, the fraction of syngas (H<sub>2</sub>+CO) in the reformed products is decreased.

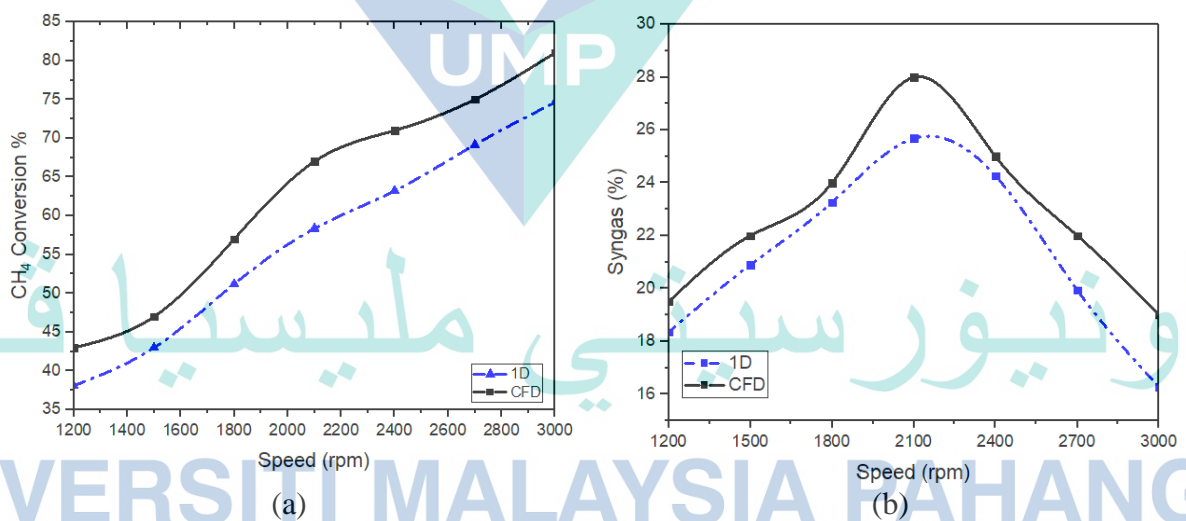


Figure 4.19 Effect of engine speed on methane conversion (a) and syngas production (b)

### 4.3.2 Effect of EGR Rate on Reforming Characteristics

Figure 4.20 demonstrates the effect of EGR rate on methane, carbon dioxide conversion and syngas production at an engine speed of 1,800 rpm. Normally, the amount of oxygen and steam in the exhaust gas mixture increase with the rise of the EGR rate. Meanwhile, the amount of methane flow rate is constant at all the EGR rate. Therefore, the rate of methane reforming increased because more amount of methane was consumed by oxidation and steam reforming reactions. However, the methane conversion gradient increased, and as more amount of methane is converted, more amount of hydrogen and carbon monoxide will be generated. It is shown that in Figure 4.20b the trend of syngas fraction increased as the EGR rate decreased because CO production is sensitive to the content of the steam in the exhaust gas mixture. This is because of the low content of oxygen in the gas mixture at lower EGR rate, which led to less generation of CO from the partial oxidation reaction. Due to the larger amount of steam in the mixture, more hydrogen was produced from steam reforming reaction. Whereas, the amount of CO produced from steam reforming reactions, further reacted with the steam into CO<sub>2</sub> in water gas shift reaction. Thus, CO<sub>2</sub> conversion decreased with the rise of EGR rate because as the amount of CO increased from steam reforming reactions, more amount of CO<sub>2</sub> would be produced from the water gas shift reaction (Zhang, et al., 2020; Zhang, Jia, et al., 2017)

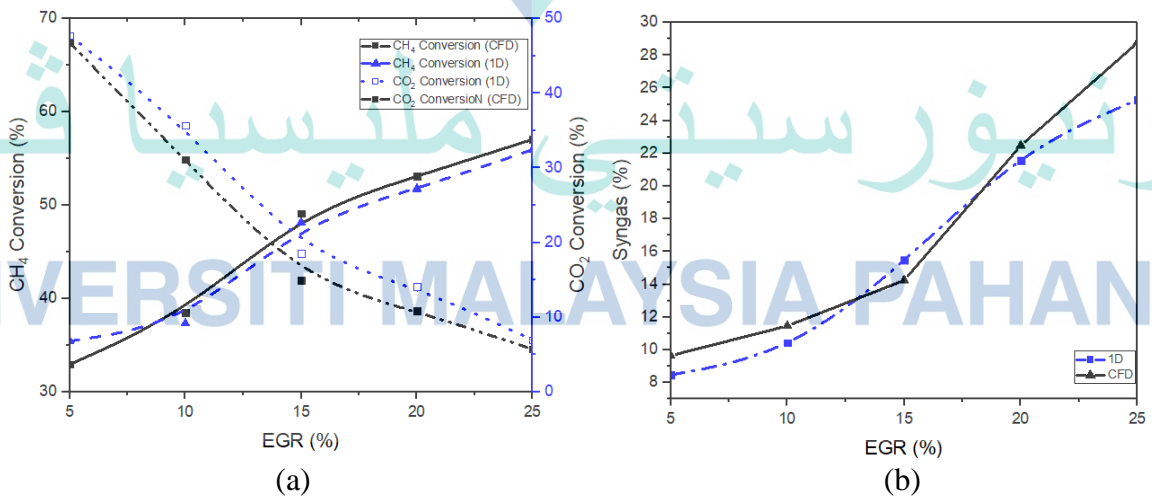


Figure 4.20 Effect of EGR rate on methane, carbon dioxide conversion (a) and syngas production (b) in 1D and 2D at 1,800 rpm

### 4.3.3 Effect of Steam Addition on Reforming Characteristics

Figure 4.21 shows the effect of steam addition on the methane conversion and hydrogen production at engine speed 1,800 rpm which has inlet temperature of 816 K. It is noticed that the methane conversion increased with the rise of the amount of steam until  $W/F = 1.75$ . It also is seen that at a higher rate, methane conversion started to be constant because to achieve more conversion, more temperature and oxygen amount will be needed; therefore, the methane conversion became stable. Meanwhile, the amount of hydrogen produced tended to increase first and then decreased because of the relative reduction of methane compared to the amount of steam. Thus, the amount of produced hydrogen started to decrease at the water to fuel (Methane) ratio of 3. The amount of produced syngas reached its maximum value when the water to fuel ratio is 1.5. This is because the amount of steam was sufficient compared to lower water to fuel rate, whereas the amount of methane was insufficient at higher rate water to fuel. These outcomes meets with study conducted by Z. Zhang et al (Zhang, et al., 2018)

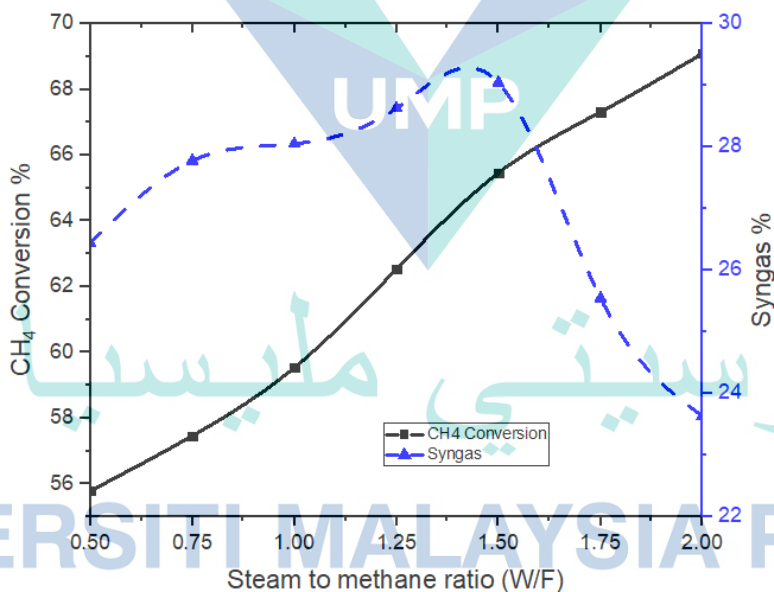


Figure 4.21 Effect of steam addition on methane conversion and syngas production at 1800 rpm.

#### 4.3.4 Effect of Air Addition on Reforming Characteristics

The effect of  $O_2/C$  ratio on the reforming characteristics is illustrated in Figure 4.22. It is noticed that there is a linear relationship between the conversion of methane and  $O_2$  quantity. As the amount of air increased, more methane conversion was achieved. This is an expected result since, with higher amount of  $O_2$  in the feed, more methane was oxidized, and more heat is released as shown in Figure 4.22. This increase was a reflection of the heat release, which motivated the methane conversion by the total oxidation reaction. Meanwhile, the production of the  $H_2$  and  $CO$  slightly reduced, since the rise of the air in the air in the reactants led to a higher amount of steam and carbon dioxide by the total oxidation reaction. The rise of the steam in the mixture affected the steam reforming reaction negatively

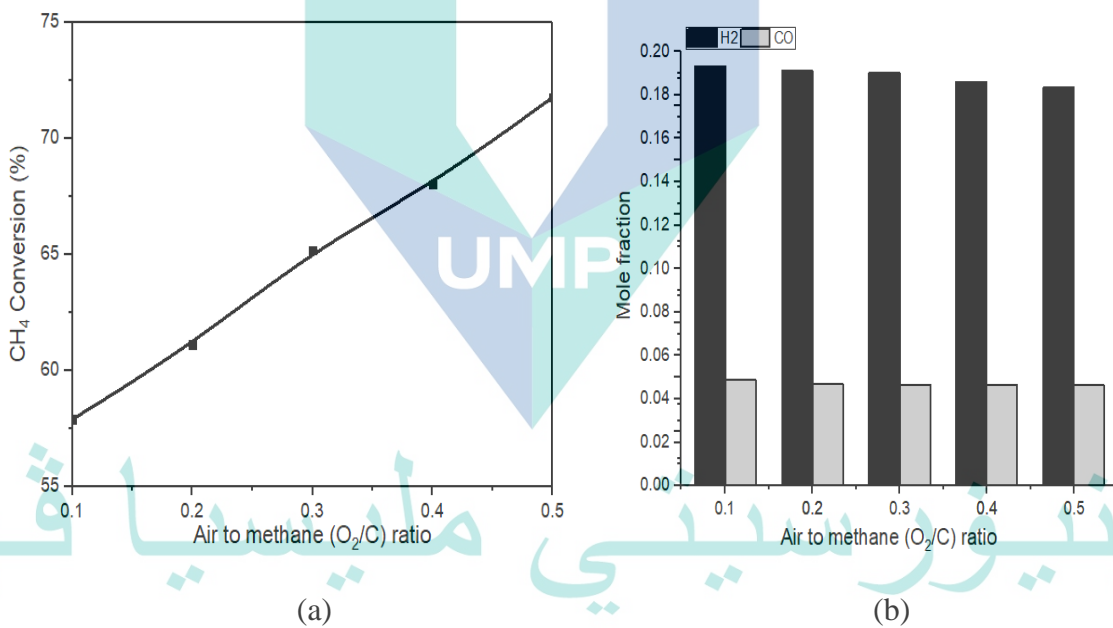


Figure 4.22 Effect of  $O_2/C$  ratio in methane conversion (a),  $H_2$  and  $CO$  fraction at the reformer outlet at 1,800 rpm

#### 4.3.5 Effect of Wall Temperature on Reforming Characteristics

Figure 4.23 shows the effect of wall temperature on the variation of the conversion rate of methane and hydrogen to carbon monoxide ratio at the reformer outlet.

It is noticed that methane conversion increased exponentially with the rise of wall temperature. Meanwhile, the ratio of hydrogen to carbon monoxide has increased, which indicated that the production of carbon monoxide increased at higher wall temperature. As the value of  $H_2/CO$  ratio reduced, the amount of carbon monoxide tended to be closer to the amount of the produced hydrogen. This variation is due to the change of steam reforming rate of methane with the wall temperature, which contributed to the increasing of the reaction temperature. As the reaction temperature increased, the steam reforming and oxidation reaction rate increased, which led to more consumption of methane and higher generation of hydrogen and carbon monoxide. The great reduction of the ratio of  $H_2$  to  $CO$  because the water gas shift reaction is exothermic, which has depressed with the rise of temperature. As results, more carbon monoxide formation is produced by steam reforming reaction and palatial oxidation reaction which led to a lower molar ratio of  $H_2$  to  $CO$ . Similar results were obtained by Zhang et al. (2018).

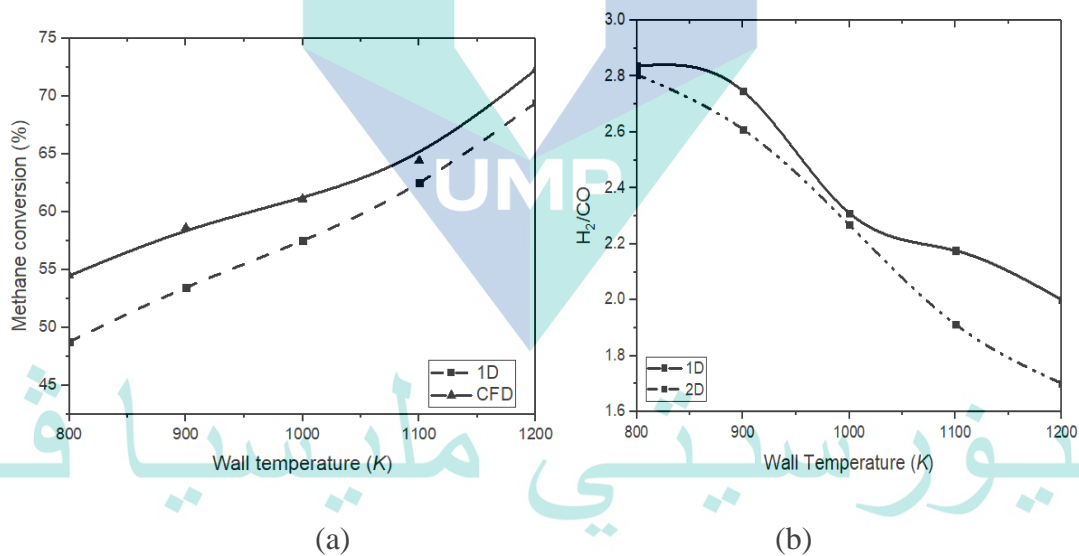


Figure 4.23 Effect of wall temperature on methane conversion (a) and  $H_2/CO$  ratio (b)

#### 4.4 Effect Of Reformmate Gas On The Combustion Characteristics

3D CFD simulation studies conducted to evaluate the effect of reformed gas (Exhaust gas reforming products) on the combustion characteristics in an SI engine. The combustion characteristics are evaluated by in-cylinder pressure, heat release rate (HRR)

and mass burned fraction (MBF). The simulation is reformed at an engine speed of 18,00 rpm and 25% EGR rate. The simulation is performed in two stages. The cold flow is used to observe flow inside the combustion chamber, whereas the combustion to evaluate the effect of the reformed gas on the combustion characteristics..

#### 4.4.1 Cold Flow

The cold flow analysis has involved the simulation of airflow in the transient engine without any reactions take place. There is no combustion process during the cold flow analysis. The goal is to observe the airflow and streamline in the engine when the intake valve and the exhaust valve open and close.

##### 4.4.1.1 Airflow for the four strokes

Figure 4.24 shows the airflow for the four strokes from the air intake to the open of the exhaust valve. Figure 4.24a demonstrates the open valve at the crank angle of 12° CA BTDC. It is shown that the flow of the air intake to the combustion chamber. Meanwhile, the exhaust valve remains closed. Then compression of the stage started, as shown in Figure 4.24b and the intake valve was closed at angle 48° CA ABDC. Finally, the exhaust valve was opened at 45 BTDC, as shown in Figure 4.24 (c) at 10° CA ATDC, which shows how the flow has higher values at the open valve.

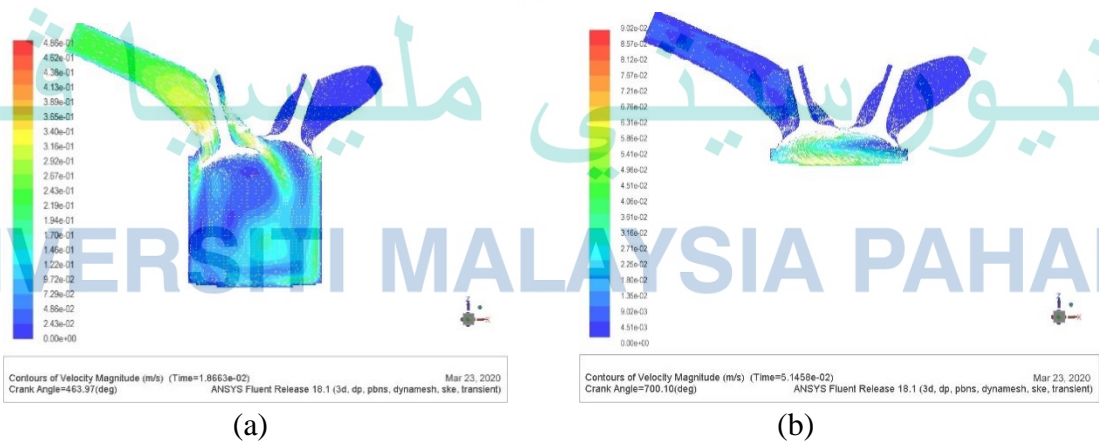


Figure 4.24 The airflow velocity from the intake flow (a), compression stage (b) and the open of exhaust valve (c)

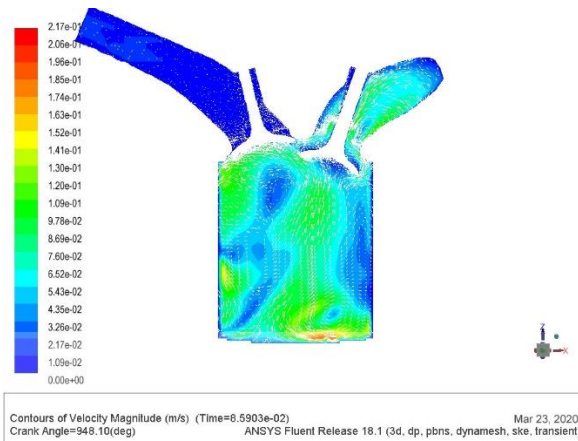


Figure 4.24 Continued

#### 4.4.2 Fuel Injection

Since the simulation is a dual fuel system, two injectors are used. The primary fuel injection is used for the natural gas. Whereas the injection of EGR addition is considered as a secondary fuel injector.

##### 4.4.2.1 Natural Gas Injection

Figure 4.25 shows the injection stage of natural gas from the side (a) and (b) and top views (c) and (c). The injection is tested to observe the flow behaviour of primary fuel. It is illustrated that the flow of the natural gas is matched with the footprint points that are created in the geometry (Chapter 3).

اوديزور سيني مالنيسيا قهغ

UNIVERSITI MALAYSIA PAHANG

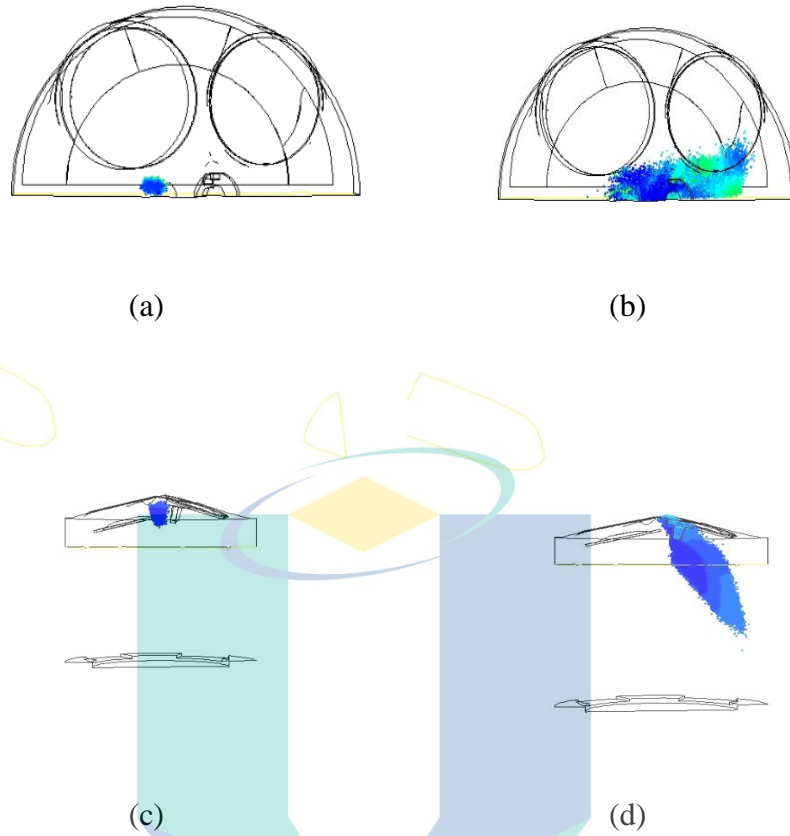


Figure 4.25 Natural gas injection to the combustion chamber (Countinued)

#### 4.4.2.2 EGR Addition

Figure 4.26 shows the reformed gas addition to the air manifold. The aim of reformed gas is to enhance the combustion stability of natural gas by the hydrogen presence in the fuel mixture. Therefore, the injection of reformed gas needed to be observed to ensure that the flow of the EGR is alined with created footprint points in the main geometry presented in Chpater 3.

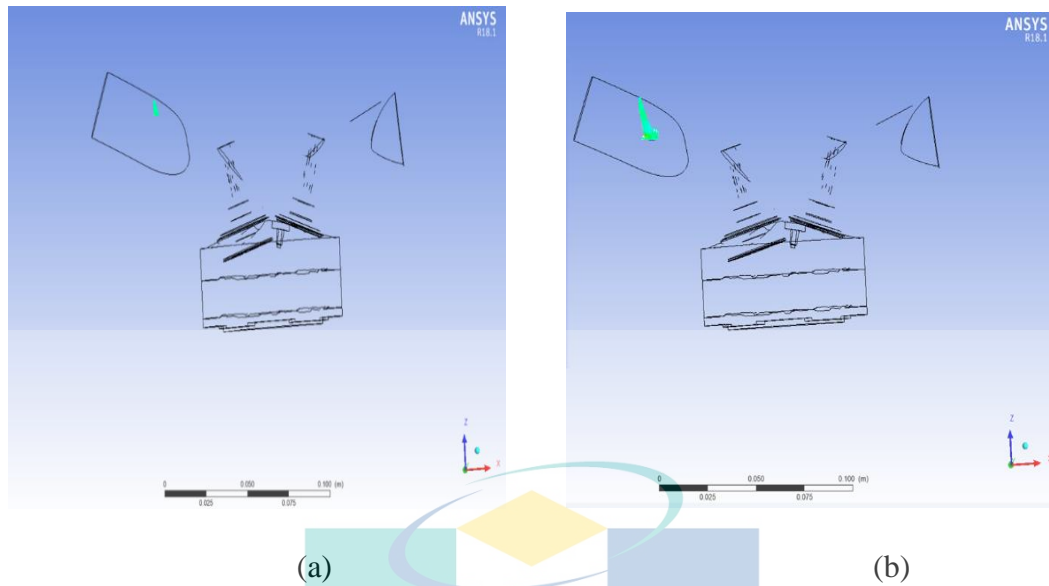


Figure 4.26 EGR addition to air manifold to the combustion chamber

#### 4.4.2.3 Volumetric Efficiency

Volumetric efficiency is the percentage of the mass of air and fuel and that is trapped by the cylinder during air induction. This is divided by the mass that would occupy the displaced volume if the air density in the cylinder were equal to the ambient air density. Therefore, volumetric efficiency in the case of EGR addition gets reduced due to the displacement of sucked air by the reformat gas and this case is common in dual fueling system (Alrazen, et al., 2018; H. Chen, et al., 2018; Sahoo, et al., 2012). The volumetric efficiency in the case of the pure natural gas was 73.73% and it dropped to 68.50% in the case of reformat gas addition. Therefore, it is expected that, the combustion enhancement that should occur due to the hydrogen addition might be affected slightly.

#### 4.4.3 Combustion Characteristics

Figure 4.27 indicates the effect of reformed gas added to natural gas on the in-cylinder pressure compared to pure natural gas (CNG) at 1,800 rpm. It is shown that the pure natural gas has the lower pressure, which is 76.7 bar compared to the CNG with the addition of reformed gas (EGR) which has a pressure of 79.69 bar. The rise of the

pressure in the case of EGR addition is due to the higher amount of fuel compared to CNG which is 0.3603 g/s, whereas the flow rate of the fuel in the case of EGR addition is  $(1.234+0.3603 \text{ CNG})$  g/s. This has led to higher pressure because of the higher density of gas in the combustion chamber. Also, the amount of syngas ( $\text{H}_2+\text{CO}$ ) in the EGR which represent 23.19%. Besides, the higher energy released from the combustion of (CNG+EGR) compared to pure CNG.

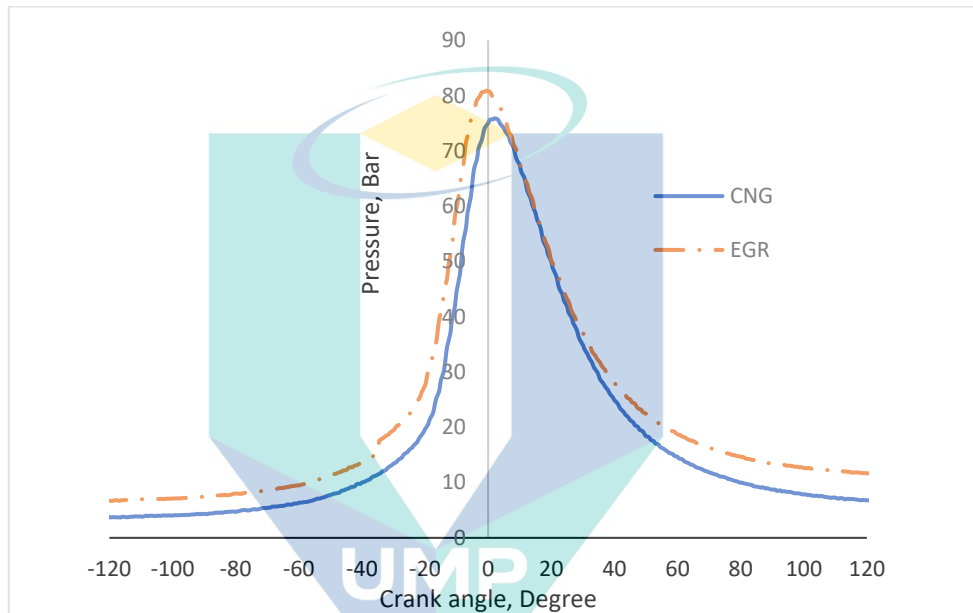


Figure 4.27 Variation of in-cylinder pressure with crank angle degree at 1800 RPM in pure natural gas and natural gas with the addition of the reformed gas (continued)

Figure 4.28 shows the variation of the heat release rate of the combustion of the pure natural gas and natural gas with the addition of reformed gas which has a concentration of syngas ( $\text{H}_2+\text{CO}$ ). It is indicated that the combustion with the addition of EGR has a higher heat release. This higher HRR is due to the presence of hydrogen concentrations which has higher calorific value compared to natural gas. The heat release rate depends on the calorific value, and as the calorific value increased, more heat release is achieved. Therefore, the case of EGR addition has higher HRR due to the presence of syngas which contributed to the calorific value increment. Besides, the presence of hydrogen in EGR mixture speeded up the flame growth and propagation at an earlier stage of combustion. This promotion in combustion led to an increase in the peak of heat release rate.

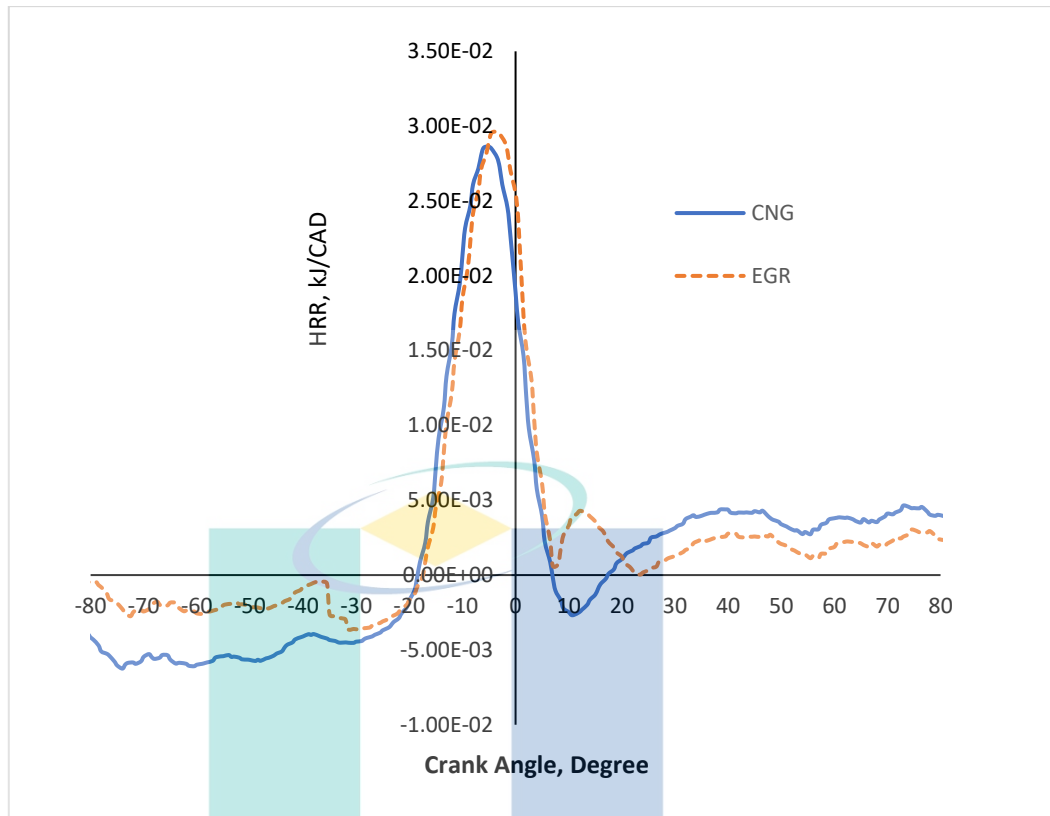


Figure 4.28 Effect of EGR addition on the heat release rate at 1,800 rpm

Figure 4.29 indicates the comparison between the mass burned fraction of the natural gas and natural gas with the added reformed gas. It is shown that the mass burned fraction started to be consumed before the natural gas. This faster MBF of EGR is due to the higher concentration of  $H_2$ , which led to faster flame propagation. The content of the hydrogen in the mixture besides the higher density of EGR and natural gas compared with a pure natural gas contributed to reducing the ignition delay.

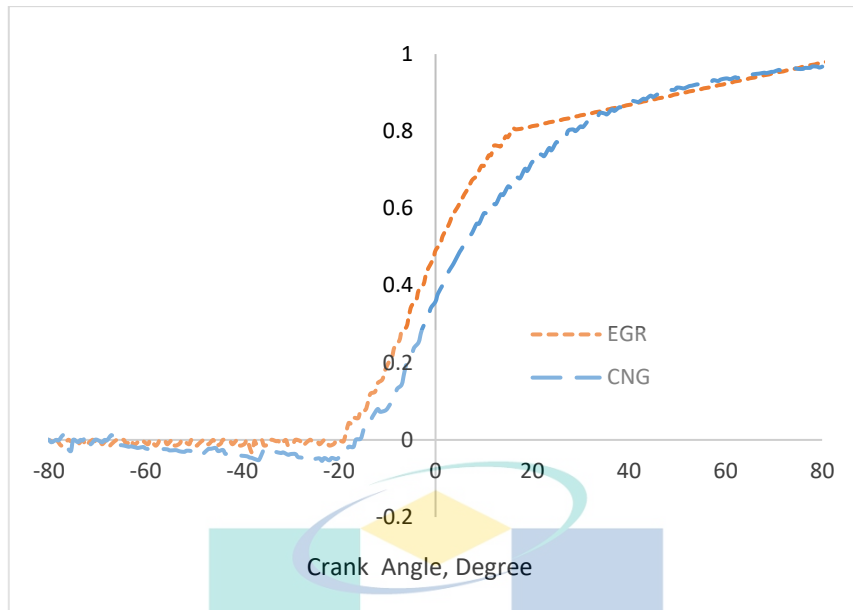


Figure 4.29 Effect of EGR addition on the mass burned fraction at 1,800 rpm

Mainly, in spark ignition engines, the laminar flame velocity (LFV) of the air-fuel mixture is an important factor that affects the combustion process and engine performance as well. The flame burning velocity of the combustible gases in the fuel mixture are ( $H_2=2.10$  m/s,  $CH_4=0.40$  m/s,  $CO=0.285$  m/s) (Korb, et al., 2016). The higher flame velocity of the hydrogen can improve the total flame speed of the mixture and thermal efficiency of the engine as well and this is the main reason beyond the reduction of the combustion duration. As shown in Table 4.6, the laminar flame velocity of the natural gas with the reformat addition is higher than pure natural gas. Therefore, the combustion duration was reduced which was  $60.5$  °CA and  $38.5$  °CA in pure natural gas and natural gas with reformat addition, respectively. Similar combustion characteristics outcomes were obtained by Z. He et al. (Zhuoyao He, Zhan Gao, Lei Zhu, Shujing Li b, Ang Li, Wugao Zhang, 2016)

Table 4.6 Calculated laminar flame velocity, combustion duration and adiabatic flame temperature

Fuel	LFV (m/s)	Combustion Duration °CA	Adiabatic flame Temperature
Natural gas	0.232	60.5	1785.0
Natural gas + EGR	0.260	38.5	1805.5

## CHAPTER 5

### CONCLUSION AND RECOMMENDATIONS

#### 5.1 Introduction

The objective of this study was to study the on-board production of hydrogen-rich syngas through the exhaust gas reforming in spark-ignition engine fueled by natural gas. Moreover, it was also aimed to investigate the effect of the produced hydrogen-rich syngas addition on the combustion characteristics of an SI engine compared with a pure natural gas combustion. The exhaust gas reforming process is performed at full-load, and the engine speed is varied from 1,200-3,000 rpm with an interval of 300 rpm.

The exhaust gas reforming is conducted in a catalytic reactor. Therefore, in this study, a fixed-bed catalytic reactor is modelled using 1D mathematical modelling to investigate the required amount of catalyst and natural gas flow rate at each engine speed. The CCD RSM optimization is used to select a fixed natural gas flow rate and fixed catalyst mass for all the engine speeds used in this study. Then, after the catalyst mass and natural gas flow rate are selected, the reactor is sized by selecting its length and diameter based on the catalyst mass and density. The sized reactor is further simulated through a 2D CFD porous medium model at various conditions. Finally, the 3D CFD model is conducted to study the effect of reformat gas addition on the engine combustion characteristics compared with the pure natural gas.

Exhaust gas reforming of natural gas is mainly evaluated by the achieved methane conversion and hydrogen-rich syngas production. The effect of reformat addition on the combustion characteristics is evaluated by observing the change of in-cylinder pressure, heat release rate and mass burned fraction in the case of pure natural gas use and in the case of the reformat gas addition.

In conclusion all the objectives of this study were achieved. It was found that the exhaust gas reforming process is beneficial for spark ignition engine that powered by natural gas. Thus, the exhaust gas reforming can convert methane and exhaust gas to syngas that can be used for combustion enhancement. It was also shown by CFD simulation that the addition of the reforming products can lead to a significant enhancement in the combustion characteristics of SI engine. Thus, the reforming technology can produce the sufficient amount of hydrogen-rich syngas needed for combustion and performance enhancement in natural gas engines.

## 5.2 Conclusion Remarks

The evaluation of the reforming process and combustion characteristics are as follows:

### 5.2.1 Objective 1

- The effect of engine speed on the reforming characteristics is investigated by 1D mathematical modelling using reactor design algorithms and chemical kinetic. It is found that as the engine speed increased, more natural gas and less catalyst mass is needed. The methane conversion has increased with the rise of the engine speed. The amount of syngas ( $H_2+CO$ ) in the reformat mixture has increased with the higher engine speeds from 1,200-2,100 rpm and then reduced at engine speeds higher than 2,100 rpm.
- The results of the 1D modelling showed that the amount of catalyst mass at the lowest and highest engine speed use in this study are 850 g and 350 g, respectively. The natural gas flow rate at 1,200 rpm and 3,000 rpm are reported at 21.43 mol/hr and 62.85 mol/hr, respectively.
- In order to have a fixed catalyst mass and natural gas flow rate, CCD RSM optimization was used to determine the minimum catalyst mass and natural gas flow rate to achieve the maximum possible methane conversion and syngas concentrations in the reformat mixture. RSM optimization has shown that the amount of natural gas and catalyst mass needed to achieve the desired syngas production and methane

conversion are 35 Mol/hr and 850 g. The maximum syngas production is achieved at 2,100 rpm with 25.3023%. The maximum methane conversion is achieved at 3,000 rpm with 73.033%.

### 5.2.2 Objective 2

- The size of the fixed reactor is selected from the optimization study, and the dimension of the reformer is selected and simulated by 2D CFD. It is found that the temperature increased along the reactor at each engine speed. Methane conversion increase with the engine speed is noticed. The syngas concentration in the mixture has increased and then started to decrease above 2,100 rpm. The rise in EGR rate has led to lower methane conversion and higher carbon dioxide consumption. Whereas the syngas production reduced with the rise of the EGR rate. The effect of steam addition on the methane conversion and syngas production is also simulated. It is found that the addition of steam led to higher methane conversion and syngas concentration in the reformat mixture, but as the amount of steam became much higher the amount of methane, less conversion is achieved. The effect of air addition on the reforming characteristics is investigated at 1,800 rpm. It is found that the addition of more air resulted in higher methane conversion, but at the same time, the amount of hydrogen has decreased with the rise of the air in the reactant due to the higher water content generated from the complete oxidation reaction. Also, the effect of wall temperature on the reforming characteristics is tested. It is found that the amount of hydrogen and carbon dioxide production has increased with the higher wall temperature, which is represented by the lower ratio of  $H_2/CO$  with the rise of wall temperature. It is also noticed that the, higher methane conversion is obtained with a higher wall temperature.
- It was found that the maximum percentage syngas and methane conversion could be achieved were 28% and 77% by 2D CFD simulation at 2,100 rpm. Whereas in 1D modelling, the percentage of generated syngas and converted methane were 26% and 74% at 2,100 rpm.

### 5.2.3 Objective 3

- 3D CFD simulation is performed to evaluate the effect of the addition of the reformat on the combustion characteristics. It is found that the addition of the reformat gas enhanced the combustion characteristics. Higher in-cylinder pressure and higher heat release rate are achieved, and a faster mass burned fraction is observed in the case of the reformat gas addition as compared to the pure natural gas combustion. The enhancement of the combustion is due to the higher calorific value and density in the case of the reformat addition which led to higher energy release from the combustion of the syngas beside the main combustion of the natural gas.

### 5.3 Recommendations

1. This study is conducted by mathematical modelling and CFD simulation. Therefore, further experimental and optimization are required for optimum reformer design and combustion evaluation.
2. This study has neglected coke formation and catalyst activity. Therefore, the coke formation and catalyst activation time are required to be investigated to avoid any catalyst deactivation, which may affect the reforming performance.
3. The reformer should be evaluated using the real exhaust components by including the components that are neglected in this study. This study is important to avoid any negative effect of the hydrocarbons (HC) or  $\text{NO}_x$  on the catalyst activity and reforming performance as well.
4. This study focused on the effect of the reformat gas on the combustion characteristics. Therefore, another study needs to be conducted to investigate the effect of the reformat gas on the exhaust gas emission because the high-temperature release from hydrogen combustion may lead to higher  $\text{NO}_x$  emission.
5. The reformer should be fabricated and to be installed with the engine setup to test the combustion, engine performance and exhaust gas emission experimentally.

## REFERENCES

- Abdullah, B., Abd Ghani, N. A., & Vo, D. V. N. (2017a). Recent advances in dry reforming of methane over Ni-based catalysts. *Journal of Cleaner Production*, 162, 170–185. <https://doi.org/10.1016/j.jclepro.2017.05.176>
- Abdullah, B., Abd Ghani, N. A., & Vo, D. V. N. (2017b). Recent advances in dry reforming of methane over Ni-based catalysts. *Journal of Cleaner Production*, 162, 170–185. <https://doi.org/10.1016/j.jclepro.2017.05.176>
- Aboosadi, Z. A., Jahanmiri, A. H., & Rahimpour, M. R. (2011). Optimization of tri-reformer reactor to produce synthesis gas for methanol production using differential evolution ( DE ) method. *Applied Energy*, 88(8), 2691–2701. <https://doi.org/10.1016/j.apenergy.2011.02.017>
- Açikgöz, B., Çelik, C., Soyhan, H. S., Gökalp, B., & Karabağ, B. (2015). Emission characteristics of an hydrogen-CH<sub>4</sub> fuelled spark ignition engine. *Fuel*, 159(x), 298–307. <https://doi.org/10.1016/j.fuel.2015.06.043>
- Aghamohammadi, S., Haghghi, M., & Maleki, M. (2017). Sequential impregnation vs . sol-gel synthesized Ni / Al<sub>2</sub>O<sub>3</sub> -CeO<sub>2</sub> nanocatalyst for dry reforming of methane : Effect of synthesis method and support promotion. *Molecular Catalysis*, 431, 39–48. <https://doi.org/10.1016/j.mcat.2017.01.012>
- Alrazen, H. A., & Ahmad, K. A. (2018). HCNG fueled spark-ignition ( SI ) engine with its effects on performance and emissions. *Renewable and Sustainable Energy Reviews*, 82(July 2016), 324–342. <https://doi.org/10.1016/j.rser.2017.09.035>
- Altın, İ., Bilgin, A., & Çeper, B. A. (2017). Parametric study on some combustion characteristics in a natural gas fueled dual plug SI engine. *Energy*, 139, 1237–1242. <https://doi.org/10.1016/j.energy.2017.04.026>
- Alvarez-Galvan, C., Melian, M., Ruiz-Matas, L., Eslava, J. L., Navarro, R. M., Ahmadi, M., Cuenya, B. R., & Fierro, J. L. G. (2019). Partial oxidation of methane to syngas over nickel-based catalysts: Influence of support type, addition of rhodium, and preparation method. *Frontiers in Chemistry*, 7(MAR), 1–16. <https://doi.org/10.3389/fchem.2019.00104>
- Angeli, S. D., Monteleone, G., Giaconia, A., & Lemonidou, A. A. (2014a). State-of-the-art catalysts for CH<sub>4</sub> steam reforming at low temperature. *International Journal of Hydrogen Energy*, 39(5), 1979–1997. <https://doi.org/10.1016/j.ijhydene.2013.12.001>
- Angeli, S. D., Monteleone, G., Giaconia, A., & Lemonidou, A. A. (2014b). State-of-the-art catalysts for CH<sub>4</sub> steam reforming at low temperature. *International Journal of Hydrogen Energy*, 39(5), 1979–1997. <https://doi.org/10.1016/j.ijhydene.2013.12.001>

Antonius Indarto, J. P. (2007). *SYNGAS PRODUCTION, APPLICATIONS AND ENVIRONMENTAL IMPACT* No. Nova.

Aramouni, N. A. K., Touma, J. G., Tarboush, B. A., Zeaiter, J., & Ahmad, M. N. (2018a). Catalyst design for dry reforming of methane: Analysis review. *Renewable and Sustainable Energy Reviews*, 82(November 2017), 2570–2585. <https://doi.org/10.1016/j.rser.2017.09.076>

Aramouni, N. A. K., Touma, J. G., Tarboush, B. A., Zeaiter, J., & Ahmad, M. N. (2018b). Catalyst design for dry reforming of methane: Analysis review. *Renewable and Sustainable Energy Reviews*, 82(November 2017), 2570–2585. <https://doi.org/10.1016/j.rser.2017.09.076>

Arku, P., Regmi, B., & Dutta, A. (2018). A review of catalytic partial oxidation of fossil fuels and biofuels: Recent advances in catalyst development and kinetic modelling. *Chemical Engineering Research and Design*, 136, 385–402. <https://doi.org/10.1016/j.cherd.2018.05.044>

Arman, A., Hagos, F. Y., Abdullah, A. A., Mamat, R., Aziz, A. R. A., & Cheng, C. K. (2020). Syngas production through steam and CO<sub>2</sub> reforming of methane over Ni-based catalyst-A Review. *IOP Conference Series: Materials Science and Engineering*, 736(4). <https://doi.org/10.1088/1757-899X/736/4/042032>

Baudouin, D., Rodemerck, U., Krumeich, F., Mallmann, A. De, Szeto, K. C., Ménard, H., Veyre, L., Candy, J., Webb, P. B., Thieuleux, C., & Copéret, C. (2013). Particle size effect in the low temperature reforming of methane by carbon dioxide on silica-supported Ni nanoparticles. *Journal of Catalysis*, 297, 27–34. <https://doi.org/10.1016/j.jcat.2012.09.011>

Baxter, R., Hastings, N., Law, A., & Glass, E. J. . (2008a). Hydrogen and Syngas Production and Purification Technologies. In *A John Wiley & Sons* (Vol. 39, Issue 5). A John Wiley & Sons.

Baxter, R., Hastings, N., Law, A., & Glass, E. J. . (2008b). Industrial Gases Processing. In *WILEY-VCH Verlag GmbH & CO. KGaA* (Vol. 39, Issue 5).

Bogarra, M., Herreros, J. M., Tsolakis, A., York, A. P. E., Millington, P. J., & Martos, F. J. (2017). Impact of exhaust gas fuel reforming and exhaust gas recirculation on particulate matter morphology in Gasoline Direct Injection Engine. *Journal of Aerosol Science*, 103, 1–14. <https://doi.org/10.1016/j.jaerosci.2016.10.001>

Bradford, M. C. J., & Vannice, M. A. (1996). Catalytic reforming of methane with carbon dioxide over nickel catalysts I. Catalyst characterization and activity. *Applied Catalysis A: General*, 142(1), 73–96. [https://doi.org/10.1016/0926-860X\(96\)00065-8](https://doi.org/10.1016/0926-860X(96)00065-8)

Bruce E. Poling, George H. Thomson, Daniel G. Friend, Richard L. Rowley, W. V. W. (2008). *Perry 's Chemical Engineers, Physical and Chemical Data* (D. W. G. Robert H. Perry (ed.)). McGRAW-HILL. <https://doi.org/10.1036/0071511253>

- Bulutoglu, P. S., Koc, S., & Avci, A. K. (2015). ScienceDirect Simulation of exhaust gas reforming of natural gas in a microchannel reactor. *International Journal of Hydrogen Energy*, 41(19), 8184–8192.  
<https://doi.org/10.1016/j.ijhydene.2015.10.126>
- Changpeng Liu, Wang, Z., Song, H., Qi, Y., A, Y. L., Li, F., Zhang, W., & He, X. (2018). Experimental and numerical investigation on H<sub>2</sub> / CO formation and their effects on combustion characteristics in a natural gas SI engine. *Energy*, 143, 597–605. <https://doi.org/10.1016/j.energy.2017.11.024>
- Chen, D., Ignatius, J., Sun, D., Goh, M., & Zhan, S. (2018). Impact of congestion pricing schemes on emissions and temporal shift of freight transport. *Transportation Research Part E: Logistics and Transportation Review*, 118(July), 77–105. <https://doi.org/10.1016/j.tre.2018.07.006>
- Chen, H., He, J., & Zhong, X. (2018). Engine combustion and emission fuelled with natural gas : A review. *Journal of the Energy Institute*, 1–14.  
<https://doi.org/10.1016/j.joei.2018.06.005>
- Choi, S., Bae, J., Lee, J., & Cha, J. (2017a). Exhaust gas fuel reforming for hydrogen production with CGO-based precious metal catalysts. *Chemical Engineering Science*, 163, 206–214. <https://doi.org/10.1016/j.ces.2017.01.010>
- Choi, S., Bae, J., Lee, J., & Cha, J. (2017b). Exhaust gas fuel reforming for hydrogen production with CGO-based precious metal catalysts. *Chemical Engineering Science*, 163, 206–214. <https://doi.org/10.1016/j.ces.2017.01.010>
- Christian Enger, B., Lødeng, R., & Holmen, A. (2008). A review of catalytic partial oxidation of methane to synthesis gas with emphasis on reaction mechanisms over transition metal catalysts. *Applied Catalysis A: General*, 346(1–2), 1–27.  
<https://doi.org/10.1016/j.apcata.2008.05.018>
- Companies, T. M. (1999). *Perry 's Chemical Engineers ' (D. W. G. Perry, Robert H. (ed.)). The Mcgraw-hill.*
- Dai, X., Ji, C., Wang, S., Liang, C., Liu, X., & Ju, B. (2012). Effect of syngas addition on performance of a spark-ignited gasoline engine at lean conditions. *International Journal of Hydrogen Energy*, 37(19), 14624–14631.  
<https://doi.org/10.1016/j.ijhydene.2012.07.039>
- Delgado, K., Maier, L., Tischer, S., Zellner, A., Stotz, H., & Deutschmann, O. (2015). Surface Reaction Kinetics of Steam- and CO<sub>2</sub>-Reforming as Well as Oxidation of Methane over Nickel-Based Catalysts. *Catalysts*, 5(2), 871–904.  
<https://doi.org/10.3390/catal5020871>
- Deposition, C. (2017). *Computational Fluid Dynamics Study of the Dry Reforming of Methane over Ni / Al<sub>2</sub> O<sub>3</sub> Catalyst in a Membrane Reactor .* 58(3), 328–329.  
<https://doi.org/10.1134/S0023158417030028>

- Dwivedi, A., Gudi, R., & Biswas, P. (2017). ScienceDirect An improved tri-reforming based methanol production process for enhanced CO<sub>2</sub> valorization. *International Journal of Hydrogen Energy*, 42(36), 23227–23241. <https://doi.org/10.1016/j.ijhydene.2017.07.166>
- Elsayed, N. H., Roberts, N. R. M., Joseph, B., & Kuhn, J. N. (2015). Applied Catalysis B : Environmental Low temperature dry reforming of methane over Pt – Ni – Mg / ceria – zirconia catalysts. “*Applied Catalysis B, Environmental*,” 179, 213–219. <https://doi.org/10.1016/j.apcatb.2015.05.021>
- Fauteux-Lefebvre, C., Abatzoglou, N., Blanchard, J., & Gitzhofer, F. (2010). Steam reforming of liquid hydrocarbons over a nickel-alumina spinel catalyst. *Journal of Power Sources*, 195(10), 3275–3283. <https://doi.org/10.1016/j.jpowsour.2009.11.121>
- Fekri Lari, M., Farsi, M., & Rahimpour, M. R. (2019). Modification of a tri-reforming reactor based on the feeding policy to couple with methanol and GTL units. *Chemical Engineering Research and Design*, 144(2014), 107–114. <https://doi.org/10.1016/j.cherd.2019.01.029>
- Fennell, D., Herreros, J., Tsolakis, A., Cockle, K., Pignon, J., & Millington, P. (2015). Thermochemical recovery technology for improved modern engine fuel economy- part 1: Analysis of a prototype exhaust gas fuel reformer. *RSC Advances*, 5(44), 35252–35261. <https://doi.org/10.1039/c5ra03111g>
- Fennell, Daniel, Herreros, J., & Tsolakis, A. (2014). Improving gasoline direct injection (GDI) engine efficiency and emissions with hydrogen from exhaust gas fuel reforming. *International Journal of Hydrogen Energy*, 39(10), 5153–5162. <https://doi.org/10.1016/j.ijhydene.2014.01.065>
- Fontana, G., & Galloni, E. (2010). Experimental analysis of a spark-ignition engine using exhaust gas recycle at WOT operation. *Applied Energy*, 87(7), 2187–2193. <https://doi.org/10.1016/j.apenergy.2009.11.022>
- Fotache, C. G., Kreutz, T. G., & Law, C. K. (1997). Ignition of hydrogen-enriched methane by heated air. *Combustion and Flame*, 110(4), 429–440. [https://doi.org/10.1016/S0010-2180\(97\)00084-9](https://doi.org/10.1016/S0010-2180(97)00084-9)
- Gaber, C., Demuth, M., Prieler, R., Schluckner, C., Schroettner, H., Fitzek, H., & Hochenauer, C. (2019). Experimental investigation of thermochemical regeneration using oxy-fuel exhaust gases. *Applied Energy*, 236(December 2018), 1115–1124. <https://doi.org/10.1016/j.apenergy.2018.12.046>
- Gálvez, M. E., Albarazi, A., & Costa, P. Da. (2015). Applied Catalysis A : General Enhanced catalytic stability through non-conventional synthesis of Ni / SBA-15 for methane dry reforming at low temperatures. “*Applied Catalysis A, General*,” 504, 143–150. <https://doi.org/10.1016/j.apcata.2014.10.026>
- García, L. (2015). Hydrogen production by steam reforming of natural gas and other

nonrenewable feedstocks. In *Compendium of Hydrogen Energy*. Elsevier Ltd. <https://doi.org/10.1016/b978-1-78242-361-4.00004-2>

- Ghoneim, S. A., El-Salamony, R. A., & El-Temtamy, S. A. (2016). Review on Innovative Catalytic Reforming of Natural Gas to Syngas. *World Journal Of Engineering and Technology*, 4(February), 116–139. <https://doi.org/10.4236/wjet.2016.41011>
- Golunski, S. (2010). What is the point of on-board fuel reforming? *Energy Environ. Sci.*, 3(12), 1918–1923. <https://doi.org/10.1039/C0EE00252F>
- Gosiewski, K., Bartmann, U., Moszczyński, M., & Mleczko, L. (1999). Effect of the intraparticle mass transport limitations on temperature profiles and catalytic performance of the reverse-flow reactor for the partial oxidation of methane to synthesis gas. In *Chemical Engineering Science - CHEM ENG SCI* (Vol. 54). Chemical Engineering Science - CHEM ENG SCI. [https://doi.org/10.1016/S0009-2509\(99\)00132-3](https://doi.org/10.1016/S0009-2509(99)00132-3)
- Guo, D., Wen, J. H., & Wang, G. C. (2019). Coordination dependence of carbon deposition resistance in partial oxidation of methane on Rh catalysts. *Catalysis Today*, February, 1–13. <https://doi.org/10.1016/j.cattod.2019.07.017>
- Hagos, F. Y., Aziz, A. R. A., & Sulaiman, S. A. (2014a). Syngas (H<sub>2</sub>/CO) in a spark-ignition direct-injection engine. Part 1: Combustion, performance and emissions comparison with CNG. *International Journal of Hydrogen Energy*, 39(31), 17884–17895. <https://doi.org/10.1016/j.ijhydene.2014.08.141>
- Hagos, F. Y., Aziz, A. R. A., & Sulaiman, S. A. (2014b). Trends of syngas as a fuel in internal combustion engines. *Advances in Mechanical Engineering*, 2014(January). <https://doi.org/10.1155/2014/401587>
- Halabi, M. H., Croon, M. H. J. M. De, Schaaf, J. Van Der, Cobden, P. D., & Schouten, J. C. (2008). Modeling and analysis of autothermal reforming of methane to hydrogen in a fixed bed reformer. *Chemical Engineering Journal*, 137, 568–578. <https://doi.org/10.1016/j.cej.2007.05.019>
- Hossain, M. A., Ayodele, B. V., Cheng, C. K., & Khan, M. R. (2019). Optimization of renewable hydrogen-rich syngas production from catalytic reforming of greenhouse gases (CH<sub>4</sub> and CO<sub>2</sub>) over calcium iron oxide supported nickel catalyst. *Journal of the Energy Institute*, 92(1), 177–194. <https://doi.org/10.1016/j.joei.2017.10.010>
- Ilsen Önsan, Z., & Avcı, A. K. (2011). Reactor Design for Fuel Processing. In *Fuel Cells: Technologies for Fuel Processing*. <https://doi.org/10.1016/B978-0-444-53563-4.10014-8>
- Imran, M., Yasmeen, T., Ijaz, M., Farooq, M., & Wakeel, M. (2016). Research progress in the development of natural gas as fuel for road vehicles : A bibliographic review ( 1991 – 2016 ). *Renewable and Sustainable Energy Reviews*, 66, 702–741.

<https://doi.org/10.1016/j.rser.2016.08.041>

Inc., A. (2016). ANSYS Fluent Theory Guide v17.1. *ANSYS 17.1 Documentation*, 15317(April), 850.

Iulianelli, A., Ribeirinha, P., Mendes, A., & Basile, A. (2014). Methanol steam reforming for hydrogen generation via conventional and membrane reactors: A review. *Renewable and Sustainable Energy Reviews*, 29, 355–368. <https://doi.org/10.1016/j.rser.2013.08.032>

Janardhanan, V. M., Appari, S., Jayanti, S., & Deutschmann, O. (2011). Numerical study of on-board fuel reforming in a catalytic plate reactor for solid-oxide fuel cells. *Chemical Engineering Science*, 66(3), 490–498. <https://doi.org/10.1016/j.ces.2010.11.023>

Jang, W. J., Jeong, D. W., Shim, J. O., Kim, H. M., Roh, H. S., Son, I. H., & Lee, S. J. (2016). Combined steam and carbon dioxide reforming of methane and side reactions: Thermodynamic equilibrium analysis and experimental application. *Applied Energy*, 173, 80–91. <https://doi.org/10.1016/j.apenergy.2016.04.006>

Jang, W. J., Shim, J. O., Kim, H. M., Yoo, S. Y., & Roh, H. S. (2018). A review on dry reforming of methane in aspect of catalytic properties. *Catalysis Today*, July, 0–1. <https://doi.org/10.1016/j.cattod.2018.07.032>

Ji, G., Zhao, M., & Wang, G. (2018). Computational fluid dynamic simulation of a sorption-enhanced palladium membrane reactor for enhancing hydrogen production from methane steam reforming. *Energy*, 147, 884–895. <https://doi.org/10.1016/j.energy.2018.01.092>

Jiménez-González, C., Gil-Calvo, M., De Rivas, B., González-Velasco, J. R., Gutiérrez-Ortiz, J. I., & López-Fonseca, R. (2016). Oxidative Steam Reforming and Steam Reforming of Methane, Isooctane, and N-Tetradecane over an Alumina Supported Spinel-Derived Nickel Catalyst. *Industrial and Engineering Chemistry Research*, 55(14), 3920–3929. <https://doi.org/10.1021/acs.iecr.6b00461>

Kakaee, A. H., Paykani, A., & Ghajar, M. (2014). The influence of fuel composition on the combustion and emission characteristics of natural gas fueled engines. *Renewable and Sustainable Energy Reviews*, 38, 64–78. <https://doi.org/10.1016/j.rser.2014.05.080>

Kakaee, A., & Paykani, A. (2013). Research and development of natural-gas fueled engines in Iran. *Renewable and Sustainable Energy Reviews*, 26, 805–821. <https://doi.org/10.1016/j.rser.2013.05.048>

Kamil, M., & Rahman, M. M. (2015). Performance prediction of spark-ignition engine running on gasoline-hydrogen and methane-hydrogen blends. *Applied Energy*, 158, 556–567. <https://doi.org/10.1016/j.apenergy.2015.08.041>

Kathiraser, Y., Oemar, U., Saw, E. T., Li, Z., & Kawi, S. (2015). Kinetic and

mechanistic aspects for CO<sub>2</sub> reforming of methane over Ni based catalysts. *Chemical Engineering Journal*, 278, 62–78. <https://doi.org/10.1016/j.cej.2014.11.143>

- Keiski, R. L., Ojala, S., Huuhtanen, M., Kolli, T., & Leiviskä, K. (2011). Partial oxidation (POX) processes and technology for clean fuel and chemical production. In *Advances in Clean Hydrocarbon Fuel Processing: Science and Technology*. Woodhead Publishing Limited. <https://doi.org/10.1533/9780857093783.3.262>
- Korb, B., Kawauchi, S., & Wachtmeister, G. (2016). Influence of hydrogen addition on the operating range, emissions and efficiency in lean burn natural gas engines at high specific loads. *Fuel*, 164, 410–418. <https://doi.org/10.1016/j.fuel.2015.09.080>
- Kumar, J., & Bansal, A. (2013). Photocatalytic degradation in annular reactor: Modelization and optimization using computational fluid dynamics (CFD) and response surface methodology (RSM). *Journal of Environmental Chemical Engineering*, 1(3), 398–405. <https://doi.org/10.1016/j.jece.2013.06.002>
- Kumar, P., Sun, Y., & Idem, R. O. (2007). Nickel-Based Ceria, Zirconia, and Ceria–Zirconia Catalytic Systems for Low-Temperature Carbon Dioxide Reforming of Methane. *Energy & Fuels*, 21(6), 3113–3123. <https://doi.org/10.1021/ef7002409>
- Li, X., Hu, Q., Yang, Y., Wang, Y., & He, F. (2012). Studies on stability and coking resistance of Ni/BaTiO<sub>3</sub>-Al<sub>2</sub>O<sub>3</sub> catalysts for lower temperature dry reforming of methane (LTDRM). *Applied Catalysis A: General*, 413–414, 163–169. <https://doi.org/10.1016/j.apcata.2011.11.004>
- Liao, C., & Horng, R. (2017). ScienceDirect Experimental study of syngas production from methane dry reforming with heat recovery strategy. *International Journal of Hydrogen Energy*, 42(40), 25213–25224. <https://doi.org/10.1016/j.ijhydene.2017.01.238>
- Liu, C., Li, F., Song, H., & Wang, Z. (2018). Effects of H<sub>2</sub> / CO addition on knock tendency and lean limit in a natural gas SI engine. *Fuel*, 233(June), 582–591. <https://doi.org/10.1016/j.fuel.2018.06.102>
- Long, Y., Li, G., Zhang, Z., & Liang, J. (2018). ScienceDirect Effects of reformed exhaust gas recirculation on the HC and CO emissions of a spark-ignition engine fueled with LNG. *International Journal of Hydrogen Energy*, 43(45), 21070–21078. <https://doi.org/10.1016/j.ijhydene.2018.09.077>
- Lu, H., Deng, J., Hu, Z., Wu, Z., Li, L., Yuan, F., Xie, D., Yuan, S., & Shen, Y. (2016). *Study on Fuel Economy Improvement by Low Pressure Water-Cooled EGR System on a Downsized Boosted Gasoline Engine*. SAE International . <https://doi.org/10.4271/2016-01-0678>
- Ma, R., Xu, B., & Zhang, X. (2019). Catalytic partial oxidation (CPOX) of natural gas and renewable hydrocarbons/oxygenated hydrocarbons—A review. *Catalysis Today*, 338(June), 18–30. <https://doi.org/10.1016/j.cattod.2019.06.025>

- Nathan, A. J., & Scobell, A. (2012). FUEL CELLS: TECHNOLOGIES FOR FUEL PROCESSING. In *Foreign Affairs* (Vol. 91, Issue 5).  
<https://doi.org/10.1017/CBO9781107415324.004>
- O. Deutschmann. (2008). *Computational Fluid Dynamics Simulation of Catalytic Reactors, Handbook of Heterogeneous Catalysis*.
- Özener, O., & Özkan, M. (2020). Fuel consumption and emission evaluation of a rapid bus transport system at different operating conditions. *Fuel*, 265(November 2019), 117016. <https://doi.org/10.1016/j.fuel.2020.117016>
- Pakhare, D., & Spivey, J. (2014). A review of dry (CO<sub>2</sub>) reforming of methane over noble metal catalysts. *Chemical Society Reviews*, 43(22), 7813–7837.  
<https://doi.org/10.1039/c3cs60395d>
- Pashchenko, D. (2019). Numerical study of steam methane reforming over a pre-heated Ni-based catalyst with detailed fluid dynamics. *Fuel*, 236(September 2018), 686–694. <https://doi.org/10.1016/j.fuel.2018.09.033>
- Qader, B. S., Supeni, E. E., Ariffin, M. K. A., & Talib, A. R. A. (2019). RSM approach for modeling and optimization of designing parameters for inclined fins of solar air heater. *Renewable Energy*, 136, 48–68.  
<https://doi.org/10.1016/j.renene.2018.12.099>
- Ravindra, K., Wauters, E., Tyagi, S. K., Mor, S., & Van Grieken, R. (2006). Assessment of air quality after the implementation of compressed natural gas (CNG) as fuel in public transport in Delhi, India. *Environmental Monitoring and Assessment*, 115(1–3), 405–417. <https://doi.org/10.1007/s10661-006-7051-5>
- Raviteja, S., & Kumar, G. N. (2015). Effect of hydrogen addition on the performance and emission parameters of an SI engine fueled with butanol blends at stoichiometric conditions. *International Journal of Hydrogen Energy*, 40(30), 9563–9569. <https://doi.org/10.1016/j.ijhydene.2015.05.171>
- Richardson, J. T., Garrat, M., & Hung, J. K. (2003). Carbon dioxide reforming with Rh and Pt-Re catalysts dispersed on ceramic foam supports. *Applied Catalysis A: General*, 255(1), 69–82. [https://doi.org/10.1016/S0926-860X\(03\)00645-8](https://doi.org/10.1016/S0926-860X(03)00645-8)
- Sadeghi, M., Jafari, M., Yari, M., & Mahmoudi, S. M. S. (2018). Exergoeconomic assessment and optimization of a syngas production system with a desired H<sub>2</sub>/CO ratio based on methane tri-reforming process. *Journal of CO<sub>2</sub> Utilization*, 25(April), 283–301. <https://doi.org/10.1016/j.jcou.2018.04.009>
- Sahoo, B. B., Saha, U. K., & Sahoo, N. (2011). Theoretical performance limits of a syngas-diesel fueled compression ignition engine from second law analysis. *Energy*, 36(2), 760–769. <https://doi.org/10.1016/j.energy.2010.12.045>
- Sahoo, B. B., Sahoo, N., & Saha, U. K. (2012). Effect of H<sub>2</sub>:CO ratio in syngas on the performance of a dual fuel diesel engine operation. *Applied Thermal Engineering*,

49, 139–146. <https://doi.org/10.1016/j.applthermaleng.2011.08.021>

- Schmal, M., Toniolo, F. S., & Kozonoe, C. E. (2018). Applied Catalysis A , General Perspective of catalysts for ( Tri ) reforming of natural gas and flue gas rich in. *Applied Catalysis A, General*, 568(July), 23–42. <https://doi.org/10.1016/j.apcata.2018.09.017>
- Schneider, A., Mantzaras, J., & Jansohn, P. (2006). *Experimental and numerical investigation of the catalytic partial oxidation of CH<sub>4</sub> / O<sub>2</sub> mixtures diluted with H<sub>2</sub> O and CO<sub>2</sub> in a short contact time reactor*. 61, 4634–4649. <https://doi.org/10.1016/j.ces.2006.02.038>
- Schwiedernoch, R., Tischer, S., Correa, C., & Deutschmann, O. (2003). Experimental and numerical study on the transient behavior of partial oxidation of methane in a catalytic monolith. *Chemical Engineering Science*, 58(3–6), 633–642. [https://doi.org/10.1016/S0009-2509\(02\)00589-4](https://doi.org/10.1016/S0009-2509(02)00589-4)
- Sengodan, S., Lan, R., Humphreys, J., Du, D., Xu, W., Wang, H., & Tao, S. (2018). Advances in reforming and partial oxidation of hydrocarbons for hydrogen production and fuel cell applications. *Renewable and Sustainable Energy Reviews*, 82(July 2017), 761–780. <https://doi.org/10.1016/j.rser.2017.09.071>
- Smith, M. W., & Shekhawat, D. (2011). Catalytic Partial Oxidation. In *Fuel Cells: Technologies for Fuel Processing*. Elsevier. <https://doi.org/10.1016/B978-0-444-53563-4.10005-7>
- Soria, M. A., & Rodemerck, U. (2013). Applied Catalysis B : Environmental Transient studies of low-temperature dry reforming of methane over. “*Applied Catalysis B, Environmental*,” 129, 450–459. <https://doi.org/10.1016/j.apcatb.2012.09.052>
- Subramani, V., Sharma, P., Zhang, L., & Liu, K. (2009). Catalytic Steam Reforming Technology for the Production of Hydrogen and Syngas. In *Hydrogen and Syngas Production and Purification Technologies*. <https://doi.org/doi:10.1002/9780470561256.ch2>
- Tartakovsky, L., & Sheintuch, M. (2018). Fuel reforming in internal combustion engines. *Progress in Energy and Combustion Science*, 67, 88–114. <https://doi.org/10.1016/j.pecs.2018.02.003>
- Trimm, D. L., & Lam, C.-W. (1980). The combustion of methane on platinum—alumina fibre catalysts—I: kinetics and mechanism. *Chemical Engineering Science*, 35(6), 1405–1413. [https://doi.org/10.1016/0009-2509\(80\)85134-7](https://doi.org/10.1016/0009-2509(80)85134-7)
- Trimm, D. L., & Önsan, Z. I. (2011). Catalysis Reviews : Science and Engineering ONBOARD FUEL CONVERSION FOR HYDROGEN-FUEL- CELL-DRIVEN VEHICLES. *Catalysis Reviews*, 43(November 2012), 31–84. <https://doi.org/10.1081/CR-100104386>
- Tu, X., & Whitehead, J. C. (2012). *Applied Catalysis B : Environmental Plasma-*

*catalytic dry reforming of methane in an atmospheric dielectric barrier discharge : Understanding the synergistic effect at low temperature. 125, 439–448.*  
<https://doi.org/10.1016/j.apcatb.2012.06.006>

Usman, M., Wan Daud, W. M. A., & Abbas, H. F. (2015). Dry reforming of methane: Influence of process parameters - A review. *Renewable and Sustainable Energy Reviews, 45*, 710–744. <https://doi.org/10.1016/j.rser.2015.02.026>

Wang, S. (1999). A Comprehensive Study on Carbon Dioxide Reforming of Methane over Ni/ $\gamma$ -Al<sub>2</sub>O<sub>3</sub> Catalysts. *Industrial & Engineering Chemistry Research, 38*(7), 2615–2625. <https://doi.org/10.1021/ie980489t>

Wang, Y., Yao, L., Wang, S., Mao, D., & Hu, C. (2018). Low-temperature catalytic CO<sub>2</sub> dry reforming of methane on Ni-based catalysts: A review. *Fuel Processing Technology, 169*(October 2017), 199–206. <https://doi.org/10.1016/j.fuproc.2017.10.007>

Wang, Y., Yao, L., Wang, Y., Wang, S., Zhao, Q., Mao, D., & Hu, C. (2018). Low-Temperature Catalytic CO<sub>2</sub> Dry Reforming of Methane on Ni-Si/ZrO<sub>2</sub> Catalyst. *ACS Catalysis, 8*(7), 6495–6506. <https://doi.org/10.1021/acscatal.8b00584>

Yabe, T., Mitarai, K., Oshima, K., Ogo, S., & Sekine, Y. (2017). Low-temperature dry reforming of methane to produce syngas in an electric field over La-doped Ni / ZrO<sub>2</sub> catalysts. *Fuel Processing Technology, 158*, 96–103. <https://doi.org/10.1016/j.fuproc.2016.11.013>

Yao, L., Shi, J., Xu, H., Shen, W., & Hu, C. (2016). Low-temperature CO<sub>2</sub> reforming of methane on Zr-promoted Ni / SiO<sub>2</sub> catalyst. *Fuel Processing Technology, 144*, 1–7. <https://doi.org/10.1016/j.fuproc.2015.12.009>

Yao, L., Wang, Y., Shi, J., Xu, H., Shen, W., & Hu, C. (2017). *The influence of reduction temperature on the performance of ZrO<sub>x</sub> / Ni-MnO<sub>x</sub> / SiO<sub>2</sub> catalyst for low-temperature CO<sub>2</sub> reforming of methane. 281, 259–267.*  
<https://doi.org/10.1016/j.cattod.2016.05.031>

Zhang, Z., Jia, P., Feng, S., Liang, J., Long, Y., & Li, G. (2018). Numerical simulation of exhaust reforming characteristics in catalytic fixed-bed reactors for a natural gas engine. *Chemical Engineering Science, 191*, 200–207. <https://doi.org/10.1016/j.ces.2018.06.061>

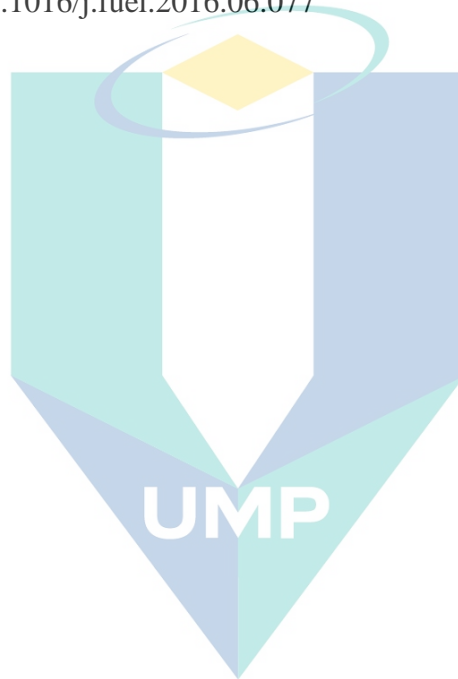
Zhang, Z., Jia, P., Zhong, G., Liang, J., & Li, G. (2017). Numerical study of exhaust reforming characteristics on hydrogen production for a marine engine fueled with LNG. *Applied Thermal Engineering, 124*, 241–249. <https://doi.org/10.1016/j.applthermaleng.2017.06.012>

Zhang, Z., Wu, R., Feng, S., Long, Y., & Li, G. (2020). Numerical investigation of tubular exhaust reformer with thermochemical recuperation for LNG engine. *International Journal of Heat and Mass Transfer, 146*, 118743. <https://doi.org/10.1016/j.ijheatmasstransfer.2019.118743>

Zhang, Z., Xie, Q., Liang, J., & Li, G. (2017). Numerical study of combustion characteristics of a natural gas HCCI engine with closed loop exhaust-gas fuel reforming. *Applied Thermal Engineering*, 119, 430–437. <https://doi.org/10.1016/j.applthermaleng.2017.03.079>

Zhao, X., Cao, Y., Li, H., Zhang, J., Shi, L., & Zhang, D. (2017). Sc promoted and aerogel confined Ni catalysts for coking-resistant dry reforming of methane. *RSC Advances*, 4735–4745. <https://doi.org/10.1039/c6ra27266e>

Zhuoyao He , Zhan Gao , Lei Zhu , Shujing Li b, Ang Li , Wugao Zhang, Z. H. (2016). Effects of H<sub>2</sub> and CO enrichment on the combustion, emission and performance characteristics of spark ignition natural gas engine. *Fuel*, 183, 230–237. <https://doi.org/10.1016/j.fuel.2016.06.077>



اونيور سيطي ملايسيا قهغ

UNIVERSITI MALAYSIA PAHANG

Appendix A Chemkin code of surface of surface mechanism reaction of CH4 Over Rhodium

!SURFACE MECHANISM OF OXIDATION AND STEAM/DRY REFORMING OF CH4 OVER RHODIUM

!\*\*\*\*\*

!\*\*\*\* \*  
!\*\*\*\* CH4/O2/H2O/CO2 OVER RH - SURFACE MECHANISM \*

!\*\*\*\* thermodynamically constant (273 - 1273K) \*

!\*\*\*\* \*  
!\*\*\*\* References: \*  
!\*\*\*\* C. Karakaya, L. Maier, O. Deutschmann, \*  
!\*\*\*\* Applied Catalysis A: General, submitted (2013) \*  
!\*\*\*\* www.detchem.com/mechanisms \*  
!\*\*\*\* KIT (Karlsruhe Institute of Technology) \*  
!\*\*\*\* Contact: mail@detchem.com (O. Deutschmann) \*  
!\*\*\*\* www.detchem.com/mechanisms \*

!\*\*\*\* \*  
!\*\*\*\* UMP \*  
!\*\*\*\* \*

!\*\*\*\* Kinetic data: \*  
!\*\*\*\*  $k = A * T^{*b} * \exp(-Ea/RT)$  A b Ea \*  
!\*\*\*\* (cm,mol,s) - kJ/mol \*

اونيور سیتی ملیسیا قهق

!\*\*\*\* STICK: A in next reaction is initial sticking coefficient \*

UNIVERSITI MALAYSIA PAHANG

!\*\*\*\* \*  
!\*\*\*\* \*

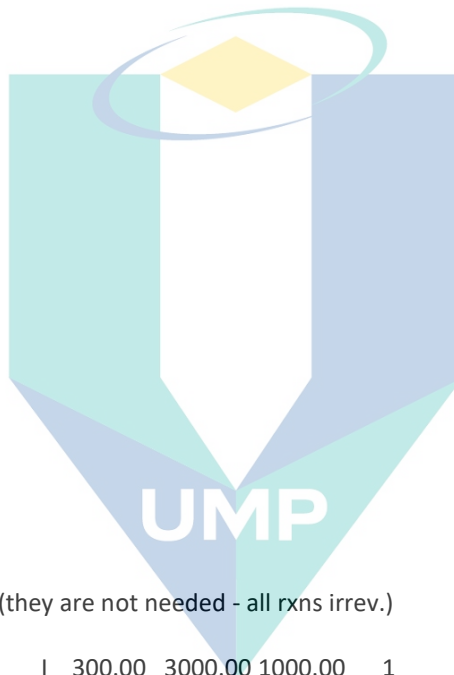
!\*\*\*\* (CHEMKIN format) \*

!\*\*\*\* \*

!\*\*\*\*\*

SITE/Rh\_surface/ SDEN/2.72E-9/

Rh(s)  
H2O(s)  
H(s)  
OH(s)  
CO(s)  
C(s)  
CH3(s)  
CH2(s)  
CH(s)  
CH4(s)  
O(s)  
CO2(s)  
COOH(s)



END

THERMO

300.0 1000.0 3000.0

! all data are dummy data (they are not needed - all rxns irrev.)

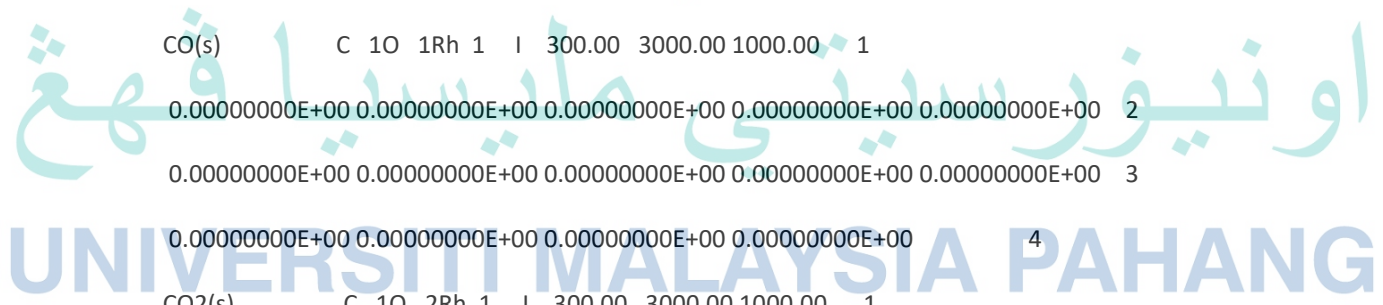
O(s) O 1Rh 1 I 300.00 3000.00 1000.00 1  
0.00000000E+00 0.00000000E+00 0.00000000E+00 0.00000000E+00 0.00000000E+00 2  
0.00000000E+00 0.00000000E+00 0.00000000E+00 0.00000000E+00 0.00000000E+00 3  
0.00000000E+00 0.00000000E+00 0.00000000E+00 0.00000000E+00 4

اونیورسیتی مالیزیاء  
UNIVERSITI MALAYSIA PAHANG

O2(s) O 2Rh 1 I 300.00 3000.00 1000.00 1  
0.00000000E+00 0.00000000E+00 0.00000000E+00 0.00000000E+00 0.00000000E+00 2  
0.00000000E+00 0.00000000E+00 0.00000000E+00 0.00000000E+00 0.00000000E+00 3  
0.00000000E+00 0.00000000E+00 0.00000000E+00 0.00000000E+00 4

H(s) H 1Rh 1 I 300.00 3000.00 1000.00 1  
0.00000000E+00 0.00000000E+00 0.00000000E+00 0.00000000E+00 0.00000000E+00 2

0.00000000E+00 0.00000000E+00 0.00000000E+00 0.00000000E+00 0.00000000E+00 3  
 0.00000000E+00 0.00000000E+00 0.00000000E+00 0.00000000E+00 4  
 H2(s) H 2Rh 1 I 300.00 3000.00 1000.00 1  
 0.00000000E+00 0.00000000E+00 0.00000000E+00 0.00000000E+00 0.00000000E+00 2  
 0.00000000E+00 0.00000000E+00 0.00000000E+00 0.00000000E+00 0.00000000E+00 3  
 0.00000000E+00 0.00000000E+00 0.00000000E+00 0.00000000E+00 4  
 H2O(s) O 1H 2Rh 1 I 300.00 3000.00 1000.00 1  
 0.00000000E+00 0.00000000E+00 0.00000000E+00 0.00000000E+00 0.00000000E+00 2  
 0.00000000E+00 0.00000000E+00 0.00000000E+00 0.00000000E+00 0.00000000E+00 3  
 0.00000000E+00 0.00000000E+00 0.00000000E+00 0.00000000E+00 4  
 OH(s) O 1H 1Rh 1 I 300.00 3000.00 1000.00 1  
 0.00000000E+00 0.00000000E+00 0.00000000E+00 0.00000000E+00 0.00000000E+00 2  
 0.00000000E+00 0.00000000E+00 0.00000000E+00 0.00000000E+00 0.00000000E+00 3  
 0.00000000E+00 0.00000000E+00 0.00000000E+00 0.00000000E+00 4  
 Rh(s) Rh 1 S 300.00 3000.00 1000.00 1  
 0.00000000E+00 0.00000000E+00 0.00000000E+00 0.00000000E+00 0.00000000E+00 2  
 0.00000000E+00 0.00000000E+00 0.00000000E+00 0.00000000E+00 0.00000000E+00 3  
 0.00000000E+00 0.00000000E+00 0.00000000E+00 0.00000000E+00 4  
 CO(s) C 1O 1Rh 1 I 300.00 3000.00 1000.00 1  
 0.00000000E+00 0.00000000E+00 0.00000000E+00 0.00000000E+00 0.00000000E+00 2  
 0.00000000E+00 0.00000000E+00 0.00000000E+00 0.00000000E+00 0.00000000E+00 3  
 0.00000000E+00 0.00000000E+00 0.00000000E+00 0.00000000E+00 4  
 CO2(s) C 1O 2Rh 1 I 300.00 3000.00 1000.00 1  
 0.00000000E+00 0.00000000E+00 0.00000000E+00 0.00000000E+00 0.00000000E+00 2  
 0.00000000E+00 0.00000000E+00 0.00000000E+00 0.00000000E+00 0.00000000E+00 3  
 0.00000000E+00 0.00000000E+00 0.00000000E+00 0.00000000E+00 4  
 C(s) C 1Rh 1 I 300.00 3000.00 1000.00 1



0.0000000E+00 0.0000000E+00 0.0000000E+00 0.0000000E+00 0.0000000E+00 2  
 0.0000000E+00 0.0000000E+00 0.0000000E+00 0.0000000E+00 0.0000000E+00 3  
 0.0000000E+00 0.0000000E+00 0.0000000E+00 0.0000000E+00 4

CH(s) C 1H 1Rh 1 | 300.00 3000.00 1000.00 1

0.0000000E+00 0.0000000E+00 0.0000000E+00 0.0000000E+00 0.0000000E+00 2  
 0.0000000E+00 0.0000000E+00 0.0000000E+00 0.0000000E+00 0.0000000E+00 3  
 0.0000000E+00 0.0000000E+00 0.0000000E+00 0.0000000E+00 4

CH2(s) C 1H 2Rh 1 | 300.00 3000.00 1000.00 1

0.0000000E+00 0.0000000E+00 0.0000000E+00 0.0000000E+00 0.0000000E+00 2  
 0.0000000E+00 0.0000000E+00 0.0000000E+00 0.0000000E+00 0.0000000E+00 3  
 0.0000000E+00 0.0000000E+00 0.0000000E+00 0.0000000E+00 4

CH3(s) C 1H 3Rh 1 | 300.00 3000.00 1000.00 1

0.0000000E+00 0.0000000E+00 0.0000000E+00 0.0000000E+00 0.0000000E+00 2  
 0.0000000E+00 0.0000000E+00 0.0000000E+00 0.0000000E+00 0.0000000E+00 3  
 0.0000000E+00 0.0000000E+00 0.0000000E+00 0.0000000E+00 4

CH4(s) C 1H 4Rh 1 | 300.00 3000.00 1000.00 1

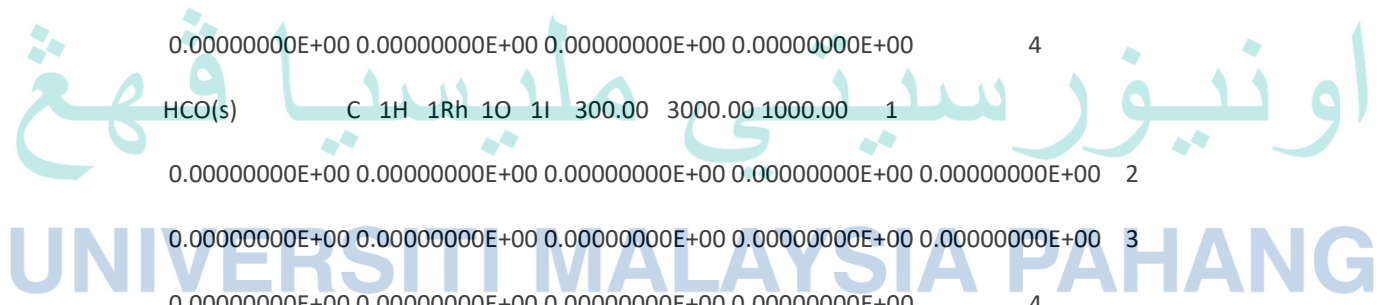
0.0000000E+00 0.0000000E+00 0.0000000E+00 0.0000000E+00 0.0000000E+00 2  
 0.0000000E+00 0.0000000E+00 0.0000000E+00 0.0000000E+00 0.0000000E+00 3  
 0.0000000E+00 0.0000000E+00 0.0000000E+00 0.0000000E+00 4

HCO(s) C 1H 1Rh 1O 1 | 300.00 3000.00 1000.00 1

0.0000000E+00 0.0000000E+00 0.0000000E+00 0.0000000E+00 0.0000000E+00 2  
 0.0000000E+00 0.0000000E+00 0.0000000E+00 0.0000000E+00 0.0000000E+00 3  
 0.0000000E+00 0.0000000E+00 0.0000000E+00 0.0000000E+00 4

CH4 (adjust) C 1H 4 0 0 300.00 5000.00 1000.00 1

1.68347883E+00 1.02372356E-02 -3.87512864E-06 6.78558487E-10 -4.50342312E-14 2  
 -1.00807871E+04 9.62339497E+00 7.78741479E-01 1.74766835E-02 -2.78340904E-05 3  
 3.04970804E-08 -1.22393068E-11 -9.82522852E+03 1.37221947E+01 4



O2 (adjust) O 2 0 0 0 300.00 5000.00 1000.00 1  
3.61221390E+00 7.48531660E-04-1.98206470E-07 3.37490080E-11-2.39073740E-15 2  
-1.19781510E+03 3.67033070E+00 3.78371350E+00-3.02336340E-03 9.94927510E-06 3  
-9.81891010E-09 3.30318250E-12-1.06381070E+03 3.64163450E+00 4

CO (adjust) C 1O 1 0 0 300.00 5000.00 1000.00 1  
3.02507806E+00 1.44268852E-03-5.63082779E-07 1.01858133E-10-6.91095156E-15 2  
-1.42683496E+04 6.10821772E+00 3.26245165E+00 1.51194085E-03-3.88175522E-06 3  
5.58194424E-09-2.47495123E-12-1.43105391E+04 4.84889698E+00 4

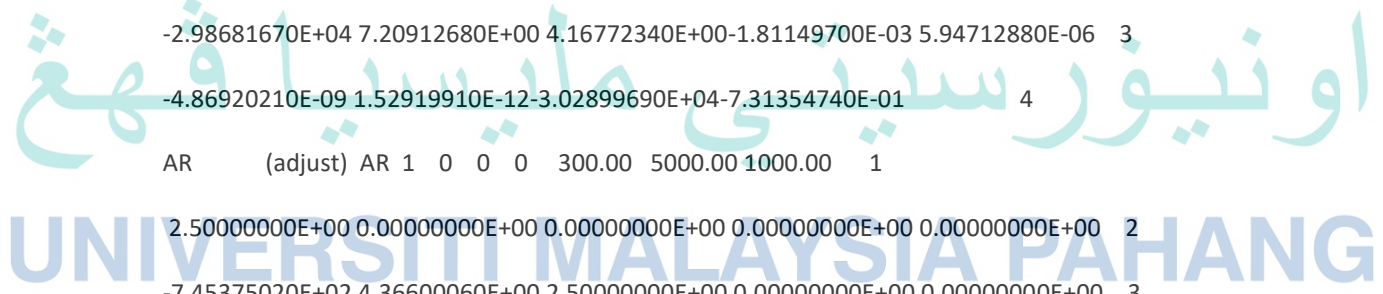
CO2 (adjust) C 1O 2 0 0 300.00 5000.00 1000.00 1  
4.45362282E+00 3.14016873E-03-1.27841054E-06 2.39399667E-10-1.66903319E-14 2  
-4.89669609E+04-9.55395877E-01 2.27572465E+00 9.92207229E-03-1.04091132E-05 3  
6.86668678E-09-2.11728009E-12-4.83731406E+04 1.01884880E+01 4

H2 (adjust) H 2 0 0 0 300.00 5000.00 1000.00 1  
3.06670950E+00 5.74737550E-04 1.39383190E-08-2.54835180E-11 2.90985740E-15 2  
-8.65474120E+02-1.77984240E+00 3.35535140E+00 5.01361440E-04-2.30069080E-07 3  
-4.79053240E-10 4.85225850E-13-1.01916260E+03-3.54772280E+00 4

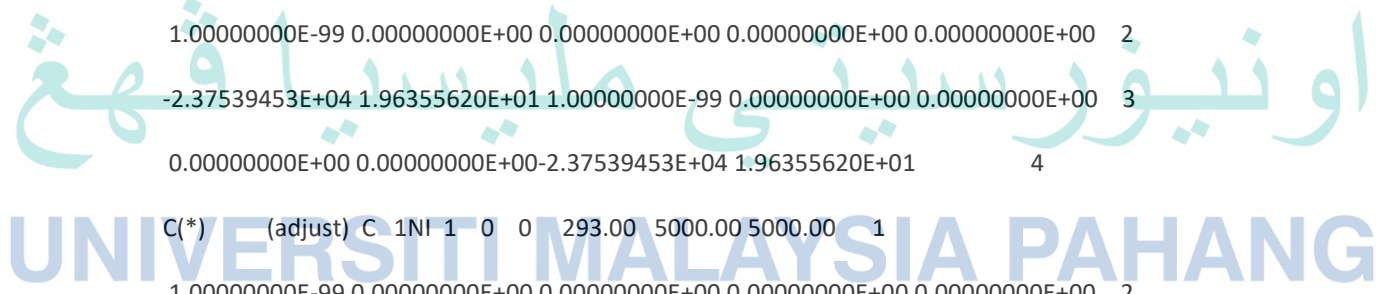
H2O (adjust) H 2O 1 0 0 300.00 5000.00 1000.00 1  
2.61104720E+00 3.15631300E-03-9.29854380E-07 1.33315380E-10-7.46893510E-15 2  
-2.98681670E+04 7.20912680E+00 4.16772340E+00-1.81149700E-03 5.94712880E-06 3  
-4.86920210E-09 1.52919910E-12-3.02899690E+04-7.31354740E-01 4

AR (adjust) AR 1 0 0 0 300.00 5000.00 1000.00 1  
2.50000000E+00 0.00000000E+00 0.00000000E+00 0.00000000E+00 0.00000000E+00 2  
-7.45375020E+02 4.36600060E+00 2.50000000E+00 0.00000000E+00 0.00000000E+00 3  
0.00000000E+00 0.00000000E+00-7.45374980E+02 4.36600060E+00 4

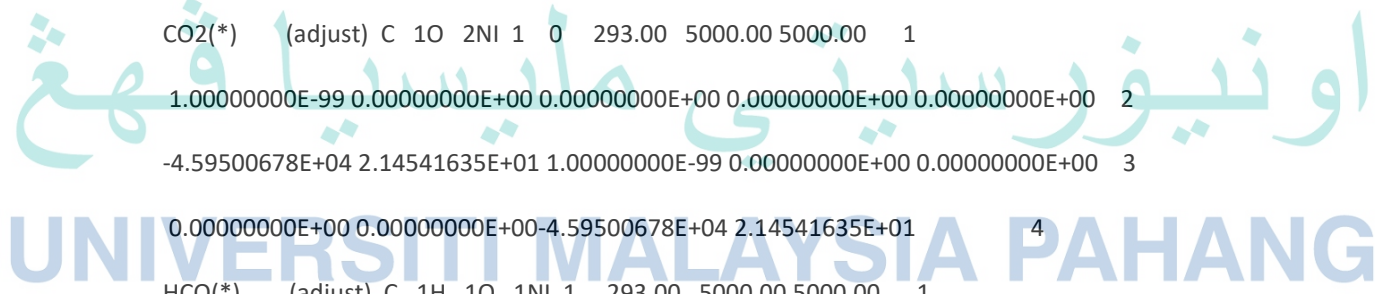
NI(\*) (adjust) NI 1 0 0 0 300.00 3000.00 1000.00 1  
0.00000000E+00 0.00000000E+00 0.00000000E+00 0.00000000E+00 0.00000000E+00 2  
0.00000000E+00 0.00000000E+00 0.00000000E+00 0.00000000E+00 0.00000000E+00 3



0.0000000E+00 0.0000000E+00 0.0000000E+00 0.0000000E+00 4  
 H2O(\*) (adjust) H 2O 1NI 1 0 293.00 5000.00 5000.00 1  
 1.0000000E-99 0.0000000E+00 0.0000000E+00 0.0000000E+00 0.0000000E+00 2  
 -3.28621348E+04 1.57219174E+01 1.0000000E-99 0.0000000E+00 0.0000000E+00 3  
 0.0000000E+00 0.0000000E+00 -3.28621348E+04 1.57219174E+01 4  
 H(\*) (adjust) H 1NI 1 0 0 293.00 5000.00 5000.00 1  
 1.0000000E-99 0.0000000E+00 0.0000000E+00 0.0000000E+00 0.0000000E+00 2  
 -3.82656399E+03 4.89898398E+00 1.0000000E-99 0.0000000E+00 0.0000000E+00 3  
 0.0000000E+00 0.0000000E+00 -3.82656399E+03 4.89898398E+00 4  
 COOH(\*) (adjust) C 1H 1O 2NI 1 300.00 5000.00 1000.00 1  
 0.0000000E+00 0.0000000E+00 0.0000000E+00 0.0000000E+00 0.0000000E+00 2  
 0.0000000E+00 0.0000000E+00 0.0000000E+00 0.0000000E+00 0.0000000E+00 3  
 0.0000000E+00 0.0000000E+00 0.0000000E+00 0.0000000E+00 4  
 OH(\*) (adjust) H 1O 1NI 1 0 293.00 5000.00 5000.00 1  
 1.0000000E-99 0.0000000E+00 0.0000000E+00 0.0000000E+00 0.0000000E+00 2  
 -2.31833113E+04 1.28038592E+01 1.0000000E-99 0.0000000E+00 0.0000000E+00 3  
 0.0000000E+00 0.0000000E+00 -2.31833113E+04 1.28038592E+01 4  
 CO(\*) (adjust) C 1O 1NI 1 0 293.00 5000.00 5000.00 1  
 1.0000000E-99 0.0000000E+00 0.0000000E+00 0.0000000E+00 0.0000000E+00 2  
 -2.37539453E+04 1.96355620E+01 1.0000000E-99 0.0000000E+00 0.0000000E+00 3  
 0.0000000E+00 0.0000000E+00 -2.37539453E+04 1.96355620E+01 4  
 C(\*) (adjust) C 1NI 1 0 0 293.00 5000.00 5000.00 1  
 1.0000000E-99 0.0000000E+00 0.0000000E+00 0.0000000E+00 0.0000000E+00 2  
 -9.60170600E+02 -9.94267012E+00 1.0000000E-99 0.0000000E+00 0.0000000E+00 3  
 0.0000000E+00 0.0000000E+00 -9.60170600E+02 -9.94267012E+00 4  
 CH3(\*) (adjust) C 1H 3NI 1 0 293.00 5000.00 5000.00 1  
 1.0000000E-99 0.0000000E+00 0.0000000E+00 0.0000000E+00 0.0000000E+00 2



-3.58843376E+03 3.36230167E+00 1.00000000E-99 0.00000000E+00 0.00000000E+00 3  
 0.00000000E+00 0.00000000E+00 -3.58843376E+03 3.36230167E+00 4  
 CH2(\*) (adjust) C 1H 2NI 1 0 293.00 5000.00 5000.00 1  
 1.00000000E-99 0.00000000E+00 0.00000000E+00 0.00000000E+00 0.00000000E+00 2  
 5.94161025E+03 2.12413716E+00 1.00000000E-99 0.00000000E+00 0.00000000E+00 3  
 0.00000000E+00 0.00000000E+00 5.94161025E+03 2.12413716E+00 4  
 CH(\*) (adjust) C 1H 1NI 1 0 293.00 5000.00 5000.00 1  
 1.00000000E-99 0.00000000E+00 0.00000000E+00 0.00000000E+00 0.00000000E+00 2  
 1.22543876E+04 -2.56790500E+00 1.00000000E-99 0.00000000E+00 0.00000000E+00 3  
 0.00000000E+00 0.00000000E+00 1.22543876E+04 -2.56790500E+00 4  
 CH4(\*) (adjust) C 1H 4NI 1 0 293.00 5000.00 5000.00 1  
 1.00000000E-99 0.00000000E+00 0.00000000E+00 0.00000000E+00 0.00000000E+00 2  
 -7.27928907E+03 8.44319611E+00 1.00000000E-99 0.00000000E+00 0.00000000E+00 3  
 0.00000000E+00 0.00000000E+00 -7.27928907E+03 8.44319611E+00 4  
 O(\*) (adjust) O 1NI 1 0 0 293.00 5000.00 5000.00 1  
 1.00000000E-99 0.00000000E+00 0.00000000E+00 0.00000000E+00 0.00000000E+00 2  
 -2.66580549E+04 4.68860658E+00 1.00000000E-99 0.00000000E+00 0.00000000E+00 3  
 0.00000000E+00 0.00000000E+00 -2.66580549E+04 4.68860658E+00 4  
 CO2(\*) (adjust) C 1O 2NI 1 0 293.00 5000.00 5000.00 1  
 1.00000000E-99 0.00000000E+00 0.00000000E+00 0.00000000E+00 0.00000000E+00 2  
 -4.59500678E+04 2.14541635E+01 1.00000000E-99 0.00000000E+00 0.00000000E+00 3  
 0.00000000E+00 0.00000000E+00 -4.59500678E+04 2.14541635E+01 4  
 HCO(\*) (adjust) C 1H 1O 1NI 1 293.00 5000.00 5000.00 1  
 1.00000000E-99 0.00000000E+00 0.00000000E+00 0.00000000E+00 0.00000000E+00 2  
 -1.21882034E+04 1.49580180E+01 1.00000000E-99 0.00000000E+00 0.00000000E+00 3  
 0.00000000E+00 0.00000000E+00 -1.21882034E+04 1.49580180E+01 4  
 C3H8(s) (adjust) C 3H 8Rh 1 300.00 3000.00 1000.00 1



```

0.0000000E+00 0.0000000E+00 0.0000000E+00 0.0000000E+00 0.0000000E+00 2
-0.0000000E+00-0.0000000E+00 0.0000000E-00 0.0000000E+00 0.0000000E+00 3
0.0000000E+00 0.0000000E+00-0.0000000E+00-0.0000000E+00 4
C2H3(s) (adjust) C 2H 3Rh 1 I 300.00 3000.00 1000.00 1
0.0000000E+00 0.0000000E+00 0.0000000E+00 0.0000000E+00 0.0000000E+00 2
-0.0000000E+00-0.0000000E+00 0.0000000E-00 0.0000000E+00 0.0000000E+00 3
0.0000000E+00 0.0000000E+00-0.0000000E+00-0.0000000E+00 4
C3H7(s) (adjust) C 3H 7Rh 1 I 300.00 3000.00 1000.00 1
0.0000000E+00 0.0000000E+00 0.0000000E+00 0.0000000E+00 0.0000000E+00 2
-0.0000000E+00-0.0000000E+00 0.0000000E-00 0.0000000E+00 0.0000000E+00 3
0.0000000E+00 0.0000000E+00-0.0000000E+00-0.0000000E+00 4
C3H6(s) (adjust) C 3H 6Rh 1 I 300.00 3000.00 1000.00 1
0.0000000E+00 0.0000000E+00 0.0000000E+00 0.0000000E+00 0.0000000E+00 2
-0.0000000E+00-0.0000000E+00 0.0000000E-00 0.0000000E+00 0.0000000E+00 3
0.0000000E+00 0.0000000E+00-0.0000000E+00-0.0000000E+00 4
C3H8 120186C 3H 8 G 0300.00 5000.00 1000.00 1
0.07525217E+02 0.01889034E+00-0.06283924E-04 0.09179373E-08-0.04812410E-12 2
-0.16464548E+05-0.01784390E+03 0.08969208E+01 0.02668986E+00 0.05431425E-04 3
-0.02126000E-06 0.09243330E-10-0.13954918E+05 0.01935533E+03 4
COOH(s) C 1H 1O 2Rh 1I 300.00 3000.00 1000.00 1
0.30016165E+01 0.54084505E-02-0.40538058E-06-0.53422466E-09 0.11451887E-12 2
-0.32752722E+04-0.10965984E+02 0.12919217E+01 0.72675603E-02 0.98179476E-06 3
-0.20471294E-08 0.90832717E-13-0.25745610E+04-0.11983037E+01 4

```

END

!

REACTIONS MWOFF KJOULES/MOLE

H2 + Rh(s) + Rh(s) => H(s) + H(s) 3.000E-02 0.000 0.000

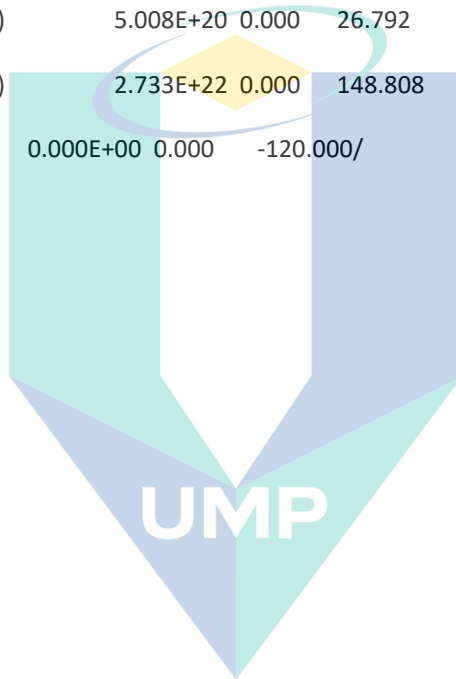
STICK			
$O_2 + Rh(s) + Rh(s) \Rightarrow O(s) + O(s)$	1.000E-02	0.000	0.000
STICK			
$H_2O + Rh(s) \Rightarrow H_2O(s)$	1.000E-01	0.000	0.000
STICK			
$CO_2 + Rh(s) \Rightarrow CO_2(s)$	4.800E-02	0.000	0.000
STICK			
$CO + Rh(s) \Rightarrow CO(s)$	4.971E-01	0.000	0.000
STICK			
$CH_4 + Rh(s) \Rightarrow CH_4(s)$	1.300E-02	0.000	0.000
STICK			
$H(s) + H(s) \Rightarrow Rh(s) + Rh(s) + H_2$	5.574E+19	0.239	59.691
$O(s) + O(s) \Rightarrow Rh(s) + Rh(s) + O_2$	5.329E+22	-0.137	386.995
$H_2O(s) \Rightarrow Rh(s) + H_2O$	6.858E+14	-0.280	44.993
$CO(s) \Rightarrow Rh(s) + CO$	1.300E+13	0.295	134.070
COV/CO(s)	0.000E+00	0.000	-47.000/
$CO_2(s) \Rightarrow Rh(s) + CO_2$	3.920E+11	0.315	20.505
$CH_4(s) \Rightarrow Rh(s) + CH_4$	1.523E+13	-0.110	26.018
$O(s) + H(s) \Rightarrow OH(s) + Rh(s)$	8.826E+21	-0.048	73.365
$OH(s) + Rh(s) \Rightarrow O(s) + H(s)$	1.000E+21	0.045	48.041
$OH(s) + H(s) \Rightarrow H_2O(s) + Rh(s)$	1.743E+22	-0.127	41.731
$H_2O(s) + Rh(s) \Rightarrow OH(s) + H(s)$	5.408E+22	0.129	98.220
$OH(s) + OH(s) \Rightarrow O(s) + H_2O(s)$	5.736E+20	-0.081	121.594
$O(s) + H_2O(s) \Rightarrow OH(s) + OH(s)$	1.570E+22	0.081	203.407
$O(s) + C(s) \Rightarrow CO(s) + Rh(s)$	1.173E+22	0.000	92.142
COV/C(s)	0.000E+00	0.000	-120.000/
$CO(s) + Rh(s) \Rightarrow O(s) + C(s)$	6.390E+21	0.000	174.758

COV/CO(s)	0.000E+00	0.000	-47.000/
O(s) + CO(s) => CO2(s) + Rh(s)	6.183E+21	0.034	129.982
COV/CO(s)	0.000E+00	0.000	-47.000/
CO2(s) + Rh(s) => O(s) + CO(s)	5.752E+22	-0.175	106.492
CO(s) + OH(s) => COOH(s) + Rh(s)	2.922E+20	0.000	55.334
COV/CO(s)	0.000E+00	0.000	-47.000/
COOH(s) + Rh(s) => CO(s) + OH(s)	2.738E+21	0.000	48.375
COOH(s) + Rh(s) => CO2(s) + H(s)	1.165E+19	0.160	5.610
CO2(s) + H(s) => COOH(s) + Rh(s)	1.160E+20	-0.160	14.480
COOH(s) + H(s) => CO(s) + H2O(s)	5.999E+19	-0.188	33.552
CO(s) + H2O(s) => COOH(s) + H(s)	2.258E+19	0.051	97.078
COV/CO(s)	0.000E+00	0.000	-47.000/
CO(s) + OH(s) => CO2(s) + H(s)	3.070E+19	0.000	82.938
COV/CO(s)	0.000E+00	0.000	-47.000/
CO2(s) + H(s) => CO(s) + OH(s)	2.504E+21	-0.301	84.767
C(s) + OH(s) => CO(s) + H(s)	4.221E+20	0.078	30.038
COV/C(s)	0.000E+00	0.000	-120.000/
CO(s) + H(s) => C(s) + OH(s)	3.244E+21	-0.078	138.262
COV/CO(s)	0.000E+00	0.000	-47.000/
CH4(s) + Rh(s) => CH3(s) + H(s)	4.622E+21	0.136	72.262
CH3(s) + H(s) => CH4(s) + Rh(s)	2.137E+21	-0.058	46.770
CH3(s) + Rh(s) => CH2(s) + H(s)	1.275E+24	0.078	107.563
CH2(s) + H(s) => CH3(s) + Rh(s)	1.073E+22	-0.078	39.537
CH2(s) + Rh(s) => CH(s) + H(s)	1.275E+24	0.078	115.388
CH(s) + H(s) => CH2(s) + Rh(s)	1.073E+22	-0.078	52.612
CH(s) + Rh(s) => C(s) + H(s)	1.458E+20	0.078	23.088
C(s) + H(s) => CH(s) + Rh(s)	1.122E+23	-0.078	170.712

اونیورسیتی ملیسیا پاهانگ

UNIVERSITI MALAYSIA PAHANG

COV/C(s)	0.000E+00	0.000	-120.000/
CH4(s) + O(s) => CH3(s) + OH(s)	3.465E+23	0.051	77.708
CH3(s) + OH(s) => CH4(s) + O(s)	1.815E+22	-0.051	26.892
CH3(s) + O(s) => CH2(s) + OH(s)	4.790E+24	0.000	114.517
CH2(s) + OH(s) => CH3(s) + O(s)	2.858E+21	0.000	20.883
CH2(s) + O(s) => CH(s) + OH(s)	4.790E+24	0.000	141.792
CH(s) + OH(s) => CH2(s) + O(s)	2.858E+21	0.000	53.408
CH(s) + O(s) => C(s) + OH(s)	5.008E+20	0.000	26.792
C(s) + OH(s) => CH(s) + O(s)	2.733E+22	0.000	148.808
COV/C(s)	0.000E+00	0.000	-120.000/
END			



اونیورسیتی ملیسیا قهغ

UNIVERSITI MALAYSIA PAHANG

Appendix B Chemkin code of H<sub>2</sub>/CO combustion mechanism

!

=====  
 =====

ELEMENTS

C H N O A R H E

END

SPECIES

H	H2	O	O2	OH	OH*
H2O	N2	HO2	H2O2	AR	
CO	CO2	HE	HCO		

END

REACTIONS

!REF:HONG ET AL., PROC. COMBUST.INST. 33(1) (2011) 309–316.

H+O2<=>O+OH 1.04E+14 0.00 15286

!REF:SUTHERLAND ET AL., 21ST SYMPOSIUM, P. 929 (1986)

O+H2<=>H+OH 5.080E+04 2.67 6.292E+03

!REF:LAM ET AL. (STANFORD) SUBMITTED TO IJCK (2012)

OH+H2<=>H+H2O 4.38E+13 0.0 6990.0

!REF:SUTHERLAND ET AL., 23RD SYMPOSIUM, P. 51 (1990)

O+H2O<=>OH+OH 2.97E+06 2.02 1.340E+04

!REF:TSANG AND HAMPSON, J. PHYS. CHEM. REF. DATA, 15:1087  
(1986)

H2+M<=>H+H+M 4.577E+19 -1.400 1.044E+05

H2/2.5/ H2O/12/ CO/1.9/ CO2/3.8/ HE/.83/

O+O+M<=>O2+M 6.165E+15 -0.500 0.000E+00

H2/2.5/ H2O/12/ AR/.83/ CO/1.9/ CO2/3.8/ HE/.83/

O+H+M<=>OH+M 4.714E+18 -1.000 0.000E+00

H2/2.5/ H2O/12/ AR/.75/ CO/1.5/ CO2/2/ HE/.75/

!REF: LI INT. J. CHEM. KINET. 36(10) (2004) 566-575.

H+OH+M<=>H2O+M 3.5E+22 -2.000 0.000E+00

H2/ .73/ H2O/3.65/ AR/ .38/

!----- H+O2(+M) = HO2 (+M)-----

!REF: FERNANDES ET AL.,PHYS. CHEM. CHEM. PHYS. 10(29) (2008)  
4313-4321

H+O2(+M)<=>HO2(+M) 4.650E+12 0.440 0.000E+00

LOW / 1.737E+19 -1.23 0.000E+00 /

TROE / 0.67 1E-30 1E30 1E30 /

H2/1.3/ CO/1.9/ CO2/3.8/ HE/0.0/ H2O/10.0/ AR/0.00/

H+O2(+HE)<=>HO2(+HE) 4.650E+12 0.440 0.000E+00

LOW / 9.192E+18 -1.20 0.000E+00 / ! FERNANDES

X 1.5

TROE / 0.59 1E-30 1E30 1E30 /

H+O2(+AR)<=>HO2(+AR) 4.650E+12 0.440 0.000E+00

!REF: BATES ET AL. PHYS. CHEM. CHEM. PHYS. 3(12) (2001) 2337–2342.

LOW / 6.810E+18 -1.200 0.0/

TROE /0.70 1.0E-30 1.0E+30 1.0E+30/

!-----

!REF MUELLER ET AL., INT. J. CHEM. KINET. 31(10) (1999) 705–724.

HO2+H<=>OH+OH 7.079E+13 0.00 2.950E+02

!REF: MICHAEL ET AL., PROC. COMBUST. INST. 28(2) (2000) 1471–1478.

H2+O2<=>H+HO2 5.176E+05 2.433 53502.0

!REF:BAULCH ET AL., J. PHYS. CHEM. REF DATA, 21(3) (1992) 411-734

HO2+O<=>OH+O2 3.250E+13 0.000 0.000E+00

!REF:KEYSER, J. PHYS. CHEM. 92 (1988) 1193–1200. REDUCED BY 15%

HO2+OH<=>H2O+O2 2.456E+13 0.000 -4.970E+02

!REF:HIPPLER ET AL., J. CHEM. PHYS. 93(3) (1990) 1755–1760.

HO2+HO2 = O2+H2O2 1.300E+11 0.000 -1630.00

DUPLICATE

HO2+HO2 = O2+H2O2 3.658E+14 0.000 12000.00 !HIPPLER

X 0.87

DUPLICATE

!----- H2O2(+M) = OH+OH(+M)-----

-----

!REF: TROE, COMBUST. FLAME 158(4) (2011) 594–601.

H2O2(+M) = OH+OH(+M) 2.00E+12 0.90 4.8749+04

!DEFINED IN ARGON

LOW/2.49E+24 -2.30 4.8749+04/

TROE/0.43 1E-30 1E+30/

H2O/0.0/ CO2/1.6/ N2/1.5/ O2/1.2/ HE/0.65/ H2O2/7.7/

! EFFICIENCIES FOR H2 AND CO TAKEN FROM LI ET AL., INT. J. CHEM. KINET. 36:566-575 (2004)

H2/3.7/ CO/2.8/

H2O2(+H2O)<=>OH+OH(+H2O) 2.00E+12 0.90 4.8749+04

LOW/ 1.865E+25 -2.30 4.8749+04 /

TROE/ 0.51 1E-30 1E+30 /

!-----

!REF:TSANG AND HAMPSON, J. PHYS. CHEM. REF. DATA 15 (1986) 1087–1280.

H2O2+H<=>H2O+OH 2.410E+13 0.000 3.970E+03

!REF: ELLINGSON ET AL., J. PHYS. CHEM. A 111(51) (2007) 13554–13566.

(FIT TO THE THEORETICAL RATE)

H2O2+H<=>H2+HO2 2.150E+10 1.000 6.000E+03

!REF:TSANG AND HAMPSON, J. PHYS. CHEM. REF. DATA 15 (1986) 1087–1280.

H2O2+O<=>OH+HO2 9.550E+06 2.000 3.970E+03

!REF: HONG ET AL., J. PHYS. CHEM. A 114(18) (2010) 5718–5727.

H2O2+OH<=>H2O+HO2 1.74E+12 0.000 3.18E+02

DUPLICATE

H2O2+OH<=>H2O+HO2 7.59E+13 0.000 7.269E+03

DUPLICATE

!-----

!-----END OF H2 MECHANISM-----

!REF: TROE, J. PHYS. CHEM. 83 (1979) 114–126. X 0.76

CO+O(+M)=CO2(+M) 1.362E+10 0.000 2384.00

!REF: WESTMORELAND ET AL, AICHE JOURNAL 32(12) (1986) 1971–1979. X 0.87

LOW / 1.173E+24 -2.79 4191. /

H2/2.0/ H2O/12/ CO/1.75/ CO2/3.6/ AR/0.7/ HE/0.7/

!REF: TSANG AND HAMPSON, J. PHYS. CHEM. REF. DATA 15 (1986) 1087–1280.

CO+O2 = CO2+O 1.119E+12 0.000 47700.00

!REF: JOSHI AND WANG, INT. J. CHEM. KINET. 38(1) (2006) 57–73.

CO+OH<=>CO2+H 7.015E+04 2.053 -355.67

DUPLICATE

CO+OH<=>CO2+H 5.757E+12 -0.664 331.83

DUPLICATE

!REF: YOU ET AL. J. PHYS. CHEM. A 111(19) (2007) 4031–4042.

CO+HO2<=>CO2+OH 1.570E+05 2.180 1.794E+04

!REF: LI ET AL. INT. J. CHEM. KINET. 39(3) (2007) 109–136.

HCO+M<=>H+CO+M 4.750E+11 0.660 1.487E+04

H2/2/ H2O/12/ CO/1.5/ CO2/2/

!REF: TIMONEN ET AL., J. PHYS. CHEM. 92(3) (1988) 651–655.

HCO+O2<=>CO+HO2 7.580E+12 0.000 4.100E+02

!REF: TIMONEN ET AL., J. PHYS. CHEM. 91(3) (1987) 692–694.

HCO+H<=>CO+H2 7.340E+13 0.000 0.000E+00

!REF: TSANG AND HAMPSON, J. PHYS. CHEM. REF. DATA 15 (1986)  
1087–1280.

HCO+O<=>CO+OH 3.020E+13 0.000 0.000E+00

HCO+O<=>CO2+H 3.000E+13 0.000 0.000E+00

!REF: BAULCH ET AL., J. PHYS. CHEM. REF. DATA 21(3) (1992) 411–734.

HCO+OH<=>CO+H2O 1.020E+14 0.000 0.000E+00

!REF: TSANG AND HAMPSON, J. PHYS. CHEM. REF. DATA 15 (1986)  
1087–1280.

HCO+HO2=>CO2+H+OH 3.000E+13 0.000 0.000E+00

HCO+HCO=>H2+CO+CO 3.000E+12 0.000 0.000E+00

!-----

!-----END OF H2/CO MECHANISM-----

-----

!-----

!-----OH\* MECHANISM-----

-----

!REF: KATHROTIA ET AL., COMBUST. FLAME 157(7) (2010) 1261–1273

H+O+M<=>M+OH\* 1.50E+13 0.0 5.975E3

H2/1/ H2O/6.5/ O2/0.4/ N2/0.4/ AR/0.35/

!REF: TAMURA ET AL., COMBUST. FLAME 114(3-4) (1998) 502–514.

OH\*+H2O<=>OH+H2O 5.930E+12 0.5 -8.60E2

OH\*+H2<=>OH+H2 2.950E+12 0.5 -4.44E2

OH\*+N2<=>OH+N2 1.080E+11 0.5 -1.242E3

OH\*+OH<=>OH+OH 6.010E+12 0.5 -7.64E2

OH\*+H<=>OH+H 1.310E+12 0.5 -1.67E2

OH\*+O2<=>OH+O2 2.100E+12 0.5 -4.78E2

OH\*+CO2<=>OH+CO2 2.750E+12 0.5 -9.68E2

OH\*+CO<=>OH+CO 3.230E+12 0.5 -7.87E2

!REF: PAUL ET AL., J. CHEM. PHYS. 102(21) (1995) 8378–8384.

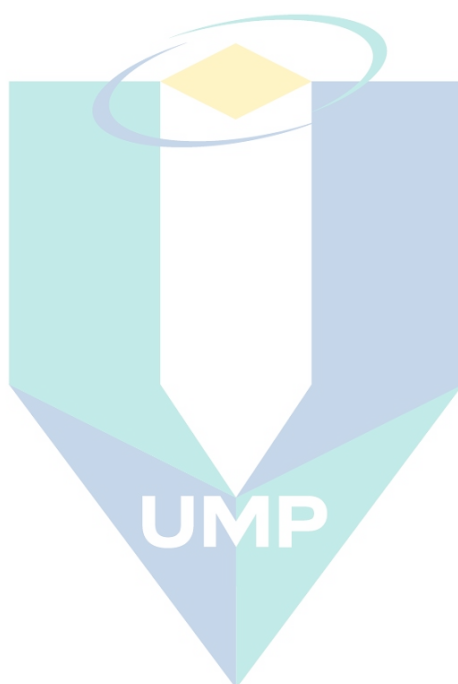
OH\*+AR<=>OH+AR 1.690E+12 0.0 4.135E3

!REF: SMITH ET AL., COMBUST. FLAME 131(1-2) (2002) 59–69.

OH\* $\rightleftharpoons$ OH+HV                      1.450E+06    0.0    0.0

!-----END OH\* MECHANISM-----

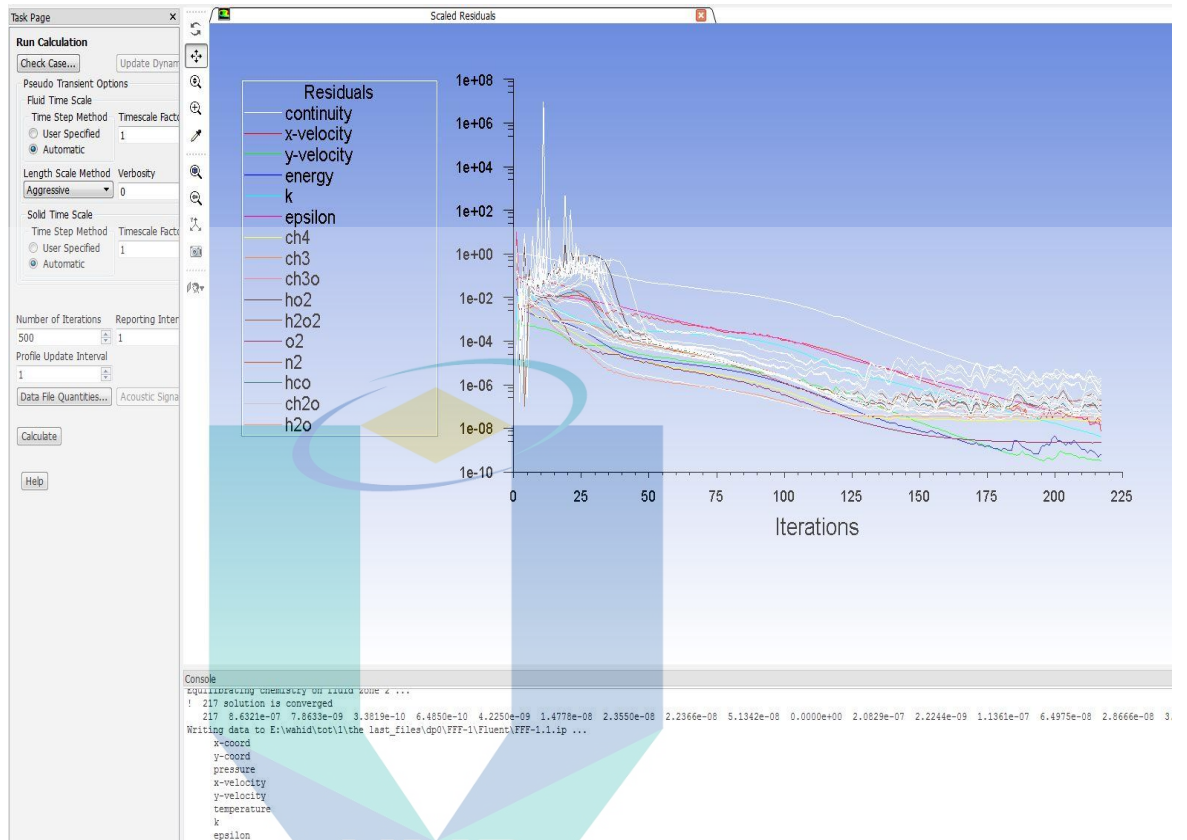
-----  
END



اونيورسيتي مليسيا قهغ

UNIVERSITI MALAYSIA PAHANG

## Appendix C CFD scaled residual.



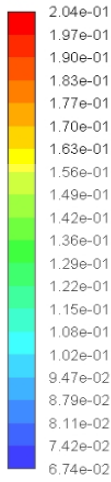
UMP

اونیورسیتی ملیسیا قهق

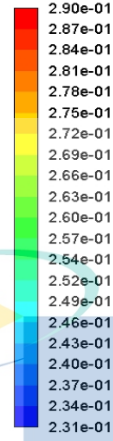
UNIVERSITI MALAYSIA PAHANG

## Appendix D CFD Validation Contours

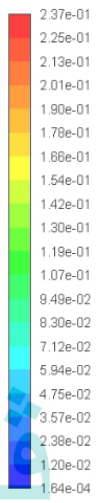
contour-3  
Mole fraction of ch4



contour-3  
Mole fraction of co2



contour-3  
Mole fraction of h2



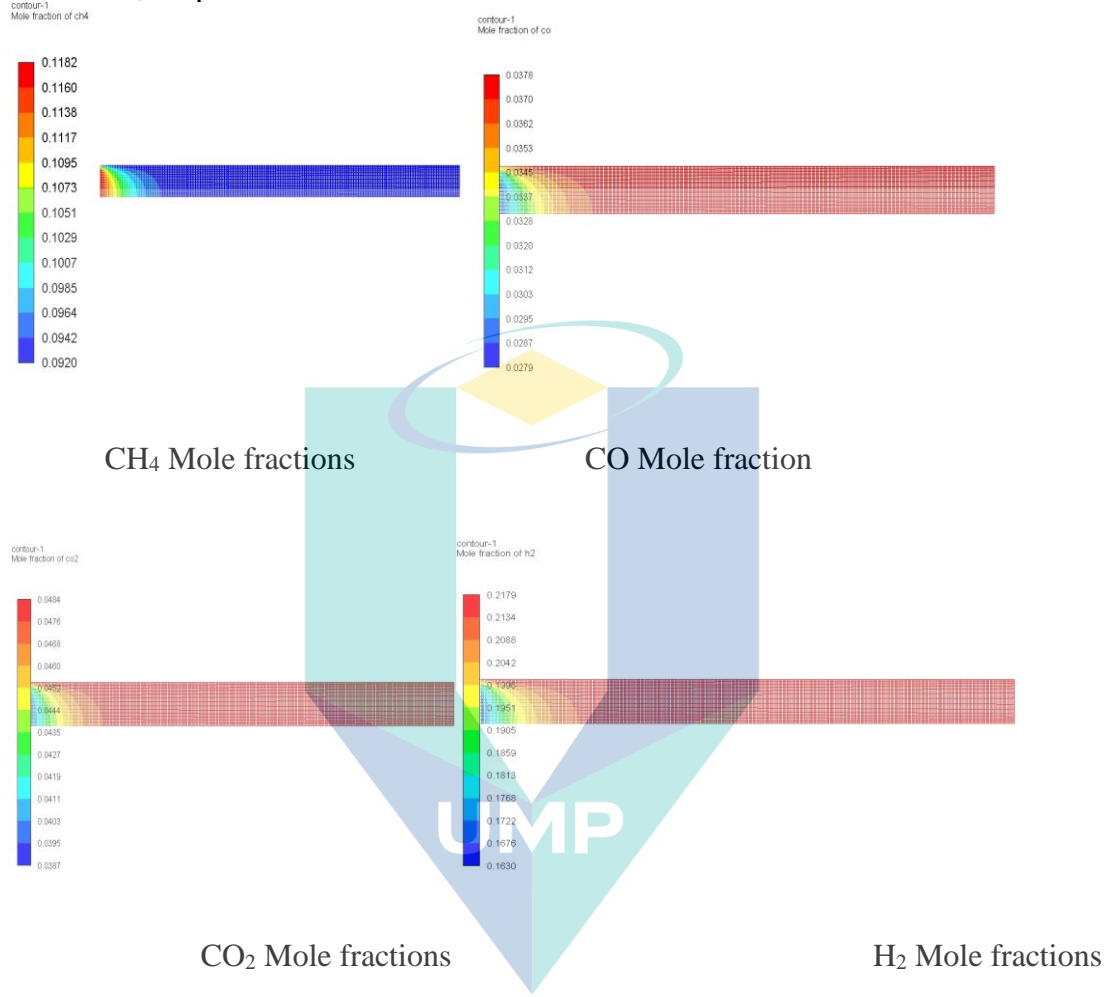
contour-3  
Mole fraction of h2o



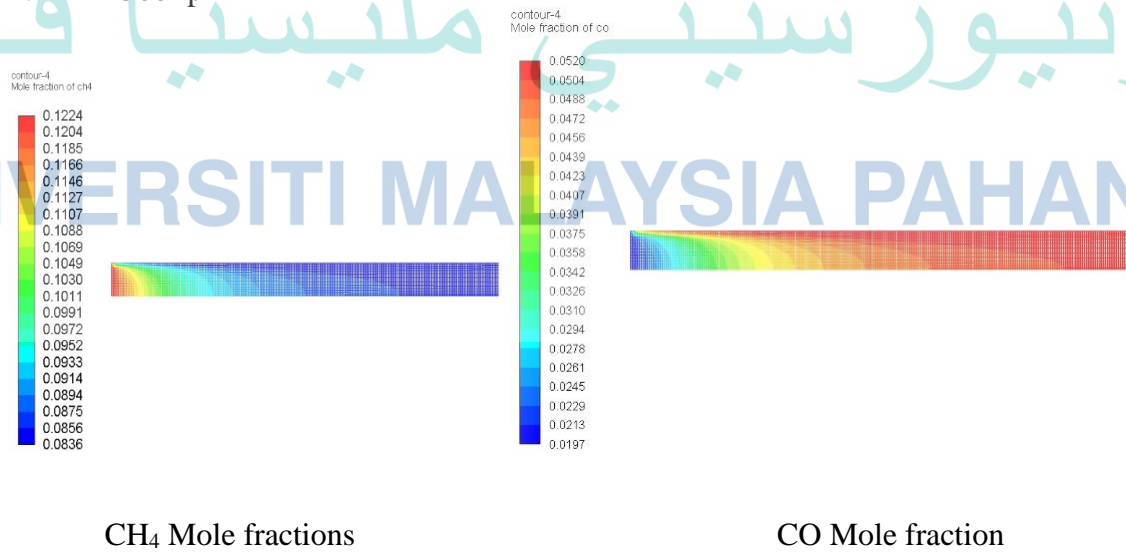
اونيورسيتي ملايسيا هانغ  
UNIVERSITI MALAYSIA PAHANG

Appendix E CFD Contours of reforming characteristics of the optimized model

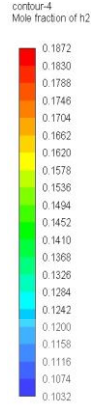
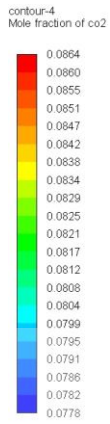
1. 12,00 rpm



2. 1500 rpm

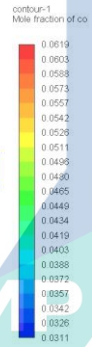
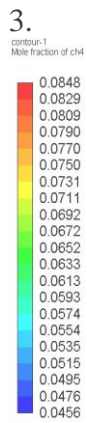


اونيور سیتی ملیسیا قهغ  
UNIVERSITI MALAYSIA PAHANG



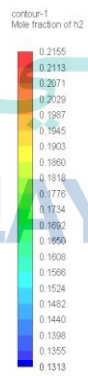
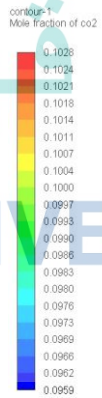
CO<sub>2</sub> Mole fractions

H<sub>2</sub> Mole fractions



CH<sub>4</sub> Mole fractions

CO Mole fraction



CO<sub>2</sub> Mole fractions

H<sub>2</sub> Mole fractions

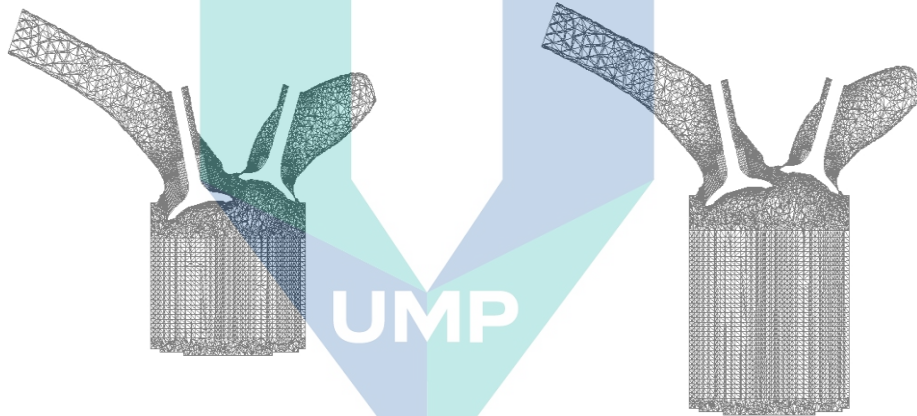
اونيورسيتي مليسيا هغ  
UNIVERSITI MALAYSIA PAHANG

## Appendix F Dynamic Mesh



Mesh (Time=0.0000e+00) ANSYS Fluent Release 18.1 (3d, dp, pbns, dynamesh, pdf20, ANSYS Fluent Release 18.1 (3d, dp, pbns, dynamesh

Surface Grid (Time=1.8924e-03) Crank Angle=336.63(deg) ANSYS Fluent Release 18.1 (3d, dp, pbns, dynamesh



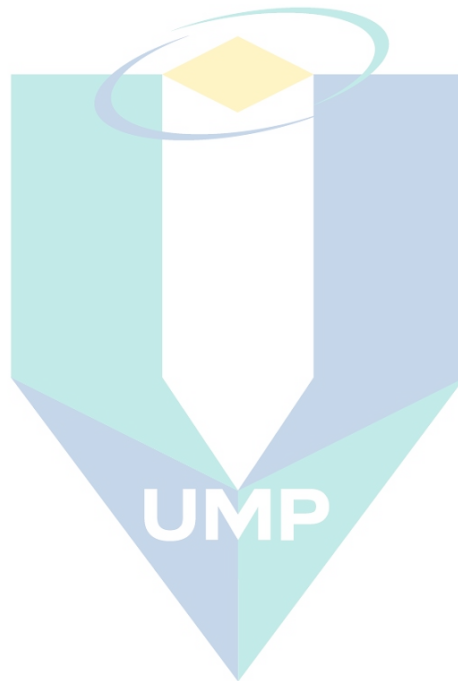
Surface Grid (Time=1.6951e-02) Crank Angle=445.05(deg) ANSYS Fluent Release 18.1 (3d, dp, pbns, dynamesh, ANSYS Fluent Release 18.1 (3d, dp, pbns, dynamesh,

Surface Grid (Time=2.2674e-02) Crank Angle=486.25(deg) ANSYS Fluent Release 18.1 (3d, dp, pbns, dynamesh,

اونيور سيني ملايسيا قهغ  
UNIVERSITI MALAYSIA PAHANG

## Appendix G List of publications

1. Arman, Abdulwahid, Ftwi Yohannes Hagos, Abdul Adam Abdullah, Abd Rashid Abd Aziz, Rizalman Mamat, Chin Kui Cheng, and Dai-Viet N. Vo. "Kinetic and CFD Modeling of Exhaust Gas Reforming of Natural Gas in a Catalytic Fixed-Bed Reactor for Spark Ignition Engines." *Chemical Engineering & Technology* 43, no. 4 (2020): 705-718.. (ISI: Q<sub>2</sub> Journal, IF=2.7)
2. Arman, A., F. Y. Hagos, A. A. Abdullah, R. Mamat, A. R. A. Aziz, and C. K. Cheng. "Syngas production through steam and CO<sub>2</sub> reforming of methane over Ni-based catalyst-A Review." *MS&E* 736, no. 4 (2020): 042032. (Scopus indexed)

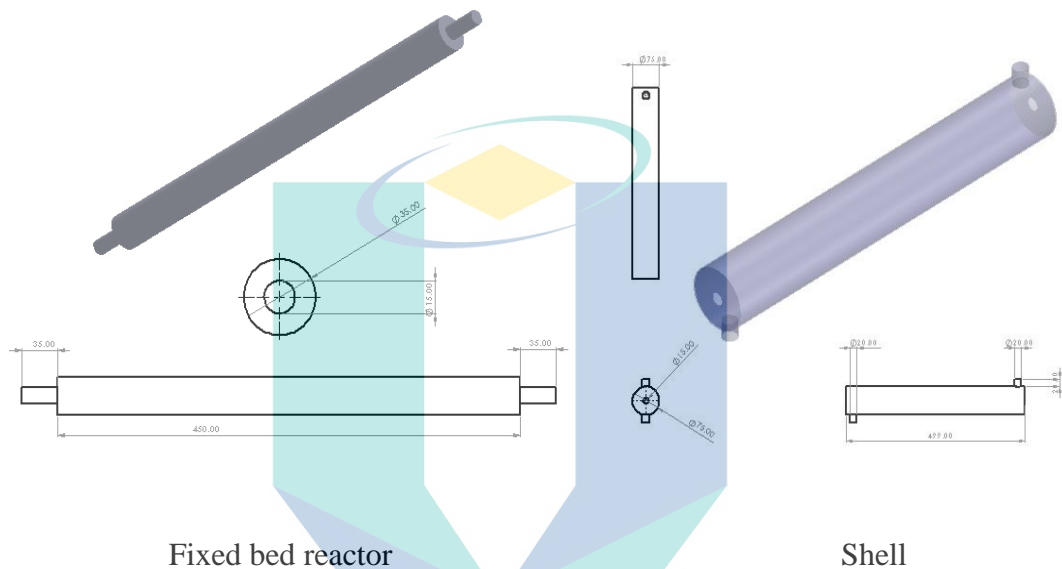


اونيورسيتي ملايسيا قهغ

UNIVERSITI MALAYSIA PAHANG

Appendix H Sugessted Reformer design

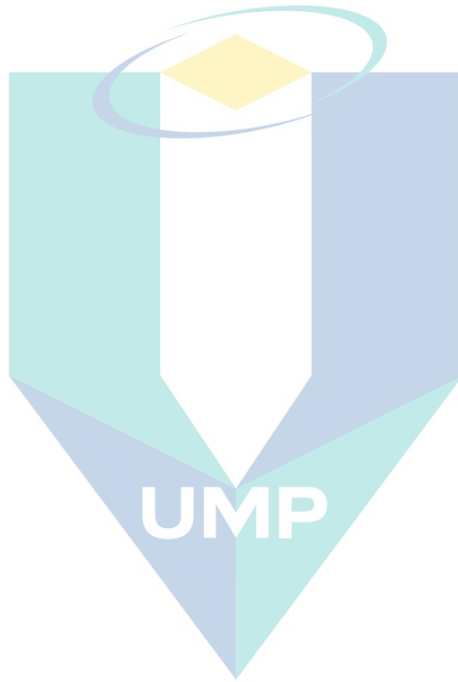
Fixed Bed rector (Shell and tube heat exchanger reactor )



UMP



Final reactor design



اونيورسيتي ملايسيا قهغ

UNIVERSITI MALAYSIA PAHANG